FACULDADE DE ENGENHARIA DA UNIVERSIDADE DO PORTO

Power Loss Modelling of a 2.5 MW Bosch Rexroth GPV500 Wind Turbine Gearbox

Rui Pedro Ferreira

MASTER OF SCIENCE DISSERTATION



Master Degree in Mechanical Engineering

Supervisor: Professor Carlos M.C.G. Fernandes

Co-Supervisors: Doctor Pedro M.T. Marques
Professor Jorge H.O. Seabra

July 21, 2021

Power Loss Modelling of a 2.5 MW Bosch Rexroth GPV500 Wind Turbine Gearbox

Rui Pedro Ferreira

Master Degree in Mechanical Engineering

July 21, 2021

Abstract

With the constant growth in the demand for higher efficiencies and shorter development times, it has become essential to find an alternative to the time consuming and expensive experimental tests in order to analyse power loss in a gearbox. That being said, this work is focused on developing a power loss model for a 2.5 MW Bosch Rexroth wind turbine gearbox.

A reverse engineering process was performed in order to obtain gearbox geometry data essential to the power loss calculation. Next, a gearbox model was created using KISSsoft/KISSsys, making it possible to perform power loss calculations using this same software. Further power loss models were applied on different software aiming to establish a comparison with KISSsoft results.

Due to the gearbox complexity, a heat dissipation model based on one directional heat transfer was suggested in an effort to accurately represent thermal phenomena in the case under study. Although the model allows to obtain wall temperatures and provides knowledge concerning lubricant temperature fluctuation, it still lacks experimental validation. Further calculations were performed in order to predict gear bulk temperature using pre-existing models, as well as bearing bulk temperature to which a model that stems from the combination of pre-existing ones was implemented.

Analysing the results obtained from the models, allows to understand that the lubricant used and the operating conditions to which the gearbox is submitted are crucial factors to the efficiency results. Furthermore, the most relevant power loss sources and gearbox's critical elements are easily noted.

Resumo

Com o constante crescimento na procura de altas eficiências e curtos períodos de desenvolvimento, torna-se essencial econtrar uma alternativa aos tão caros e demorados testes experimentais realizados no âmbito da potência dissipada. Assim, este trabalho é focado em desenvolver um modelo capaz de calcular a potência dissipada numa caixa multiplicadora, 2.5 MW Bosch Rexroth, aplicada em turbinas eólicas.

Foi usado um processo de engenharia inversa de forma a obter dados relativos à geometria desta caixa essenciais ao cálculo da potência dissipada. De seguida, um modelo da caixa foi criado em KISSsoft/KISSsys, permitindo assim a realização de cálculos no âmbito da potência dissipada neste mesmo *software*. Modelos adicionais, no toca à potência dissipada, foram aplicados em *software* diferente para que fosse possível establecer uma comparação com os resultados obtidos através do KISSsoft.

Dada a alta complexidade da caixa multiplicadora, sugeriu-se um modelo de dissipação de calor baseado em transferência de calor unidirecional com o intuito de representar de forma mais precisa os fenómenos térmicos no caso em análise. Ainda que este modelo permita o cálculo das temperaturas de parede, bem como forneça informação relativa à variação da temperatura do lubrificante, carece ainda de validação experimental. Foram realizados cálculos adicionais, de forma a prever a temperatura de massa de engrenagens, realizados com base em modelos pré-existentes, e ainda temperatura de massa de rolamentos para a qual foi usado um modelo que deriva da combinação de modelos pré-existentes.

Pela a análise dos resultados obtidos através dos modelos implementados, pode perceber-se que tanto o lubrificante como as condições de operação a que a caixa é submetida, são fatores muito relevantes na sua eficiência. Além disto, tanto as fontes de dissipação de potência mais relevantes como os elementos críticos desta caixa, tornam-se evidentes.

Acknowledgements

My first word of gratitude needs to be addressed to my supervisors, without whom the development of this project would not be as fulfilling as it was: Professor Carlos Fernandes, for the opportunity of developing this work, as well as for all the resources and knowledge transmitted over the whole journey; Doctor Pedro Marques, for his patience and readiness at all times, specially in the most difficult ones; and of course, Professor Jorge Seabra, for the motivation and wise advice when it was most needed.

I am also grateful to everyone working at CETRIB for the warm welcome and for providing an extremely healthy work environment over the last few months.

I could not forget to thank two of my closest friends, James Hooton and Tiago Meireles, for their companionship and assertive suggestions, which made this road a lot easier to walk than it would be otherwise

Finally, and most importantly, a very special thank you to my parents and brother, for the support provided at all times and the values instilled in me that led me to where I am today.

An honest thank you to you all...

"Audaces fortuna juvat"

Latin proverb

Contents

1 Introduction **1**
- 1.1 Problem Statement . . . 1
- 1.2 Purpose . . . 2
- 1.3 Thesis Layout . . . 2

2 Power Loss Models **5**
- 2.1 Gear Losses . . . 6
  - 2.1.1 Load Independent Losses . . . 6
  - 2.1.2 Load Dependent Losses . . . 7
- 2.2 Rolling Bearing Losses . . . 9
- 2.3 Shaft Seal Losses . . . 12
- 2.4 Auxiliary Losses . . . 13
- 2.5 Heat Dissipation . . . 13

3 Flash and Bulk Temperatures **17**
- 3.1 Gear Bulk Temperature . . . 17
  - 3.1.1 Flash Temperature Method . . . 17
  - 3.1.2 Integral Temperature Method . . . 20
- 3.2 Bearing Bulk Temperature . . . 23

4 Gearbox - Reverse Engineering **25**
- 4.1 Drawing Scaling . . . 27
- 4.2 Shaft Sizing . . . 27
- 4.3 Bearings . . . 28
- 4.4 Seals . . . 29
- 4.5 Gear Sizing . . . 30
  - 4.5.1 Normal Module and Helix Angle . . . 30
  - 4.5.2 Iterative Process . . . 31
- 4.6 Gearbox Kinematics . . . 36
  - 4.6.1 Planetary Stages Kinematics . . . 38

5 Gearbox Modelling **41**
- 5.1 KISSsoft Model . . . 42
  - 5.1.1 Planetary Stages . . . 42
  - 5.1.2 Helical Gear Pair . . . 43
- 5.2 KISSsys Model . . . 43
  - 5.2.1 Assembling a Planetary Stage . . . 44
  - 5.2.2 Assembling Last Stage . . . 46

5.2.3 Establishing Boundary Conditions . . . 47
5.2.4 Mainline Coaxial Shaft Calculation . . . 54
5.2.5 Creating User Interface Table . . . 56
5.3 Power Loss Model . . . 56
5.3.1 KISSsys Power Loss Model . . . 56
5.3.2 Excel Power Loss Model . . . 58
5.4 Heat Dissipation Model . . . 59
5.4.1 Activating KISSsys Heat Transfer Model . . . 59
5.4.2 One Directional Heat Dissipation Model . . . 60
5.4.3 Lubricant Heat Dissipation . . . 60
5.5 Bulk Temperatures . . . 61
5.5.1 Gear Bulk Temperatures . . . 61
5.5.2 Bearing Bulk Temperatures . . . 62

6 Results and Discussion **65**
6.1 Power Loss . . . 66
6.1.1 Gear Power Loss . . . 66
6.1.2 Bearing Power Loss . . . 68
6.1.3 Gearbox Power Loss . . . 70
6.1.4 Gearbox Efficiency . . . 71
6.2 Thermal Model . . . 76
6.3 Bulk Temperatures . . . 81
6.3.1 Gear Bulk Temperatures . . . 81
6.3.2 Bearing Bulk Temperatures . . . 84

7 Conclusions and Future Work **89**
7.1 Conclusions . . . 89
7.2 Future Work . . . 90

A Sliding Speed Distributions **95**

B KISSsoft Reports **99**

List of Figures

1.1 Photograph of the 2.5 MW Bosch Rexroth GPV500 wind turbine gearbox, taken at SERMEC GROUP. . . . 2

2.1 Power loss sources. . . . 5
2.2 Splash oil factor according to Mauz, adapted from ISO TR 14179-2. . . . 6
2.3 Gearbox thermal zones. . . . 14

3.1 Parameter on the line of action. . . . 18
3.2 Load distribution along the path of contact . . . 19

4.1 Power flow on the first stage of the gearbox. . . . 25
4.2 Power flow on the second stage of the gearbox. . . . 26
4.3 Power flow on the third stage of the gearbox. . . . 26
4.4 Power flow on the fourth stage of the gearbox. . . . 26
4.5 Iterative process used in gear sizing. . . . 33
4.6 Gearbox kinematics. . . . 37
4.7 Kinematics of a planetary stage. . . . 38

5.1 KISSsys gearbox model. . . . 41
5.2 Planetary calculation - KISSsoft. . . . 42
5.3 KISSsoft rating tab and definition of X_L and K_A parameters. . . . 43
5.4 Helical gear pair calculation - KISSsoft. . . . 43
5.5 Stage 1 KISSsys tree structure. . . . 44
5.6 Stage 1 planet pin KISSsoft calculation. . . . 45
5.7 Planetary gear 3D representation on KISSsys. . . . 45
5.8 Output and pump shafts KISSsys tree structure. . . . 46
5.9 Schematic representation of stage 1 kinematics. . . . 48
5.10 Three dimensional model of the first stage. . . . 48
5.11 Schematic representation of stage 1 and 2 kinematics. . . . 49
5.12 Three dimensional model of the first and second stages. . . . 49
5.13 Schematic representation of stage 1 to 3 kinematics. . . . 50
5.14 Three dimensional model of the first, second and third stages. . . . 51
5.15 Three dimensional model of the gearbox stages. . . . 51
5.16 Schematic representation of stage 1 to 4 kinematics. . . . 52
5.17 KISSsys dialog window for the input boundary condition. . . . 53
5.18 Overall KISSsys tree structure of the gearbox. . . . 53
5.19 Schematic representation of the gearbox kinematics. . . . 54
5.20 Mainline KISSsys tree structure. . . . 54
5.21 Mainline coaxial shaft KISSsoft calculation. . . . 55

5.22 User interface table. . . . 56
5.23 Output shaft KISSsys tree structure. . . . 57
5.24 KISSsys efficiency table. . . . 57
5.25 KISSsys heat dissipation sources. . . . 60
5.26 KISSsoft rating tab, calculation and report buttons. . . . 61

6.1 Load distribution and sliding speed along the path of contact of sun-planet gear pair -first planetary stage. . . . 67
6.2 Gear load-dependent power loss for six operating conditions and two gearbox oils. 68
6.3 Bearing power loss for six operating conditions and two gearbox oils. . . . 69
6.4 Total power loss for six operating conditions and two gearbox oils. . . . 71
6.5 Efficiency values for six operating conditions, gearbox lubricated with mineral oil. 72
6.6 Efficiency values for six operating conditions, gearbox lubricated with PAO oil. . 72
6.7 Efficiency curve for the mineral lubricant, $R^2 = 0,9$. . . . 73
6.8 Efficiency curve for the PAO lubricant, $R^2 = 0,9$. . . . 73
6.9 Comparison between the efficiency curves of both lubricants for lower values of input power. . . . 74
6.10 Comparison between the efficiency curves of both lubricants for higher values of input power. . . . 74
6.11 Gearbox efficiency maps. . . . 75
6.12 Gearbox thermal zones and heat transfer coefficients. . . . 76
6.13 Thermal model sensitivity. . . . 78
6.14 Oil temperature fluctuation, mineral oil. . . . 79
6.15 Oil temperature fluctuation, synthetic oil. . . . 79
6.16 Oil temperature fluctuation using the cooler second speed, mineral oil. . . . 80
6.17 Oil temperature fluctuation using the cooler second speed, synthetic oil. . . . 80
6.18 Percentage of heat dissipated per source and operating condition. . . . 81
6.19 Flash temperature distribution along the path of contact for sun-planet gear pair of the first stage. . . . 82
6.20 Gear bulk temperatures calculated with the flash temperature method, mineral oil lubricated. . . . 83
6.21 Gear bulk temperatures calculated with the flash temperature method, PAO oil lubricated. . . . 83
6.22 Highest contact temperature per gear pair and operating condition, mineral oil lubricated. . . . 84
6.23 Highest contact temperature per gear pair and operating condition, PAO oil lubricated. . . . 84
6.24 Bearing temperature for the six different operating conditions. . . . 85
6.25 Bearing temperature for the sixth operating condition. . . . 86
6.26 Temperature variation for set of tapered bearings "Timken H936349-H936310 + SKF 30234". . . . 87

A.1 Sliding speed distribution along the path of contact of the planet-ring gear pair - first planetary stage. . . . 95
A.2 Sliding speed distribution along the path of contact of the sun-planet gear pair - second planetary stage. . . . 96
A.3 Sliding speed distribution along the path of contact of the planet-ring gear pair - second planetary stage. . . . 96

A.4 Sliding speed distribution along the path of contact of the sun-planet gear pair - third planetary stage. 97
A.5 Sliding speed distribution along the path of contact of the planet-ring gear pair - third planetary stage. 97

List of Tables

2.1 Oil formulation parameter. . . . 9
2.2 SKF μ_{EHL} values. . . . 11
2.3 Values for μ_{EHL} and μ_{bl} proposed by Fernandes *et al.*. . . . 11

4.1 Drawing scaling factors. . . . 27
4.2 Relevant bearings for power loss calculation on stage 1. . . . 28
4.3 Relevant bearings for power loss calculation on stage 2. . . . 28
4.4 Relevant bearings for power loss calculation on stage 3. . . . 28
4.5 Relevant bearings for power loss calculation on stage 4. . . . 29
4.6 Relevant seals for power loss calculation on stage 1. . . . 29
4.7 Relevant seals for power loss calculation on stage 4. . . . 29
4.8 Gear modules. . . . 30
4.9 Helix angle. . . . 31
4.10 Input data on KISSsoft calculations for iterative process. . . . 32
4.11 Final iteration for stage 1 gears. . . . 34
4.12 Final iteration for stage 2 gears. . . . 35
4.13 Final iteration for stage 3 gears. . . . 35
4.14 Final iteration for stage 4 gears. . . . 36

5.1 Gear load dependent power loss model validation. . . . 58
5.2 Bearing power loss model validation. . . . 59
5.3 Flash temperature method. . . . 62
5.4 Integral temperature method. . . . 62

6.1 Gearbox operating conditions. . . . 65
6.2 Lubricant properties. . . . 66
6.3 Schlenk's approach (Excel) vs Niemann's approach (KISSsoft). . . . 66
6.4 Results produced with SKF's values vs Fernandes' values of μ_{EHL} and μ_{bl}. . . . 69
6.5 Wall temperatures and power dissipated through the gearbox housing. . . . 77

List of Symbols

a'	Working centre distance	mm
A	Heat transfer area	mm^2
A_r	Bearing seating surface	mm^2
B	Bearing width	mm
b	Gear width	mm
b_0	Reference value of gear width	mm
B_{Mi}	Thermal contact coefficient of the element i	$N/((mm \cdot m \cdot s)^{1/2} \cdot K)$
c'	Single stiffness according to ISO 6336-1	$N/(mm \cdot \mu m)$
c_γ	Mesh stiffness according to ISO 6336-1	$N/(mm \cdot \mu m)$
$C_{1,2}$	Width/depth factors	-
C_{ai}	Tip relief of element i	µm
C_{eff}	Optimal tip relief	µm
c_{Mi}	Specific heat per unit of mass of element i	$J/(kg \cdot K)$
C_{Sp}	Splash oil factor	-
d	Roller bearing bore diameter	mm
D	Roller bearing outside diameter	mm
d_i	Reference pitch diameter of the element i	mm
d_{sh}	Shaft diameter	mm
d_a	Gear addendum diameter	mm
d_b	Gear base diameter	mm
d_f	Gear root diameter	mm
d_m	Bearing mean diameter	mm
d_s	Seal counterface diameter	mm
e	Wall thickness	m
E_i	Modulus of elasticity of element i	N/mm^2
E_r	Reduced modulus of elasticity	N/mm^2
F_{bt}	Transverse force to tooth flank	N
F_N	Local load per unit of length	N/mm
G_{rr}	Variable depending on bearing data	-
G_{sl}	Variable depending on bearing data	-
H	Oil level	mm
h_c	Height of point of contact above the lowest point of the immersing gear	mm
$h_{e,max}$	Maximum tip circle immersion depth with stationary oil level	mm
h_{e0}	Reference value of immersion depth	mm
$h_{e1,e2}$	Tip circle immersion depth with oil level stationary	mm
H_{VL}	Gear loss factor	-
k	Addendum correction factor	-
K_A	Application factor	-

$K_{B\alpha}$	Transverse load factor (scuffing)	-
$K_{B\beta}$	Face load factor (scuffing)	-
$K_{B\lambda}$	Helical load factor (scuffing)	-
K_{BE}	Geometry factor at pinion tooth tip	-
K_{mp}	Multiple path factor	-
K_{rs}	Replenishment/starvation constant	-
K_{S1}	Constant depending on seal and bearing type	-
K_{S2}	Constant depending on seal and bearing type	-
K_L	Bearing type related constant	-
K_V	Dynamic factor	-
K_z	Bearing type related constant	-
l_h	Hydraulic length	mm
$l^i(x,y)$	Single contact line length at given position (x,y)	mm
m	Normal gear module	mm
M	Total frictional moment	$\mathrm{N}\cdot\mathrm{mm}$
M_{drag}	Frictional moment of drag losses	$\mathrm{N}\cdot\mathrm{mm}$
M_{rr}	Rolling frictional moment	$\mathrm{N}\cdot\mathrm{mm}$
M_{seal}	Frictional moment of seals	$\mathrm{N}\cdot\mathrm{mm}$
M_{sl}	Sliding frictional moment	$\mathrm{N}\cdot\mathrm{mm}$
m_t	Transverse gear module	mm
n	Rotational speed	rpm
n_p	Number of planets	-
P_{IN}	Mesh input power	W
P_{IN}^g	Gearbox input power	W
p_b	Base pitch	mm
$\dot{Q}_c$	Conduction heat transferred per unit of time	W
$\dot{Q}_{cv}$	Convection heat transferred per unit of time	W
$\dot{Q}_L$	Heat flow dissipated by the lubricant	kW
$\dot{Q}_{rad}$	Radiation heat transferred per unit of time	W
$\dot{Q}_s$	Heat flow dissipated via the bearing seating surfaces	kW
r_b	Base radius	mm
Ra	Average absolute surface roughness	µm
Ra	Average absolute surface roughness	µm
T_∞	Surrounding fluid temperature	K
T_{Wall}	Wall temperature	K
T_H	Hydraulic torque loss	$\mathrm{N}\cdot\mathrm{m}$
U	Perimeter	mm
u	Gear ratio	-
$v_{\Sigma C}$	Sum of velocities at pitch point	$\mathrm{m/s}$
v_{t0}	Reference tangential speed	$\mathrm{m/s}$
v_{tb}	Absolute tangential speed on base plane	$\mathrm{m/s}$
v_g	Sliding speed	$\mathrm{m/s}$
$\dot{V}_L$	Oil flow in the bearing	$\mathrm{L/min}$
$\dot{V}_{Lmax}$	Maximum oil flow in the bearing	$\mathrm{L/min}$
V_M	Drag loss factor	-
v_t	Pitch line velocity	$\mathrm{m/s}$
w_{Bt}	Transverse unit load	$\mathrm{N/mm}$

x	Profile shift coefficient	-
X_ε	Contact ratio factor	-
X_Γ	load sharing factor	-
$X_{\alpha\beta}$	Angle factor	-
X_{Ca}	Tip relief factor	-
X_E	Run-in factor	-
X_G	Geometry factor	-
X_J	Approach factor	-
X_L	Lubricant formulation parameter	-
X_M	Thermo-elastic factor	-
X_Q	Approach factor	-
X_R	Roughness factor according to Niemann	-
X_S	Lubrication system factor	-
z_i	Number of teeth of the element i	-
α_{ext}	Heat transfer coefficient, exterior of the gearbox	$\mathrm{W}/(\mathrm{m}^2 \cdot \mathrm{K})$
α_{int}	Heat transfer coefficient, interior of the gearbox	$\mathrm{W}/(\mathrm{m}^2 \cdot \mathrm{K})$
α	Gear reference pressure angle	°
α'	Gear working pressure angle	°
β	Helix angle	°
β_{seal}	Exponent depending on seal and bearing type	-
ε	Emissivity	-
ε_a	Recess contact ratio	-
ε_f	Approach contact ratio	-
ε_i	Addendum contact ratio of the element i	-
ε_α	Contact ratio	-
η	Dynamic viscosity	mPa
Γ_y	Parameter on the line of action at generic point y	-
λ	Wall thermal conductivity	$\mathrm{W}/(\mathrm{m} \cdot \mathrm{K})$
λ_{Mi}	Heat conductivity of element i	$\mathrm{N}/(\mathrm{s} \cdot \mathrm{K})$
μ_{bl}	Constant depending on movement	-
μ_{EHL}	Sliding friction coefficient in full-film conditions	-
μ_{mZ}	Average coefficient of friction along the path of contact	-
μ_{sl}	Sliding friction coefficient	-
ν_i	Poisson's ratio of element i material	-
ω_{ij}	Angular velocity of body i, frame of reference attached to j	rad/s
ϕ_{bl}	Weighting factor for the sliding friction coefficient	-
ϕ_{ish}	Inlet shear heating reduction factor	-
ϕ_{rs}	Kinematic replenishment/starvation reduction factor	-
ρ_{Mi}	Density of element i	kg/m^3
ρ_{redC}	Equivalent contact radius on pitch point	mm
σ	Stefan-Boltzmann constant	$\mathrm{W}/(\mathrm{m}^2 \cdot \mathrm{K}^4)$
θ_{fl}	Flash temperature	°C
θ_{flm}	Average flash temperature	°C
θ_{oil}	Oil temperature	°C
θ_B	Contact temperature	°C
θ_M	Bulk temperature	°C
υ	Operating viscosity of the oil	mm^2/s
ϑ_{flaE}	Flash temperature at pinion tooth tip when load sharing is neglected	°C

ϑ_{flaint}	Mean flash temperature	°C
ϑ_M	Bulk temperature	°C
	Subscripts	
1	Index meaning the data is associated to pinion	-
2	Index meaning the data is associated to wheel	-
plan	Index meaning the data is associated to planet gear	-
pump	Index meaning the data is associated to pump gear	-
ring	Index meaning the data is associated to ring gear	-
sun	Index meaning the data is associated to sun gear	-

Chapter 1

Introduction

1.1 Problem Statement

Renewable energies are a must for human kind's path to sustainability. As climate change repercussions become more evident by the year and non-renewable sources scarcer, diversifying energy production methods is of utmost importance [1].

Wind being a clean, unlimited and free source of renewable energy makes it one of the most promising to be explored. For such reasons, fast growth over the past years has been noticed in world's wind energy capacity [2–5].

Electricity generated from wind power represented 5.9% of global demand at the end of 2019 [6]. For Portugal, this value goes up to 27%, with a total installed wind power capacity of 5437 MW and a total electrical energy output from wind of 13,7 TWh [7].

Turbines used in wind energy farms are considered to take only a small fraction of their life span to produce the same energy amount as the one spent in their manufacturing process, thus creating the possibility of generating an energy quantity, over their lifetime, many times greater than that embodied in their production [8].

Such machines are capable of turning the kinetic energy from the wind into mechanical energy. Nevertheless, the relatively low rotational speeds of the blades, around 20 revolutions per minute, are not suitable for using an electrical generator. Solving this problem requires a multiplying gearbox before the electrical generator [9].

The efficiency of such gearboxes is often wrongly overlooked. An improvement of this factor will lead to lower heat dissipation and consequently lower lubricant operation temperature, which in turn will minimize oil degradation and the risk of failure [10].

Furthermore, a 1% increase in the efficiency of a 2.5 MW wind turbine will lead to an additional 25 kW of output power, in a single machine, which is enough to power several households. If such improvement would be made to wind farms across the globe, the increment in amount of energy generated without the need for additional equipment could be a decisive point in sustainability.

1.2 Purpose

The main goal of this work is to create a power loss model that can accurately predict power losses in a 2.5 MW Bosch Rexroth GPV500 wind turbine gearbox, as the one shown in Figure 1.1. Ultimately, the model will allow to understand what causes are behind such losses without the need for experimental measurements. Additionally, it will provide valuable data concerning the gearbox machine elements, such as temperatures and the amount of power lost by each of those elements. Therefore providing knowledge on how to act in order to improve gearbox efficiency.



Figure 1.1: Photograph of the 2.5 MW Bosch Rexroth GPV500 wind turbine gearbox, taken at SERMEC GROUP.

In order to achieve these goals, a reverse engineering process needs to be done as a means to obtain crucial gearbox data to the modelling process. Next, a model using KISSsys/KISSsoft will be created based on the data obtained from the reverse engineering process, followed by the application of power loss and heat dissipation models.

1.3 Thesis Layout

Chapter 2, entitled **"Power Loss Models"**, approaches the models used to calculate power loss in the different sources present in the gearbox under study. Additionally, a model used to perform calculations concerning heat dissipation is presented.

Chapter 3, entitled **"Flash and Bulk Temperatures"**, presents the models behind the calculations done in order to obtain bulk temperatures in the gearbox elements.

Chapter 4, entitled **"Gearbox - Reverse Engineering"**, covers the reverse engineering process used to obtain crucial information, from the scarce data available, in order to properly model the gearbox.

Chapter 5, entitled **"Gearbox Modelling"**, goes into detail on what concerns the implementation of previously mentioned models. This chapter contains information regarding software usage in order to achieve the final model of the gearbox.

Chapter 6, entitled **"Results/Discussion"**, presents the results obtained from the models implemented. Here, the information is arranged in tables and charts, providing an easier analysis. Additionally, these results are briefly analysed and commented.

Chapter 7, entitled **"Conclusions and Future Work"**, where final conclusions regarding this thesis are drawn. Furthermore, several suggestions for future work in this field are made.

Chapter 2

Power Loss Models

Power loss in a gearbox is the combination of gear, bearing, seal and in some cases auxiliary losses from devices coupled to the mechanism *e.g.* oil pumps have to be taken into consideration [11]. Gear and bearing power losses can be divided in load dependent and load independent (Figure 2.1). The first type will occur even without power transmission, depending mainly on lubricant properties, density and viscosity, as well as rotational speed, internal housing design and immersion depth of the components in a sump lubricated gearbox [12], while load dependent ones will be influenced by transmitted load, coefficient of friction and sliding velocity in the contact areas of the components [13].

Gearbox testing can be used to obtain power loss values, but being such a time demanding and expensive option with complex technical aspects to overcome, makes it less appealing when compared to a model capable of predicting these same values at the design stage when no physical components exist yet.

Since there are infinite combinations of machine elements, lubricant formulations and operating conditions to be used, the real challenge is to create models capable of including such large number of variables and accurately predict the losses in any gearbox [14].

This chapter is dedicated to presenting some of the existing models used to predict power loss from different sources in a gearbox. The selected models are either used by commercial software based on standards or research articles, in some cases experimentally validated.

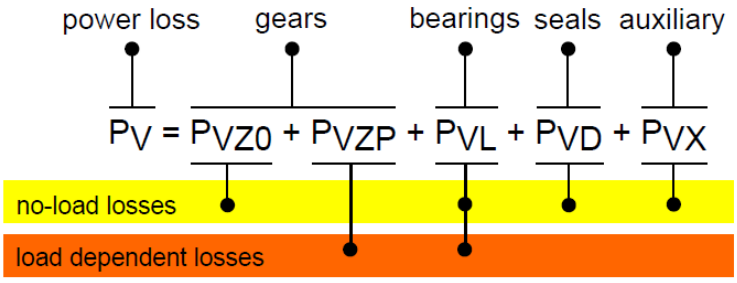


Figure 2.1: Power loss sources [15].

2.1 Gear Losses

2.1.1 Load Independent Losses

The first studies to be conducted in this subject can be attributed to the work of Daily *et al.* (1960) [16] and Mann *et al.* (1961) [17]. At the time, the drag torque and secondary flows on a disk rotating submerged in fluid were being studied.

Since then, several subsequent studies on the power loss due to the churning of the gears in an oil bath were conducted, such as the work of Terekhov (1975) [18], Walter (1982) [19], Lauster (1983) [20], Mauz (1985) [21], Boness (1989) [22] and Changenet (2011) [23].

More recent studies are trying to predict churning losses in planetary gears, such as Boni *et al.* (2019) [24], which admits the formation of an oil ring around the ring shaft. The conditions required for the formation of such ring were defined in June 2021, by the same authors [25].

Mauz's model, as seen in Figure 2.2, is part of ISO TR 14179-2 [26] and used by KISSsoft to calculate the load-independent gear losses. According to this model, the total hydraulic torque loss of a splash lubricated gear stage is determined as following:

$$T_H = C_{Sp} \cdot C_1 \cdot e^{C_2 \cdot \left(\frac{\nu_L}{\nu_{f0}}\right)} \tag{2.1}$$

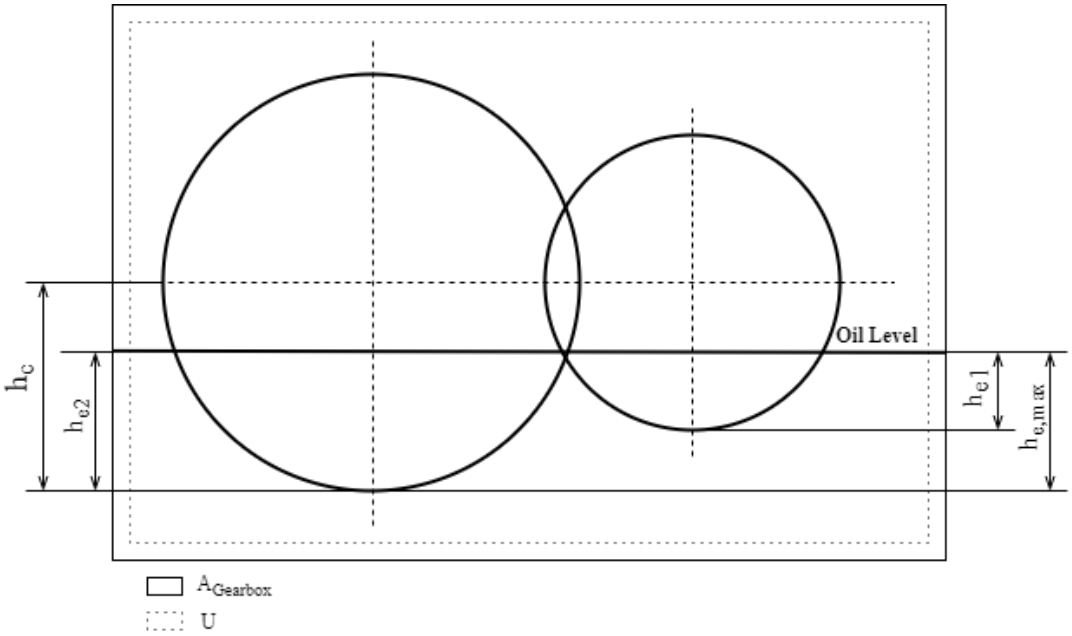


Figure 2.2: Splash oil factor according to Mauz, adapted from ISO TR 14179-2 [26].

Hydraulic length can be obtained from equation (2.2):

$$l_h = \frac{4 \cdot A_{Gearbox}}{U} \tag{2.2}$$

The splash oil factor, C_{Sp}, depends on the immersion depth as shown in Figure 2.2. Factors C_1 and C_2 are used to account for the effect of tooth width and immersion depth.

Since no viscosity effect was measurable in low depths and for high immersion depth the effects were contradictory, this formulation does not account such an effect.

$$C_{Sp} = \left(\frac{4h_{e,max}}{3h_c}\right)^{1,5} \cdot \frac{2h_c}{l_h} \tag{2.3}$$

$$C_1 = 0,063 \cdot \left(\frac{h_{e1}+h_{e2}}{h_{e0}}\right) + 0,0128 \cdot \left(\frac{b}{b_0}\right)^3 \tag{2.4}$$

$$C_2 = \frac{h_{e1}+h_{e2}}{80 \cdot h_{e0}} + 0,2 \tag{2.5}$$

Where the reference values for immersion depth, gear width and tangential speed are defined as follows: $h_{e0} = 10$ mm, $b_0 = 10$ mm and $v_{t0} = 10$ m/s.

On any gearbox, gear load-independent power loss will be the sum of each stage no-load gear loss. This type of loss can be calculated by multiplying the no-load torque loss with the angular velocity.

$$P_{VZ0} = \sum_{i=1}^{n} T_{H,i} \cdot \frac{\pi \cdot n_i}{30} \tag{2.6}$$

With n as the number of stages.

Equally important to note, is the fact that even though KISSsoft uses this model to predict load independent power losses, there are models capable of accounting for lubricant viscosity [18] and different flow regimes [23].

2.1.2 Load Dependent Losses

In 1949, a first approach to this type of losses was done by Buckingham [27]. Few years later, Ohlendorf (1958) [28] was able to present an approach to the power loss generated between gear tooth contact, resulting in equation (2.7) [14].

$$P_{VZP} = P_{IN} \cdot H_{VL} \cdot \mu_{mZ} \tag{2.7}$$

With H_{VL} representing the gear loss factor and μ_{mZ} the coefficient of friction, which is usually assumed constant along the path of contact [29].

The input power can be obtained as following:

$$P_{IN} = F_{bt} \cdot \omega \cdot r_b \tag{2.8}$$

Where, in the case of a parallel gear pair, the tangential force on the base plane is calculated using equation (2.9).

$$F_{bt} = \frac{P_{IN}^{g}}{v_t \cdot cos\alpha} \tag{2.9}$$

Nonetheless, for a planetary stage in order to account for the number of planets, it is calculated using equation (2.10) [30].

$$F_{bt} = \frac{P_{IN}^{g}}{n_p \cdot v_t \cdot cos\alpha} \tag{2.10}$$

Since Buckingham first approached this matter [27], numerous other authors have been doing it in the attempt to develop formulations that better predict this type of losses for any type of gear under analysis. As a result, several formulations are now known to establish gear loss factors, for instance the formulations of Merritt (1971) [31], Henriot (1978) [32], Niemman and Winter (1989) [33] and Velex (2009) [34].

However, these formulations are valid for spur gears without profile shift corrections. More recently, Wimmer [35] was able to solve this problem by developing equation (2.11). In order to solve it, FVA RIKOR was used and a solution for the load distribution ($F_N(x,y)$) along the path of contact was obtained considering elastic effects, in contrast to what had been done by Ohlendorf [28] years prior.

$$H_{VL} = \frac{1}{p_b} \int_0^b \int_A^E \frac{F_N(x,y)}{F_{bt}} \cdot \frac{v_g(x,y)}{v_{tb}} dxdy \tag{2.11}$$

Calculation of the load distribution along the path of contact can be done through equation (2.12).

$$F_N(x,y) = F_{bt} \cdot \frac{1}{\sum_{i=1}^{n} l^i(x,y)} \tag{2.12}$$

With n as the number of points defined along the path of contact.

Similarly to the gear loss factor, several formulations to obtain the coefficient of friction in meshing gears have been developed throughout the years, many of which disregarding at least one important geometrical or oil formulation parameter.

Michaelis [36] was able to present a formulation that accounts for oil viscosity, load applied, gear geometry and surface finishing. Besides oil viscosity, Schlenk [37] was even able to add a factor accounting for the oil formulation [14].

Nowadays, software such as KISSsoft uses Niemann's approach (equation (2.13)), as presented in [33], with the addition of X_L factor developed by Schlenk in order to account for the oil formulation.

$$\mu_{mZ} = 0,045 \cdot \left(\frac{F_{bt}/b}{v_{\Sigma C} \cdot \rho_{redC}} \right)^{0,2} \cdot \eta^{-0,05} \cdot X_R \tag{2.13}$$

$$X_R = 3,8 \cdot \sqrt[4]{\frac{Ra}{d_1}} \tag{2.14}$$

Equation (2.15) presents Schlenk's [37] formulation.

$$\mu_{mZ} = 0.048 \cdot \left(\frac{F_{bt}/b}{\nu_{\sum C} \cdot \rho_{redC}} \right)^{0,2} \cdot \eta^{-0,05} \cdot R_a^{0,25} \cdot X_L \tag{2.15}$$

In recent years, in a study published by Fernandes *et al.*, adjusted X_L values were proposed in order to minimize the difference between experimental values and the ones obtained from equation (2.15) [29]. Table 2.1 shows the values for X_L factor.

Table 2.1: Oil formulation parameter.

Oil	X_L **(Fernandes) [29]**	X_L **(Schlenk) [26]**
MINR	0,846	1
PAOR	0,666	0.8
MINE	0,751	1
PAGD	0,585	$0,75 \cdot \left(\frac{6}{\nu_{\sum C}}\right)^{0,2}$

The lubricants shown in Table 2.1, correspond to specific ISO VG 320 wind turbine gearbox oils according to [29] (a mineral (MINR), a poly-alpha-olefin (PAOR), a mineral with viscosity modifier (MINE) and a poly-alkyleneglycol (PAGD)).

2.2 Rolling Bearing Losses

For a better understanding of the processes that leads to rolling bearing power losses, they can be arranged into four main loss mechanisms.

Rolling friction is one of this mechanisms, it can be explained by the roller being under a normal load, rolling over its raceway. This work condition will lead to the formation of a bulge, and consequently a depression, on the raceway. The occurrence of this bulge means the roller now has to overcome an additional obstacle, meaning an additional tangential force will be needed to keep the rolling motion [14].

The major source of power loss in a rolling bearing is sliding friction. The slightest misalignment can cause one surface to slip over the other, depending on the coefficient of friction and the elastic properties of the surfaces involved, causing energy to be lost. Moreover, on a rolling bearing under simple radial load, pure rolling can only occur on points contained in two specific lines of contact, meaning at all other points sliding may occur [14].

In addition, the drag friction has to be accounted for. Lubricant is used to cool and lubricate bearings, nonetheless the lubrication film between the rolling elements and their raceway is built

using only a small portion of the lubricant. Lubricant surplus will generate additional drag forces and therefore a power loss, depending on its viscosity and rotational speed [14].

Rolling bearing seals also play a role in power loss. Used to prevent impurity from getting in and lubricant from getting out of the housing, tight spacing between the rubber of the seal and the shaft is essential. The friction generated by this interaction is a source of power loss, depending mainly on the rotational speed [14].

Many models have been presented to predict power losses in rolling bearings. Some of which were developed by the main rolling bearing manufacturers, being supported by a great amount of experimental results makes this models some of the most trustworthy [14]. KISSsoft uses by default SKF's model, even though it allows the calculations to be done according to other models.

SKF Torque Loss Model

According to SKF [38] the total torque loss is calculated using equation (2.16).

$$M_t = M_{rr} + M_{sl} + M_{seal} + M_{drag} \tag{2.16}$$

With the rolling frictional moment given by equation (2.17).

$$M_{rr} = \phi_{ish} \cdot \phi_{rs} \cdot G_{rr} \cdot (\upsilon \cdot n)^{0.6} \tag{2.17}$$

where G_{rr} depends on bearing and application data, can be obtained at SKF's catalogue.

As explained before, only a fraction of the lubricant is used to generate the hydrodynamic film. Thus, the excess is repelled and produces a reverse flow, shearing the lubricant and generating heat, consequently lowering the oil viscosity. In order to account for this effect, inlet shear heating reduction factor is estimated using:

$$\phi_{ish} = \frac{1}{1 + 1.84 \times 10^{-9} \cdot (n \cdot d_m)^{1.28} \cdot \upsilon^{0.64}} \tag{2.18}$$

In some lubrication conditions, *e.g.* cases where oil bath level is lower than the centre of the lowest rolling element and grease lubricated applications, a displacement of the lubricant from the raceways may occur due to continuous over-rolling. In high-speed applications or when working with high viscosities, the lubricant may not have sufficient time to replenish the raceways, promoting a "kinematic starvation" effect. The kinematic starvation/replenish factor can be estimated using equation (2.19).

$$\phi_{rs} = \frac{1}{e^{K_{rs} \cdot \upsilon \cdot n \cdot (d+D) \cdot \sqrt{\frac{K_Z}{2 \cdot (D-d)}}}} \tag{2.19}$$

where $K_{rs} = 3 \times 10^{-8}$ for low level oil bath and oil jet lubrication, or $K_{rs} = 6 \times 10^{-8}$ for grease and oil-air lubrication. K_Z is a bearing type related constant, can be obtained from SKF's catalogue.

The sliding frictional moment can be obtained from equation (2.20).

$$M_{sl} = G_{sl} \cdot \mu_{sl} \tag{2.20}$$

With the sliding friction coefficient calculated as following:

$$\mu_{sl} = \phi_{bl} \cdot \mu_{bl} + (1 - \phi_{bl}) \cdot \mu_{EHL} \tag{2.21}$$

where the weighting factor for the sliding friction coefficient is defined as:

$$\phi_{bl} = \frac{1}{e^{2.6\times10^{-8}(n\cdot\upsilon)^{1.4}d_m}} \tag{2.22}$$

and $\mu_{bl} = 0,12$ for $n \neq 0$, or $\mu_{bl} = 0,15$ for the starting torque calculation ($n = 0$). The μ_{EHL} values are shown in Table 2.2.

Table 2.2: SKF μ_{EHL} values.

	μ_{EHL}
Cylindrical Roller Bearings	0,02
Tapered Roller Bearings	0,002
Other Bearings	
Mineral Oil Lubricated	0,05
Synthetic Oil Lubricated	0,04
Transmission Fluids Lubricated	0,1

Based on the findings of Fernandes *et al.* [39], it can be argued that the values for μ_{bl} and μ_{EHL} presented in Table 2.3 provide more accurate power loss predictions for wind turbine gear oils.

Table 2.3: Values for μ_{EHL} and μ_{bl} proposed by Fernandes *et al.* [39].

Oil		**TBB**	**RTB**
MINR	μ_{bl}	0,058	0,035
	μ_{EHL}	0,056	0,018
PAOR	μ_{bl}	0,049	0,039
	μ_{EHL}	0,044	0,010
MINE	μ_{bl}	0,044	0,044
	μ_{EHL}	0,027	0,008
PAGD	μ_{bl}	0,054	0,025
	μ_{EHL}	0,044	0,010

The values presented are to be used on bearings that are not tapered roller bearings. The thrust ball bearings (TBB) values, can be used in calculations related to elliptic contact bearings, similarly the roller thrust bearings (RTB) values can be used for line contact bearings.

The seal frictional moment is given by equation (2.23).

$$M_{seal} = K_{S1} \cdot d_S^{\beta_{seal}} + K_{S2} \tag{2.23}$$

where K_{S1},β_{seal},K_{S2} are constants depending on seal and bearing type and size. The three constants can be obtained from SKF's catalogue.

As for the frictional moment of drag losses for roller bearings, it can be obtained from equation (2.24).

$$M_{drag} = 4 \cdot V_M \cdot K_{roll} \cdot C_w \cdot B \cdot d_m^4 \cdot n^2 + 1,093 \times 10^{-7} \cdot n^2 \cdot d_m^3 \cdot \left(\frac{n \cdot d_m^2 \cdot f_t}{\upsilon} \right)^{-1,379} \cdot R_s \tag{2.24}$$

The variables and functions used in the equation for frictional moment of drag losses are defined in SKF's torque loss model [38], exactly as:

$$K_{roll} = \frac{K_L \cdot K_Z \cdot (d+D)}{D-d} \cdot 10^{-12} \tag{2.25}$$

$$C_w = 2,789 \times 10^{-10} \cdot I_D^3 - 2,786 \times 10^{-4} \cdot I_D^2 + 0,0195 \cdot I_D + 0,6439 \tag{2.26}$$

$$I_D = 5 \cdot \frac{K_L \cdot B}{d_m} \tag{2.27}$$

$$f_t = \begin{cases} \sin\ (0,5 \cdot t), & \text{when } 0 \leq t \leq \pi \\ 1, & \text{when } \pi < t < 2\pi \end{cases} \tag{2.28}$$

$$R_S = 0,36 \cdot d_m^2 \cdot (t - \sin\ t) \cdot f_A \tag{2.29}$$

$$t = 2 \cdot \cos^{-1} \left(\frac{0,6 \cdot d_m - H}{0,6 \cdot d_m} \right) \text{ ; when } H \geq 1,2 \cdot d_m \text{ , use } H = 1,2 \cdot d_m \tag{2.30}$$

$$f_A = 0,05 \cdot \frac{K_z \cdot (D+d)}{D-d} \tag{2.31}$$

2.3 Shaft Seal Losses

The fact that the contact zone in this elements is very small, makes this type of losses very difficult to parametrize, and is one of the main reasons why this problem is not very well understood yet.

Nonetheless, Freudenberg Simrit was able to understand the seal losses were varying with the seal diameter and speed of the shaft. From a large number of measurements, Simrit was able to establish an equation (2.32) to predict this type of losses.

$$P_{VD} = 7,69 \times 10^{-6} \cdot d_{sh}^2 \cdot n \tag{2.32}$$

Linke (1996) [40] and Kettler (2002) [41], later developed equations that account for the oil viscosity, however the results produced by such equations do not seem to be consistent for all operating conditions and lubricants.

More recently, Organisciak presented a model to predict this type of losses [42], which accounts for oil viscosity and factors such as real contact area at the surface roughness level. The amount of data needed to apply the model is very extensive and obtained by performing measurements which made it impossible to apply to this work.

2.4 Auxiliary Losses

Every dissipative source that is not generated by gears, bearings or seals, should be considered in this group.

Specifically in this work, there is a gear pump that should be given some attention in order to determine if it is a relevant source of power loss, as well as the losses produced by the planet carriers.

2.5 Heat Dissipation

Power loss in the gearbox will be converted into the form of heat. Therefore, understanding the heat dissipation in this gearbox is of utmost importance. In order to so, the balance between power loss and heat dissipation must be established, allowing to understand the conditions to which thermal equilibrium is achieved and the correspondent temperatures.

KISSsys calculation for heat dissipation through the housing is based on ISO/TR 14179 [26], which in time uses Hohn's model presented in [11].

This model can accurately predict the losses in smaller, less complex gearboxes. Nonetheless, the simplifications it assumes may lead to significant differences in the prediction of heat transfer in gearboxes with such complexity and size as the one under study in this work.

Therefore, a one directional heat transfer model (equation(2.33)) was used to predict the heat transfer through the wall. This approximation had to be done with arbitrary heat transfer coefficients for air, which later on should be adjusted according to experimental data on the wall temperatures.

$$\dot{Q}_{cv_{Int}} = \dot{Q}_c = \dot{Q}_{cv_{Ext}} \tag{2.33}$$

Rearranging equation (2.33) by applying the convection and conduction heat transfer equations, leads to equation (2.34).

$$\begin{cases} \alpha_{Int} \cdot (T_{\infty_{Int}} - T_{Wall_{Int}}) = \lambda \cdot \dfrac{T_{Wall_{Int}} - T_{Wall_{Ext}}}{e} \\ \\ \lambda \cdot \dfrac{T_{Wall_{Int}} - T_{Wall_{Ext}}}{e} = \alpha_{Ext} \cdot (T_{Wall_{Ext}} - T_{\infty_{Ext}}) \end{cases} \tag{2.34}$$

As for the oil heat transfer coefficient, it was selected based on the data presented in [43], which shows a variation for this coefficient between 100 $\mathrm{W}/(\mathrm{m}^2 \cdot \mathrm{K})$ and 500 $\mathrm{W}/(\mathrm{m}^2 \cdot \mathrm{K})$.

The equilibrium (2.34) allows the calculation of wall temperatures, based on heat transfer coefficients, wall thickness and thermal conductivity, as well as ambient and gearbox's interior temperature.

Furthermore, the gearbox was split into three different thermal zones (Figure 2.3). Such division allows to account for the presence of lubricant in the lower zone, an air-oil mixture in the second zone and a third air-only zone. For each one of the zones, equilibrium (2.34) was applied, therefore obtaining wall temperatures and heat flow per unit area.

Obtaining the wall temperatures, allows to account for the radiation effect, through the application of the equation (2.35).

$$\dot{Q}_{rad} = \varepsilon \cdot \sigma \cdot A \cdot T^4_{wall_{Ext}} \tag{2.35}$$

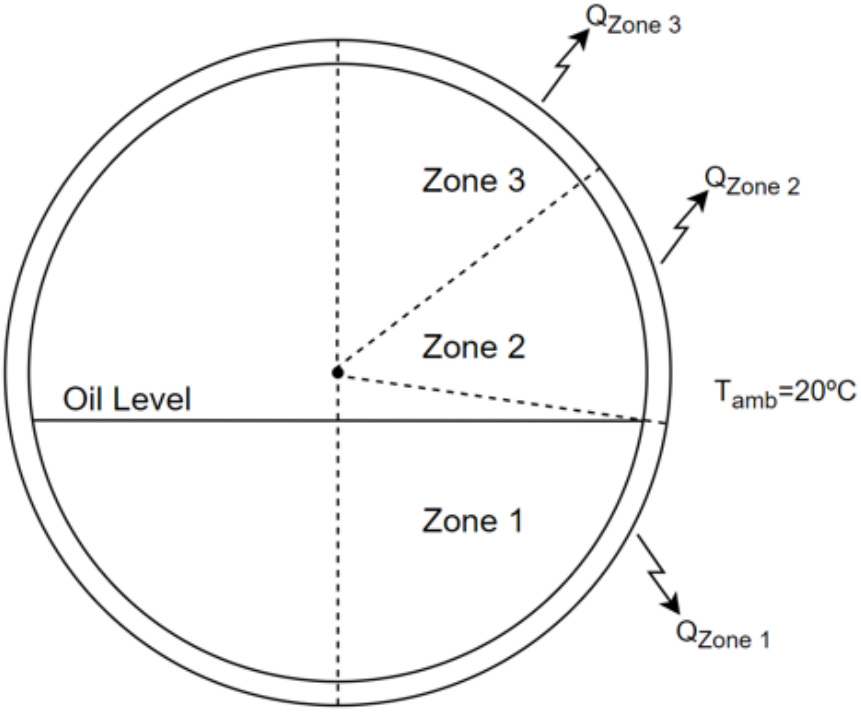


Figure 2.3: Gearbox thermal zones.

Calculating the area of each zone, allows to obtain the heat transferred through the wall, as well as the heat transferred via radiation. The total heat transferred through the housing is the sum of the heat transferred through the wall with the one transferred via radiation.

Heat transfer via shafts and couplings, as well as via foundations will be disregarded. Therefore, the heat transfer calculation might have to be adjusted through a safety factor in order to compensate the absence of this two effects.

In a subsequent stage of the project, when further experimental data is available, the model should be adjusted in order to account for all the effects.

Chapter 3

Flash and Bulk Temperatures

Two rubbing surfaces will generate frictional heat through sliding action in the contact area, meaning this area is made to assume the role of a heat source. Hence, particularly in the contact area, but also in the adjacent parts of the two rubbing bodies in a minor extent, substantial temperature develops for very short periods of time, known as flash temperature.

In the middle 1920's, the flash temperature relevance became more evident as the first attempts were undertaken to put hypoid gears to good use in automobile rear-axles. Soon, similar troubles occurred with spur gears, both in aircraft and automobiles [44]. Nowadays, this situation must be accounted for by mechanical designers in every field and for the majority of machine elements.

There is sliding inherent to the meshing of gear teeth, which results in heat generation. The sliding spot moving along the tooth flank, will result in a substantial increase in temperatures at the sliding contact for very short periods of time, these are called flash temperatures. Their effects will negatively impact gear operation, to the point where, according to Blok's hypothesis, a critical value might be reached, resulting in oil film break down and consequently rapid scuffing of the contact surfaces.

The temperature on the sub-surface of the tooth, constant regardless of being in contact, is known as bulk temperature. Its importance during operation should not be neglected, since it affects the properties of gear materials. In some cases, as the case of polymer gears, it may result in general yielding and failure. [45]

In the following sections, models used in order to predict these temperatures will be presented.

3.1 Gear Bulk Temperature

The methods for gear bulk temperature are described in ISO TR-13989:2000 part one and two [46; 47], as flash temperature method and integral temperature method, respectively. Such models will be approached in detail on subsequent sections.

3.1.1 Flash Temperature Method

The following equations are based on ISO TR-13989-1:2000 [46].

The flash temperature formula adapted for cylindrical gears reads:

$$\theta_{fl} = \mu_{mZ} \cdot X_M \cdot X_J \cdot X_G \cdot (X_\Gamma \cdot w_{Bt})^{3/4} \cdot \frac{v_{tb}^{1/2}}{a^{1/4}} \tag{3.1}$$

Where:

μ_{mZ} is calculated according to equation (2.15).

X_M is the thermo-elastic factor, accounts for the influence of the material properties of the pinion and wheel.

$$X_M = E_r^{1/4} \cdot \frac{(1+\Gamma_y)^{1/2} + (1-\Gamma_y/u)^{1/2}}{B_{M1} \cdot (1+\Gamma_y)^{1/2} + B_{M2} \cdot (1-\Gamma_y/u)^{1/2}} \tag{3.2}$$

with E_r as the reduced modulus of elasticity, in N/mm^2,

$$E_r = \frac{2}{(1-\nu_1^2)/E_1 + (1-\nu_2^2)/E_2} \tag{3.3}$$

Γ_y as the parameter on the line of action. A generic point y on the line of action is indicated by a dimensionless linear parameter Γ_y. This parameter takes the value -1 in the tangent point to the base circle of the driving gear and 0 in the pitch point.

$$\Gamma_y = \frac{\tan\alpha_y}{\tan\alpha'} - 1 \tag{3.4}$$

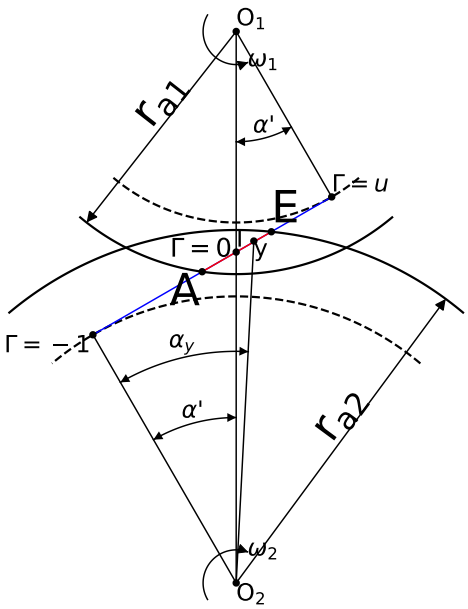


Figure 3.1: Parameter on the line of action.

B_{Mi} as the thermal contact coefficient of the element i.

$$B_{Mi} = (0,001 \cdot \lambda_{Mi} \cdot \rho_{Mi} \cdot c_{Mi})^{1/2} \tag{3.5}$$

X_J is the approach factor. If the pinion drives the wheel:

$$\begin{cases} X_J = 1, & \text{for } \Gamma_y \geq 0 \\ X_J = 1 + \dfrac{C_{eff} - C_{a2}}{50} \cdot \left(\dfrac{-\Gamma_y}{\Gamma_E - \Gamma_A} \right)^3, & \text{provided } X_J \geq 1, \text{for } \Gamma_y < 0 \end{cases} \tag{3.6}$$

If the wheel drives the pinion:

$$\begin{cases} X_J = 1, & \text{for } \Gamma_y \leq 0 \\ X_J = 1 + \dfrac{C_{eff} - C_{a1}}{50} \cdot \left(\dfrac{\Gamma_y}{\Gamma_E - \Gamma_A} \right)^3, & \text{provided } X_J \geq 1, \text{for } \Gamma_y > 0 \end{cases} \tag{3.7}$$

X_G is the geometry factor. For an external gear pair:

$$X_G = 0.51 \cdot X_{\alpha\beta} \cdot (u+1)^{1/2} \cdot \frac{|1 + \Gamma_y - 1 - \Gamma_y/u|}{(1+\Gamma_y)^{1/4} \cdot (u - \Gamma_y)^{1/4}} \tag{3.8}$$

For an internal gear pair

$$X_G = 0.51 \cdot X_{\alpha\beta} \cdot (u-1)^{1/2} \cdot \frac{|1 + \Gamma_y - 1 + \Gamma_y/u|}{(1+\Gamma_y)^{1/4} \cdot (u + \Gamma_y)^{1/4}} \tag{3.9}$$

with

$$X_{\alpha\beta} = 1,22 \cdot \sin^{1/4} \alpha' \cdot \cos^{-1/2} \alpha' \cdot \cos^{1/2} \beta \tag{3.10}$$

X_Γ is the load sharing factor. The load distribution was assumed as shown in Figure 3.2, based on [48].

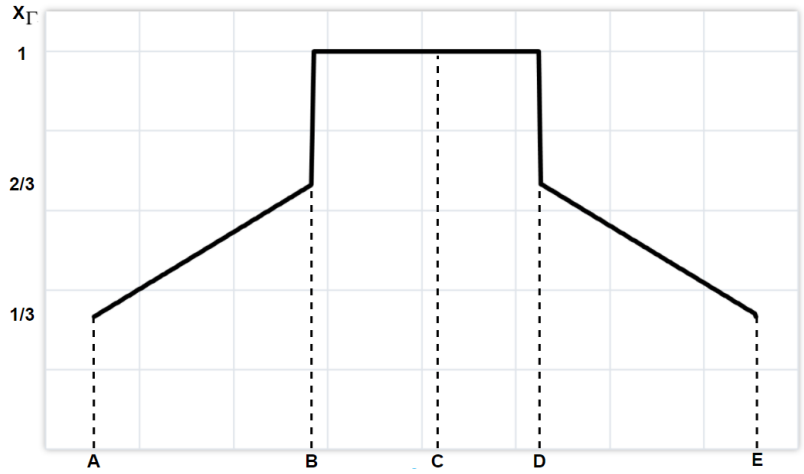


Figure 3.2: Load distribution along the path of contact.

W_{Bt} is the transverse unit load.

$$w_{Bt} = K_A \cdot K_V \cdot K_{B\beta} \cdot K_{B\alpha} \cdot K_{mp} \cdot \frac{F_{bt}}{b} \tag{3.11}$$

According to ISO 6336-1 [48]:

The application factor, K_A, adjusts the nominal load in order to account for additional external forces. This factor mainly depends on the characteristics of the driving and driven machines.

The dynamic factor, K_V, makes allowance for gear tooth accuracy and modifications. A large number of parameters affect this factor, such as design parameters, manufacturing considerations and dynamic response effects.

As for the face load factor, $K_{B\beta}$, takes into account the load distribution over the face width.

The transverse load factor, $K_{B\alpha}$, accounts for the effect of non-uniform transverse load distribution between several pairs of simultaneously contacting gear teeth.

The multiple path factor, K_{mp}, accounts for the maldistribution in multiple path transmissions.

Finally, the bulk temperature can be given as:

$$\theta_M = \theta_{Oil} + 0.47 \cdot X_S \cdot X_{mp} \cdot \theta_{flm} \tag{3.12}$$

where θ_{Oil} is the oil temperature.

$$\begin{cases} X_S = 1,2 & \text{for spray lubrication;} \\ X_S = 1,0 & \text{for dip lubrication;} \\ X_S = 1,0 & \text{for meshes with additional spray for cooling purpose;} \\ X_S = 0,2 & \text{for gears submerged in oil, provided sufficient cooling.} \end{cases} \tag{3.13}$$

$$X_{mp} = \frac{1+n_p}{2} \tag{3.14}$$

and θ_{flm} is the average flash temperature along the path of contact.

$$\theta_{flm} = \frac{\int_A^E \theta_{fl} \cdot d\Gamma_y}{\Gamma_E - \Gamma_A} \tag{3.15}$$

The contact temperature is the sum of bulk and flash temperature.

$$\theta_B = \theta_M + \theta_{fl} \tag{3.16}$$

3.1.2 Integral Temperature Method

The following equations are based on ISO TR-13989-2:2000 [47].

The flash temperature at pinion tooth tip can be calculated as follows:

$$\vartheta_{flaE} = \mu_{mZ} \cdot X_M \cdot X_{BE} \cdot X_{\alpha\beta} \cdot \frac{(K_{B\lambda} \cdot w_{Bt})^{0,75} \cdot v_{tb}^{0,5}}{|a|^{0,25}} \cdot \frac{X_E}{X_Q \cdot X_{Ca}} \tag{3.17}$$

Where μ_{mZ}, X_M, $X_{\alpha\beta}$ and w_{Bt} are calculated as shown in the previous section.

X_{BE} is the geometry factor at tip of pinion. It takes into account Hertzian stress and sliding velocity at tooth tip.

$$X_{BE} = 0,51 \cdot \sqrt{\frac{|z_2|}{z_2} \cdot (u+1)} \cdot \frac{\sqrt{\rho_{E1}} - \sqrt{\frac{\rho_{E2}}{u}}}{(\rho_{E1} \cdot |\rho_{E2}|)^{0,25}} \tag{3.18}$$

with the radius of curvature at tooth tip as:

$$\rho_{E1} = 0,5 \cdot \sqrt{d_{a1}^2 - d_{b1}^2} \tag{3.19}$$

$$\rho_{E2} = a \cdot \sin\alpha' - \rho_{E1} \tag{3.20}$$

$K_{B\lambda}$ is the helical load factor.

$$\begin{cases} K_{B\lambda} = 1 & \text{for } \varepsilon_\lambda \leq 2 \\ K_{B\lambda} = 1 + 0,2 \cdot \sqrt{(\varepsilon_\lambda - 2) \cdot (5 - \varepsilon_\lambda)} & \text{for } 2 < \varepsilon_\lambda < 3,5 \\ K_{B\lambda} = 1,3 & \text{for } \varepsilon_\lambda \geq 3,5 \end{cases} \tag{3.21}$$

Gears should not run under full load conditions before a proper run-in, this is due to the fact that often scuffing occurs in the first few hours of service. In order to account for this effect, X_E, run-in factor, is used.

$$X_E = 1 + (1 - \Phi_E) \cdot \frac{30 \cdot Ra}{\rho_{redC}} \tag{3.22}$$

with

$$\begin{cases} \Phi_E = 1, & \text{full run-in} \\ \Phi_E = 0, & \text{newly manufactured} \end{cases} \tag{3.23}$$

X_Q is the approach factor. It takes into account impact loads in areas of high sliding.

$$\begin{cases} X_Q = 1,00 & \text{for } \dfrac{\varepsilon_f}{\varepsilon_a} \leq 1,5 \\ X_Q = 1,40 - \dfrac{4}{15} \cdot \dfrac{\varepsilon_f}{\varepsilon_a} & \text{for } 1,5 < \dfrac{\varepsilon_f}{\varepsilon_a} < 3 \\ X_Q = 0,60 & \text{for } 3 \leq \dfrac{\varepsilon_f}{\varepsilon_a} \end{cases} \tag{3.24}$$

When the pinion drives the wheel:

$$\begin{cases} \varepsilon_f = \varepsilon_2 \\ \varepsilon_a = \varepsilon_1 \end{cases} \tag{3.25}$$

When the pinion is driven by the wheel:

$$\begin{cases} \varepsilon_f = \varepsilon_1 \\ \varepsilon_a = \varepsilon_2 \end{cases} \tag{3.26}$$

with ε_i as:

$$\varepsilon_i = \frac{z_i}{2\pi} \cdot \left[\sqrt{\left(\frac{d_{ai}}{d_{bi}}\right)^2 - 1} - \tan\alpha' \right] \tag{3.27}$$

High impact loads at tooth tips in areas of high sliding may occur due to elastic deformations of loaded teeth. X_{Ca}, tip relief factor, takes into account the influence of profile modifications on such loads.

$$X_{Ca} = 1 + \left[0,06 + 0,18 \left(\frac{C_a}{C_{eff}} \right) \right] \cdot \varepsilon_{max} + \left[0,02 + 0,69 \left(\frac{C_a}{C_{eff}} \right) \right] \cdot \varepsilon_{max}^2 \tag{3.28}$$

with ε_{max} as the maximum value between ε_1 and ε_2.

When the pinion drives the wheel with $\varepsilon_1 > 1,5 \cdot \varepsilon_2$, or the pinion is driven by the wheel with $\varepsilon_1 > (2/3) \cdot \varepsilon_2$,

$$C_a = C_{a1} \quad \text{for} \quad C_{a1} \leq C_{eff} \tag{3.29}$$

$$C_a = C_{eff} \quad \text{for} \quad C_{a1} > C_{eff} \tag{3.30}$$

when the pinion drives the wheel with $\varepsilon_1 \leq 1,5 \cdot \varepsilon_2$, or the pinion is driven by the wheel with $\varepsilon_1 < (2/3) \cdot \varepsilon_2$,

$$C_a = C_{a2} \quad \text{for} \quad C_{a2} \leq C_{eff} \tag{3.31}$$

$$C_a = C_{eff} \quad \text{for} \quad C_{a2} > C_{eff} \tag{3.32}$$

Where C_{eff} is the effective tip relief. This factor is used to compensate for the elastic deformation of the teeth in single pair contact.

$$C_{eff} = \frac{K_A \cdot F_{bt}}{b \cdot c'} \quad \text{for spur gears} \tag{3.33}$$

$$C_{eff} = \frac{K_A \cdot F_{bt}}{b \cdot c_\gamma} \quad \text{for helical gears} \tag{3.34}$$

In order to obtain the bulk temperature using the integral method, ϑ_{flaint} is needed.

$$\vartheta_{flaint} = \vartheta_{flaE} \cdot X_\varepsilon \tag{3.35}$$

where X_ε, contact ratio factor, is used to convert the flash temperature at the tip of the pinion tooth to a mean value over the path of contact without the need to account for the load sharing.

For $\varepsilon_\alpha < 1, \varepsilon_1 < 1, \varepsilon_2 < 1$:

$$X_\varepsilon = \frac{1}{2 \cdot \varepsilon_\alpha \cdot \varepsilon_1} \cdot \left(\varepsilon_1^2 + \varepsilon_2^2\right) \tag{3.36}$$

For $1 \leq \varepsilon_\alpha < 2, \varepsilon_1 < 1, \varepsilon_2 < 1$:

$$X_\varepsilon = \frac{1}{2 \cdot \varepsilon_\alpha \cdot \varepsilon_1} \cdot \left[0,70 \cdot \left(\varepsilon_1^2 + {\varepsilon_2}^2\right) - 0,22 \cdot \varepsilon_\alpha + 0,52 - 0,60 \cdot \varepsilon_1 \cdot \varepsilon_2\right] \tag{3.37}$$

For $1 \leq \varepsilon_\alpha < 2, \varepsilon_1 \geq 1, \varepsilon_2 < 1$:

$$X_\varepsilon = \frac{1}{2 \cdot \varepsilon_\alpha \cdot \varepsilon_1} \cdot \left(0,18 \cdot \varepsilon_1^2 + 0,70 \cdot \varepsilon_2^2 + 0,82 \cdot \varepsilon_1 - 0,52 \cdot \varepsilon_2 - 0,30 \cdot \varepsilon_1 \cdot \varepsilon_2\right) \tag{3.38}$$

For $1 \leq \varepsilon_\alpha < 2, \varepsilon_1 < 1, \varepsilon_2 \geq 1$:

$$X_\varepsilon = \frac{1}{2 \cdot \varepsilon_\alpha \cdot \varepsilon_1} \cdot \left(0,70 \cdot \varepsilon_1^2 + 0,18 \cdot \varepsilon_2^2 - 0,52 \cdot \varepsilon_1 + 0,82 \cdot \varepsilon_2 - 0,30 \cdot \varepsilon_1 \cdot \varepsilon_2\right) \tag{3.39}$$

For $2 \leq \varepsilon_\alpha < 3, \varepsilon_1 \geq \varepsilon_2$:

$$X_\varepsilon = \frac{1}{2 \cdot \varepsilon_\alpha \cdot \varepsilon_1} \cdot \left(0,44 \cdot \varepsilon_1^2 + 0,59 \cdot \varepsilon_2^2 + 0,30 \cdot \varepsilon_1 - 0,30 \cdot \varepsilon_2 - 0,15 \cdot \varepsilon_1 \cdot \varepsilon_2\right) \tag{3.40}$$

For $2 \leq \varepsilon_a < 3, \varepsilon_1 < \varepsilon_2$:

$$X_\varepsilon = \frac{1}{2 \cdot \varepsilon_\alpha \cdot \varepsilon_1} \cdot \left(0,59 \cdot \varepsilon_1^2 + 0,44 \cdot \varepsilon_2^2 - 0,30 \cdot \varepsilon_1 + 0,30 \cdot \varepsilon_2 - 0,15 \cdot \varepsilon_1 \cdot \varepsilon_2\right) \tag{3.41}$$

Contact ratio, ε_α, is given by the sum of the addendum contact ratios from pinion and wheel.

$$\varepsilon_\alpha = \varepsilon_1 + \varepsilon_2 \tag{3.42}$$

Finally, the bulk temperature can be obtained as follows:

$$\vartheta_M = \vartheta_{oil} + C_1 \cdot X_{mp} \cdot \vartheta_{flaint} \cdot X_S \tag{3.43}$$

Where X_{mp} and X_S factors are calculated according to equations (3.14) and (3.13) respectively. C_1 is the constant accounting for heat transfer conditions obtained from experimental results, $C_1 = 0,7$.

3.2 Bearing Bulk Temperature

Several bearing manufacturers have presented models to calculate the heat transfer in a bearing with the ultimate purpose of understanding what will be the thermally safe operating speed. The

basis of this calculation is the thermal balance in the bearing.

Achieving an equilibrium between the heat generated from the frictional losses, which depend on rotational speed, and the heat dissipated to the bearing surroundings will allow to understand what will be the rotational speed causing the bearing exceed its critical temperature.

The problem with these generic heat transfer models, is that they are not prepared to account for the heat conduction through gearbox housing walls. Instead, it is considered that the bearing is directly contacting with a surface at room temperature, which is not true to the case in study.

In order to solve this problem and predicting bearing temperature, a model based on the pre-existing ones as well as one directional heat conduction was implemented.

SKF's model, shown in [49], admits that it is possible to determine the maximum oil flow, above which no significant temperature reduction is obtained, depending on bearing characteristics, using:

$$\dot{V}_{Lmax} = \frac{D \cdot B}{12500} \tag{3.44}$$

Furthermore, Schaeffler [50] admits the heat dissipated through the lubricant in a bearing can be calculated as follows:

$$\dot{Q}_L = 0,0286 \cdot \dot{V}_L \cdot (T_{bearing} - T_{oil}) \tag{3.45}$$

Assuming the bearing is in thermal equilibrium with its housing, the heat dissipation via the bearing seating surfaces through the housing is:

$$\dot{Q}_s = \lambda \cdot A_r \cdot \frac{T_{bearing} - T_{housing}}{e} \tag{3.46}$$

With A_r, bearing seating surface, calculated according to Schaeffler's model [50] as:

$$\begin{cases} A_r = \dfrac{\pi}{2} \cdot (D^2 - d^2) & \text{for axial bearings} \\ A_r = \pi \cdot B \cdot (D + d) & \text{for radial bearings} \end{cases} \tag{3.47}$$

Obtaining the bearing power loss, P_{VL}, as shown in section 2.2 and the housing temperatures from equation (2.34), will allow to determine bearing temperature by solving:

$$\begin{cases} P_{VL} = \dot{Q}_L + \dot{Q}_s \\ \dot{Q}_s = \lambda \cdot A_r \cdot \dfrac{T_{bearing} - T_{housing}}{e} \\ \dot{Q}_L = 0,0286 \cdot \dot{V}_L \cdot (T_{bearing} - T_{oil}) \end{cases} \tag{3.48}$$

Varying the oil flow, $\dot{V}_L$, allows the determination of bearing minimum temperature, for the maximum flow from equation (3.44), as well as its maximum theoretical temperature considering no oil flow would cool the bearing, for each operating condition.

Chapter 4

Gearbox - Reverse Engineering

Scarcity of information on the gearbox was one of the main hindrances to the development of this project. One can summarize the available information as an exploded view in the form of animation, parts list and an assembly drawing.

Solving such problem required using a reverse engineering process to obtain every dimension needed on subsequent steps of the work. This process is of extreme relevance, since it will directly influence every output later on; any mistake obtaining these dimensions may result in poor, inconsistent outcome.

From an initial look at the assembly drawing and exploded view animation it is possible to gather some general information about the gearbox, namely the fact that it has four stages, the first three being planetary with three planets each and the last one a cylindrical gear pair.

Concerning the first stage, it can be understood that the power input is done in the planet carrier, while the output is done by the sun gear, as shown in Figure 4.1. In this stage the ring gear is stationary.

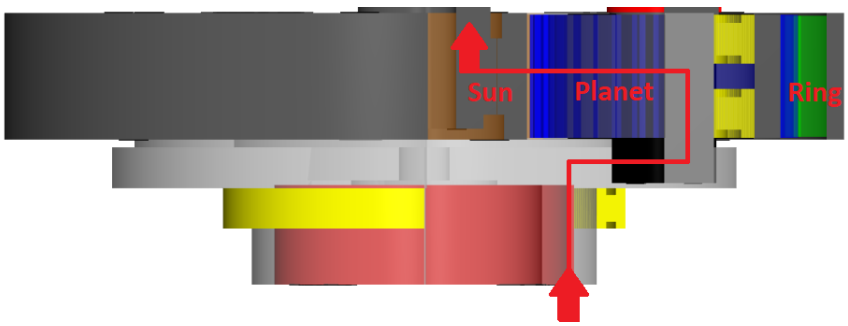


Figure 4.1: Power flow on the first stage of the gearbox.

In the second stage, the power input is done in the ring gear and the output done by the sun gear, as it can be seen on Figure 4.2. Here, the planet carrier is stationary.

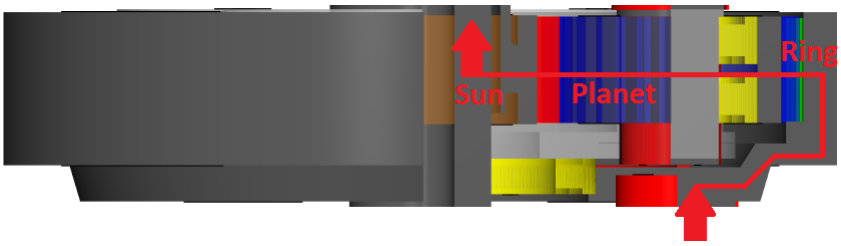


Figure 4.2: Power flow on the second stage of the gearbox.

As for the third stage, it has no stationary elements. The power input is done both on planet carrier and ring gear. Similarly to previous stages, the output is done by the sun gear, as shown in Figure 4.3.

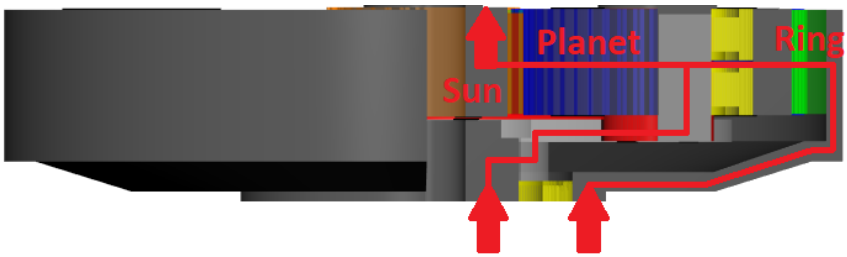


Figure 4.3: Power flow on the third stage of the gearbox.

Analysing the fourth stage of this gearbox it can be seen that, geared with the wheel there is also a second pinion with the meaning to power an oil pump. Furthermore, it is possible to understand from the exploded view animation, that the gears in this stage are helical. The power input is done on the wheel, while the output is done two the both pinions previously mentioned, as it can be seen on Figure 4.4.

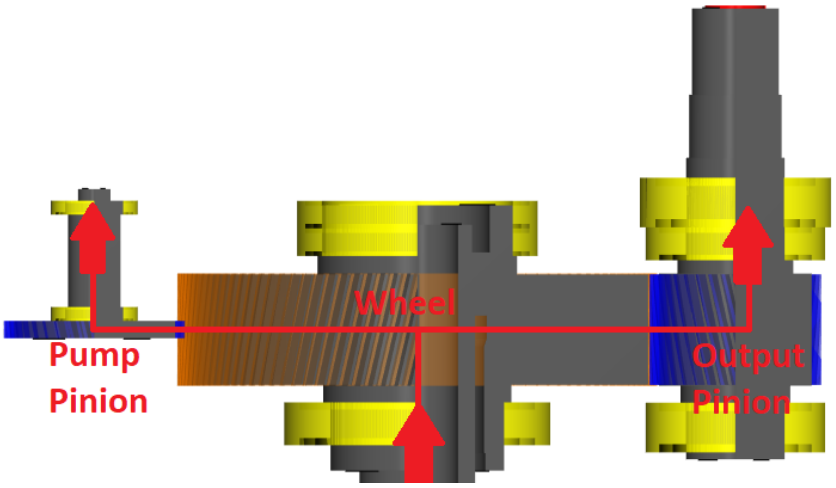


Figure 4.4: Power flow on the fourth stage of the gearbox.

This chapter will be a detailed explanation on how the dimensions from the elements in this gearbox were obtained, as well as the purpose of each step along the way. Additionally, kinematic relationships concerning the gearbox stages will be approached in detail.

4.1 Drawing Scaling

In order to take measurements, it was necessary to use an image manipulation software that had an available measurement tool, since measuring the physical version would result in lower precision measurements.

To make sure the drawing was correctly scaled, a control measurement had to be taken. Making this verification required measuring a standardized element on every stage of the gearbox, *e.g.* bearings, and comparing it to the known dimension. This process allowed to understand if the values obtained through the image manipulation software were correct or if they would need to be applied a correction factor.

For the first three stages the standard elements used were bearings, NJ2244EM for the first, NJ2240EM and NJ2236EMC3 for the second and third stages respectively. As for fourth stage, the centre distance was given in the assembly drawing and it was used as a reference to create the scaling factor. Table 4.1 shows the scaling factors obtained for all stages.

Table 4.1: Drawing scaling factors.

	1st Stage		**2nd Stage**		**3rd Stage**		**4th Stage**	
	Reference	**Measured**	**Reference**	**Measured**	**Reference**	**Measured**	**Reference**	**Measured**
d / mm	220	215,52	200	196,45	180	176,95	550,00	543,63
D / mm	400	393,51	360	355,03	320	315,95		
Scaling Factor	1,018		1,016		1,015		1,012	

It was assumed the drawing scaling was not manipulated in any way. Consequently, for subsequent measurements taken from the assembly drawing, each scaling factor present in Table 4.1 was applied to the correspondent stage, in order to have those measurements closer to real values.

4.2 Shaft Sizing

Pertinent shaft information for power loss calculation could be measured in the assembly drawing without the need for further calculation. Therefore, the dimensions used to create KISSsys model are the result of measurements taken from the assembly drawing to which the scaling factors shown in section 4.1 were applied.

4.3 Bearings

Relevant dimensions for power loss calculation regarding bearings, stems from a thorough analysis of the parts list and assembly drawing.

Bearings shown in this section were obtained from KISSsoft catalogue to build the gearbox model. All of them are exactly the same as the ones present in the gearbox parts list, with the exception of Timken H936349-H936310, in the fourth stage.

The correspondent bearing in the gearbox was specifically manufactured for the application, meaning there is no way to represent it exactly as it is on KISSsoft, the chosen bearing for this effect has very similar dimensions and it is not expected that it will affect the power loss prediction in a meaningful way.

Tables 4.2 to 4.5, present information concerning the bearings in this gearbox, each table is dedicated to one of the gearbox's stages.

Table 4.2: Relevant bearings for power loss calculation on stage 1.

Designation	Quantity	Observations
SKF NJ2244ECML	6	Planet pin bearings (2 on each planet)
SKF L183449/410	1	Bearing supporting carrier shaft
Timken EE647220-647285	1	Bearing between planet pin and stage 2 carrier shaft

Table 4.3: Relevant bearings for power loss calculation on stage 2.

Designation	Quantity	Observations
SKF NJ2240 ECML	6	Planet pin bearings (2 on each planet)

Table 4.4: Relevant bearings for power loss calculation on stage 3.

Designation	Quantity	Observations
SKF NJ2236 ECML	6	Planet pin bearings (2 on each planet)
Timken LL778149-LL778110	1	Bearing supporting ring shaft
SKF NU 1880 MP	1	Bearing between ring shaft and carrier shaft

Table 4.5: Relevant bearings for power loss calculation on stage 4.

Designation	Quantity	Observations
SKF NU 1060 MA	1	Bearing supporting wheel shaft
Timken L860048-L860010	2	Bearing supporting wheel shaft
SKF NU2234 ECML	1	Bearing supporting pinion shaft
SKF 30234	1	Bearing supporting pinion shaft
Timken H936349-H936310	1	Bearing supporting pinion shaft

4.4 Seals

As for the seals, KISSsoft has no catalogue for these elements. Therefore, the relevant seals for the power loss calculation in this gearbox, will be presented in this section exactly as they are defined in the assembly drawing and respective parts list. The way in which their power loss was represented in the model will be approached in detail on section 5.3.1.

Tables 4.6 and 4.7 show the seals accounted for in the power loss calculation, each table concerning a gearbox stage. Equally important to note is the fact that only the first and last stages hold relevant seals in the power loss calculation.

Table 4.6: Relevant seals for power loss calculation on stage 1.

Designation	Quantity	Observations
O-Ring 110x5	1	Carrier Shaft Seal
O-Ring 100x5	2	Carrier Shaft Seal
V-Ring V 750L	1	Carrier Shaft Seal

Table 4.7: Relevant seals for power loss calculation on stage 4.

Designation	Quantity	Observations
Labyrinth Seal 500D	1	Output Shaft Seal
Labyrinth Seal 510D	1	Output Shaft Seal
O-Ring 69,44x3,53	1	Output Shaft Seal

4.5 Gear Sizing

In order to properly define all gears in this gearbox an iterative process, relying on software such as Microsoft Office Excel and KISSsoft, was used.

From the exploded view animation, it was possible to understand - gears in the first three stages are spur gears, while the ones in the last stage are helical. Also, the number of teeth was know since it was indicated in the assembly drawing.

No more information about the gearbox was available at the moment.

4.5.1 Normal Module and Helix Angle

Finding each stage module was the first step on sizing gears. Since the number of teeth was already given in the assembly drawing, only the pitch diameter was needed to get the module.

Pitch circle was then measured and the correspondent correction factor was applied, as previously explained. Obtaining an approximated module, using equation (4.1), was the next step. Followed by an approximation to the closer standard module value, according to DIN 780-1 [51]. Table 4.8 presents the gear modules obtained using this process.

$$m = \frac{d_i}{z_i} \tag{4.1}$$

Table 4.8: Gear modules.

	1st Stage	**2nd Stage**	**3rd Stage**	**4th Stage**
z_i	30	32	33	113
d_i / mm	483,956	515,130	310,598	811,195
$m_{calculated}$ / mm	16,132	16,098	9,412	7,179
$m_{standard}$ / mm	16	16	9	7

At this point the information available was enough to start an iterative process for the planetary stages. However, the helix angle was required to start iterating for the last stage.

$$m_t = \frac{m}{\cos\beta} \tag{4.2}$$

When analysing an helical gear, the value given by equation (4.1) is considered to be the transverse module. Comparing this value with one obtained from equation (4.2) allowed to get an approximated value for the helix angle.

Wheel and pinion were measured, resulting in two different values for transverse module from equation (4.1), which led to two different helix angle values from equation (4.2). The results were compared and the closer standard value to both was assumed as a starting point for subsequent iterations. Table 4.9 presents the helix angle values obtained through this process.

Table 4.9: Helix angle.

	Pinion	**Wheel**
m_t / mm	7,207	7,179
m / mm	7	
β / °	13,76	12,88
$\beta_{standard}$ / °	13	

4.5.2 Iterative Process

Many gear geometric characteristics were still unknown at this point and yet, only a few could be measured at the assembly drawing. Creating an iterative process that could methodically lead to adequate values was a laborious, time-consuming process. Finally, an iterative method relying on KISSsoft was used to obtain more precise information about the gears.

The measurements that could be taken from the assembly drawing are addendum, root and reference pitch diameters, as well as gear width and working centre distance. These measurements were performed for all the gears and stages in this gearbox.

Width and centre distance were measured and used as an input on KISSsoft calculations. Additionally, number of teeth - given in the drawing, module and helix angle - calculated as shown in section 4.5.1, as well as number of planets for the planetary stages were also used as input data. The values used as input data on KISSsoft in order to start the iterative process are presented on Table 4.10.

Table 4.10: Input data on KISSsoft calculations for iterative process.

	1st Stage	**2nd Stage**	**3rd Stage**	**4th Stage**
a' / mm	530	516	393	550
β / °	-	-	-	13
$nplanets$	3	3	3	-
z_{sun}/z_1	30	32	33	39
z_{plan}/z_2	34	31	52	113
z_{ring}/z_{pump}	99	94	198	41
b_{sun}/b_1 / mm	280	224	183	194,5
b_{plan}/b_2 / mm	272	219	178	191
b_{ring}/b_{pump} / mm	267,5	213	174	30

On the contrary, factors such as reference profile, reference pressure angle, addendum correction factor and profile shift coefficient were used as iteration factors. These factors were changing between iterations seeking to get closer results to the drawings.

Moreover, there were control factors which allowed to control the output from KISSsoft and to know how close to the drawings the results were. Addendum diameter and root diameter were used as such factors, since they could be measured on the assembly drawing and they were also an output of KISSsoft calculations.

An Excel file was created, where KISSsoft output values could be written and compared to the measurements taken from the assembly drawing. Analysing differences in control factors allowed to understand which iterative factor should be given more attention and to decide when to stop the iterative process.

On the first iteration of each stage, addendum correction factor was calculated to achieve minimum bottom clearance. As for the profile shift coefficient, it was calculated for minimum specific sliding.

As for the reference pressure angle, a value of 20° was selected and the reference profile was defined as ISO 53:1998 profile A. The decision on imposing these values as a starting point was due to the fact they are commonly used on standard gearing.

Concerning the iterative process per se, the criteria to vary iteration factors were defined based in the conclusions drawn from the differences between measured diameters and KISSsoft diameters, as shown in Figure 4.5.

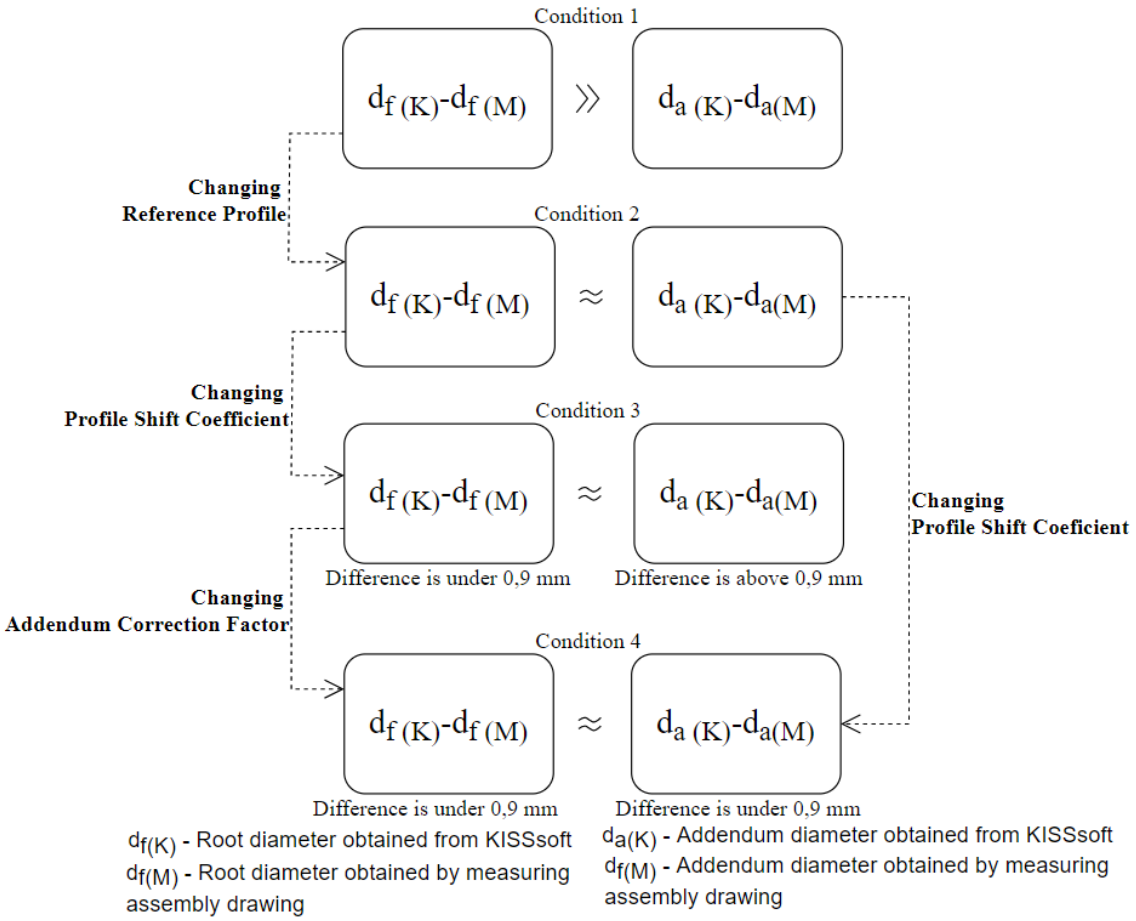


Figure 4.5: Iterative process used in gear sizing.

From one condition to the other, an input of KISSsoft values in the Excel spreadsheet was needed in order to draw conclusions about the next step to take.

This process was applied one stage at a time, which in some cases meant applying it to three different gears at the same time. The main challenge was making iterations with a fixed working centre distance which meant dependency between the profile shift of each gear in the same stage, making it harder to find a balanced solution to get out of condition 2. By balanced solution, one can assume profile shifts that will not weaken any of the gears, nor will they require an exaggerated addendum correction factor to get to condition 4.

Any changes applied to the reference pressure angle were producing worse final results, this factor was considered correct as assumed in the first iteration. The threshold of 0,9 mm to stop the process, was motivated by the poor scaling and large line thickness of assembly drawing from where the measured values were taken. In addition, this diameter difference represents a deviation under 0,25% from the measured values.

No information was available on gear tooth profile modification, which lead to the assumption none was made.

Tables 4.11 to 4.14 show the final results obtained from the iteration process, each table corresponding to one of the four stages. Even though some addendum correction factors may seem too high, without additional information on the gears, it was not possible to get a more realistic approximation. Furthermore, it was possible to obtain different values for the radius measured, depending on which side of the drawing the measure was taken. Therefore, showing the poor quality of the drawing available to obtain and validate the gear information.

Equally important to note, is the fact that a negative profile shift coefficient on the ring, produces a thicker tooth.

Table 4.11: Final iteration for stage 1 gears.

	Sun	**Planets**	**Ring**
a' / mm		530	
m / mm		16	
α / °		20	
α' / °		24,8	22,785
z_i	30	34	99
b / mm	280	272	267,5
Reference Profile	D (1,40/0,39/1,0)	D (1,40/0,39/1,0)	A(1,25/0,38/1,0)
x	0,6183	0,6406	-1,308
$k \cdot m$ / mm	-0,181	-0,801	-1,465
d_a / mm	531,424	594,896	1596,666
d_f / mm	454,629	519,340	1666,520

Table 4.12: Final iteration for stage 2 gears.

	Sun	**Planets**	**Ring**
a' / mm		516	
m / mm		16	
α / °		20	
α' / °		23,39	23,39
z_i	32	31	94
b / mm	224	219	213
Reference Profile	D (1,40/0,39/1,0)	D (1,40/0,39/1,0)	A(1,25/0,38/1,0)
x	0,5397	0,2727	-1,0852
$k \cdot m$ / mm	-0,999	-0,999	-2,1858
d_a / mm	559,272	534,729	1510,972
d_f / mm	484,112	459,5715	1579,3858

Table 4.13: Final iteration for stage 3 gears.

	Sun	**Planets**	**Ring**
a' / mm		393	
m / mm		9	
α / °		20	
α' / °		23,853	22,279
z_i	33	52	138
b / mm	183	178	174
Reference Profile	D (1,40/0,39/1,0)	D (1,40/0,39/1,0)	A(1,25/0,38/1,0)
x	0,5845	0,6929	-1,3967
$k \cdot m$ / mm	-0,006	-2,544	-2,11
d_a / mm	325,509	493,385	1253,235
d_f / mm	281,9641	454,9155	1290,299

Table 4.14: Final iteration for stage 4 gears.

	Pinion	**Wheel**	**Pump Gear**
a' / mm	550		558,5
m / mm	7		
α / °	20		
α' / °	21,572		21,898
β / °	13		
z_i	39	113	41
b / mm	191	194,5	30
Reference Profile	D (1,40/0,39/1,0)	D (1,40/0,39/1,0)	D (1,40/0,39/1,0)
x	0,1718	0,4083	0,3774
$k \cdot m$ / mm	-0,103	-0,7064	-0,178
d_a / mm	296,477	830,11	313,477
d_f / mm	262,56	797,22	279,711

4.6 Gearbox Kinematics

In the beginning of the current chapter, the mechanisms in this gearbox were briefly explained. Figure 4.6, provides the information needed to fully understand how the gearbox works and how the four stages connect to each other.

The arrows on Figure 4.6, represent the power flow in the gearbox. Thus, it is possible to understand that the power input is done on the planet carrier of the first stage, while the output is done by both pinions of the last stage, as previously mentioned.

Additionally, the dotted boxes highlight the connections between stages. From box number 1, it can be understood that the planet carrier of the first stage connects to the ring gear of the second stage. Box number 2 highlights the connections of stage 1 and 2 to stage 3, it can be seen that the power output from stage 1 and 2 are input, respectively, to the planet carrier and ring gear of the third stage. Finally, box number 3 shows the power flowing to both pinions of the fourth stage.

Equally important are the "Static" highlights written in Figure 4.6. These highlights show the supports that prevent stage 1 ring gear and stage 2 planet carrier from having rotational movement.

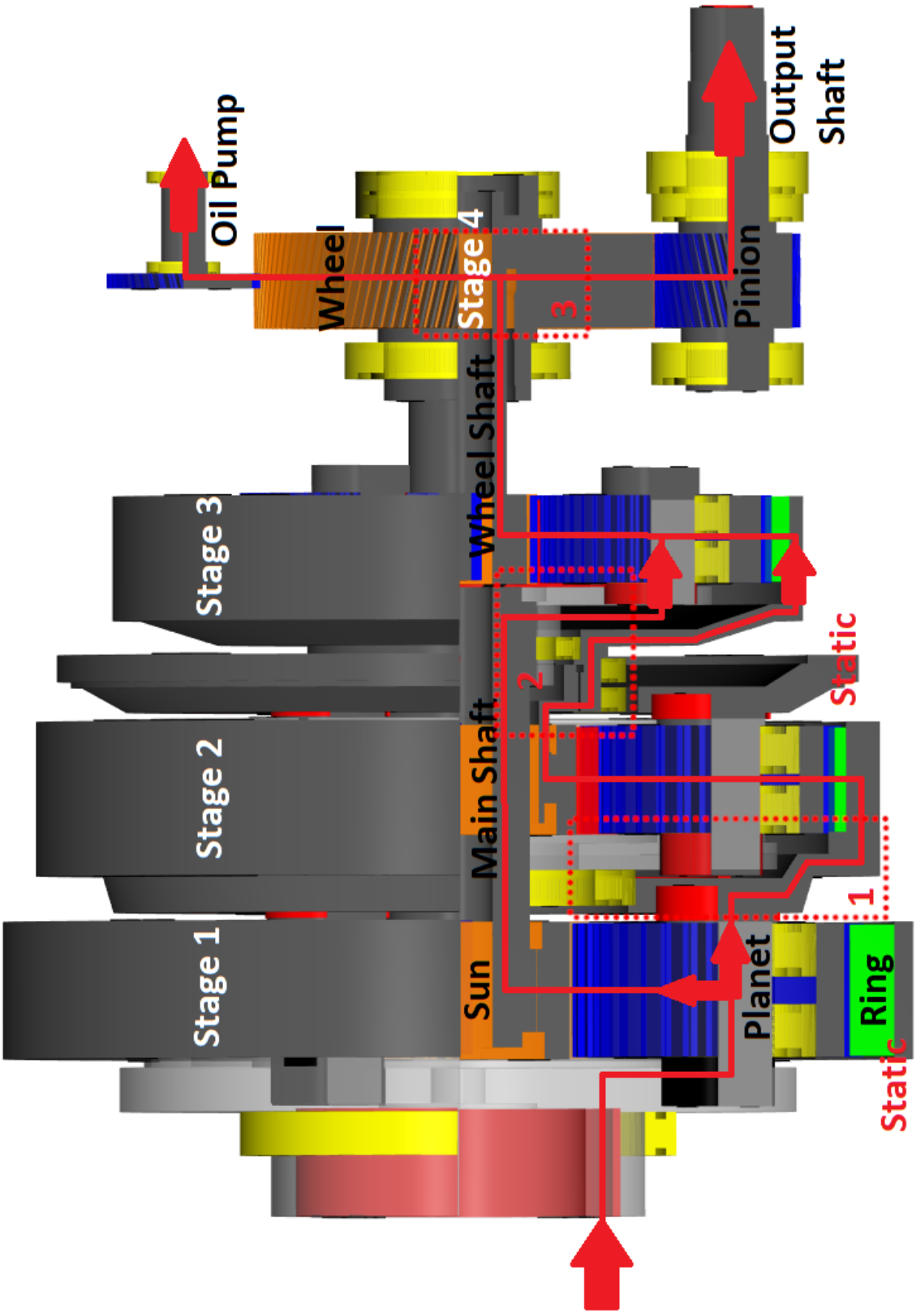


Figure 4.6: Gearbox kinematics.

4.6.1 Planetary Stages Kinematics

Planetary gears may work according to several different configurations, depending on where the input is done and if any of the elements is stationary. As previously mentioned, this gearbox has three different planetary stages, all of which working under different configurations.

For a better understanding on how the stages work, in this section the kinematics calculation will be approached for all planetary stages.

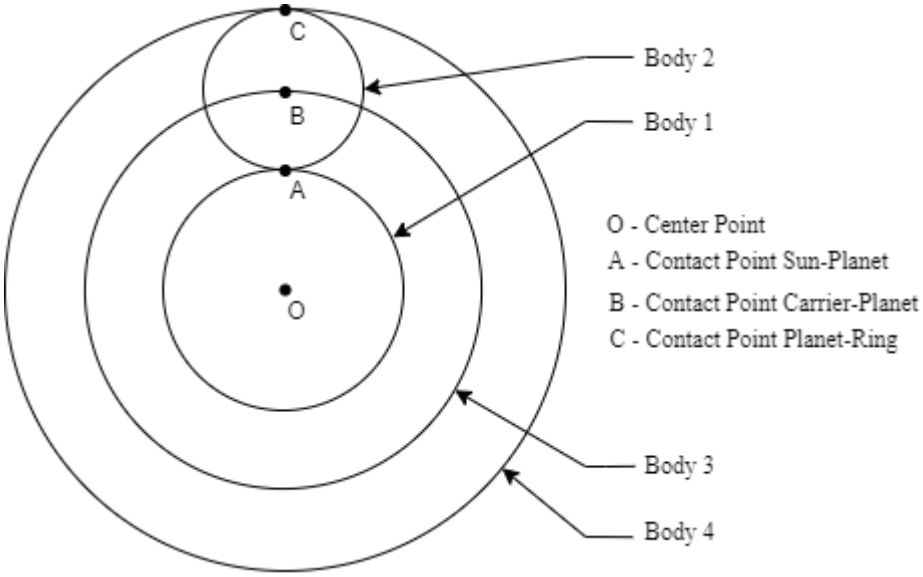


Figure 4.7: Kinematics of a planetary stage.

Since the speed input on stage 1 is done on the carrier shaft, one can assume $n_{carrier}$ is known. Resulting:

$$\omega_{30} = \frac{n_{carrier} \times \pi}{30} \tag{4.3}$$

The linear velocity in point B is the same relative to body 2 and 3, so it can be written:

$$\overrightarrow{\omega_{20}} \times \overrightarrow{BC} = \overrightarrow{\omega_{30}} \times \overrightarrow{OB} \tag{4.4}$$

Knowing, $\overrightarrow{v_{A10}} = \overrightarrow{v_{A20}}$, comes:

$$\overrightarrow{\omega_{10}} \times \overrightarrow{OA} = \overrightarrow{\omega_{30}} \times \overrightarrow{OB} + \overrightarrow{\omega_{20}} \times \overrightarrow{BA} \tag{4.5}$$

In order to obtain the relative speed of the sun gear (frame of reference attached to the carrier shaft), the speed of the carrier shaft (ω_{30}) must be subtracted to the speed of the sun gear (ω_{10}), as explained by Marques in [52]:

$$\omega_{sun} = \omega_{10} - \omega_{30} \tag{4.6}$$

The speed of the planet gear can be obtained directly from the relation between the number of teeth of both gears:

$$n_{plan} = n_{sun} \times \frac{z_{sun}}{z_{plan}} \tag{4.7}$$

As for stage 2, the input is done at the ring shaft, meaning n_{ring} is known. Similarly to what happens on stage 1, the rotational speed of both planet and sun gears can be obtained from equation 4.7.

Analysing stage 3, one can understand ω_{30} and ω_{40} are already known since the input is done to both carrier and ring shafts. However, the fact that both these shafts have movement, means that n_{ring} can not be obtained by applying equation 4.3 to ω_{40}. Instead, the relative speed between body 3 and 4 must be accounted for.

In order to find the relevant rotational speeds in this stage, ω_{20} had to be calculated. In this stage:

$$\overrightarrow{\omega_{20}} \times \overrightarrow{BC} = \overrightarrow{\omega_{40}} \times \overrightarrow{CO} + \overrightarrow{\omega_{30}} \times \overrightarrow{OB} \tag{4.8}$$

Equation 4.5 can now be applied, followed by equation 4.6 and 4.7, therefore obtaining all the relevant rotational speeds in this stage.

Chapter 5

Gearbox Modelling

In previous chapters, the models used in order to fulfil this task were presented. The equations are known by now, as well as the process of gathering crucial information.

This chapter is focused on the implementation of such models, aiming to explain every step of the way; from creating KISSsoft calculations, going through assembling the gearbox, up to power loss calculations in every element, as well as heat transfer.

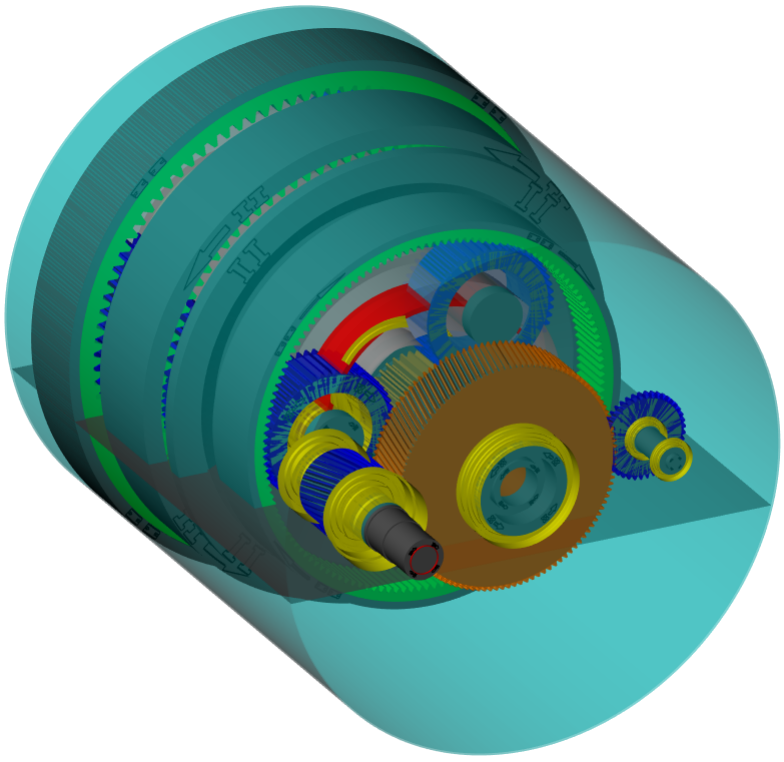


Figure 5.1: KISSsys gearbox model.

In some cases, models were implemented on other software rather than KISSsys, these models will also be presented in this chapter, as well as the reasons behind their creation and validation.

5.1 KISSsoft Model

The creation of these models, was almost complete at the time the iterative process (section 4.5.2) was finished. Containing valuable information relative to gears on each stage, it can be said such models lay the foundation of the whole gearbox model.

5.1.1 Planetary Stages

Inputting the gear data shown in the previous chapter, as it can be seen on Figure 5.2, allows to run the calculation and ask for a report containing additional information on the gear stage, from root and addendum diameters, up to length of path of contact and even gear loss factors, if the Rating tab is active on the calculations menu.

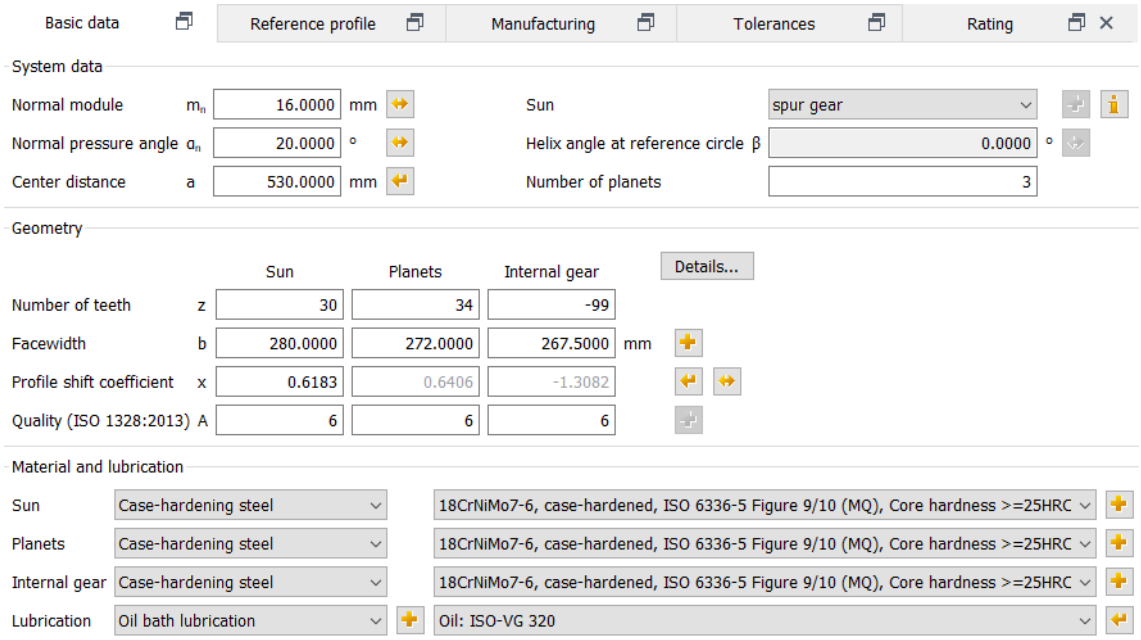


Figure 5.2: Planetary calculation - KISSsoft.

Furthermore, KISSsoft calculations allow input of several other factors which will later on be relevant to power loss calculations, such as lubricant factor, X_L, and application factor, K_A.

Lubricant information is defined on Basic data tab, Figure 5.2. Nonetheless, lubricant factor, X_L, should be defined on the Rating tab by pressing the "Details" button, as shown in Figure 5.3, in order for this option to become available. The definition of the application factor, K_A, is directly done on the Rating tab.

Without further information on working characteristics of the mechanism, application factor was defined as 1 for every stage, according to ISO 6336 [48]. As for the lubricant factor, was defined according to Fernandes's study [29], depending on the lubricant as previously shown in Table 2.1.

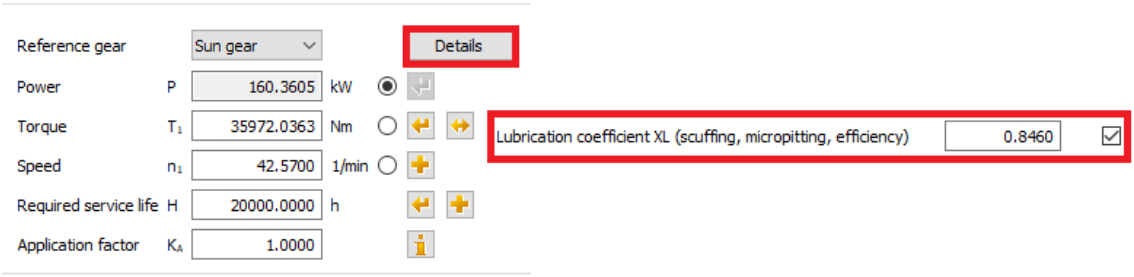


Figure 5.3: KISSsoft rating tab and definition of X_L and K_A parameters.

5.1.2 Helical Gear Pair

The calculation for an helical gear pair, is similar in every way to a planetary calculation. The main exceptions are the fact that the input information can only be done for two gears only, pinion and wheel, and also the definition of an helix angle, as shown in Figure 5.4.

As for factors in the rating tab, were defined according to the exact same standards as in the planetary case.

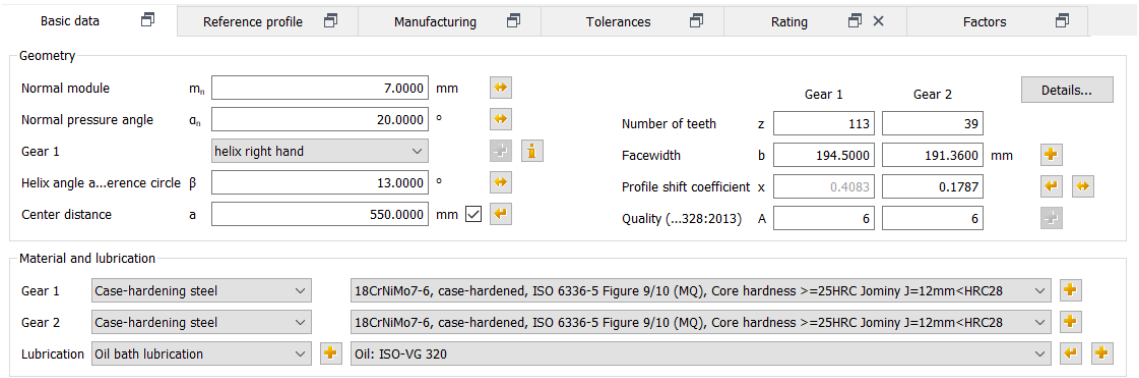


Figure 5.4: Helical gear pair calculation - KISSsoft.

5.2 KISSsys Model

KISSsoft calculations contain information relative to each stage on an isolated way. In order to assemble all the stages and establish the kinematic relationships needed, KISSsys was used.

KISSsys has numerous integrated templates of pre-made gearboxes, including multi-stage ones. Nonetheless, a gearbox like the one in study, with complex kinematic relationships between stages and several vital details, had to be created from scratch.

In order to start the modelling process, two groups were added to KISSsys element tree. The first group was named "Gearbox", the second is a sub-group of the gearbox called "Mainline". These sub-groups are needed to keep the coaxial shafts separated from each other. A coaxial shaft calculation includes all the shafts present in the same group.

5.2.1 Assembling a Planetary Stage

All the planetary stages were added to the mainline group. Assembling each one of the planetary stages was done by following "KISSsys - Tutorial 2; Assembling a One Stage Planetary Gearbox" [53] guidelines. With variations when creating couplings and supports, which vary depending on the gearbox geometry.

After adding all the elements needed from KISSsys "elements box", the stages tree structure should look as the one presented in Figure 5.5.

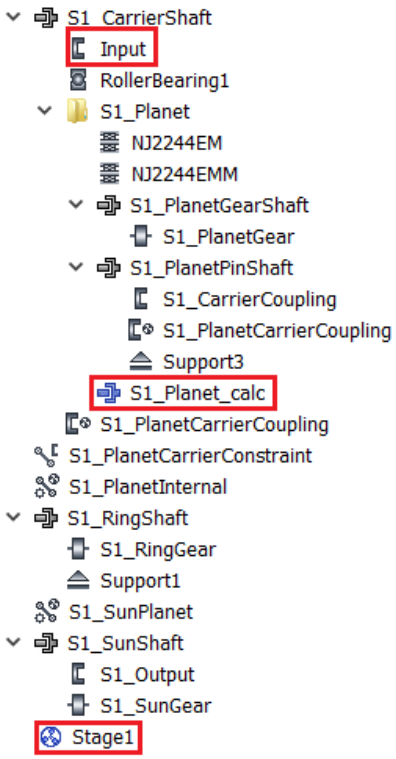


Figure 5.5: Stage 1 KISSsys tree structure.

The main differences between the planetary stages can be found in the input coupling, which defines where the power input is done for that stage. For stage 1, it is done via carrier shaft, as it can be understood from the highlighted coupling in Figure 5.5; this coupling on stage 1 is the global power input for the gearbox. Stage 2 and 3 input couplings, will be explained in section 5.2.3.

From Figure 5.5, another highlight named "Stage1" can be seen. This element is a KISSsoft calculation, it is where the previously obtained data on stage 1 gears (section 5.1.1) is loaded, therefore making the bridge between KISSsoft gear calculations and KISSsys modeling.

Equally important, is the element named "S1_Planet_calc". This type of element is a coaxial shaft calculation, and makes it possible to define the planet pin dimensions, as well as which bearings support the planet. It will be very similar for the three planetary stages, varying the size and bearings references according to the assembly drawing and parts list respectively.

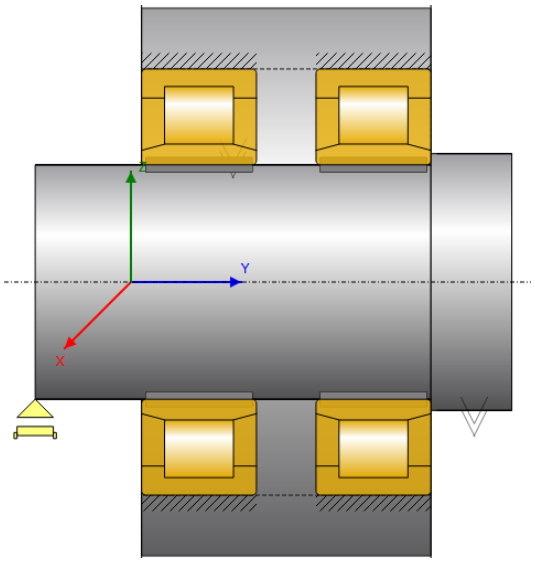


Figure 5.6: Stage 1 planet pin KISSsoft calculation.

After following these steps, KISSsys is able to generate the 3D model for the planetary gear, as shown in Figure 5.7.

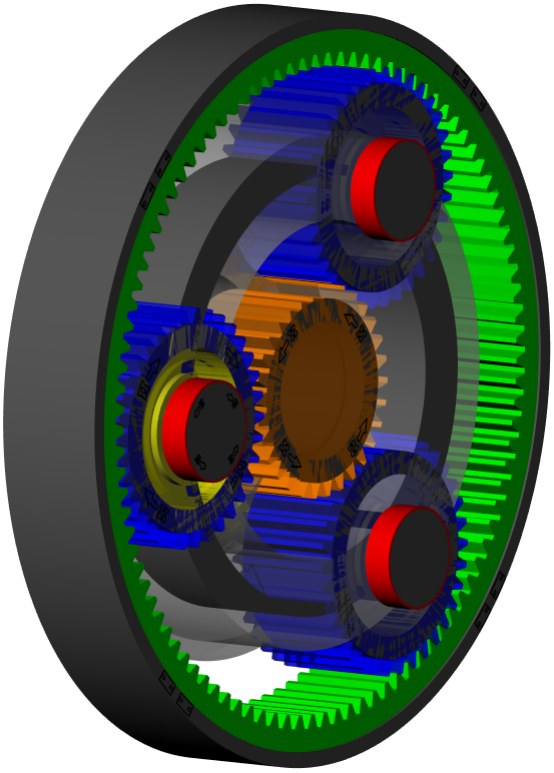


Figure 5.7: Planetary gear 3D representation on KISSsys.

5.2.2 Assembling Last Stage

Assembling the last stage required adding a wheel shaft to the main line. This shaft contains the wheel and respective bearings according to the assembly drawing.

As for the output shaft and pump group, they had to be created inside the gearbox group, but outside main line since there is no coaxiality between these shafts and the ones on mainline.

The pump group contains two shafts, as it can be seen on Figure 5.8. One contains the gear pump, while the second is responsible for establishing the connection between gear and the actual pump, as represented in the assembly drawing.

Additionally, from Figure 5.8 it is possible to see two highlighted gear pairs, as well as the respective KISSsoft calculations.

The pair named "Z10Z11", concerns stage four, wheel and pinion, that will connect to the output shaft and subsequently to the wind turbine generator. As for the pair named "Z10Z12", it shares the same wheel as the previous pair, but the pinion connects to the pump shaft, therefore taking the power to the mechanical oil pump used in this gearbox.

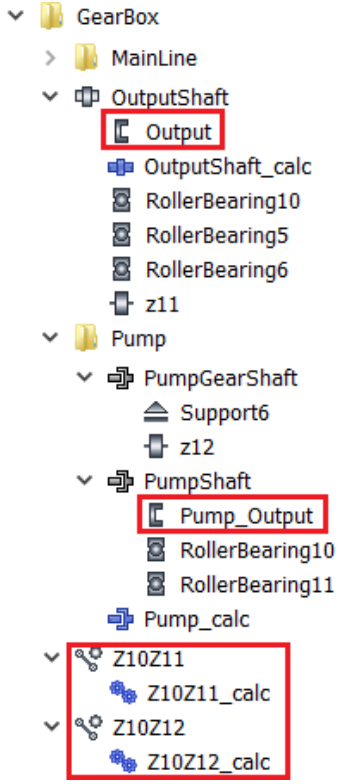


Figure 5.8: Output and pump shafts KISSsys tree structure.

Also, there are two couplings highlighted, "Output" coupling is where the global output of the gearbox will be done, in a practical way it represents the connection to the power generator. As for the "Pump_Output", it emulates the connection to the mechanical pump, in order to account for its power consumption.

5.2.3 Establishing Boundary Conditions

Correctly defining the kinematic relationships of this gearbox was a complex and challenging step. It was done by establishing boundary conditions according to what was represented in the assembly drawing. These conditions can be added to the model under many ways. In order to define kinematics, three main types were used: connection element, connecting rolling bearing and speed or force.

Connection elements are defined between two shafts (inside and outside shaft), allowing to define if their rotational movement is connected. The software allows to define it for every direction independently.

Connecting bearings are placed between two shafts, as in the planet pin and planet shaft previously shown (Figure 5.6). This type of connection provides support but makes the rotational movement independent. Another type of rolling bearings can be placed from the elements box. These bearings will only be placed on one shaft and the outer ring is assumed to be on the housing.

Speed or force conditions need to be associated with a coupling, as the ones highlighted in figures 5.5 and 5.8. Their purpose is to define if the respective coupling will be working as input or output, additionally it allows to define the type (speed or force) and if the input has a constrained value or if it is to be calculated according to the gearbox ratio.

5.2.3.1 Stage 1

Establishing stage 1 kinematics required defining ring and planet gears as driven by their shaft (input) and the sun as driving its shaft (output).

Similarly to what can be seen in the assembly drawing, a fixed support in every direction was added to the ring shaft preventing it from moving, this stage has a stationary ring.

Next, a shaft was created with the purpose of connecting stage 1 carrier to the stage 2 ring shaft. In order to establish these connections, two connection elements were added. As a result stage 2 ring shaft rotates with stage 1 carrier shaft.

A second shaft was created, this time connecting the stage 1 sun to stage 3 carrier. Again, two connection elements were added resulting in stage 3 carrier rotating with stage 1 sun gear.

A schematic representation of the established relations is produced by KISSsys, as shown on Figure 5.9. In this scheme, the power flow is represented by the arrows. Also, two connecting bearings can be seen between the planet pin shaft and the planet gear shaft. Equally important are the connection elements represented by the "hourglass" shaped symbols that can be seen in Figure 5.9, these elements will connect this stage to stages 2 and 3 as previously mentioned.

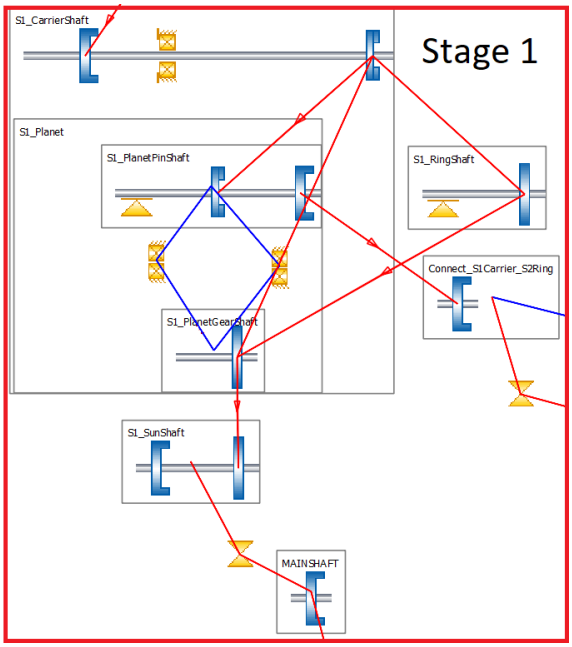


Figure 5.9: Schematic representation of stage 1 kinematics.

The three dimensional model of this stage can be seen on Figure 5.10.

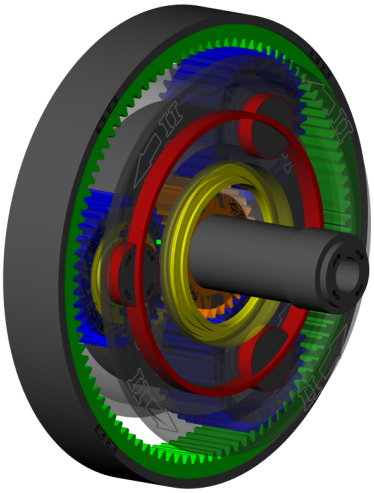


Figure 5.10: Three dimensional model of the first stage.

5.2.3.2 Stage 2

As previously mentioned, stage 2 ring shaft is rotating with stage 1 carrier, meaning ring gear had to be defined as driven by its shaft (input). In this stage the carrier is stationary, as a result planet gears were also defined as driven by their shaft, once again the output was defined to be done by sun gear.

In order to model the stage as it is represented in the drawing, an additional shaft was created and connected to the stage 2 carrier via connecting element. On the other end of the shaft a fixed support in every direction was added, resulting in a stationary carrier.

Another essential point, was the creation of a new shaft with the purpose of connecting stage 2 sun gear to stage 3 ring gear. For the effect two connection elements were added.

At this point, the kinematic relationships can be schematically represented, as shown in Figure 5.11. In this schematic representation, it can be seen a connection element, as well as a connecting bearing, connecting stages 1 and 2. Figure 5.11 also shows the power output of stages 1 and 2 done by two different shafts that will later on connect to stage 3.

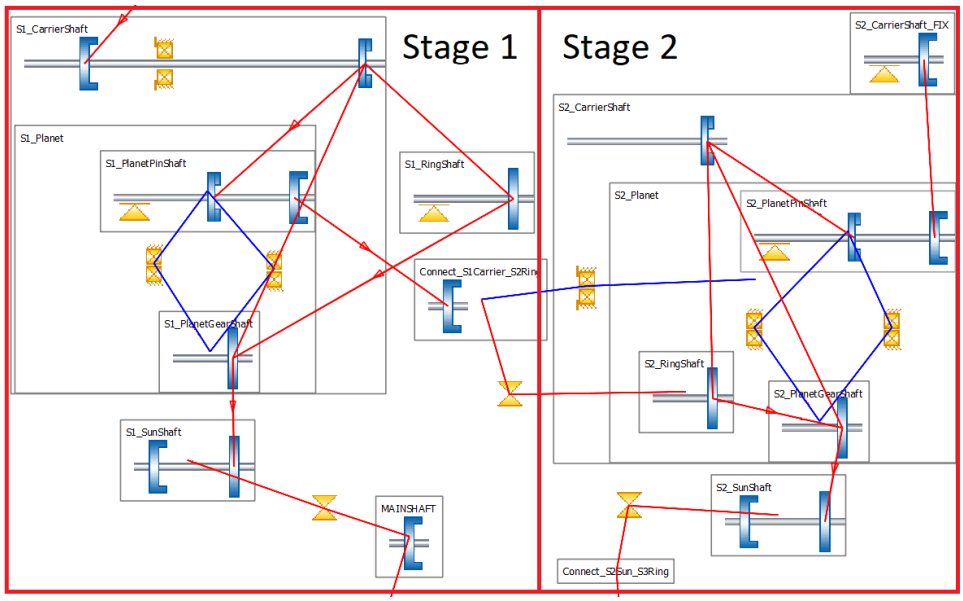


Figure 5.11: Schematic representation of stage 1 and 2 kinematics.

As for the three dimensional model of the first two stages, it can be seen on Figure 5.12.

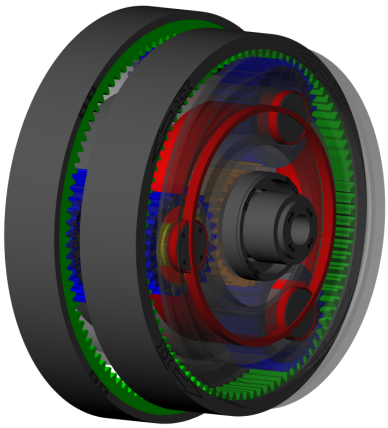


Figure 5.12: Three dimensional model of the first and second stages.

5.2.3.3 Stage 3

Stage 3 does not have stationary gears, as it can be understood from the description of previous stages.

In this stage, the carrier is rotating with stage 1 sun gear. Similarly, this stage's ring gear is rotating with stage 2 sun gear. Consequently, both ring and planet gears had to be defined as an input and the sun gear as the output.

This time, stage 3 sun shaft is connected to stage 4 wheel shaft via connection element, for this reason stage 4 wheel rotates with stage 3 sun gear.

Establishing these conditions allows to obtain the kinematic relationships shown on Figure 5.13. In this scheme, it can be seen that the power input on stage 3 is done by stages 1 and 2, respectively, on planet carrier and ring shaft, while the output is done by the sun shaft.

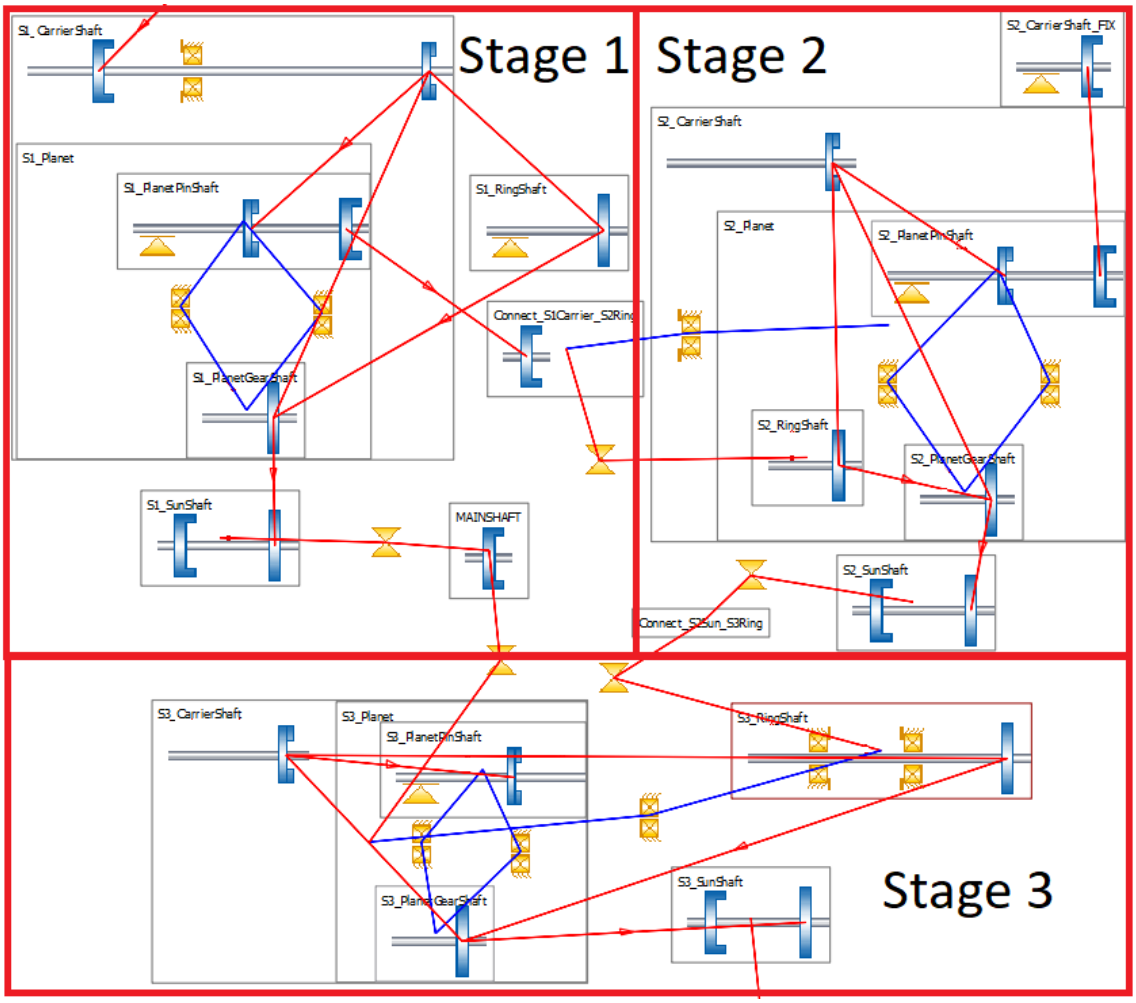


Figure 5.13: Schematic representation of stage 1 to 3 kinematics.

The three dimensional model of stages 1 to 3 is represented on Figure 5.14.

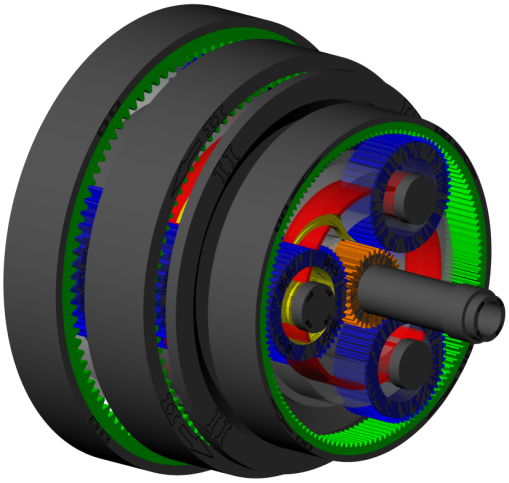


Figure 5.14: Three dimensional model of the first, second and third stages.

5.2.3.4 Stage 4

Establishing this stage's kinematic relationships did not require the creation of additional shafts nor boundary conditions. Defining the wheel as an input and both pump and output pinions as an output was enough to correctly define the kinematics.

The three dimensional model of the four stages, it is represented on Figure 5.15.

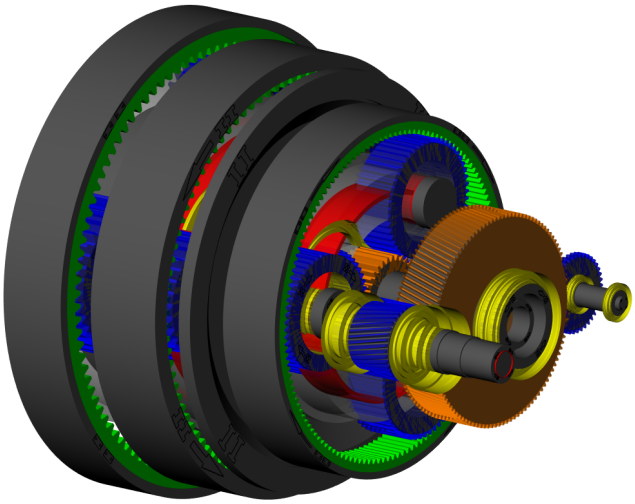


Figure 5.15: Three dimensional model of the gearbox stages.

As for the kinematic relationships of all the gearbox stages, can be schematically represented as shown on Figure 5.16. In this scheme it can be seen the connection element between the stage 3 sun shaft and the wheel shaft of the fourth stage, as well as the power output done by both shafts in the last stage.

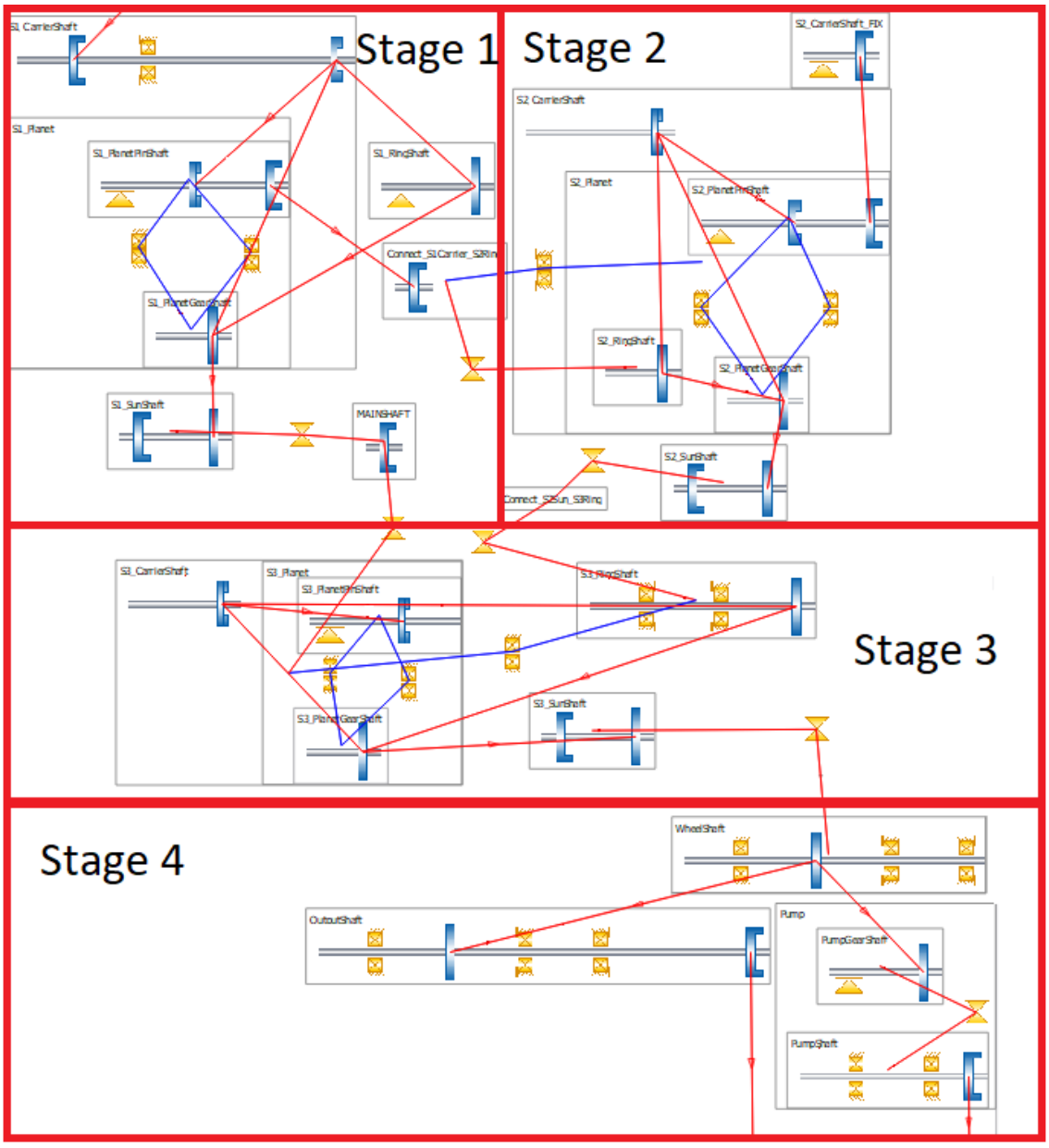


Figure 5.16: Schematic representation of stage 1 to 4 kinematics.

5.2.3.5 Global boundary conditions

In order to completely define the gearbox kinematics, three speed or force boundary conditions were applied through a software dialog window as the one shown in Figure 5.17.

The first one is associated with stage 1 input coupling. This condition was defined as constrained speed and power input that needs to be defined by the user according to the operating condition to be simulated.

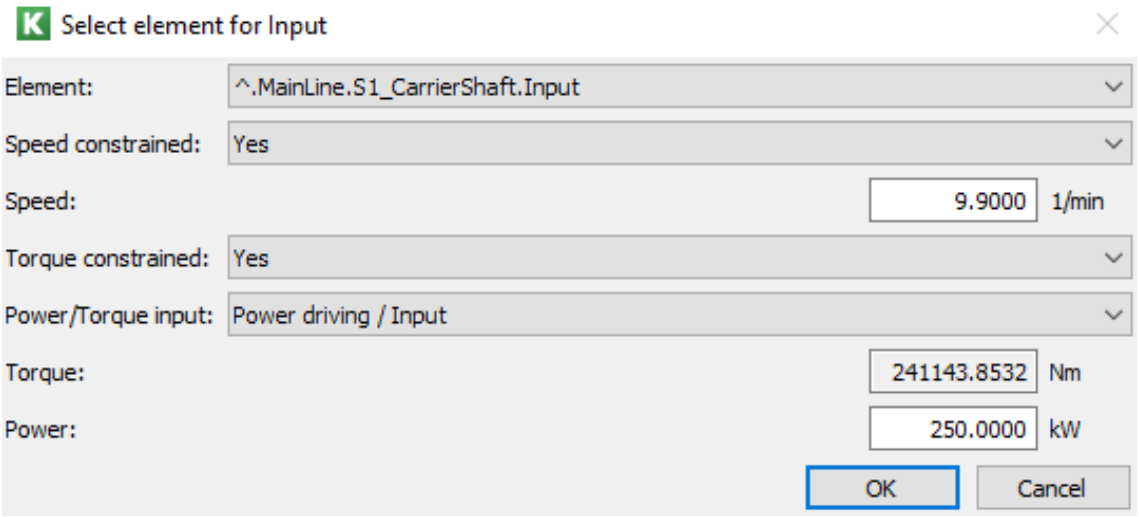


Figure 5.17: KISSsys dialog window for the input boundary condition.

Next, a condition associated with stage 4 output coupling needed to be defined. This condition was defined as not constrained speed and power output, therefore allowing the software to calculate the amount of speed and power to output, based on the model characteristics.

Finally, a boundary condition associated with the gear-pump was defined. This condition was defined as power constrained, with a fixed value of 1.1 kW (pump power). Concerning speed, the condition was not constrained allowing the software to make its calculation.

The overall KISSsys tree structure is represented in Figure 5.18, the three highlights mark the speed or force boundary conditions.

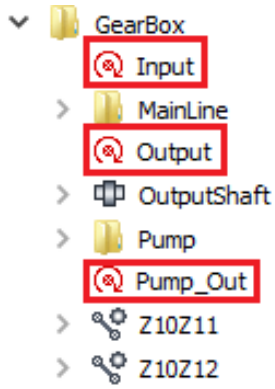


Figure 5.18: Overall KISSsys tree structure of the gearbox.

These three conditions can also be seen in the overall schematic representation of the kinematic relationships, as shown on Figure 5.19.

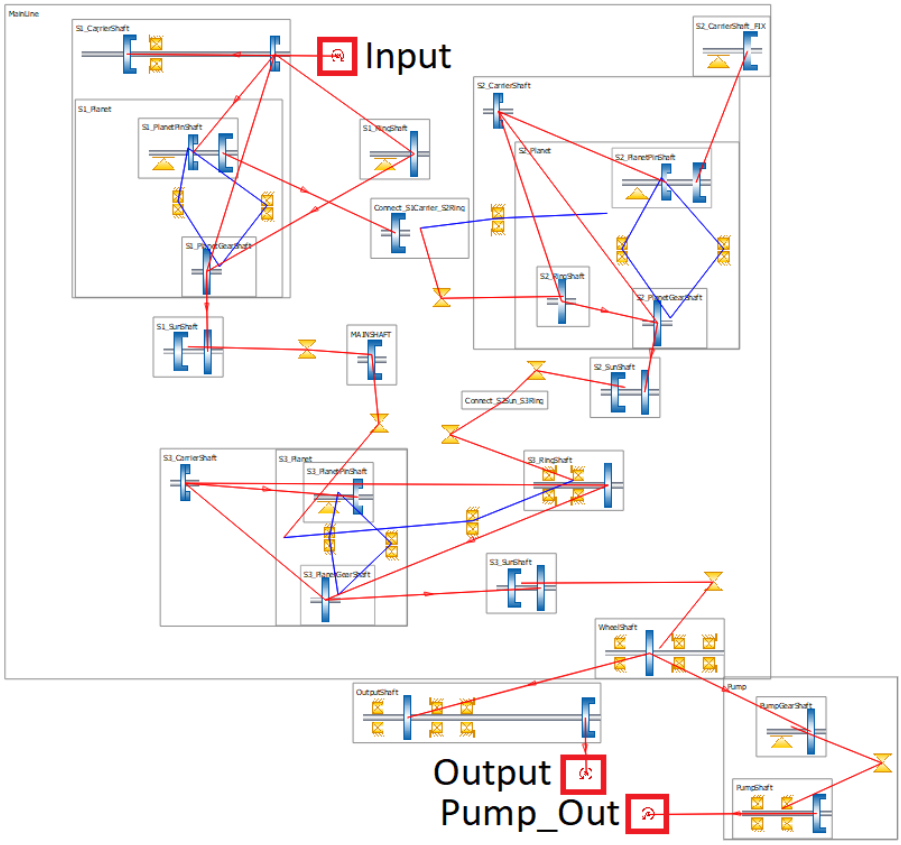


Figure 5.19: Schematic representation of the gearbox kinematics.

5.2.4 Mainline Coaxial Shaft Calculation

From previous sections it is possible to understand the mainline group holds several machine elements and even sub-groups, as shown in Figure 5.20.

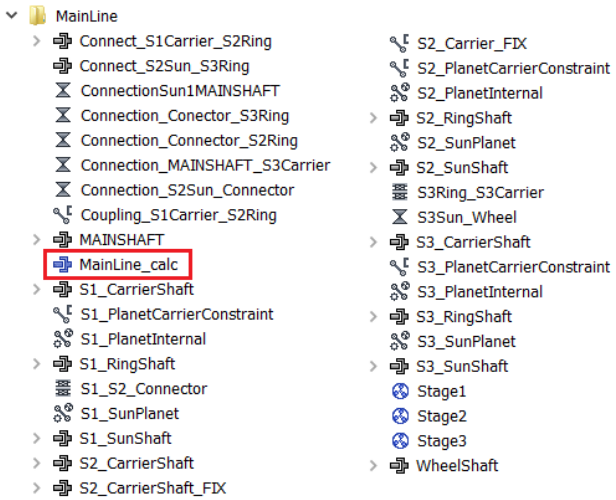


Figure 5.20: Mainline KISSsys tree structure.

Arranging these machine elements, defining their relative positions and placing standard components along the mainline, was achieved by adding a coaxial shaft KISSsoft calculation to the mainline group, highlighted in Figure 5.20.

Furthermore, through this calculation it was possible to define the geometry and dimensions of all the shafts previously mentioned, as it can be seen on Figure 5.21.

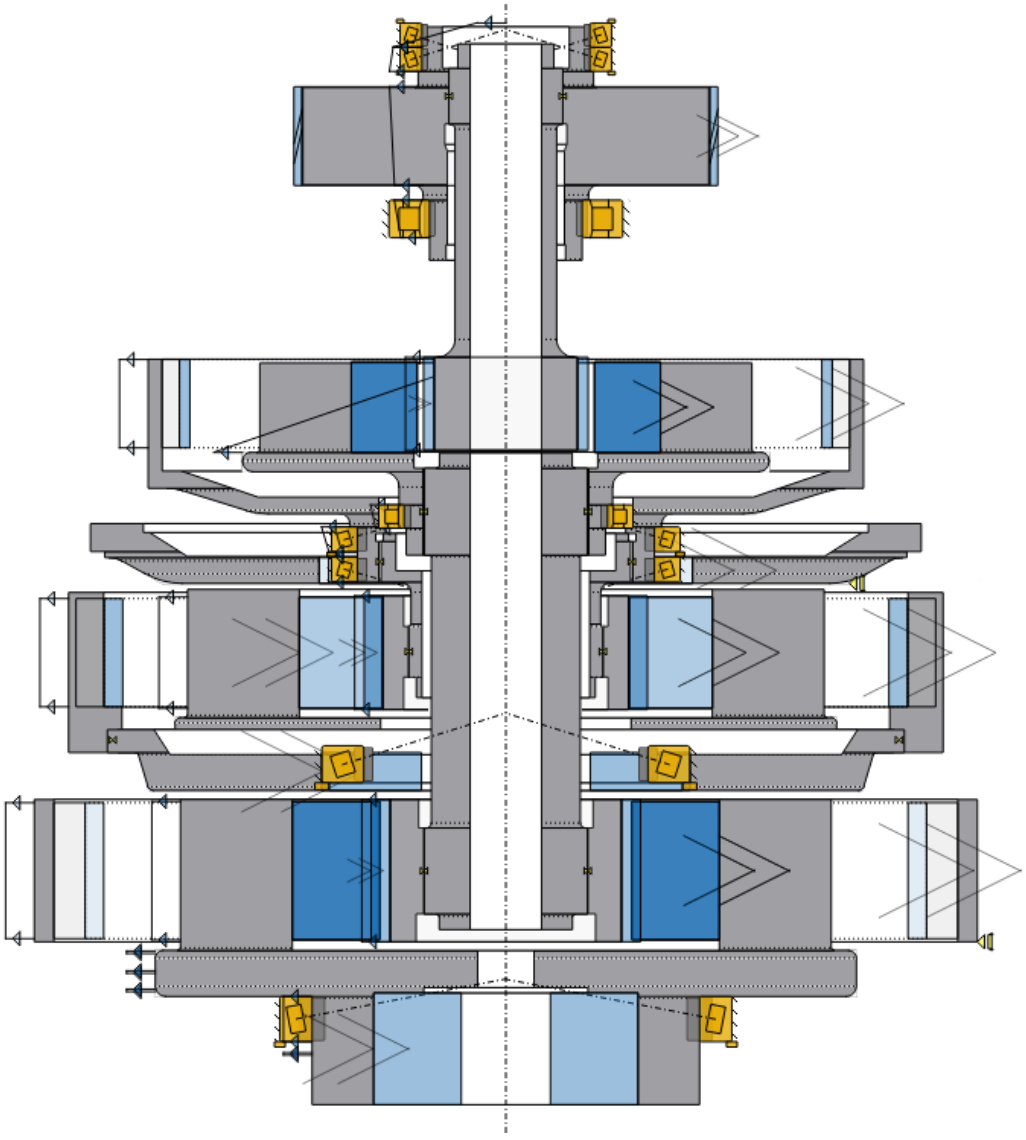


Figure 5.21: Mainline coaxial shaft KISSsoft calculation.

5.2.5 Creating User Interface Table

At this point the gearbox was assembled and the kinematics established. Nonetheless, changing the operating conditions was not an intuitive process.

There were several parameters to input, whose values were important to vary between simulations. In order to make this process more user-friendly and avoiding the trouble of going to numerous different tabs and windows every time the operating conditions changed, a user interface table was created, as shown in Figure 5.22.

Oil Sump. Temp. [deg]	Room Temp [deg]	Sequence Applied	
64	20	5	
Sequence	Power [kW]	Speed [rpm]	Oil Sump. Temp. [deg]
1	250	9.9	58
2	500	12.4	60
3	1000	15.5	62
4	1500	16.3	62
5	2000	16.4	64
6	2500	16.5	65
7	2500	16.4	65

Figure 5.22: User interface table.

In addition, using KISSsys integrated programming language, an expression was programmed in every variable property window. Therefore, allowing to easily change those variable values using the user interface table.

Changing the number under "Sequence Applied", as it can be seen on Figure 5.22, will automatically apply the corresponding values from the table shown in the same figure. Sequences one to six have fixed values, while sequence seven was programmed to allow the user to input any value.

5.3 Power Loss Model

KISSsys has an integrated feature that performs the power loss calculation based on the gearbox model created and a few other input parameters.

Nonetheless, in order to compare and understand the results produced by the KISSsys model, power loss models were implemented on different software. In this section, these models will be further explained.

5.3.1 KISSsys Power Loss Model

Activating KISSsys efficiency calculation feature will result in two main modifications to the gearbox model.

Firstly, a power loss element for every machine element present on the model will be automatically added to the tree structure next to the element it concerns, as seen in Figure 5.23. Later on, when running the power loss calculation a power loss value will be calculated for each one of these elements.

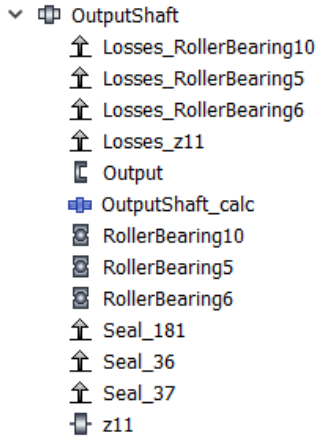


Figure 5.23: Output shaft KISSsys tree structure.

Since there is no seal catalogue in KISSsys, or any other way to add seals to the model, a power loss element needs to be manually added from the elements box to the shaft where the seal is placed in order to obtain seal losses .

After adding the necessary elements to represent the seals, accessing the KISSsoft shaft calculation and correctly placing the power loss elements is the next step. A fixed value of power loss can then be attributed to this type of elements.

However, in order to correctly calculate seal losses, regardless of the operating condition, the Simrit equation for seal losses (equation (2.32)) was programmed in the properties window of all the seal losses added. This way, KISSsys automatically calculates seals losses too.

The second main difference in the model caused by activating the efficiency feature, is the efficiency table which becomes available. This table allows to define essential data for the power loss calculation, type of lubrication, oil level, housing and foundation characteristics, ventilation data and lubricant temperature can be defined in this table. Here, the user can also choose to show the housing and oil level in the three dimensional model of the gearbox for visual purposes only.

Calculation method can also be changed in the same table, as shown in Figure 5.24.

Requested Result	Efficiency		Units	W
Calculation Method	ISO TR 14179-2		Contact Analysis	No
Housing	Settings	Ventilation	Lubrication	Oil Cooler

Figure 5.24: KISSsys efficiency table.

5.3.2 Excel Power Loss Model

As mentioned in the beginning of this section, power loss models were implemented in different software. In order to easily understand the changes in the final power loss result produced by varying the factors used in these models, Microsoft Office Excel was used to programme the models that focus on gear load dependent losses and bearing losses.

5.3.2.1 Gear Load Dependent Losses

The model created for the calculation of gear load dependent losses uses the equations presented in section 2.1.2. As mentioned in the same section, KISSsoft calculates these losses using Niemann's approach [33] for the coefficient of friction in meshing gears using the lubricant factor, X_L.

There are several advantages brought by the Excel model. First, it allows the calculation to be done according to both Niemann's and Schlenk's approach for the coefficient of friction in meshing gears, therefore allowing to compare both results and later on comparing them with experimental values, hence understanding which one will be a better approximation.

Next, this model allows to input the lubricant base and automatically updates the X_L factor according to the ones presented by Fernandes in [29].

Besides the lubricant base, the user only needs to input operating conditions in order to obtain the power loss on each stage and comparing it with KISSsoft results. Nonetheless, the user is allowed to change the gear data in case there is the need to apply the model to other planetary stages.

Obtaining the gear loss factor from equation (2.11), demands solving the integral along the path of contact. For this reason, the model also includes a feature calculating the path of contact for both gear pairs in the planetary stage. Also, the load distribution and sliding speed values along the path of contact are calculated and output in the model.

The model was validated by comparing torque loss values obtained using the Excel model for the C40 gear, in K5 load stage with a wheel speed of 400 rpm, with the values from Fernandes's published work [54]. These values are presented on Table 5.1.

Table 5.1: Gear load dependent power loss model validation.

	Experimental [54]	**Excel Model**
Torque Loss / N · m	3,75	3,67
Deviation	2,04%	

5.3.2.2 Bearing Losses

Similarly to the model presented in the previous section, the bearing power loss model uses the equations presented in section 2.2.

This model allows to simultaneously calculate the power loss values for the same bearing using μ_{bl} and μ_{EHL} from SKF catalogue and from Fernandes' published work [39]. Therefore, allowing to easily compare both results.

Furthermore, the model only requires the user to input bearing dimensions and operating conditions. All further data needed, must be selected from list boxes according to the bearing characteristics, the model will then automatically update all the coefficients according SKF's catalogue.

All the parcels adding to the total torque loss (equation (2.16)), are calculated separately and their results can be easily obtained and compared.

Even though the model is prepared to calculate losses in both cylindrical and tapered roller bearings, validation was only possible for the cylindrical roller bearings case. It was done by comparing the frictional moment obtained from the model, for a NJ406 cylindrical roller bearing (2393 N radial load, 200 rpm), with the one obtained from SKF's online bearing calculating tool as well as with the one published by Fernandes's in [39], such values are presented on Table 5.2.

Table 5.2: Bearing power loss model validation.

	Total frictional moment / $\mathrm{N/mm}$	**Deviation**
SKF Bearing Calculating Tool	66,42	0,35%
Excel Model (SKF)	66,66	
Fernandes' Work [39]	65	0,31%
Excel Model (Fernandes's Work)	65,20	

5.4 Heat Dissipation Model

As mentioned in section 2.5, results obtained from KISSsys heat dissipation model do not represent accurately the reality of the gearbox under study. Hence, a uni directional heat dissipation model was implemented to obtain a better prediction of the heat transfer phenomena in the case under study.

In this section, the necessary procedure to activate KISSsys heat transfer model, as well as the one directional model implemented in excel will be approached in detail.

5.4.1 Activating KISSsys Heat Transfer Model

Activating KISSsys heat transfer model can be done by changing the requested result, in the efficiency table to heat transfer, as shown in Figure 5.24. Depending on the data input, the software will then proceed with the calculation and output the amount of heat transferred through the different dissipation sources.

The calculation can be performed to all the sources, however the user may decide to switch some of them off, depending on the case under study. In the same table where the heat dissipation

Heat Dissipated	Correction Factors
Housing [W]	0
Foundations [W]	0
Input/Output Shafts [W]	0
Oil Cooler [W]	0
Total Dissipation [W]	0

Figure 5.25: KISSsys heat dissipation sources.

results can be consulted, correction factors can be applied in order to bring these values closer to reality, in case there are available results for validation.

5.4.2 One Directional Heat Dissipation Model

This model allows to perform heat dissipation calculations through the housing depending on several data input. Factors such as heat transfer coefficient outside the gearbox, ambient temperature, thermal conductivity and emissivity of the walls as well as heat transfer coefficients inside the gearbox may be easily adjusted.

Therefore, this model allows to expeditiously perform a sensitivity analysis, in order to understand which factors may have higher influence in the heat dissipated, highlighting some of them in contrast to the others that may not have as high influence as expected.

Furthermore, the inside and outside temperatures of the wall will be output by the model, as well as the total amount of heat dissipated for the operating condition under study.

Also, there is the possibility for the user to apply a correction factor to the model in order to bring the results closer to experimental results that may be available in the future.

5.4.3 Lubricant Heat Dissipation

The one directional model is capable of accounting for the heat dissipated through the housing. Nonetheless, there is heat being dissipated via lubricant due to the existence of an oil cooler, consequently a model to account for such dissipation had to be created.

At the time this model was developed, the only information available concerning the intercooler was the fact it could work with two different speeds, resulting in an oil flow of 53 L/min for the first speed or 105 L/min for the second speed. Also, it was known the first speed would be activated for an oil sump temperature of 62 °C and deactivated for 55 °C, as for the second speed, the window was known to be 65 to 58 °C.

For a certain working condition, the total power loss must be the same as the total heat transferred in order to achieve thermal equilibrium in the gearbox. Therefore, the heat dissipated via

lubricant can be easily obtained from the difference between the total power loss and the heat transferred through the housing.

As a result, from the heat dissipated via lubricant, the oil flow and the working intervals of the cooler, it was possible to create a model to predict the temperature differences caused by the cooler for each condition, as well as inlet and outlet oil temperatures in the oil sump.

5.5 Bulk Temperatures

5.5.1 Gear Bulk Temperatures

KISSsoft runs the calculation for gear bulk and flash temperatures by default. This means when a gear pair, or planetary stage, is created on KISSsoft, as long as the rating tab is active (Figure 5.26), running the calculations will automatically calculate bulk temperature, using both the flash temperature method [46] as well as the integral temperature method [47]. Asking for the report of such calculation will not only output the mentioned temperatures, but additional pertinent data obtained in intermediate steps of the calculation is also presented, such as average flash temperature, contact temperature and even some of the factors mentioned in chapter 3, such as tip relief factor.

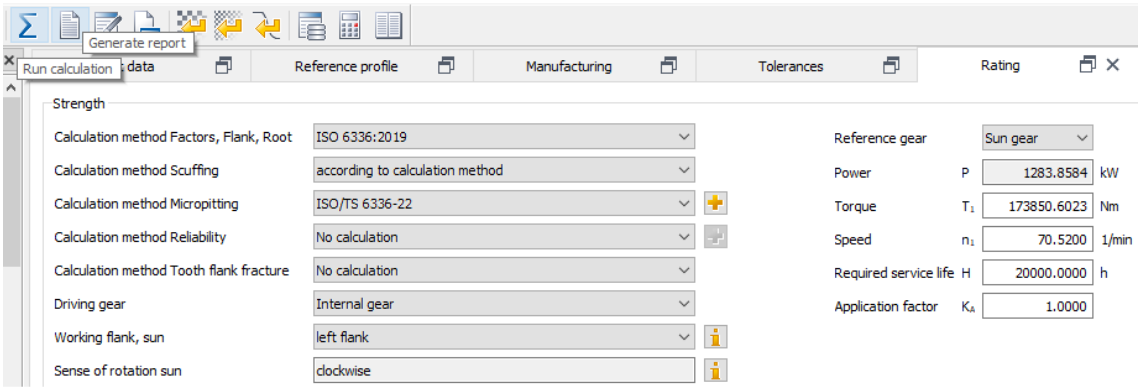


Figure 5.26: KISSsoft rating tab, calculation and report buttons.

In order to better understand KISSsoft results, as well as being able to obtain the whole distribution of temperatures along the path of contact, the author implemented these models in Excel. Both integral and flash temperature methods were implemented and their output values compared with KISSsoft. Due to the lack of information related to the tip relief, the factors depending on this data were applied with the same value as given by KISSsoft. As for the factors needed to obtain the transverse unit load, were all set to 1, since there is no information that would help in their definition according to ISO 6336-1 [48].

The bulk temperature calculation was done for the first planetary stage, specifically for sun-planet gear pair. The input conditions on the gearbox considered for this calculation were 2,5 MW at 16 rpm, with the oil sump at 64 °C.

In order to correctly compare the Excel model results and the ones obtain from KISSsoft for the flash temperature method, the mean coefficient of friction on the model had to be defined according to the one presented on KISSsoft. There are small differences on these values, since the one on the model is calculated according to Schlenk's approach, and the one on KISSsoft is calculated according to ISO TR-13989-1:2000 [46]. After such adjustment the deviations on Table 5.3 were obtained.

Table 5.3: Flash temperature method.

	Average Flash Temp. / °C	**Bulk Temp. / °C**	**Highest Contact Temp. / °C**
KISSsoft	10,37	73,75	91,34
Excel Model	9,65	73,07	84,90
Deviation	6,94%	0,92%	7,05%

Comparing the results from the integral method did not require any adjustment, since the equation for the mean coefficient of friction on ISO TR-13989-2:2000 [47] is already resulting in values close to Schlenk's approach. The values obtained from such comparison are presented on Table 5.4.

Table 5.4: Integral temperature method.

	Mean Flash Temp. / °C	**Bulk Temp. / °C**	**Integral Temp. / °C**
KISSsoft	5,35	71,49	79,51
Excel Model	5,63	71,89	80,33
Deviation	5,27%	0,55%	1,04%

5.5.2 Bearing Bulk Temperatures

Implementing bearing bulk temperature model in Excel, required a previous calculation of each bearing power loss in order to solve the thermal equilibrium equation, as mentioned in section 3.2.

Calculating the amount of heat dissipated via conduction, also required knowledge concerning bearing dimensions, wall thickness and temperature. Performing this calculation for a bearing contacting with the gearbox housing, required establishing the wall temperature as the outside wall temperature, which could be obtained from the thermal model. Nonetheless, some of the bearings do not contact directly with the gearbox housing, instead they are between machine elements, which in time were assumed to be in thermal equilibrium with the oil sump. In such cases the wall temperature was defined the same as the oil sump temperature.

The amount of heat dissipated via lubricant was calculated based on oil temperature, which depends on the operating condition, and the oil flow on the bearing under study, to which there is no information about.

Hence, as a starting point, the software was instructed to perform the calculation for the thermal equilibrium, considering the oil flow to be half of the maximum flow calculated according to equation (3.44). Consequently, the thermal equilibrium is solved and the output is the correspondent bearing bulk temperature. Further calculations were performed regarding different oil flows and will be approached in a subsequent section, nonetheless this model still lacks validation.

These calculations were performed using Excel solver tool.

Chapter 6

Results and Discussion

From all the models previously presented, it is possible to obtain a realistic estimation of what happens in the gearbox under study. From lubricant and machine elements temperature, to the power loss on every element and even the influence of external factors on final results, such as ambient temperature or heat transfer coefficients, is possible to be predicted.

In order to run simulations and have input data for the models that resemble real operating conditions, a table of expected operating conditions that can later on be upgraded according to the test programme was created, Table 6.1. Most of the simulations that produced the results presented in further sections, ran under such operating conditions. The results obtained with different input data shall be duly indicated in the following sections.

Table 6.1: Gearbox operating conditions.

Operating Condition	**Power /** kW	**Speed /** rpm	**Oil Sump Temp. /** °C
1	250	9.9	58
2	500	12.4	60
3	1000	15.5	62
4	1500	16.3	62
5	2000	16.4	64
6	2500	16.5	65

The conditions on Table 6.1 were established based on SCADA data, relative to wind turbines under real operating conditions.

In addition, the simulations were performed using two gearbox lubricants, with similar properties but different bases. Both lubricants were chosen from KISSsoft catalogue, with the properties shown in Table 6.2.

Table 6.2: Lubricant properties.

	ρ kg/dm^3	υ_{40} mm^2/s	υ_{100} mm^2/s	Min. Temp. °C	Max. Temp. °C	Lubricant Base
ISO VG 320	0,9000	320,00	22,00	-15,00	120,00	Mineral (MIN)
Castrol Optigear Synthetic X320	0,8540	325,00	34,90	-30,00	95,00	Polyalphaolefin (PAO)

6.1 Power Loss

In this section, results associated with the power loss in every element of the gearbox under study will be presented. Nevertheless, the 1.1 kW consumed by the mechanical pump [55] present in the fourth stage are essential to run the gearbox under optimal conditions, meaning this amount of power will not be considered as a loss. However, power losses in elements associated to the pump (bearings and gear), will be accounted for.

6.1.1 Gear Power Loss

The model implemented in Excel concerning gear load dependent power loss, allows to compare values obtained from KISSsoft, calculated with Niemann's approach (equation (2.13)) for the mean coefficient of friction, with the ones obtained using Schlenk's approach (equation (2.15)) for the same parameter. Calculations performed in this field, were done using X_L values from Fernandes's work [29].

Also, the operating condition used to obtain the data presented in Table 6.3, was an input power of 2.5 MW at 16 rpm, oil sump at 80 °C with a mineral based oil, specifically ISO VG 320. The power loss values on Table 6.3 should be looked at as a form of comparing both models only.

Table 6.3: Schlenk's approach (Excel) vs Niemann's approach (KISSsoft).

	Stage 1		**Stage 2**		**Stage 3**	
	Excel	**KISSsoft**	**Excel**	**KISSsoft**	**Excel**	**KISSsoft**
Power Loss W	10254,37	7920	7555,62	5841	8352,91	7428
μ_{mZ} Sun-Planet	0,053	0,041	0,055	0,042	0,034	0,031
μ_{mZ} Planet-Ring	0,051	0,033	0,051	0,034	0,031	0,021
Power Loss Difference	29%		29%		12%	

Since the same X_L values are used in both models, the differences observed are due to the approach used for the mean coefficient of friction. All subsequent values for gear related power

loss will be taken from KISSsoft, meaning slightly higher power loss values may be expected to be measured, in the case Schlenk's approach produces better approximations. Nonetheless, such validation can only be made by comparing model values with experimental ones which are non existent at the time.

Load distribution and sliding speed along the path of contact, for every gear pair of the planetary stages, had to be calculated in order to perform accurate calculations of the previously presented values.

Despite Figure 6.1 concerning only one of the gear pairs, the load distribution was considered the same for all gear pairs. The main divergences in the sliding speed distribution can be found in the difference between sliding speeds correspondent to point A and E, which in some cases is more accentuated. The distribution of the sliding speed along the path of contact for the remaining gear pairs in planetary stages can be found in Appendix A.

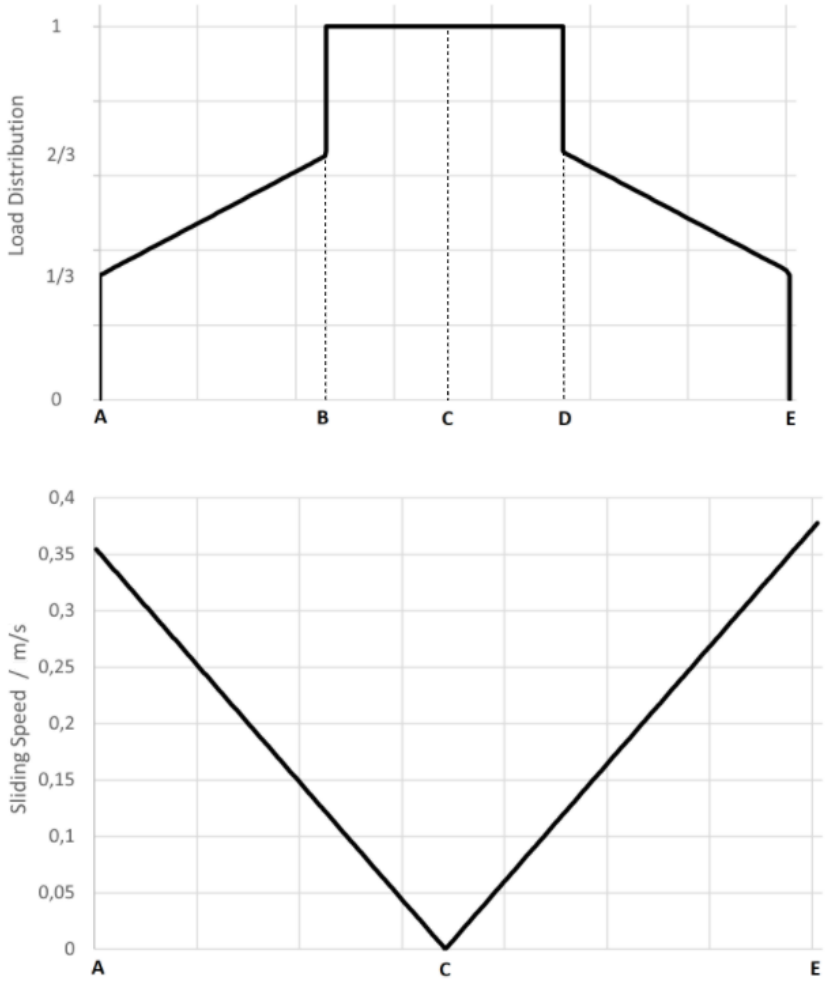


Figure 6.1: Load distribution and sliding speed along the path of contact of sun-planet gear pair -first planetary stage.

KISSsoft model allowed to run simulations with the operating conditions presented in Table 6.1, therefore providing a better understanding of what may happen in the gearbox under real operating conditions. Simulations were performed for the two gearbox oils presented on Table 6.2. Examples of the reports returned by KISSsoft when performing gear calculations are presented on Appendix B.

From Figure 6.2 it is possible to understand that gear load-dependent losses, in the same conditions, are higher for the mineral based oil. This can be justified by the fact that the X_L value for the mineral oil is higher than the correspondent value for the PAO, additionally the mineral lubricant's viscosity is lower than the one presented by the PAO, therefore resulting in a higher mean coefficient of friction for the mineral lubricant in the same operating conditions, as could be expected from equation (2.13).

Furthermore, it can be seen that the influence of stage 1 and 3 in this type of losses is slightly higher than the remaining stages. This can be explained by the higher loads in both these stages. The power split on stage 1 and 2, is responsible for the high load on stage 1, while the fact that on stage 3 the power concentrates again can be accountable for the high load on stage 3. With stage 4 being the one with higher speeds, it explains the lower load. Equally important is the fact that stage 4 has a lower gear loss factor and therefore smaller responsibility on this kind of losses.

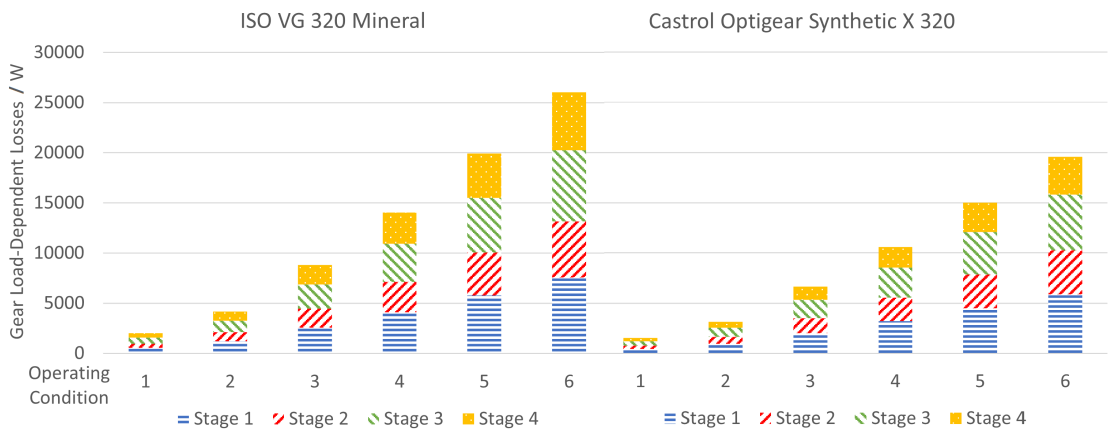


Figure 6.2: Gear load-dependent power loss for six operating conditions and two gearbox oils.

6.1.2 Bearing Power Loss

Implementing the bearing power loss model on Excel, allows to compare the results obtained by using both sets of values for μ_{EHL} and μ_{bl}, as previously mentioned.

For an input power of 2.5 MW at 16 rpm, with ISO VG 320 lubricant, it is possible to obtain the results presented in Table 6.4. Consequently, each of the bearings under analysis has a different operating condition, according to their position. The bearings shown in the table for the first three stages are the ones on the planet pins, while the one from fourth stage is placed in the output shaft.

Analysing results from the Excel model, allows to understand the differences between results obtained with SKF's and Fernandes' published values for μ_{EHL} and μ_{bl} [39]. Such differences

become smaller as the speed increases, due to the fact that higher speeds lead to lower ϕ_{bl} values (closer to full film conditions), consequently lowering the influence of μ_{bl} (parameter with higher gap) while increasing the influence of μ_{EHL} (parameter with lower gap). The differences in torque loss vary from values around 43% for speeds close to 50 rpm, up to differences of 0,4% when the speed increases to 1600 rpm.

The torque loss obtained with SKF's values is higher than the one obtained with the experimental values. This variation is justified by the fact that SKF's μ_{EHL} and μ_{bl} values for cylindrical roller bearings lubricated with mineral oil, are higher than the ones presented in [39].

Table 6.4: Results produced with SKF's values vs Fernandes' values of μ_{EHL} and μ_{bl}.

	Bearing Input Conditions		**Torque Loss /** N · mm		
	Rotational Speed rpm	Radial Load N	SKF's Values μ_{bl} and μ_{EHL}	Fernandes' Values μ_{bl} and μ_{EHL}	Difference
Stage 1 NJ2244EM	46,59	304456,00	19642,80	11017,61	43,91%
Stage 2 NJ2240EM	48,50	230045,00	13866,95	7893,13	43,08%
Stage 3 NJ2236EMC	307,32	94178,00	8998,93	8867,52	1,46%
Stage 4 NJ2234EMC	1602,44	82903,00	14513,44	14453,75	0,41%

In order to have a better understanding of what may happen in a real work environment, the procedure used for gear load-dependent losses was repeated. Using KISSsoft to perform the simulations with six different operating conditions, as presented in Table 6.1, for the same mineral and PAO oils previously mentioned, it was possible to obtain the results present in Figure 6.3.

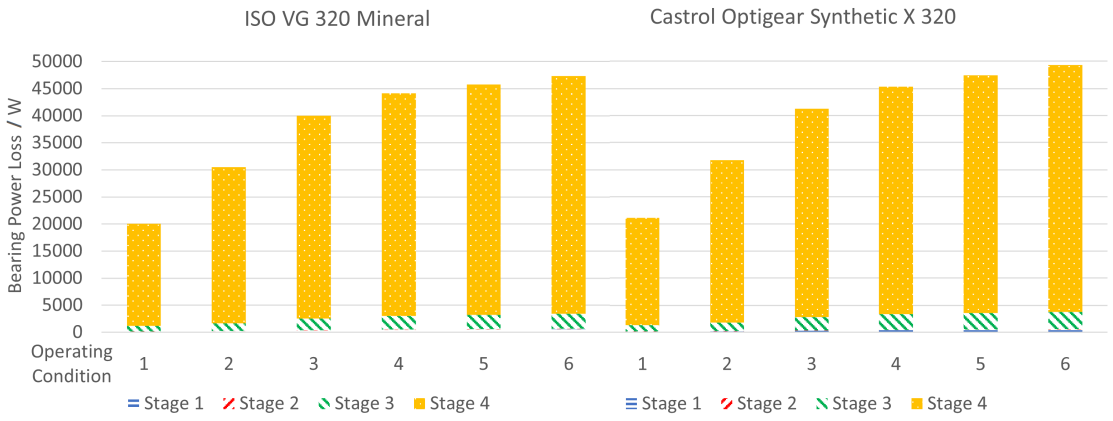


Figure 6.3: Bearing power loss for six operating conditions and two gearbox oils.

Major bearing power losses happen in the fourth stage, due to its high speed when compared to previous stages. While stage 3 bearings still make a small contribution in this power loss source, stage 1 and 2 bearings contribution is almost null when compared to the one made by stage 4 bearings.

Contrary to what happens with the gear-load dependent losses, it can be seen that for the same operating conditions, the mineral based oil generates lower bearing power losses. This is due to the lower viscosity of the mineral oil, which directly affects rolling frictional moment in bearings, as it can be seen in equation (2.17).

6.1.3 Gearbox Power Loss

KISSsoft/KISSsys simulations allow to compare and understand the global power loss in the gearbox under analysis. Values obtained with different lubricants and operating conditions can be used to predict what may happen in this gearbox under real operating conditions.

From Figure 6.4 it is possible to understand PAO produces higher losses for the first two operating conditions, while in the third condition both lubricants present very similar losses. For the last three conditions, mineral oil presents higher losses. The main difference is observed in operating condition 6 where the mineral oil produces a power loss of 86981,2 W, against 84258,4 W obtained for the PAO.

Additionally, it can be seen the influence of bearing power loss (PVL) in the total power loss is way higher than any other source. Furthermore, gear load-independent power losses (PVZ0) grouped with the churning losses generated by the planet-carrier, represented as auxiliary losses (PVX), play a very important role in the global power loss of this gearbox. These two power loss sources are represented together on Figure 6.4, since the results were taken from KISSsoft and the software does not make a distinction when presenting the results.

Moreover, gear load-dependent losses (PVZP) still have some relevance in the final power loss result, although this group only presents higher power loss values than the PVZ0+PVX group for the last two conditions, as seen in Figure 6.4. Concerning power loss generated by seals (PVD), in this gearbox, represents a small fraction of the total power loss, having little influence in the final result. This source shows its higher power loss value of 1179,5 W for operating condition 6.

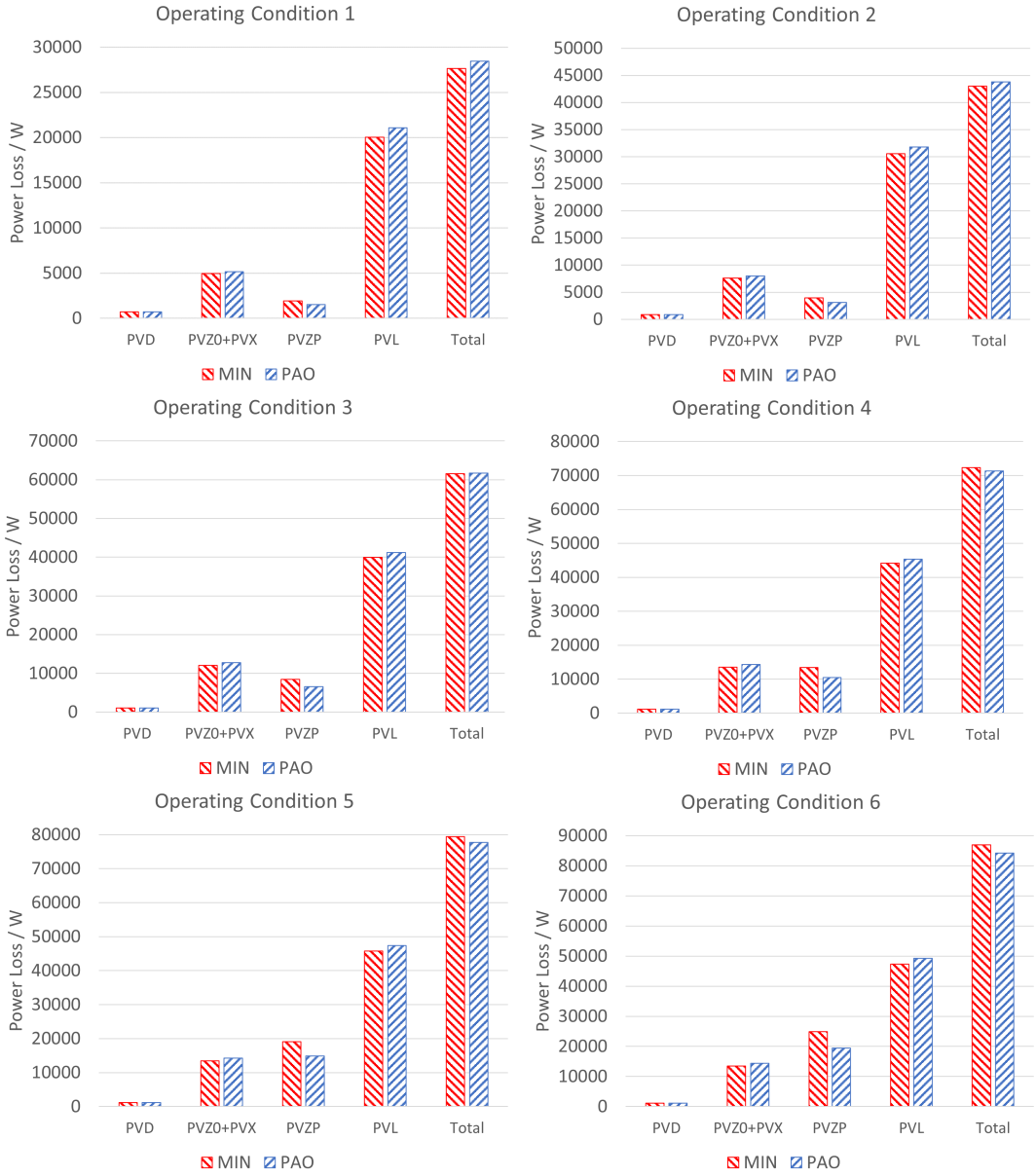


Figure 6.4: Total power loss for six operating conditions and two gearbox oils.

6.1.4 Gearbox Efficiency

Operating conditions with higher power input, will consequently result in higher power losses. In order to correctly compare operating conditions and to understand which ones result in better gearbox performance, power loss needs to be related to input power, therefore representing efficiency.

From the power loss results related to the six operating conditions, it is possible to obtain the efficiency results for both mineral (Figure 6.5) and PAO (Figure 6.6) lubricants. Analysing both figures, it is possible to understand lower input power operating conditions will result in lower efficiencies, with the results varying from around 89% up to almost 97%.

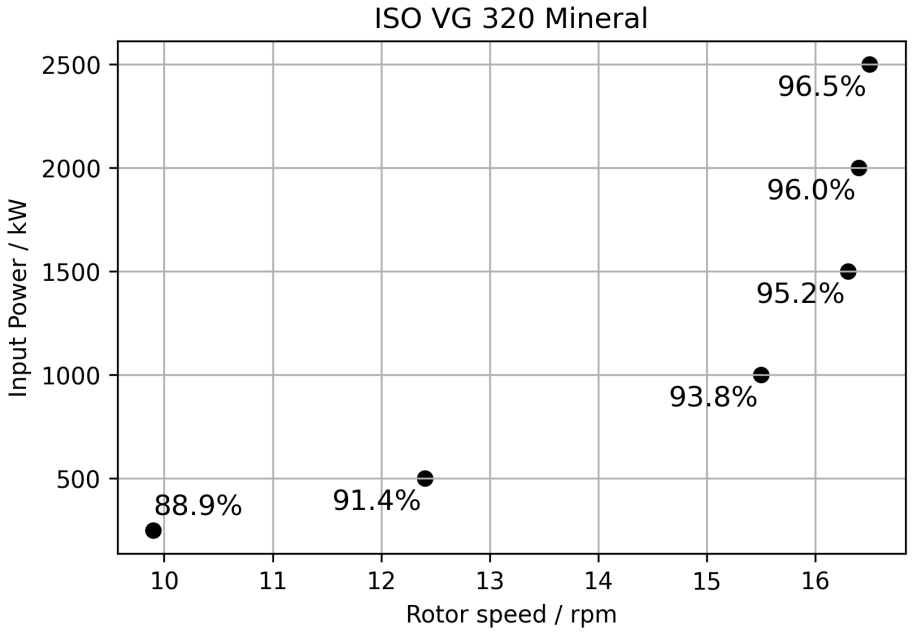


Figure 6.5: Efficiency values for six operating conditions, gearbox lubricated with mineral oil.

Comparing the results for both lubricants, allows to understand the mineral oil provides higher efficiencies for operating conditions with lower input power, while the PAO is more efficient when the operating conditions have higher input power.

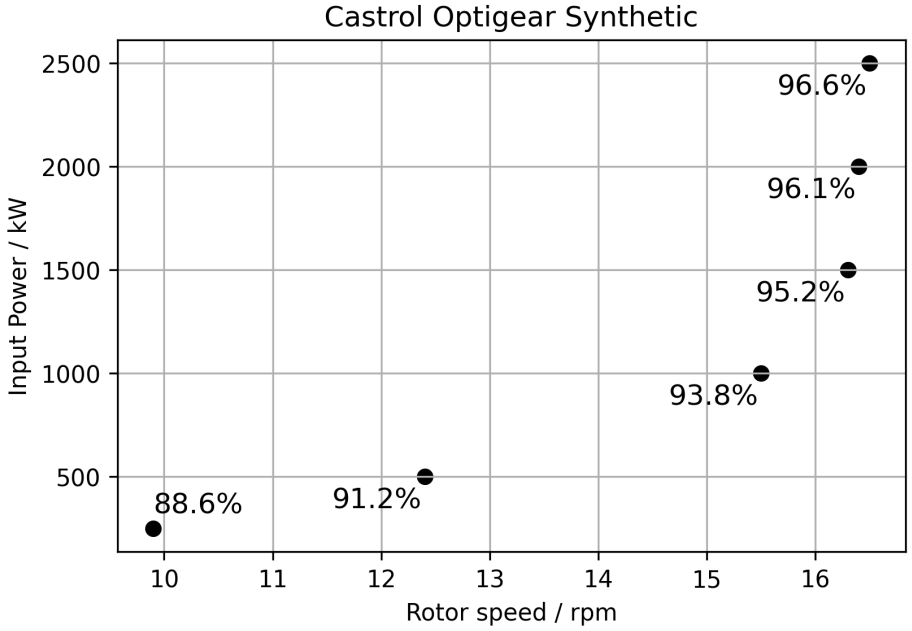


Figure 6.6: Efficiency values for six operating conditions, gearbox lubricated with PAO oil.

As a means to allow any user to predict the efficiency in this gearbox in a quick and easy way, it is possible to represent the efficiency of the gearbox depending on the input power and the lubricant used. Additionally, a polynomial curve can be used to fit the results obtained, consequently allowing the user to apply the input power in the equation of such curve and obtain a rough prediction of the correspondent efficiency for the lubricant in use.

Figure 6.7 shows the efficiency curve for the mineral lubricant and the respective equation.

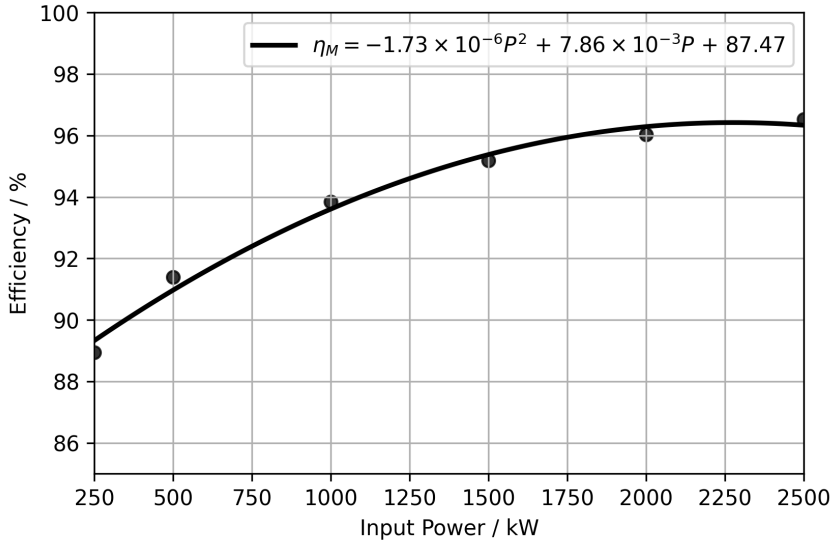


Figure 6.7: Efficiency curve for the mineral lubricant, $R^2 = 0,9$.

On Figure 6.8 it can be seen the curve for the PAO lubricant and the equation associated to this curve.

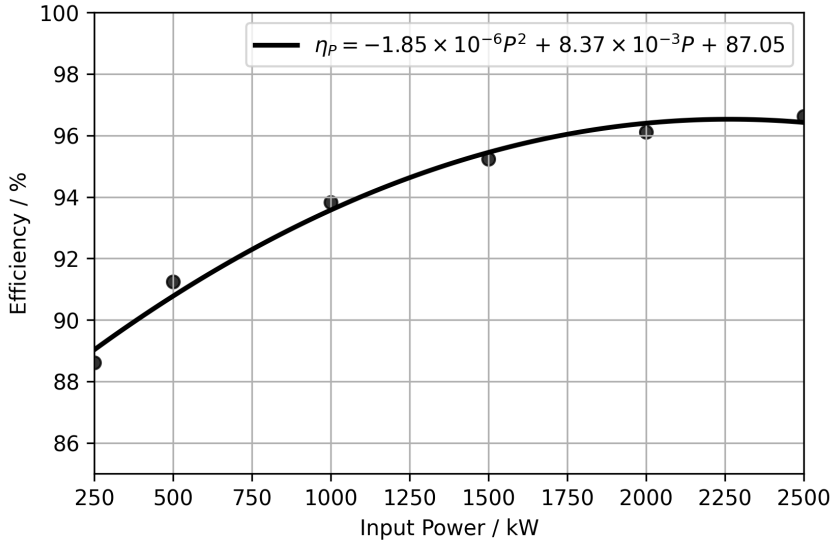


Figure 6.8: Efficiency curve for the PAO lubricant, $R^2 = 0,9$.

For an expeditious comparison between the efficiencies produced by both lubricants, it is possible to compare their efficiency curves. Such curves were plotted together and the input power split in two groups. Figure 6.9 presents the comparison for lower input power values, while Figure 6.10 establishes the efficiency curve comparison for higher input power values.

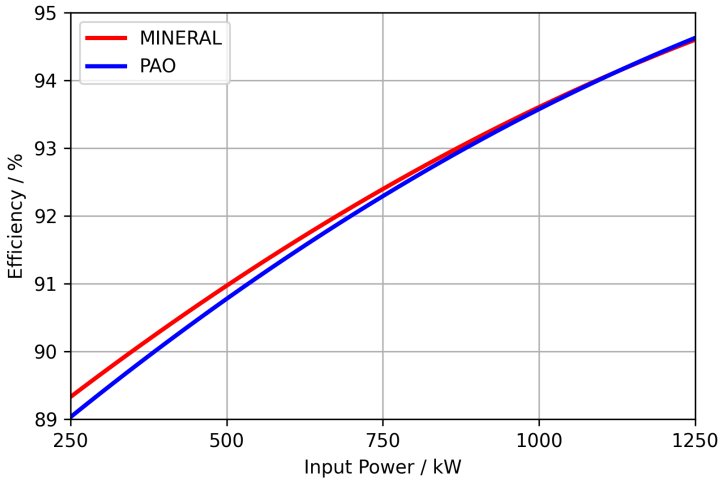


Figure 6.9: Comparison between the efficiency curves of both lubricants for lower values of input power.

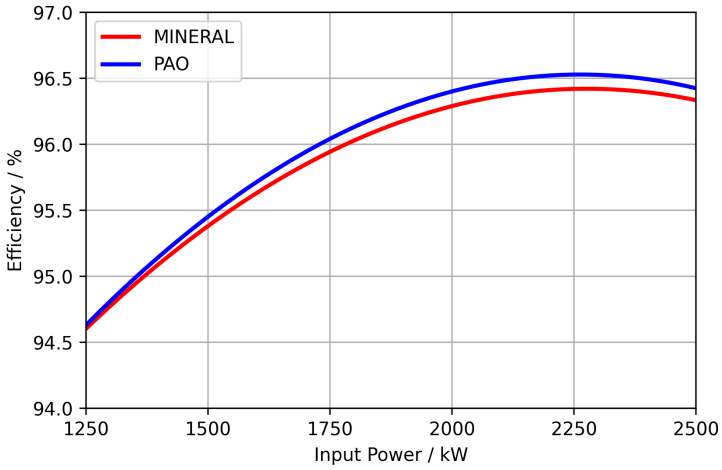


Figure 6.10: Comparison between the efficiency curves of both lubricants for higher values of input power.

By comparing figures 6.9 and 6.10, it is clear the mineral lubricant will result in higher efficiencies for lower input power values, in contrast to the PAO lubricant which results in higher efficiencies for higher input power values. In intermediate values of input power, this comparison is not so clearly represented by the curves since the efficiencies produced by both lubricants are

very similar and the number of points used to create the curves might not have been enough to cause differentiation in this zone.

In order to create the efficiency maps shown in Figure 6.11, a matrix of points which contemplates all the combinations between input power and speed, presented in table 6.1, was created and a KISSsoft/KISSsys simulation for each of those points was performed. This process was repeated for two lubricants, ISO VG 320 and Castrol Optigear Synthetic X 320, and three oil sump temperatures, 58 °C, 61,5 °C and 65 °C.

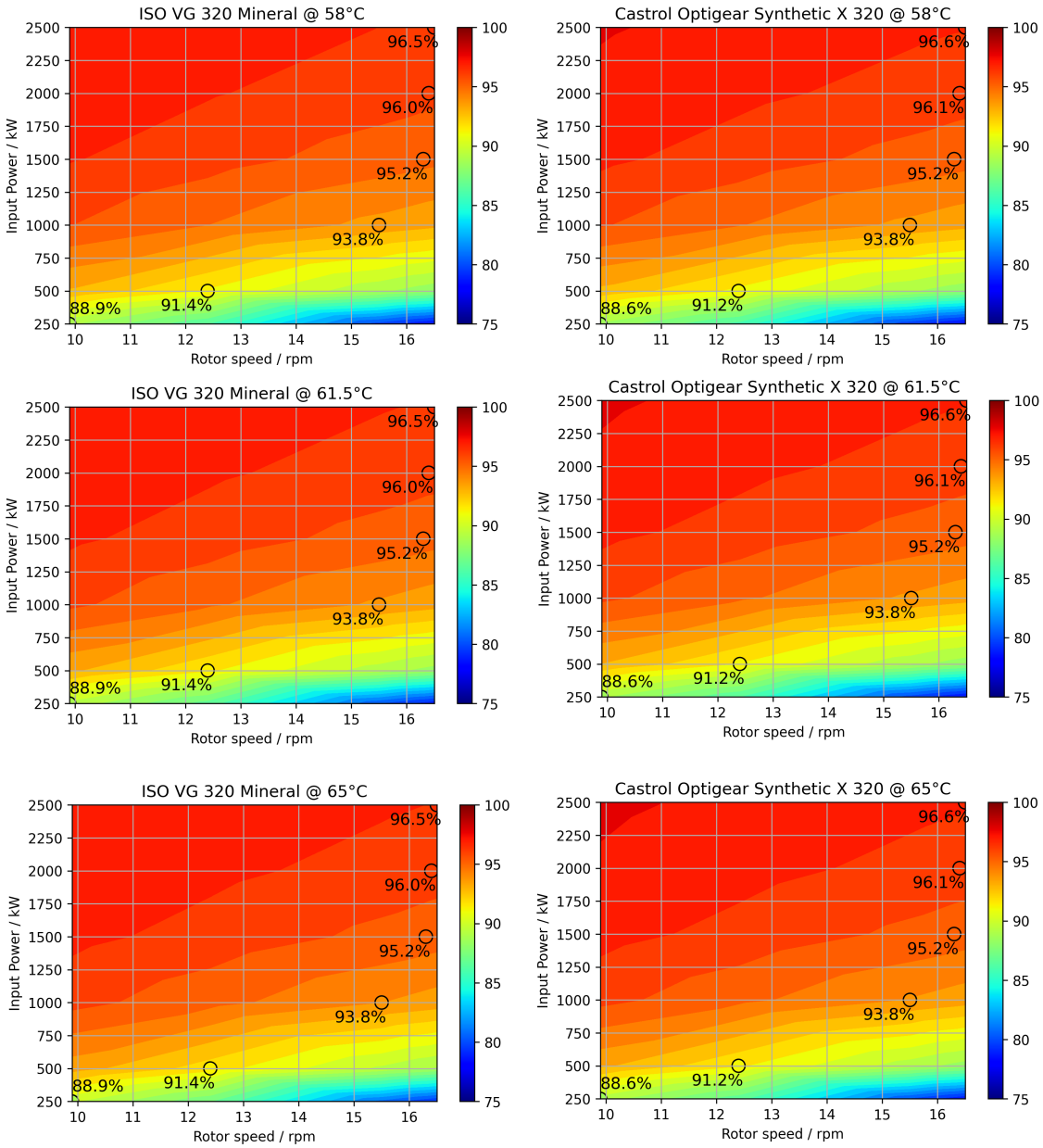


Figure 6.11: Gearbox efficiency maps.

The dark circles in Figure 6.11 represent the efficiency obtained for the correspondent lubricant

and operating conditions on table 6.1. These maps allow to estimate the gearbox efficiency for any operating condition depending on the lubricant and sump temperature.

From Figure 6.11, it can be seen that, for the same input power and speed, higher temperatures lead to higher efficiencies, this is due to the reduction in the lubricant viscosity and consequently lower bearing power loss. Additionally, for the same temperature and input speed, higher input power leads to higher efficiencies, which can be justified by the lower influence of load-independent power losses when compared to the load-dependent ones.

6.2 Thermal Model

In order to perform calculations with the thermal model, several parameters need to be defined. Such as heat transfer coefficients, ambient temperature, emissivity, wall thermal conductivity and even a wall thickness value, which is not constant along the gearbox length.

Considering three thermal zones as defined in Figure 6.12, some of the parameters do not vary regardless of the thermal zone, such as wall thickness which was defined as 0,3 m (mean value between maximum and minimum thickness), wall thermal conductivity defined as 50 $\mathrm{W}/(\mathrm{m}\cdot\mathrm{K})$ as it is a common value among cast iron and there is no information related to the wall material, as well as the emissivity of painted steel, defined as 0,95. For the ambient temperature, a value of 20 °C was assumed with an external heat transfer coefficient of 15 $\mathrm{W}/(\mathrm{m}^2\cdot\mathrm{K})$, since the heat transfer coefficient for air under natural convection may vary from 2,5 to 25 $\mathrm{W}/(\mathrm{m}^2\cdot\mathrm{K})$.

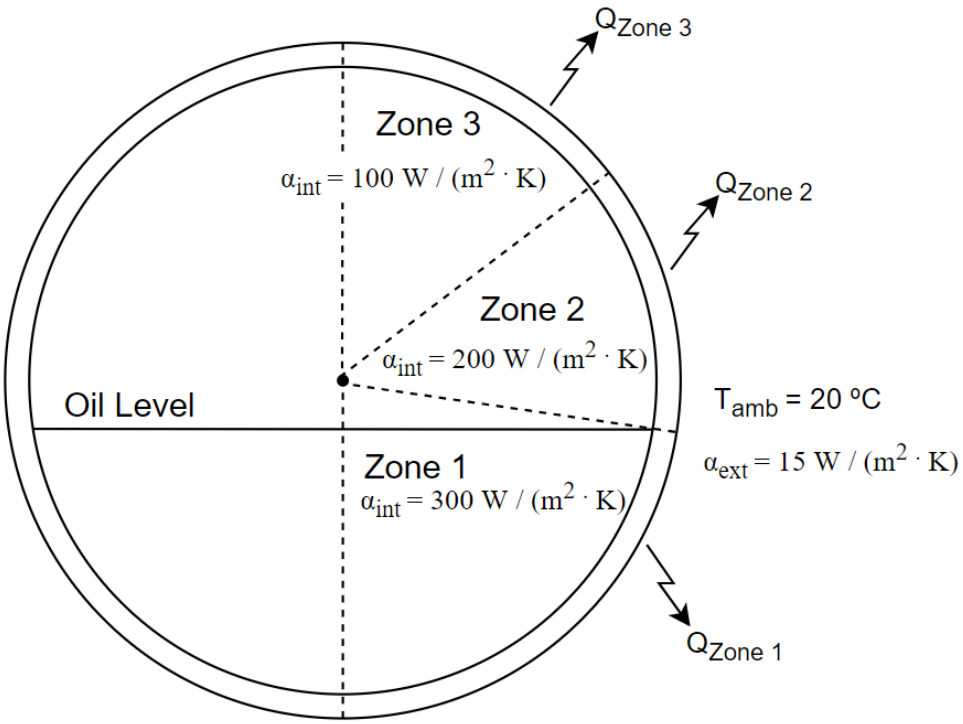


Figure 6.12: Gearbox thermal zones and heat transfer coefficients.

The remaining parameters were defined according to the thermal zone they concern. For the first zone, an internal heat transfer coefficient of 300 $W/(m^2 \cdot K)$ was defined as it is the mean value between the range of 100 $W/(m^2 \cdot K)$ to 500 $W/(m^2 \cdot K)$ obtained by Patil in [43] and the oil sump temperature was assumed as the gearbox interior temperature. Concerning the second zone, the assumed temperature was the same as in the first one, nonetheless a lower heat transfer coefficient is expected due to the presence of air-oil mixture instead of the oil sump, therefore a heat transfer coefficient of 200 $W/(m^2 \cdot K)$ is assumed. For the third and last zone, the temperature was assumed to be 90% of the one expected in the oil sump in order to account for a possible temperature gradient along the gearbox height, the heat transfer coefficient concerning this zone was defined as 100 $W/(m^2 \cdot K)$ as the mixture is expected to contain much more air.

All the previously mentioned values were estimated in order to have a good approximation of what may be the heat dissipated through the gearbox housing. Nonetheless, when further data is available on the gearbox or test conditions, such parameters should be updated in order to provide better predictions. Furthermore, the possibility of applying a correction factor to the final value is allowed by the model, even though for the calculations in this work, the correction factor is considered to be 1.

From the data presented on Table 6.5, it can be expected to have an outside wall temperature on zone 1 around 2,5 °C lower than the oil sump temperature, while on zone 3 this difference is around 11,5 °C.

Table 6.5: Wall temperatures and power dissipated through the gearbox housing.

	Zone 1		**Zone 2**		**Zone 3**		
Oil Sump Temp. °C	$T_{Wall_{Int}}$ °C	$T_{Wall_{Ext}}$ °C	$T_{Wall_{Int}}$ °C	$T_{Wall_{Ext}}$ °C	$T_{Wall_{Int}}$ °C	$T_{Wall_{Ext}}$ °C	Power Dissipated $[W]$
58	56,21	55,88	55,37	55,06	48,03	47,78	26875,98
60	58,11	57,77	57,23	56,90	49,60	49,34	27847,37
62	60,02	59,66	59,09	58,75	51,17	50,89	28824,15
64	61,92	61,55	60,96	60,59	52,73	52,44	29806,37
65	62,88	62,49	61,89	61,51	53,52	53,22	30299,55

Since many of the parameters used to obtain the results on table 6.5 were estimated, it is important to find the sensitivity of the thermal model to variations in such parameters. This type of analysis will help to understand which factors may be causing bigger deviations in the thermal model results and by doing so, allowing to perform more accurate corrections to the parameters.

The data on Figure 6.13 were obtained for an oil sump temperature of 65 °C. The α_{int} parameter concerns the heat transfer coefficient in the interior of the gearbox for zone 1. Furthermore, the parameter deviation is calculated in relation to the input parameters mentioned at the beginning of section 6.2. It is possible to understand the thermal model is much more sensitive to variations

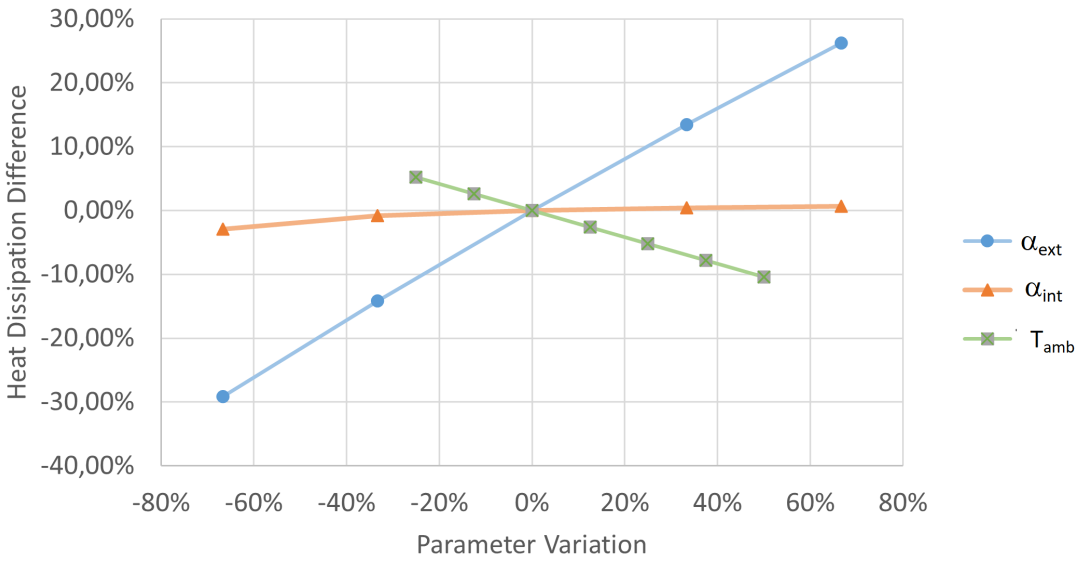


Figure 6.13: Thermal model sensitivity.

in the external heat transfer coefficient than any other parameter. Variations in the internal heat transfer coefficient will result in almost no difference in the amount of heat dissipated through the housing. As for the ambient temperature variation, even though it does not generate differences as big as the ones generated by the external heat transfer coefficient, it still produces significant differences in the amount of heat transferred and should not be overlooked since this parameter can easily oscillate.

From the difference between power dissipated through the housing, presented on Table 6.5, and the total power loss for the correspondent operating condition, the amount of power dissipated in the oil cooler can be calculated. In addition, it is known the cooler is not activated for the first and second operating conditions. For conditions 3 to 5, the first speed of the cooler (oil flow - 53 l/min) is expected to work, while the second speed (oil flow - 105 l/min) will only be activated for the last operating condition, according to the information obtained concerning the application of the gearbox under study. With such information, it is possible to predict lubricant temperature at the time it gets out of the cooler into the sump (inlet temperature). Also, lubricant temperature on the sump is imposed by the operating condition. Furthermore, the operating temperature range correspondent to each of the intercooler's speeds is also known. Therefore, it is possible to obtain the lubricant temperatures at the time it gets out of the sump into the cooler (outlet temperature), as shown in Figure 6.14 for the mineral oil and Figure 6.15 for the PAO.

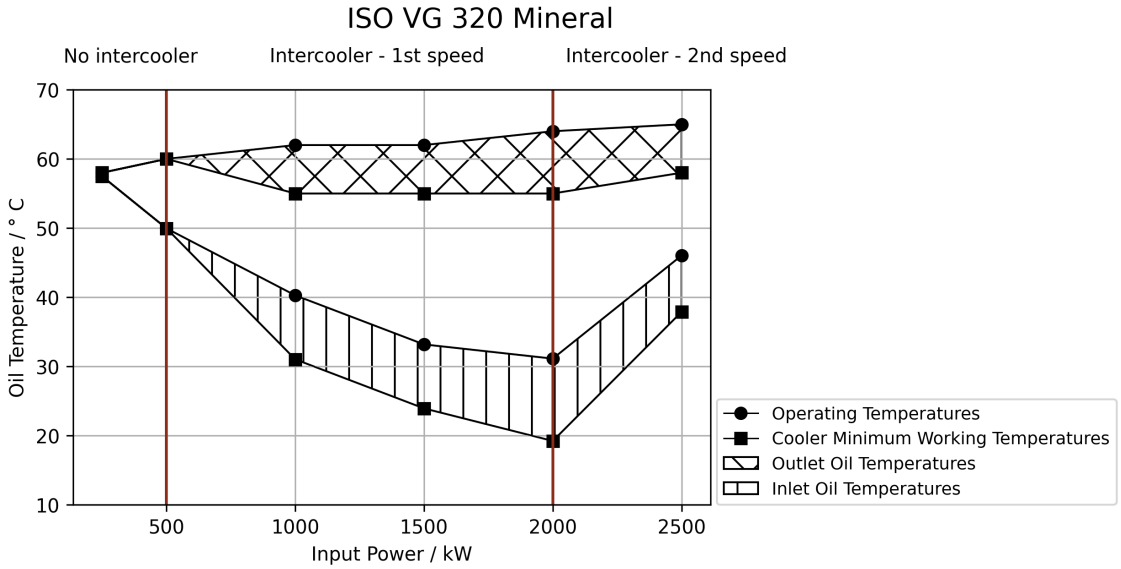


Figure 6.14: Oil temperature fluctuation, mineral oil.

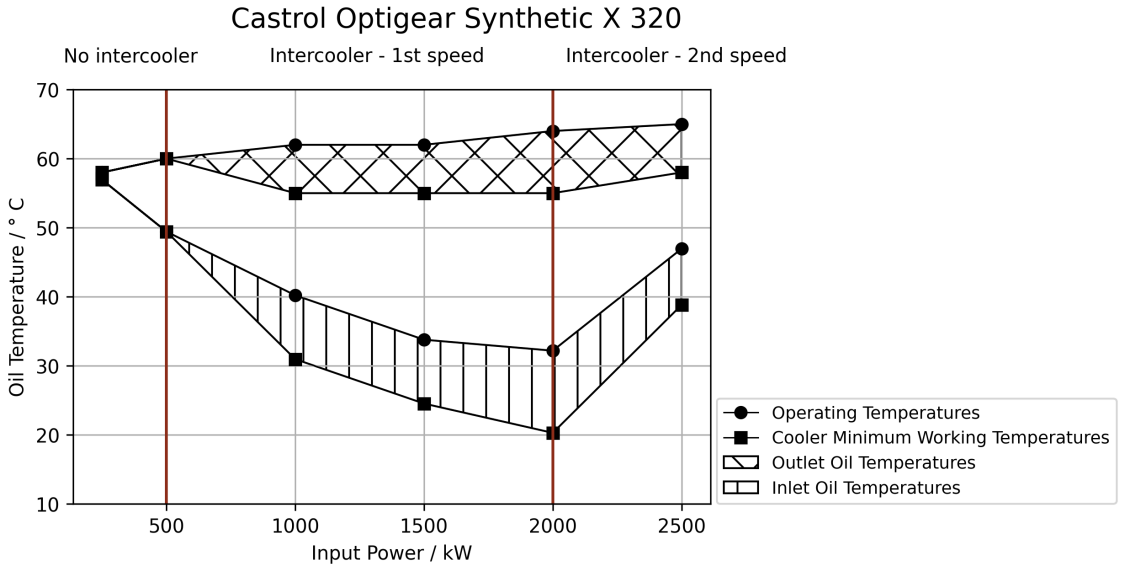


Figure 6.15: Oil temperature fluctuation, synthetic oil.

It can be observed, from figures 6.14 and 6.15, that even though the temperature fluctuation for the PAO oil is slightly smaller than the one observed for the mineral oil, the variation in the region of the intercooler's first speed is around 30 °C to 40 °C. When compared to the 10 °C to 20 °C observed for the second speed region.

In order to avoid such high temperature variation, a higher oil flow should be used. An hypothetical situation, where only the second speed is used, could result in smaller fluctuations as

shown in figures 6.16 and 6.17. From these figures, it is possible to understand that a higher oil flow could produce temperature variations under 20 °C for all the operating range considered.

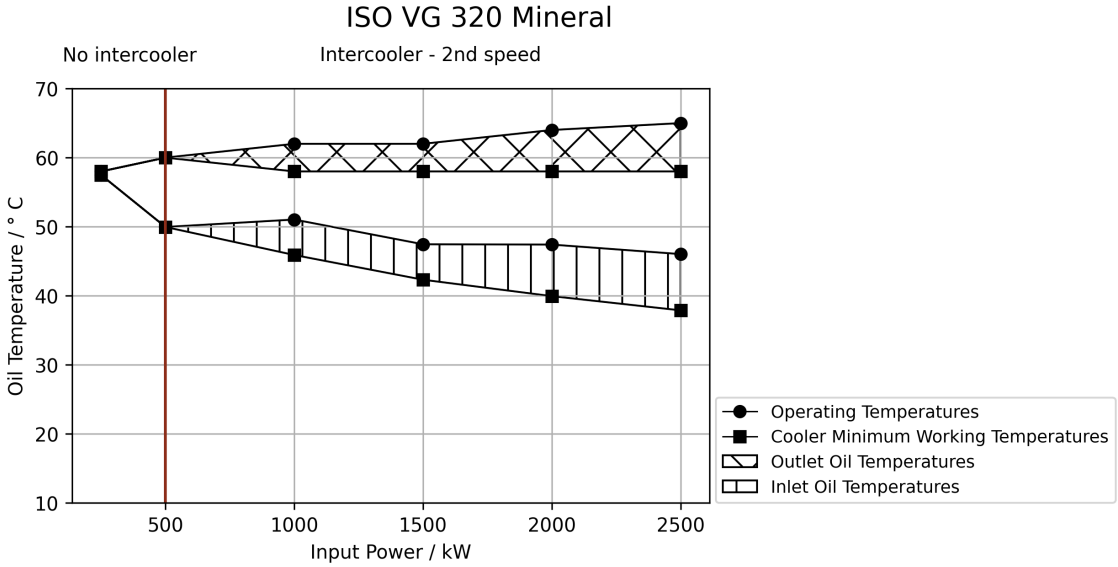


Figure 6.16: Oil temperature fluctuation using the cooler second speed, mineral oil.

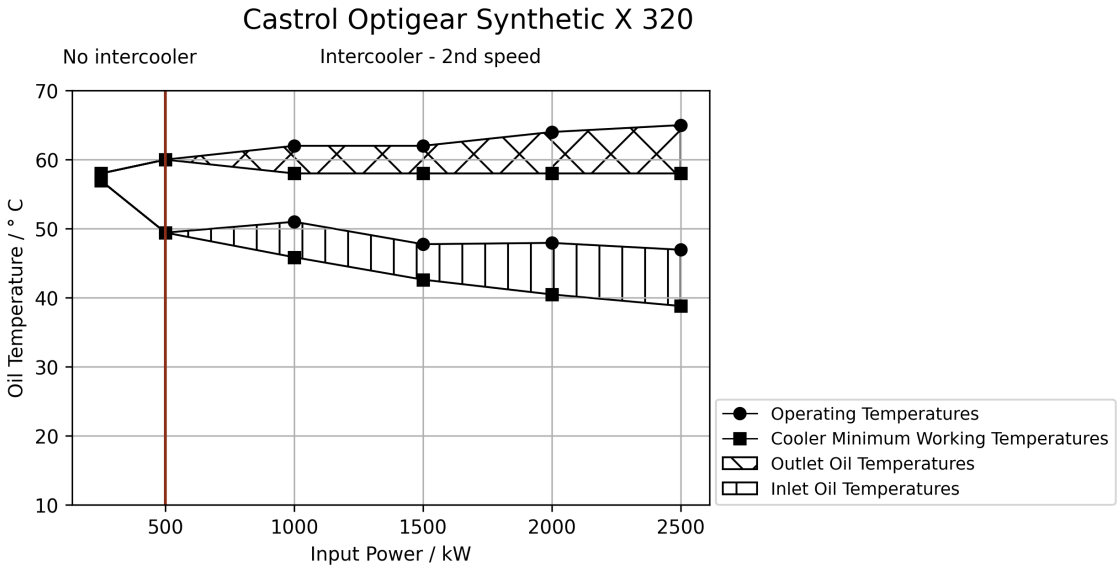


Figure 6.17: Oil temperature fluctuation using the cooler second speed, synthetic oil.

Finally, it is possible to obtain the percentage of heat dissipated by each source in every operating condition, as shown in Figure 6.18. In this figure, it is possible to see that a small percentage of heat dissipated by the "oil cooler" is represented for the first and second operating conditions. This

dissipative source represents the heat dissipated by the lubricant in the oil circuit when pumped by the mechanical pump, since the intercooler is not active for this operating condition.

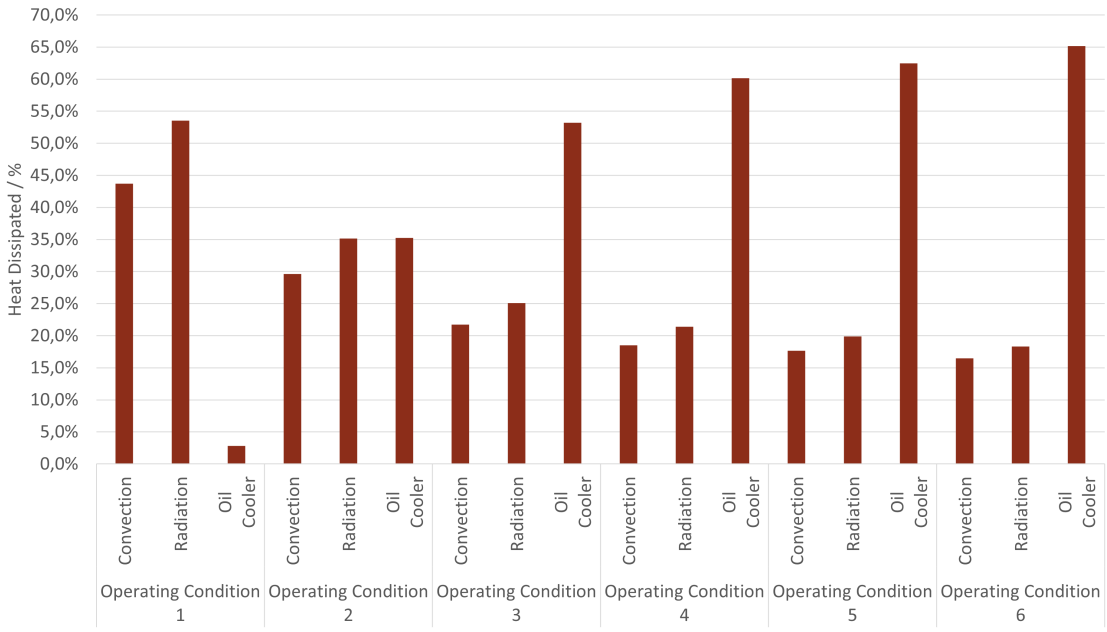


Figure 6.18: Percentage of heat dissipated per source and operating condition.

From Figure 6.18, it is also possible to understand that the oil cooler plays an increased role for operating conditions with higher input power and speed. This source shows its higher participation in operating condition 6 with 65,2 % of the heat dissipated by the oil cooler.

6.3 Bulk Temperatures

6.3.1 Gear Bulk Temperatures

From the model implemented in Excel it is possible to obtain data concerning gear bulk temperature calculated using the flash temperature method, as well as the integral temperature method.

These models were used to perform calculations concerning the sun-planet gear pair of the first stage, under 2,5 MW at 16 rpm, with the oil sump at 64 °C. For the flash temperature method, the differences obtained between the Excel and KISSsoft/KISSsys calculations, with the same input conditions, were around 7% for the average flash temperature and highest contact temperature. While for the bulk temperature, a deviation under 1% was achieved, as shown in section 5.5.1. Analysing the integral temperature method, it can be seen the differences were even lower, with a difference around 5% for the mean flash temperature and 1% for the integral temperature or even lower for the bulk temperature with 0,55%.

Such deviations, are essentially related to the equations used in the calculation of the mean coefficient of friction, similar to what happens in the gear power loss case.

Furthermore, from the flash temperature method implemented in Excel, it is possible to obtain the flash temperature distribution along the path of contact as shown in Figure 6.19.

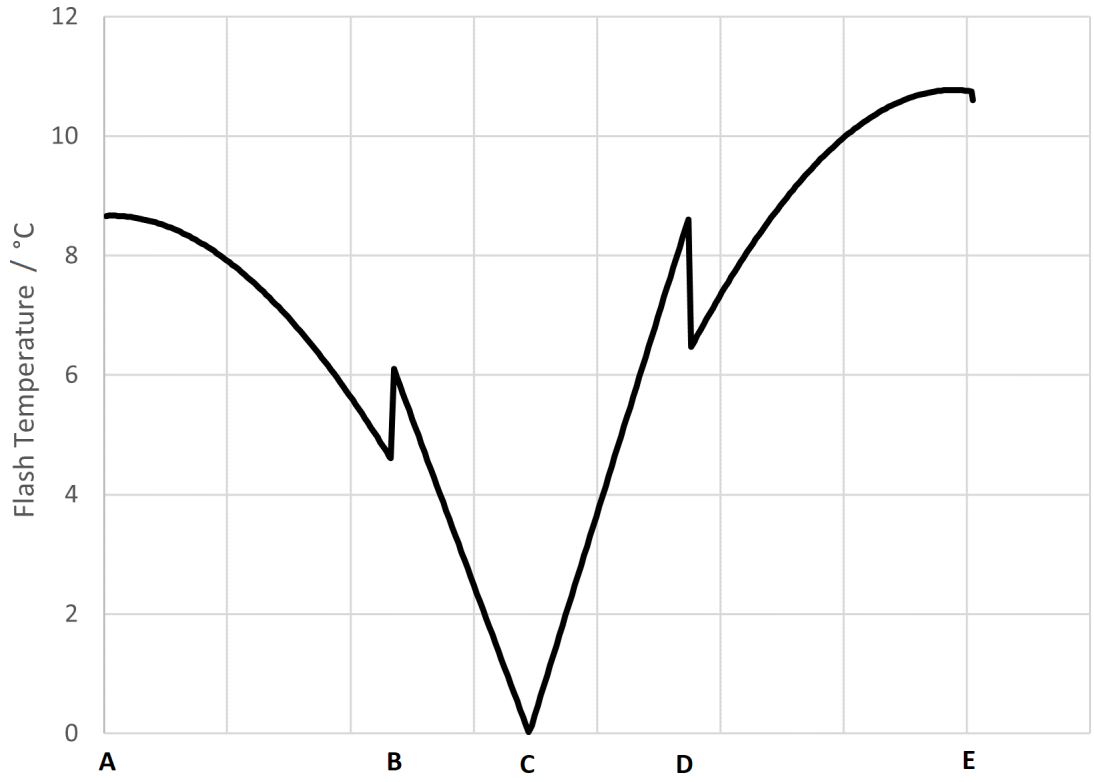


Figure 6.19: Flash temperature distribution along the path of contact for sun-planet gear pair of the first stage.

From KISSsoft/KISSsys model, it is possible to calculate gear bulk temperature using both methods. Since the values obtained using the flash temperature method are slightly higher, these are the ones shown in figures 6.20 and 6.21.

Comparing figures 6.20 and 6.21, it is possible to understand the mineral oil produces slightly higher gear bulk temperatures for the same conditions. This goes according to expected, due to the fact that a higher X_L value for the mineral oil produces a higher mean coefficient of friction, hence gear load dependent losses are higher, as previously shown. Consequently, gear bulk temperatures are also higher for this lubricant.

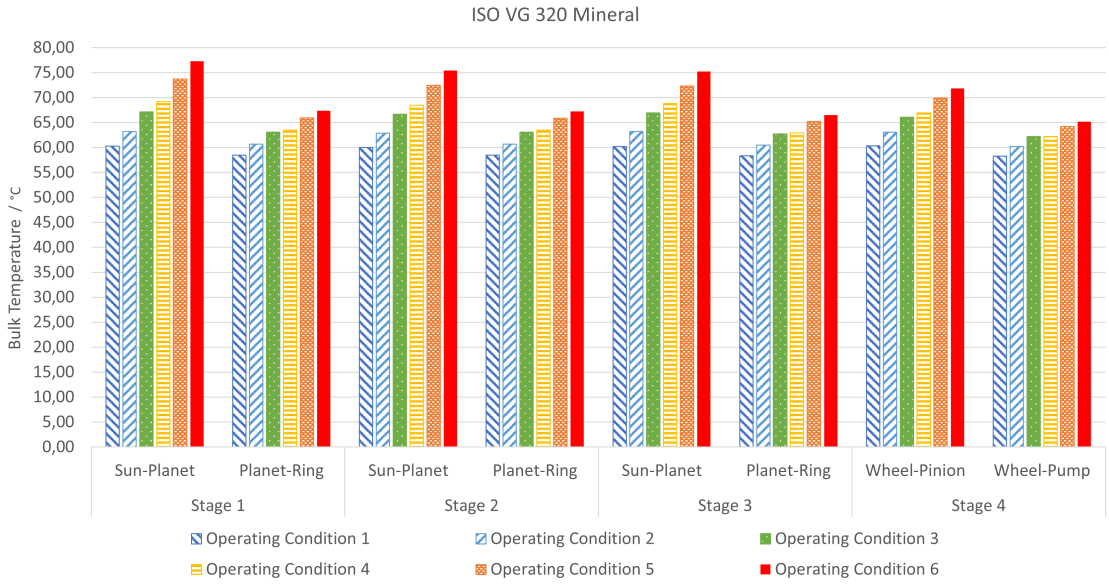


Figure 6.20: Gear bulk temperatures calculated with the flash temperature method, mineral oil lubricated.

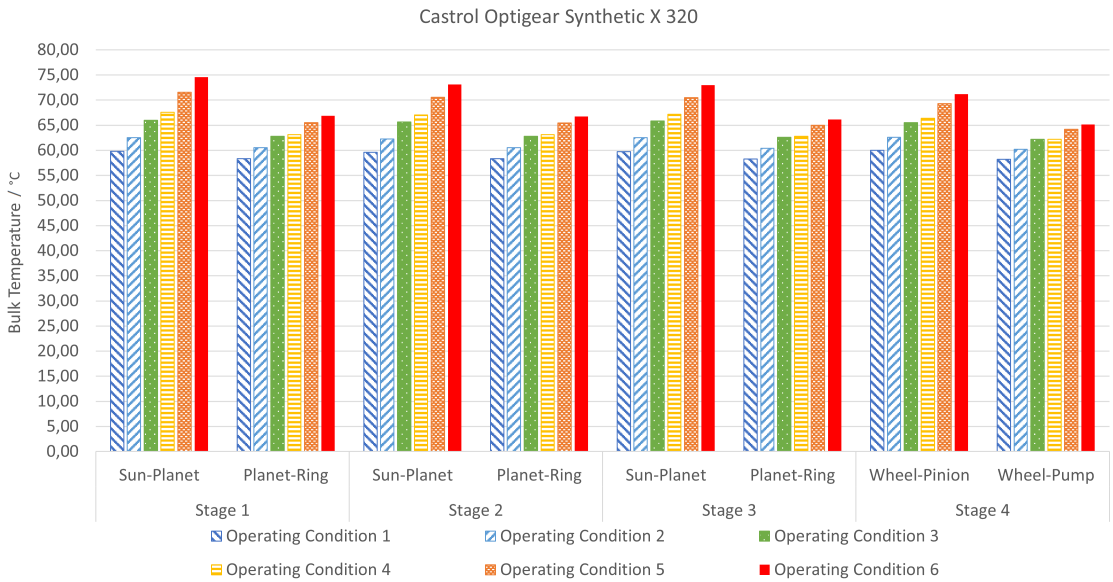


Figure 6.21: Gear bulk temperatures calculated with the flash temperature method, PAO oil lubricated.

Additionally, from KISSsoft/KISSsys model, it is possible to obtain the highest contact temperature for each gear pair in this gearbox. Figure 6.22 presents these temperatures obtained using a mineral lubricant, while Figure 6.23 shows the results obtained with a PAO lubricant.

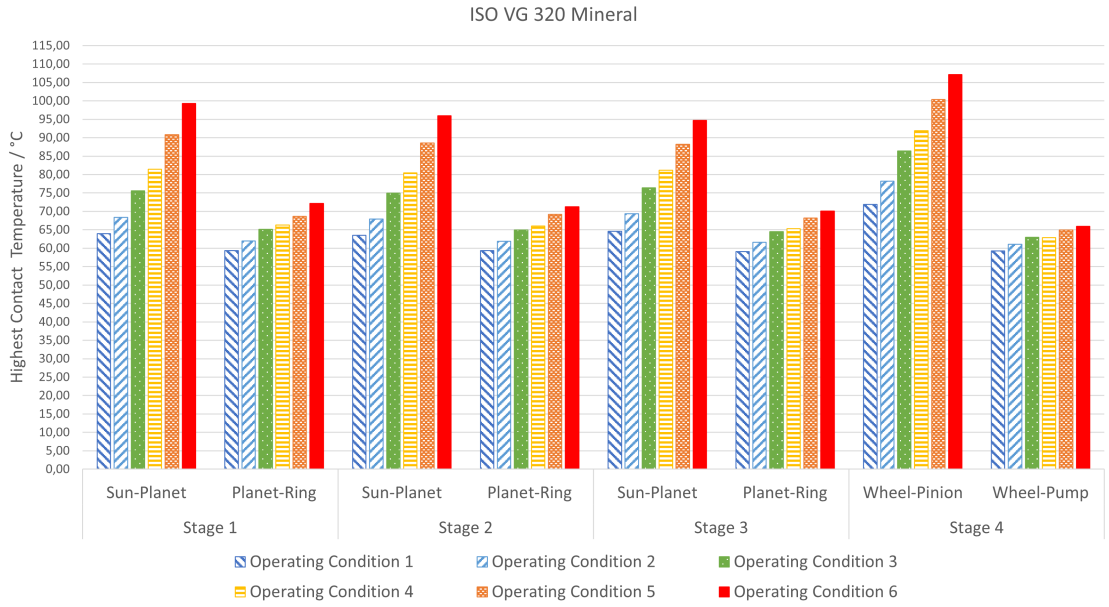


Figure 6.22: Highest contact temperature per gear pair and operating condition, mineral oil lubricated.

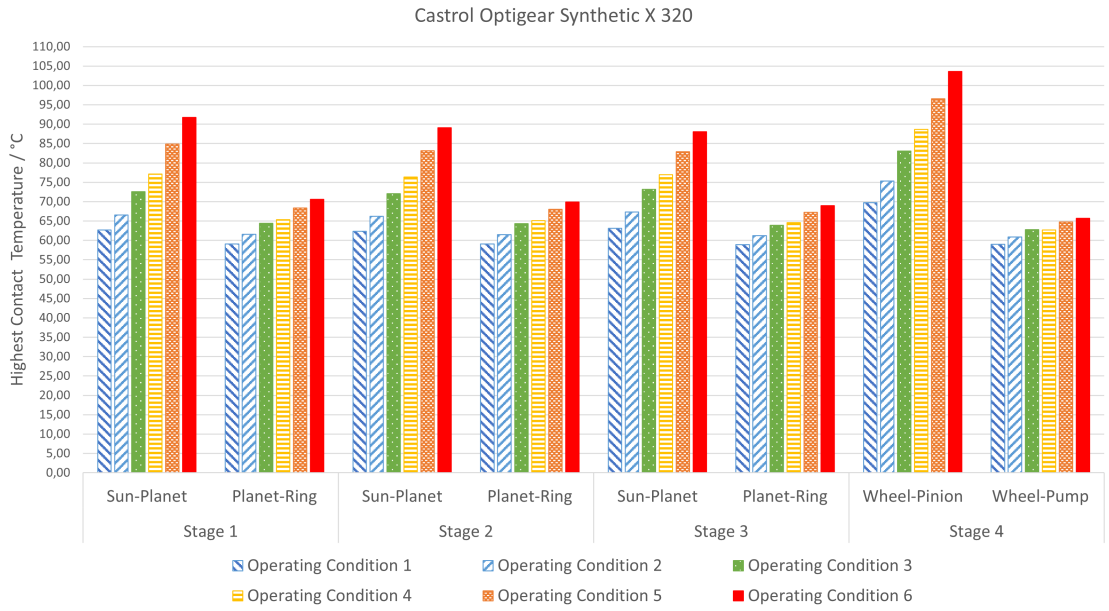


Figure 6.23: Highest contact temperature per gear pair and operating condition, PAO oil lubricated.

6.3.2 Bearing Bulk Temperatures

From bearing bulk temperature model it is possible to obtain data concerning bearing temperatures for several operating conditions, as shown in Figure 6.24.

Interesting enough, for most bearings in this gearbox regardless of the operating condition, convective heat transfer will have almost no influence. This is due to the fact that conduction heat transfer, in most cases, is enough to dissipate a big percentage of the power lost by the bearing, meaning the convective heat transfer will have small influence in bearing temperature.

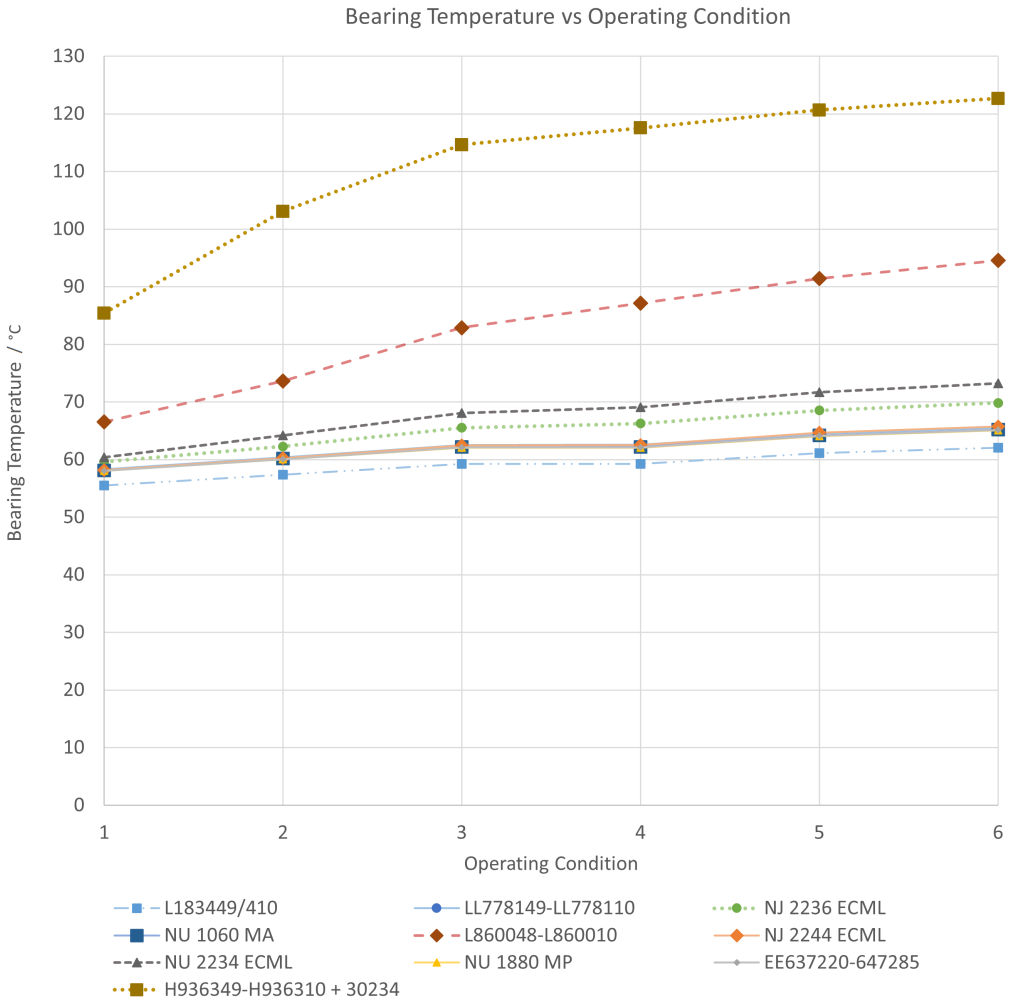


Figure 6.24: Bearing temperature for the six different operating conditions.

As an exception to this rule, there are four bearings. The first of which is the planet pin bearing on stage 3, "SKF NJ 2236 ECML". Followed by three more bearings on stage 4, "Timken L860048-L860010", "SKF NU 2234 ECML" and the set of tapered bearings "Timken H936349-H936310 + SKF 30234". These four bearing present higher power loss than the remaining ones. Their power loss is enough that the oil flow on such bearings will influence their temperature. Consequently, the thermal calculations regarding these four bearings were performed considering the oil flow was maximum.

From Figure 6.24, it possible to understand even though these four bearings show higher temperatures than the remaining ones, the set of tapered bearings on the fourth stage excels with much

higher temperatures than any other one. Furthermore, it can be seen that regardless of the bearing, the higher temperatures are reached for operating condition 6, as expected.

Figure 6.25, highlights the temperature differences in the bearings for operating condition 6.

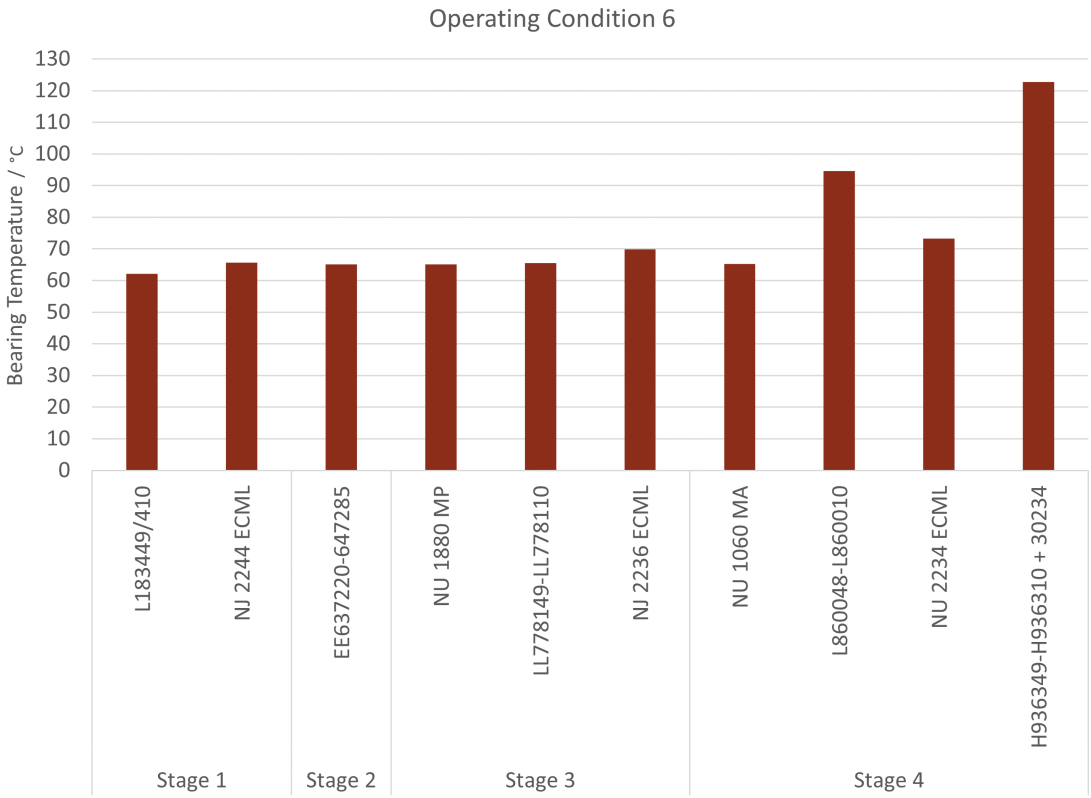


Figure 6.25: Bearing temperature for the sixth operating condition.

Additionally, it is possible to understand the set of tapered bearings in the fourth stage is the critical element regarding operating temperatures.

Since there are no experimental measurements concerning power loss or even certainty regarding the oil flow on this bearing, and its temperature already appears to be alarming, it is pertinent to analyse the temperature variation depending on a power loss ratio, relative to the bearing power loss on operating condition 6, and the oil flow on this bearing.

From Figure 6.26, it is possible to understand if the oil flow is slightly lower than the maximum flow calculated (3,5 L/min), or even if the power loss is higher than the one predicted by the model, the bearing temperature might reach critical values.

Equally important to note is the fact that Timken [56] admits that standard tapered roller bearings are dimensionally stabilized up to 120 °C. Nonetheless, upon request these bearings can be ordered to higher levels of stability, achieving maximum operating temperatures up to 350 °C, if needed.

The fact that the bearing in the output shaft of this gearbox (represented in the model by

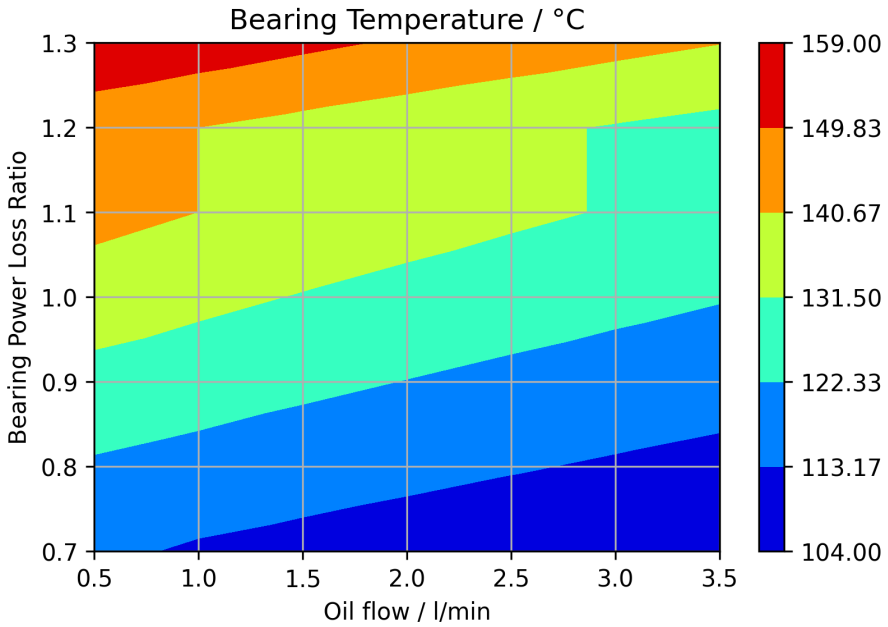


Figure 6.26: Temperature variation for set of tapered bearings "Timken H936349-H936310 + SKF 30234".

Timken H936349-H936310) has no standard dimensions, leads to the assumption it was exclusively made to this application and a special request regarding its operating temperature could have been made.

Nonetheless, based on information provided by the gearbox manufacturer, it is known the gearbox's functions are shut down whenever this bearing reaches the temperature of 95 °C. This information can be interpreted in different ways: either the gearbox does not work under conditions that lead to temperatures above 95 °C long enough for this temperature to be reached in the bearing; or the model used for the calculation of bearing bulk temperature, which is still not experimentally validated, still needs to be adjusted. The possibilities for such adjustment may lie in finding the oil flow in this bearing under real operating conditions and performing adjustments in the constant used in equation (3.45); there is also the possibility that the bearing power loss is not as high as the one predicted, since the SKF's model tends to overestimate the power loss as previously demonstrated in this work, in the beginning of section 6.1.2.

Chapter 7

Conclusions and Future Work

7.1 Conclusions

The main goal of this dissertation was to develop a power loss model for a 2.5 MW Bosch Rexroth multiplier gearbox so, the key objectives of this dissertation were achieved.

Data concerning gearbox's elements was successfully obtained through a reverse engineering process, consequently allowing the implementation of an accurate model based on very scarce initial data.

The gearbox model was implemented with success using KISSsoft/KISSsys, considering all the relevant components for the power loss calculation. Also, this model allows the user to easily input any desired operating condition in order to perform the calculations needed. Power losses correspondent to all components, including seals which had to be programmed in the software, are part of the output.

Furthermore, numerous additional models were implemented in Microsoft Office Excel, either for result comparison or in order to perform additional predictions that were not possible to be made via KISSsoft/KISSsys.

From the study of the results obtained via power loss models, it is expected mineral lubricants will produce higher gear load-dependent power loss regardless the operating condition. Despite this, lower overall power loss for operating conditions with lower input speed and power are expected for this lubricant. In contrast, for conditions of high input speed and power, PAO lubricants appear to have a better performance. Nonetheless, this second group of lubricants are expected to produce higher bearing power loss.

Finally, concerning temperature calculation, several relevant results were obtained regarding wall, lubricant, gear and bearing temperature for different operating conditions. Moreover, suggestions to improve gearbox operation, such as minimizing lubricant temperature fluctuation were made. The critical element, concerning operating temperatures, appears to be the set of tapered bearings in the pinion shaft of the fourth gear stage. Its temperature was carefully predicted for several conditions and concluded that close attention should be paid to this element, specially under more extreme operating conditions.

7.2 Future Work

This dissertation presents a model capable of predicting power loss on a complex gearbox. This could, ideally, eliminate the need for expensive and time consuming experimental tests, as well as help in the development of further projects with higher efficiencies. In order to improve the accuracy of predictions made by this model, it would be important to:

- Implement more specific models in order to predict the churning losses in planetary gears, such as Boni's [25];
- Use more complex models for seal losses prediction, capable of accounting for several more factors that may influence this type of losses, such as Organisciak's [42];
- Adjust the selected factors in the heat dissipation model, such as heat transfer coefficients;
- Apply equations to the heat dissipation model capable of accounting for the air-oil mixture, eliminating the need to split the gearbox in different zones or make assumptions related to the heat transfer coefficients;
- Perform additional calculations concerning lubricant film thickness in the gearbox machine elements;
- Obtain experimental power loss and temperature results, allowing to validate the whole model.

Bibliography

[1] Bhaba R. Sarker and Tasnim Ibn Faiz. Minimizing maintenance cost for offshore wind turbines following multi-level opportunistic preventive strategy. *Renewable Energy*, 85:104–113, 2016.

[2] S. Hur and W. E. Leithead. Collective control strategy for a cluster of stall-regulated offshore wind turbines. *Renewable Energy*, 85:1260–1270, 2016.

[3] Yonggang Lin, Le Tu, Hongwei Liu, and Wei Li. Fault analysis of wind turbines in China. *Renewable and Sustainable Energy Reviews*, 55:482–490, 2016.

[4] Asaf Varol, Cumali Ilkiliç, and Yasin Varol. Increasing the efficiency of wind turbines. *Journal of Wind Engineering and Industrial Aerodynamics*, 89(9):809–815, 2001.

[5] Ali Mostafaeipour. Productivity and development issues of global wind turbine industry. *Renewable and Sustainable Energy Reviews*, 14(3):1048–1058, 2010.

[6] International Energy Association (IEA). International Energy Association Wind TCP, Annual Report 2019. 2019.

[7] International Energy Association (IEA). International Energy Association Wind TCP, Portugal Annual Report 2019, 2019.

[8] R. H. Crawford. Life cycle energy and greenhouse emissions analysis of wind turbines and the effect of size on energy yield. *Renewable and Sustainable Energy Reviews*, 13(9):2653–2660, 2009.

[9] Carlos M.C.G. Fernandes, Luis Blazquez, Jorge Sanesteban, Ramiro C. R.C. C Martins, and Jorge H.O. Seabra. Energy efficiency tests in a full scale wind turbine gearbox. *Tribology International*, 101:375–382, sep 2016.

[10] B. R. Höhn and K. Michaelis. Influence of oil temperature on gear failures. *Tribology International*, 37(2):103–109, 2004.

[11] B.-R. R Höhn, Klaus Michaelis, and T Völlmer. Thermal Rating of Gear Drives Balance Between Power Loss and Heat Dissipation. *AGMA Technical Paper*, 96:12, 1996.

[12] C. Changenet and P. Velex. Housing influence on churning losses in geared transmissions. *Journal of Mechanical Design, Transactions of the ASME*, 130(6):0626031–0626036, 2008.

[13] Klaus Michaelis, Bernd Robert Höhn, and Michael Hinterstoißer. Influence factors on gearbox power loss. *Industrial Lubrication and Tribology*, 63(1):46–55, 2011.

[14] Carlos M.C.G. Fernandes. *Power Loss in Rolling Bearings and Gears Lubricated With Wind Turbine Gear Oils*. PhD thesis, Faculdade de Engenharia da Universidade do Porto, 2015.

[15] Carlos M.C.G. Fernandes, Maroua Hammami, Ramiro C. Martins, and Jorge Ho Seabra. Power loss prediction: Application to a 2.5 MW wind turbine gearbox. *Proceedings of the Institution of Mechanical Engineers, Part J: Journal of Engineering Tribology*, 230(8):983–995, aug 2016.

[16] J. W. Daily and R. E. Nece. Chamber dimension effects on induced flow and frictional resistance of enclosed rotating disks. *Journal of Fluids Engineering, Transactions of the ASME*, 82(1):217–230, 1960.

[17] Robert W. Mann and Charles H. Marston. Friction drag on bladed disks in housings as a function of reynolds number, axial and radial clearance, and blade aspect ratio and solidity. *Journal of Fluids Engineering, Transactions of the ASME*, 83(4):719–723, 1961.

[18] AS Terekhov. Hydraulic losses in gearboxes with oil immersion. *Russian Engineering Journal*, 55(5):7–11, 1975.

[19] P. Walter. *Anwendungsgrenzen für die Tauchschmierung von Zahnradgetrieben, Plansch- und Quetschverluste bei Tauchschmierung: Abschlußbericht; Berichtszeitraum 1976*. Forschungsvereinigung Antriebstechnik eV, 1982.

[20] E. Lauster and M. Boos. Zum wärmehaushalt mechanischer schaltgetriebe für nutzfahrzeuge. *VDI-Berichte*, (488):45–55, 1983.

[21] W. Mauz. Zahnradschmierung—leerlaufverluste. *FVA-Forschungsheft*, 185, 1985.

[22] R. J. Boness. Churning losses of discs and gears running partially submerged in oil. In *Proceedings of the ASME International Power Transmission and Gearing Conference*, volume 1, pages 355–359. Chicago, 1989.

[23] C. Changenet, G. Leprince, F. Ville, and P. Velex. A note on flow regimes and churning loss modeling. *Journal of Mechanical Design, Transactions of the ASME*, 133(12):1–5, 2011.

[24] Jean-baptiste Boni, C Changenet, and Fabrice Ville. A model for predicting churning losses in planetary gears. *Power Transmission Engineering*, (August):62–66, 2019.

[25] Jean-Baptiste Boni, Christophe Changenet, and Fabrice Ville. Analysis of flow regimes and associated sources of dissipation in splash lubricated planetary gear sets. *Journal of Tribology*, pages 1–22, 2021.

[26] ISO TR 14179-2. *Gears - Thermal capacity - Part 2: Thermal load-carrying capacity*. 2001.

[27] Earle Buckingham. *Analytical mechanics of gears*. Courier Corporation, 1988.

[28] H. Ohlendorf. *Verlustleistung und erwärmung von stirnrädern*. PhD thesis, Technische Universität München, 1958.

[29] Carlos M.C.G. Fernandes, Pedro M.T. T Marques, Ramiro C. Martins, and Jorge H.O. Seabra. Gearbox power loss. Part II: Friction losses in gears. *Tribology International*, 88:309–316, aug 2015.

[30] Carlos M.C.G. Fernandes, Pedro M.T. Marques, Ramiro C. Martins, and Jorge H.O. Seabra. Gearbox power loss. Part III: Application to a parallel axis and a planetary gearbox. *Tribology International*, 88:317–326, aug 2015.

[31] H. E. Merritt. *Gear Engineering*. London: Pitman, 1971.

[32] G. Henriot. *Traité théorique et pratique des engrenages: Theory and technology*, volume 1. Dunod, 1978.

[33] Gustav Niemann and Hans Winter. *Maschinenelemente*. Springer Berlin Heidelberg, Berlin, Heidelberg, 2003.

[34] P. Velex and F. Ville. An analytical approach to tooth friction losses in spur and helical gears-influence of profile modifications. *Journal of Mechanical Design, Transactions of the ASME*, 131(10):1010081–10100810, 2009.

[35] A. J. Wimmer. Lastverluste von stirnradverzahnungen. *Konstruktive einfüsse, wirkungsgradmaximierung, tribologie, Fakultät für Maschinenwesen der Technischen Universität München*, 2006.

[36] K. Michaelis. *Die Integraltemperatur zur Beurteilung der Fresstragfähigkeit von Stirnradgetrieben*. PhD thesis, Technische Universität München, 1987.

[37] L Schlenk. *Unterscuchungen zur Fresstragfahigkeit von Grozahnradern*. PhD thesis, Dissertation TU Munchen, Germany, 1994.

[38] SKF. The SKF model for calculating the frictional moment. *SKF*, 2017.

[39] Carlos M.C.G. Fernandes, Pedro M.T. Marques, Ramiro C. Martins, and Jorge H.O. Seabra. Gearbox power loss. Part I: Losses in rolling bearings. *Tribology International*, 88(0):298–308, aug 2015.

[40] Heinz Linke et al. *Stirnradverzahnung*. Hanser München Wien, 1996.

[41] J Kettler. *Ölsumpftemperatur von Planetengetrieben: Abschlußbericht; Forschungsvorhaben Nr. 313: Planetengetriebe-Sumpftemperatur*. FVA, 2002.

[42] Michel Organisciak, Pieter Baart, and Alex Paykin. Theoretical and experimental study of the frictional losses of radial shaft seals for industrial gearbox. *American Gear Manufacturers Association Fall Technical Meeting 2014, FTM 2014*, (June):154–165, 2014.

[43] Pravin P. Patil and Ashwani Kumar. Dynamic Structural and Thermal Characteristics Analysis of Oil-Lubricated Multi-speed Transmission Gearbox: Variation of Load, Rotational Speed and Convection Heat Transfer. *Iranian Journal of Science and Technology - Transactions of Mechanical Engineering*, 41(4):281–291, 2017.

[44] H. Blok. The flash temperature concept. *Wear*, 6(6):483–494, nov 1963.

[45] N. Anifantis and A. D. Dimarogonas. Flash and bulk temperatures of gear teeth due to friction. *Mechanism and Machine Theory*, 28(1):159–164, 1993.

[46] ISO TR-13989-1:2000. Calculation of scuffing load capacity of cylindrical, bevel and hypoid gears - Part 1: Flash temperature method.

[47] ISO TR-13989-2:2000. Calculation of scuffing load capacity of cylindrical, bevel and hypoid gears - Part 2: Integral temperature method.

[48] ISO 6336-1:2019. Calculation of load capacity of spur and helical gears - Part 1: Basic principles, introduction and general influence factors. 2019.

[49] SKF. Rolling Bearings Catalogue. *SKF*, pages 1–1722, 2018.

[50] Schaeffler. INA, FAG Rolling Bearing Catalogue. *Schaeffler*, 2014.

[51] DIN 780-1. Series of Modules for Gears. 1977.

[52] Pedro M.T. Marques. *Power Loss in planetary Gearboxes including the Influence of Gear Elastic and Dynamic Effects*. PhD thesis, Faculdade de Engenharia da Universidade do Porto, 2017.

[53] KISSsoft. *KISSsys 03/2014 - Tutorial 2. One Stage Planetary Gearbox*. 2014.

[54] Carlos M.C.G. Fernandes, Ramiro C. Martins, and Jorge H.O. Seabra. Torque loss of type C40 FZG gears lubricated with wind turbine gear oils. *Tribology International*, 70(0):83–93, feb 2014.

[55] RICKMEIER. Data Sheet - Gear Pumps R4.5/35 to R6.0/160 UNI. Technical report, RICKMEIER GmbH, 2020.

[56] Timken. Tapered Roller Bearing Catalog. *Timken*, 2016.

Appendix A

Sliding Speed Distributions

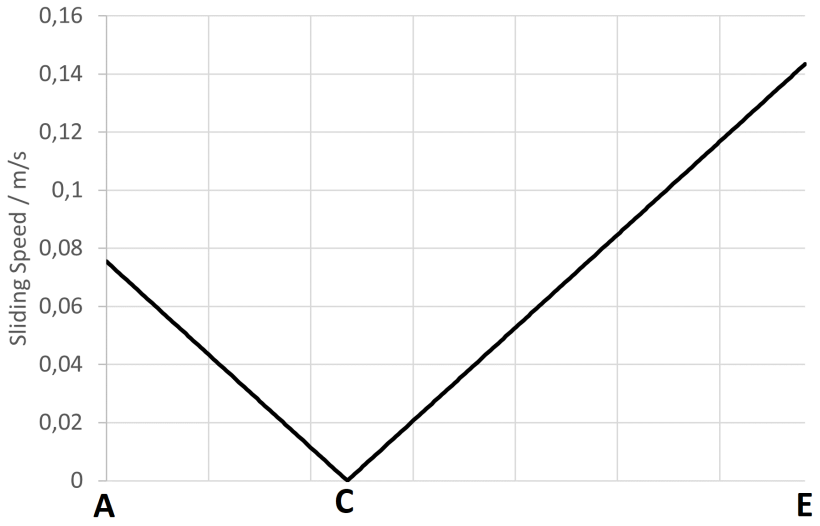


Figure A.1: Sliding speed distribution along the path of contact of the planet-ring gear pair - first planetary stage.

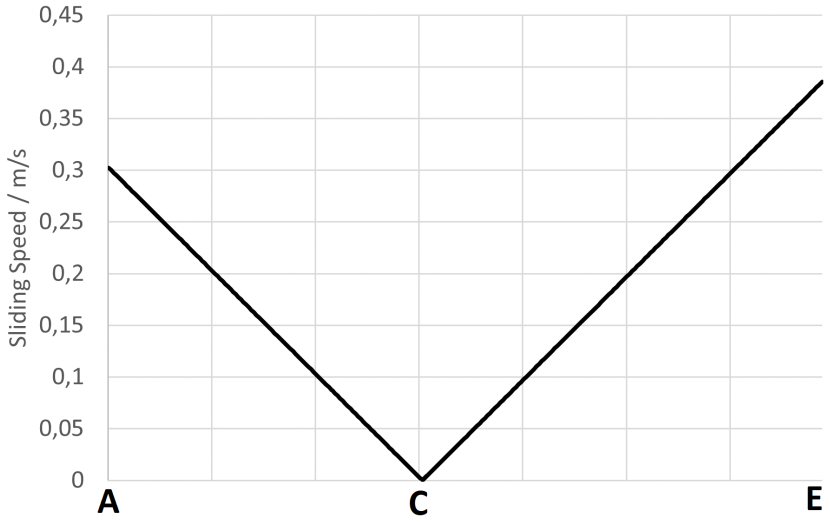


Figure A.2: Sliding speed distribution along the path of contact of the sun-planet gear pair - second planetary stage.

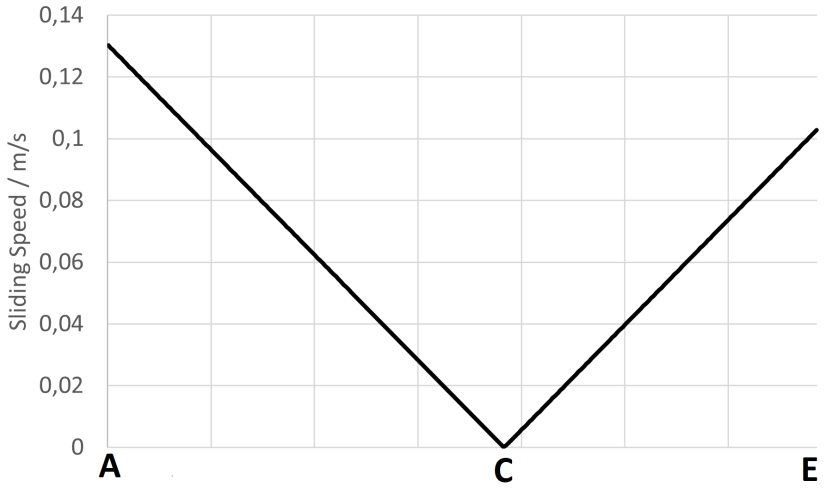


Figure A.3: Sliding speed distribution along the path of contact of the planet-ring gear pair - second planetary stage.

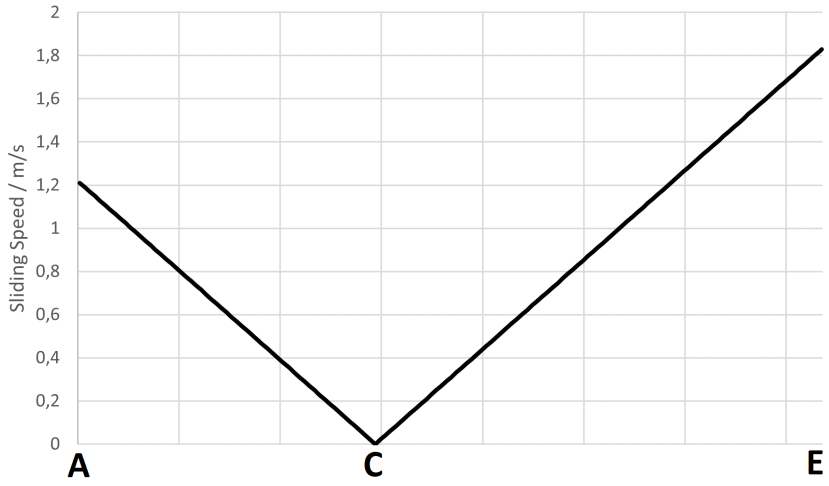


Figure A.4: Sliding speed distribution along the path of contact of the sun-planet gear pair - third planetary stage.

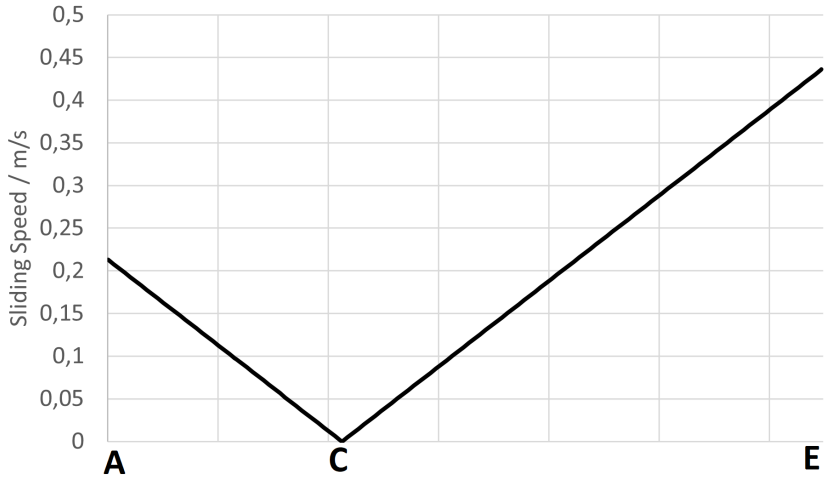


Figure A.5: Sliding speed distribution along the path of contact of the planet-ring gear pair - third planetary stage.

Appendix B

KISSsoft Reports

KISSsoft

KISSsoft Release 2020 A.1

KISSsoft University license - Universidade do Porto

File

Name : Unnamed
Changed by: Rui on: 28.06.2021 at: 20:43:52

First Planetary Stage

Calculation of a spur planetary gear stage

Drawing or article number:					
Gear 1:	0.000.0				
Gear 2:	0.000.0				
Gear 3:	0.000.0				
Calculation method	ISO 6336:2019				
		------- Sun	---------- Planets	---------- Internal gear ---	
Number of planets	[p]	1	3	1	
Power (kW)	[P]	963.168			
Speed (1/min)	[n]	70.1		0.0	
Speed difference for planet bearing calculation (1/min)		[n2]	47.5		
Speed planet carrier (1/min)	[nSteg]	16.3			
Torque (Nm)	[T]	131225.2	0.0	433043.1	
Torque Pl.-Carrier (Nm)	[TSteg]	564268.289			
Application factor	[KA]	1.00			
Distribution factor	[Kγ]	1.00			
Required service life (h)	[H]	20000.00			
Gear driving (+) / driven (-)		-	+/-	+	
Working flank gear 1:	Left flank				
Gear 1 direction of rotation:	Clockwise				
Planet carrier direction of rotation:	clockwise				

Tooth geometry and material

Geometry calculation according to	ISO 21771:2007				
		------- Gear 1	--------- Gear 2	--------- Gear 3 ---	
Center distance (mm)	[a]	530.000			
Center distance tolerance	ISO 286:2010 Measure js7				
Normal module (mm)	[mn]	16.0000			
Normal pressure angle (°)	[αn]	20.0000			
Helix angle at reference circle (°)	[β]	0.0000			
Number of teeth	[z]	30	34	-99	
Facewidth (mm)	[b]	280.00	272.00	267.50	
Hand of gear	Spur gear				
Planetary axles can be placed in regular pitch.:	120 °				
Accuracy grade	[Q-ISO 1328:2013]	A6	A6	A6	
Inner diameter (mm)	[di]	0.00	0.00		
External diameter (mm)	[di]			1777.86	
Inner diameter of gear rim (mm)	[dbi]	0.00	0.00		
Outer diameter of gear rim (mm)	[dbi]			0.00	

Material

Gear1
18CrNiMo7-6, Case-carburized steel, case-hardened
ISO 6336-5 Figure 9/10 (MQ), Core hardness >=25HRC Jominy J=12mm<HRC28

Gear2
18CrNiMo7-6, Case-carburized steel, case-hardened
ISO 6336-5 Figure 9/10 (MQ), Core hardness >=25HRC Jominy J=12mm<HRC28

Gear3

KISSsoft

18CrNiMo7-6, Case-carburized steel, case-hardened
ISO 6336-5 Figure 9/10 (MQ), Core hardness >=25HRC Jominy J=12mm<HRC28

		------- Gear 1	--------- Gear 2	--------- Gear 3 ---
Surface hardness		HRC 61	HRC 61	HRC 61
Material treatment according to ISO 6336:2006 Normal, life factors ZNT and YNT >=0.85				
Fatigue strength. tooth root stress (N/mm²)	[σFlim]	430.00	430.00	430.00
Fatigue strength for Hertzian pressure (N/mm²)	[σHlim]	1500.00	1500.00	1500.00
Tensile strength (N/mm²)	[σB]	1200.00	1200.00	1200.00
Yield point (N/mm²)	[σS]	850.00	850.00	850.00
Young's modulus (N/mm²)	[E]	206000	206000	206000
Poisson's ratio	[v]	0.300	0.300	0.300
Roughness average value DS, flank (µm)	[RAH]	0.60	0.60	0.60
Roughness average value DS, root (µm)	[RAF]	3.00	3.00	3.00
Mean roughness height, Rz, flank (µm)	[RZH]	4.80	4.80	4.80
Mean roughness height, Rz, root (µm)	[RZF]	20.00	20.00	20.00

Gear reference profile 1:

Reference profile	1.40 / 0.39 / 1.0 ISO 53:1998 Profil D		
Dedendum coefficient	[hfP*]	1.400	
Root radius factor	[ρfP*]	0.390	(ρfPmax*=0.394)
Addendum coefficient	[haP*]	1.000	
Tip radius factor	[ρaP*]	0.000	
Protuberance height coefficient	[hprP*]	0.000	
Protuberance angle	[αprP]	0.000	
Tip form height coefficient	[hFaP*]	0.000	
Ramp angle	[αKP]	0.000	
	not topping		

Gear reference profile 2:

Reference profile	1.40 / 0.39 / 1.0 ISO 53:1998 Profil D		
Dedendum coefficient	[hfP*]	1.400	
Root radius factor	[ρfP*]	0.390	(ρfPmax*=0.394)
Addendum coefficient	[haP*]	1.000	
Tip radius factor	[ρaP*]	0.000	
Protuberance height coefficient	[hprP*]	0.000	
Protuberance angle	[αprP]	0.000	
Tip form height coefficient	[hFaP*]	0.000	
Ramp angle	[αKP]	0.000	
	not topping		

Gear reference profile 3:

Reference profile	1.25 / 0.38 / 1.0 ISO 53:1998 Profil A		
Dedendum coefficient	[hfP*]	1.250	
Root radius factor	[ρfP*]	0.380	(ρfPmax*=0.472)
Addendum coefficient	[haP*]	1.000	
Tip radius factor	[ρaP*]	0.000	
Protuberance height coefficient	[hprP*]	0.000	
Protuberance angle	[αprP]	0.000	
Tip form height coefficient	[hFaP*]	0.000	
Ramp angle	[αKP]	0.000	
	not topping		

Information on final machining

Dedendum reference profile	[hfP*]	1.400	1.400	1.250
Tooth root radius Refer. profile	[ρfP*]	0.390	0.390	0.380
Addendum Reference profile	[haP*]	1.000	1.000	1.000
Protuberance height coefficient	[hprP*]	0.000	0.000	0.000
Protuberance angle (°)	[αprP]	0.000	0.000	0.000
Tip form height coefficient	[hFaP*]	0.000	0.000	0.000
Ramp angle (°)	[αKP]	0.000	0.000	0.000

Type of profile modification:	none (only running-in)					
Tip relief (µm)	[Ca L/R]	2.0	/ 2.0	2.0	/ 2.0	2.0 / 2.0

KISSsoft

Lubrication type	Oil bath lubrication	
Type of oil	ISO-VG 320	
Lubricant base	Mineral-oil base	
Oil nominal kinematic viscosity at 40°C (mm²/s)	[v40]	320.00
Oil nominal kinematic viscosity at 100°C (mm²/s)	[v100]	22.00
Specific density at 15°C (kg/dm³)	[ρ]	0.900
Oil temperature (°C)	[TS]	62.000

Gear pair 1

Overall transmission ratio	[itot]	0.233
Gear ratio	[u]	1.133
Transverse module (mm)	[mt]	16.000
Transverse pressure angle (°)	[αt]	20.000
Working pressure angle (°)	[αwt]	24.800
	[αwt.e/i]	24.808 / 24.792
Working pressure angle at normal section (°)	[αwn]	24.800
Helix angle at operating pitch circle (°)	[βw]	0.000
Base helix angle (°)	[βb]	0.000
Reference center distance (mm)	[ad]	512.000
Pitch on reference circle (mm)	[pt]	50.265
Base pitch (mm)	[pbt]	47.234
Transverse pitch on contact-path (mm)	[pet]	47.234
Sum of profile shift coefficients	[Σxi]	1.2589
Transverse contact ratio	[εα]	1.489
Transverse contact ratio with allowances	[εα.e/m/i]	1.491 / 1.488 / 1.484
Overlap ratio	[εβ]	0.000
Total contact ratio	[εγ]	1.489
Total contact ratio with allowances	[εγ.e/m/i]	1.491 / 1.488 / 1.484
Length of path of contact (mm)	[ga, e/i]	70.330 (70.414 / 70.112)
Length T1-A (mm)	[T1A]	140.502 (140.502 / 140.435)
Length T1-B (mm)	[T1B]	117.405 (117.322 / 117.557)
Length T1-C (mm)	[T1C]	104.207 (104.168 / 104.246)
Length T1-D (mm)	[T1D]	93.267 (93.267 / 93.201)
Length T1-E (mm)	[T1E]	70.171 (70.088 / 70.323)
Length T2-A (mm)	[T2A]	81.807 (81.723 / 81.956)
Length T2-B (mm)	[T2B]	104.903 (104.903 / 104.835)
Length T2-C (mm)	[T2C]	118.101 (118.057 / 118.146)
Length T2-D (mm)	[T2D]	129.041 (128.958 / 129.191)
Length T2-E (mm)	[T2E]	152.137 (152.137 / 152.069)
Length T1-T2 (mm)	[T1T2]	222.308 (222.225 / 222.392)
Minimal length of contact line (mm)	[Lmin]	272.000

Gear pair 2

Overall transmission ratio	[itot]	0.233
Gear ratio	[u]	-2.912
Transverse module (mm)	[mt]	16.000
Transverse pressure angle (°)	[αt]	20.000
Working pressure angle (°)	[αwt]	22.785
	[αwt.e/i]	22.776 / 22.794
Working pressure angle at normal section (°)	[αwn]	22.785
Helix angle at operating pitch circle (°)	[βw]	0.000
Base helix angle (°)	[βb]	0.000
Reference center distance (mm)	[ad]	520.000
Pitch on reference circle (mm)	[pt]	50.265
Base pitch (mm)	[pbt]	47.234
Transverse pitch on contact-path (mm)	[pet]	47.234
Sum of profile shift coefficients	[Σxi]	-0.6676

KISSsoft

Transverse contact ratio	[εα]	1.447
Transverse contact ratio with allowances	[εα.e/m/i]	1.453 / 1.448 / 1.444
Overlap ratio	[εβ]	0.000
Total contact ratio	[εγ]	1.447
Total contact ratio with allowances	[εγ.e/m/i]	1.453 / 1.448 / 1.444
Length of path of contact (mm)	[ga, e/i]	68.350 (68.613 / 68.191)
Length T1-A (mm)	[T1A]	152.137 (152.137 / 152.069)
Length T1-B (mm)	[T1B]	131.022 (130.759 / 131.112)
Length T1-C (mm)	[T1C]	107.366 (107.413 / 107.318)
Length T1-D (mm)	[T1D]	104.903 (104.903 / 104.835)
Length T1-E (mm)	[T1E]	83.788 (83.525 / 83.878)
Length T2-A (mm)	[T2A]	357.395 (357.485 / 357.236)
Length T2-B (mm)	[T2B]	336.280 (336.107 / 336.280)
Length T2-C (mm)	[T2C]	312.624 (312.761 / 312.486)
Length T2-D (mm)	[T2D]	310.161 (310.251 / 310.002)
Length T2-E (mm)	[T2E]	289.046 (288.873 / 289.046)
Length T1-T2 (mm)	[T1T2]	205.258 (205.348 / 205.167)
Minimal length of contact line (mm)	[Lmin]	267.500

Gear 1

Profile shift coefficient	[x]	0.6183
Tooth thickness, arc, in module	[sn*]	2.0209
Tip alteration (mm)	[k*mn]	-0.181
Reference diameter (mm)	[d]	480.000
Base diameter (mm)	[db]	451.052
Tip diameter (mm)	[da]	531.424
(mm)	[da.e/i]	531.424 / 531.354
Tip diameter allowances (mm)	[Ada.e/i]	0.000 / -0.070
Tip form diameter (mm)	[dFa]	531.424
(mm)	[dFa.e/i]	531.424 / 531.354
Root diameter (mm)	[df]	454.986
Generating Profile shift coefficient	[xE.e/i]	0.6071/ 0.6020
Generated root diameter with xE (mm)	[df.e/i]	454.628 / 454.464
Root form diameter (mm)	[dFf]	465.492
(mm)	[dFf.e/i]	465.235 / 465.117
Internal toothing: Calculation dFf with pinion type cutter (z0= 30 , x0= 0.000)		
Involute length (mm)	[l_dFa-l_dFf]	36.430
Addendum, $m_n(h_{aP}^*+x+k)$ (mm)	[ha]	25.712
(mm)	[ha.e/i]	25.712 / 25.677
Dedendum (mm)	[hf=mn*(hfP*-x)]	12.507
(mm)	[hf.e/i]	12.686 / 12.768
Tooth height (mm)	[h]	38.219
Virtual gear no. of teeth	[zn]	30.000
Normal tooth thickness at tip circle (mm)	[san]	8.731
(mm)	[san.e/i]	8.629 / 8.520
Normal tooth thickness at tip form circle (mm)	[sFan]	8.731
(mm)	[sFan.e/i]	8.629 / 8.520
Normal space width at root circle (mm)	[efn]	10.564
(mm)	[efn.e/i]	10.632 / 10.665

Gear 2

Profile shift coefficient	[x]	0.6406
Tooth thickness, arc, in module	[sn*]	2.0371
Tip alteration (mm)	[k*mn]	-0.801
Reference diameter (mm)	[d]	544.000
Base diameter (mm)	[db]	511.193
Tip diameter (mm)	[da]	594.896
(mm)	[da.e/i]	594.896 / 594.826
Tip diameter allowances (mm)	[Ada.e/i]	0.000 / -0.070
Tip form diameter (mm)	[dFa]	594.896

(mm)	[dFa.e/i]	594.896 / 594.826
Root diameter (mm)	[df]	519.698
Generating Profile shift coefficient	[xE.e/i]	0.6294/ 0.6242
Generated root diameter with xE (mm)	[df.e/i]	519.341 / 519.176
Root form diameter (mm)	[dFf]	529.757
(mm)	[dFf.e/i]	529.484 / 529.359
Internal toothing: Calculation dFf with pinion type cutter (z0= 34 , x0= 0.000)		
Involute length (mm)	[l_dFa-l_dFf]	35.827
Addendum, $m_n(h_{aP}^*+x+k)$ (mm)	[ha]	25.448
(mm)	[ha.e/i]	25.448 / 25.413
Dedendum (mm)	[hf=mn*(hfP*-x)]	12.151
(mm)	[hf.e/i]	12.330 / 12.412
Tooth height (mm)	[h]	37.599
Virtual gear no. of teeth	[zn]	34.000
Normal tooth thickness at tip circle (mm)	[san]	9.813
(mm)	[san.e/i]	9.711 / 9.605
Normal tooth thickness at tip form circle (mm)	[sFan]	9.813
(mm)	[sFan.e/i]	9.711 / 9.605
Normal space width at root circle (mm)	[efn]	10.181
(mm)	[efn.e/i]	10.233 / 10.258

Gear 3

Profile shift coefficient	[x]	-1.3082
Tooth thickness, arc, in module	[sn*]	0.6185
Tip alteration (mm)	[k*mn]	-1.465
Reference diameter (mm)	[d]	1584.000
Base diameter (mm)	[db]	1488.473
Tip diameter (mm)	[da]	1596.791
(mm)	[da.e/i]	1596.791 / 1596.666
Tip diameter allowances (mm)	[Ada.e/i]	0.000 / -0.125
Tip form diameter (mm)	[dFa]	1596.791
(mm)	[dFa.e/i]	1596.791 /1596.666
Root diameter (mm)	[df]	1665.861
Generating Profile shift coefficient	[xE.e/i]	-1.3288/ -1.3373
Generated root diameter with xE (mm)	[df.e/i]	1666.795 /1666.520
Root form diameter (mm)	[dFf]	1660.124
(mm)	[dFf.e/i]	1660.928 /1660.692
Internal toothing: Calculation dFf with pinion type cutter (z0= 32 , x0= 0.000)		
Involute length (mm)	[l_dFa-l_dFf]	34.645
Addendum, $m_n(h_{aP}^*+x+k)$ (mm)	[ha]	-6.395
(mm)	[ha.e/i]	-6.333 / -6.395
Dedendum (mm)	[hf=mn*(hfP*-x)]	40.930
(mm)	[hf.e/i]	41.260 / 41.398
Tooth height (mm)	[h]	34.535
Virtual gear no. of teeth	[zn]	99.000
Normal tooth thickness at tip circle (mm)	[san]	14.809
(mm)	[san.e/i]	14.567 / 14.416
Normal tooth thickness at tip form circle (mm)	[sFan]	14.809
(mm)	[sFan.e/i]	14.567 / 14.416
Normal space width at root circle (mm)	[efn]	5.874
(mm)	[efn.e/i]	5.797 / 5.765

Gear specific pair data Gear pair 1, Gear 1

Operating pitch diameter (mm)	[dw]	496.875
(mm)	[dw.e/i]	496.908 / 496.842
Active tip diameter (mm)	[dNa]	531.424
(mm)	[dNa.e/i]	531.424 / 531.354
Theoretical tip clearance (mm)	[c]	4.439
Effective tip clearance (mm)	[c.e/i]	4.770 / 4.583
Active root diameter (mm)	[dNf]	472.382
(mm)	[dNf.e/i]	472.472 / 472.332
Reserve (dNf-dFf)/2 (mm)	[cF.e/i]	3.677 / 3.548
Max. sliding velocity at tip (m/s)	[vga]	0.361
Specific sliding at the tip	[ζa]	0.486
Specific sliding at the root	[ζf]	-0.913

Mean specific sliding	[ζm]	0.482
Sliding factor on tip	[Kga]	0.275
Sliding factor on root	[Kgf]	-0.258
Roll angle at dFa (°)	[ξdFa.e/i]	35.695 / 35.678
Roll angle to dNa (°)	[ξdNa.e/i]	35.695 / 35.678
Roll angle to dNf (°)	[ξdNf.e/i]	17.866 / 17.806
Roll angle at dFf (°)	[ξdFf.e/i]	14.481 / 14.419
Diameter of single contact point B (mm)	[d-B]	508.512 (508.435 / 508.652)
Diameter of single contact point D (mm)	[d-D]	488.102 (488.102 / 488.051)
Addendum contact ratio	[ε]	0.768 (0.769 / 0.766)

Gear specific pair data Gear pair 1, Gear 2

Operating pitch diameter (mm)	[dw]	563.125
(mm)	[dw.e/i]	563.162 / 563.088
Active tip diameter (mm)	[dNa]	594.896
(mm)	[dNa.e/i]	594.896 / 594.826
Theoretical tip clearance (mm)	[c]	5.059
Effective tip clearance (mm)	[c.e/i]	5.390 / 5.203
Active root diameter (mm)	[dNf]	536.738
(mm)	[dNf.e/i]	536.829 / 536.687
Reserve (dNf-dFf)/2 (mm)	[cF.e/i]	3.735 / 3.601
Max. sliding velocity at tip (m/s)	[vga]	0.385
Specific sliding at the tip	[ζa]	0.477
Specific sliding at the root	[ζf]	-0.946
Mean specific sliding	[ζm]	0.482
Sliding factor on tip	[Kga]	0.258
Sliding factor on root	[Kgf]	-0.275
Roll angle at dFa (°)	[ξdFa.e/i]	34.104 / 34.088
Roll angle to dNa (°)	[ξdNa.e/i]	34.104 / 34.088
Roll angle to dNf (°)	[ξdNf.e/i]	18.372 / 18.320
Roll angle at dFf (°)	[ξdFf.e/i]	15.464 / 15.410
Diameter of single contact point B (mm)	[d-B]	552.573 (552.573 / 552.521)
Diameter of single contact point D (mm)	[d-D]	572.647 (572.572 / 572.782)
Addendum contact ratio	[ε]	0.721 (0.722 / 0.718)

Gear specific pair data Gear pair 2, Gear 2

Operating pitch diameter (mm)	[dw]	554.462
(mm)	[dw.e/i]	554.425 / 554.498
Active tip diameter (mm)	[dNa]	594.896
(mm)	[dNa.e/i]	594.896 / 594.826
Theoretical tip clearance (mm)	[c]	5.483
Effective tip clearance (mm)	[c.e/i]	6.020 / 5.777
Active root diameter (mm)	[dNf]	537.959
(mm)	[dNf.e/i]	538.015 / 537.795
Reserve (dNf-dFf)/2 (mm)	[cF.e/i]	4.328 / 4.155
Max. sliding velocity at tip (m/s)	[vga]	0.077
Specific sliding at the tip	[ζa]	0.193
Specific sliding at the root	[ζf]	-0.185
Mean specific sliding	[ζm]	0.180
Sliding factor on tip	[Kga]	0.106
Sliding factor on root	[Kgf]	-0.056
Roll angle at dFa (°)	[ξdFa.e/i]	34.104 / 34.088
Roll angle to dNa (°)	[ξdNa.e/i]	34.104 / 34.088
Roll angle to dNf (°)	[ξdNf.e/i]	18.803 / 18.723
Roll angle at dFf (°)	[ξdFf.e/i]	15.464 / 15.410
Diameter of single contact point B (mm)	[d-B]	574.443 (574.203 / 574.526)
Diameter of single contact point D (mm)	[d-D]	552.573 (552.573 / 552.521)
Addendum contact ratio	[ε]	0.948 (0.947 / 0.947)

Gear specific pair data Gear pair 2, Gear 3

Operating pitch diameter (mm)	[dw]	1614.462
(mm)	[dw.e/i]	1614.568 /1614.355

KISSsoft

Active tip diameter (mm)	[dNa]	1596.791
(mm)	[dNa.e/i]	1596.791 /1596.666
Theoretical tip clearance (mm)	[c]	8.547
Effective tip clearance (mm)	[c.e/i]	8.843 / 8.628
Active root diameter (mm)	[dNf]	1651.205
(mm)	[dNf.e/i]	1651.283 /1651.067
Reserve (dNf-dFf)/2 (mm)	[cF.e/i]	4.930 / 4.704
Max. sliding velocity at tip (m/s)	[vga]	0.108
Specific sliding at the tip	[ζa]	0.156
Specific sliding at the root	[ζf]	-0.239
Mean specific sliding	[ζm]	0.180
Sliding factor on tip	[Kga]	0.056
Sliding factor on root	[Kgf]	-0.106
Roll angle at dFa (°)	[ξdFa.e/i]	22.239 / 22.252
Roll angle to dNa (°)	[ξdNa.e/i]	22.239 / 22.252
Roll angle to dNf (°)	[ξdNf.e/i]	27.502 / 27.521
Roll angle at dFf (°)	[ξdFf.e/i]	28.348 / 28.368
Diameter of single contact point B (mm)	[d-B]	1633.367 (1633.225 / 1633.367)
Diameter of single contact point D (mm)	[d-D]	1612.561 (1612.630 / 1612.438)
Addendum contact ratio	[ε]	0.499 (0.506 / 0.496)

General influence factors

		------- Gear 1 --------- Gear 2 --------- Gear 3 ---
Nominal circum. force at pitch circle (N)	[Ft]	182257.199182257.199
Axial force (N)	[Fa]	0.0 0.0 0.0
Total axial force (N)	[Fatot=Fa* 3]	0.0 0.0
Radial force (N)	[Fr]	66336.195 66336.195
Normal force (N)	[Fnorm]	193954.1 193954.1 193954.1
Nominal circumferential force per mm (N/mm)	[w]	670.06 681.34
Only as information: Forces at operating pitch circle:		
Nominal circumferential force (N)	[Ftw]	176067.332178818.384
Axial force (N)	[Fa]	0.0
Axial force (N)	[Fa]	0.0 /0.0
Axial force (N)	[Fa]	0.0
Total axial force (N)	[Fatot=Fa* 3]	0.0 0.0
Radial force (N)	[Fr]	81353.992 75114.333
Circumferential speed reference circle (m/s)	[v]	1.35 (Planet)
Running-in value (µm)	[yp]	1.192 1.298
Running-in value (µm)	[yf]	1.500 1.500
Gear blank factor	[CR]	1.000 1.000
Correction factor	[CM]	0.800 0.800
Basic rack factor	[CBS]	0.900 0.938
Material coefficient	[E/Est]	1.000 1.000
Singular tooth stiffness (N/mm/µm)	[c']	14.216 14.058
Meshing stiffness (N/mm/µm)	[cγα]	19.429 18.771
Meshing stiffness (N/mm/µm)	[cγβ]	16.515 15.956
Reduced mass (kg/mm)	[mRed]	0.2361 1.1350
Resonance speed (min-1)	[nE1]	2888 1142
Resonance ratio (-)	[N]	0.019 0.042
Running-in value (µm)	[yα]	1.192 1.298
Planet runs on rolling bearings. Planet pin fixed on both sides in the carrier..		
lpa (mm) = 353.60 b (mm) =272.00dsh (mm) = 272.00		
Tooth trace deviation (active) (µm)	[Fβy]	7.50 9.07
from deformation of shaft (µm)	[fsh*B1]	14.91 1.00
(fsh (µm) =14.91 / 1.00, B1 = 1.00 / 1.00, fHβ5 (µm) = 11.00 / 12.00)		
Tooth trace		0 0
(0: without, 1: crowned, 2: end relief, 3: full modification)		
(4: slightly crowned, 5: helix angle modification, 6: helix angle modification with crowning)		
from production tolerances (µm)	[fmα*B2]	21.21 22.67
B2 = 1.00 / 1.00		
Tooth trace deviation, theoretical (µm)	[Fβx]	8.83 10.67
Running-in value yβ (µm)	[yβ]	1.32 1.60
Dynamic factor	[Kv=max(Kv12,Kv23)]	1.02
	[Kv12,Kv23]	1.01 1.02

Face load factor - flank	[KHβ]		1.09	1.11
- Tooth root	[KFβ]		1.08	1.09
- Scuffing	[KBβ]		1.09	1.11
Transverse load factor - flank	[KHα]		1.00	1.00
- Tooth root	[KFα]		1.00	1.00
- Scuffing	[KBα]		1.00	1.00
Number of load cycles (in mio.)	[NL]	193.6	57.0	58.7

Tooth root load capacity

Calculation of Tooth form coefficients according method: B

Internal toothing: Calculation of ρF and sFn according to ISO 6336-3:2007-04-01

Internal toothing: Calculation of YF, YS with pinion type cutter, z0= 32 , x0=0.000 , ρaP0*= 0.380

		Gear 1	Gear 2	Gear 3
Calculated with generating profile shift coefficient	[xE.i]	0.6020	0.6242	-1.3373
Tooth form factor	[YF]	1.31		
	[YF]		1.27 /1.33	
	[YF]			0.88
Stress correction factor	[YS]	2.17		
	[YS]		2.22 /2.18	
	[YS]			3.07
Bending moment arm (mm)	[hF]	19.87		
(mm)	[hF]		19.53 /20.54	
(mm)	[hF]			21.52
Load application angle (°)	[αFen]	25.14		
(°)	[αFen]		24.66 /25.10	
(°)	[αFen]			23.37
Coefficient	[fε]		1.000	1.000
Tooth thickness at root (mm)	[sFn]	37.50		
(mm)	[sFn]		37.82 /37.82	
(mm)	[sFn]			47.97
Tooth root radius (mm)	[ρF]	6.95		
(mm)	[ρF]		6.84 /6.84	
(mm)	[ρF]			4.73

hF* = 1.242 /1.220 /1.284 / 1.345sFn* = 2.344 /2.364 / 2.364 / 2.998

ρF* =0.434 /0.428 /0.428 / 0.296dsFn =460.030 / 524.805 / 524.805 /-1665.227 αsFn = 30.0 / 30.0 / 30.0 / 60.0

Helix angle factor	[Yβ]		1.00	1.00
Deep tooth factor	[YDT]		1.00	1.00
Gear rim thickness (mm)	[sr]	454.46	519.18	55.53
Gear rim factor	[YB]	1.00	1.00	1.01
Effective facewidth (mm)	[beff]	280.00		
(mm)	[beff]		272.00 /272.00	
(mm)	[beff]			267.50
Nominal stress at tooth root (N/mm²)	[σF0]	115.61		
(N/mm²)	[σF0]		117.74 /121.06	
(N/mm²)	[σF0]			115.49
Tooth root stress (N/mm²)	[σF]	127.02		
(N/mm²)	[σF]		129.36 /134.60	
(N/mm²)	[σF]			128.41
Permissible bending stress at root of Test-gear				
Notch sensitivity factor	[YdrelT]	1.002		
Notch sensitivity factor	[YdrelT]		1.002 /	1.002
Notch sensitivity factor	[YdrelT]			1.021
Surface factor	[YRrelT]	0.957	0.957	0.957
Size factor, tooth root	[YX]	0.890	0.890	0.890
Finite life factor	[YNT]	0.920	0.943	0.942
Alternating bending factor, mean stress influence coefficient				
	[YM]	1.000	0.700	1.000
Stress correction factor	[Yst]		2.00	
Yst*σFlim (N/mm²)	[σFE]	860.00	860.00	860.00
Permissible tooth root stress (N/mm²)	[σFP=σFG/SFmin]	482.05		
Permissible tooth root stress (N/mm²)	[σFP=σFG/SFmin]		346.01 /346.01	
Permissible tooth root stress (N/mm²)	[σFP=σFG/SFmin]			502.93
Limit strength tooth root (N/mm²)	[σFG]	674.86		
Limit strength tooth root (N/mm²)	[σFG]		484.42 /484.42	

Limit strength tooth root (N/mm²)	[σFG]				704.10	
Required safety	[SFmin]	1.40	1.40		1.40	
Safety for tooth root stress	[SF=σFG/σF]	5.31				
	[SF=σFG/σF]		3.74	/3.60		
	[SF=σFG/σF]				5.48	
Transmittable power (kW)	[kWRating]	3655.20				
(kW)	[kWRating]		2576.31	/2476.01		
(kW)	[kWRating]				3772.43	

Flank safety

		Gear 1	Gear 2	Gear 3	
Zone factor	[ZH]	2.21	2.32		
Elasticity factor (√N/mm²)	[ZE]	189.81	189.81		
Contact ratio factor	[Zε]	0.915	0.922		
Helix angle factor	[Zβ]	1.000	1.000		
Effective facewidth (mm)	[beff]	272.00	267.50		
Nominal contact stress (N/mm²)	[σH0]	623.24	368.70		
Contact stress at operating pitch circle (N/mm²)	[σHw]	657.15	391.47		
Single tooth contact factor	[ZB,ZD]	1.01	1.00	/1.02	1.00
Contact stress (N/mm²)	[σHB, σHD]	664.53	657.15	/397.60	391.47

Lubrication factor for NL	[ZL]	1.047	1.047 /	1.047	1.047
Speed factor for NL	[ZV]	0.958	0.958 /	0.958	0.958
Roughness factor for NL	[ZR]	1.008	1.008 /	1.038	1.038
Material hardening factor for NL	[ZW]	1.000	1.000 /	1.000	1.000
Finite life factor	[ZNT]	0.959	0.996	0.995	
Limited pitting is permitted: No					
Size factor (flank)	[ZX]	1.000	1.000	1.000	
Permissible contact stress, σHG/SHmin (N/mm²)	[σHP]	1455.96	1511.65	/1555.94	1554.52
Pitting stress limit (N/mm²)	[σHG]	1455.96	1511.65	/1555.94	1554.52

Required safety	[SHmin]	1.00	1.00	1.00		
Safety factor for contact stress at operating pitch circle	[SHw]	2.22	2.30	/3.97	3.97	
Safety for stress at single tooth contact	[SHBD=σHG/σHBD]	2.19	2.30	/3.91	3.97	
	Safety regarding transmittable torque[(SHBD)^2]		4.80	5.29 /		15.31
15.77						
Transmittable power (kW)	[kWRating]	4623.52	5096.50	/14749.91	15188.18	

Micropitting according to **ISO/TS 6336-22:2018**

Pairing Gear 1 -2 :
Calculation has not been carried out, lubricant: Load stage micropitting test not known

Pairing Gear 2 -3 :
Calculation has not been carried out, lubricant: Load stage micropitting test not known

Scuffing load capacity

Calculation method according to ISO/TS 6336-20/21:2017

Helical load factor for scuffing	[KBγ]	1.00	1.00			
Lubrication coefficient for lubrication type	[XS]	1.000				
Scuffing test and load stage	[FZGtest] FZG - Test A / 8.3 / 90 (ISO 14635 - 1)					12
Multiple meshing factor	[Xmp]	2.0	2.0			
Relative structural factor, scuffing	[XWrelT]	1.000	1.000			
Thermal contact factor (N/mm/s^.5/K)	[BM]	13.780	13.780	13.780		
Relevant tip relief (µm)	[Ca]	2.00	2.00	/ 2.00	2.00	
Optimal tip relief (µm)	[Ceff]	47.13	48.47			
Ca taken as optimal in the calculation (0=no, 1=yes)		0	0	/0	0	
Effective facewidth (mm)	[beff]	272.000	267.500			
Applicable circumferential force/facewidth (N/mm)	[wBt]	744.971	768.056			

(1) KBγ = 1.000 , wBt*KBγ =744.971
(2) KBγ = 1.000 , wBt*KBγ =768.056

Angle factor	[Xαβ]		1.047	1.018	
Flash temperature-criteria					
Lubricant factor	[XL]		0.679	0.679	
Tooth mass temperature (°C)	[θMi]		69.20	63.47	
θMi = θoil + XS*0.47*Xmp*θflm					
Average flash temperature	(°C)	[θflm]	7.65	1.56	
Scuffing temperature (°C)	[θS]		299.98	299.98	
Γ coordinates (point of highest temperature)	[Γ]		0.348	0.218	
(1) [Γ.A]= 0.348 [Γ.E]= -0.327					
(2) [Γ.A]= 0.417 [Γ.E]= -0.220					
Highest contact temp. (°C)	[θB]		81.41	66.27	
Flash factor (°K*N^-.75*s^.5*m^-.5*mm)	[XM]		50.058	50.058	
Approach factor	[XJ]		1.124	1.037	
Load sharing factor	[XΓ]		0.333	1.000	
Dynamic viscosity (mPa*s)	[ηM]		81.42	81.42	(62.0 °C)
Coefficient of friction	[μ_m]		0.052	0.043	
Required safety	[SBmin]		2.000		
Margin of safety for scuffing, flash temperature	[SB]		12.262	55.765	
Integral temperature-criteria					
Lubricant factor (Input)	[XL]		0.846		
Tooth mass temperature (°C)	[θMC]		67.57	62.86	
θMC = θoil + XS*0.70*θflaint					
Mean flash temperature	(°C)	[θflaint]	3.98	0.62	
Integral scuffing temperature (°C)	[θSint]		316.54	316.54	
Flash factor (°K*N^-.75*s^.5*m^-.5*mm)	[XM]		50.058	50.058	
Running-in factor, well run in	[XE]		1.000	1.000	
Contact ratio factor	[Xε]		0.278	0.263	
Dynamic viscosity (mPa*s)	[ηOil]		81.42	81.42	
Mean coefficient of friction	[μ_m]		0.035	0.022	
Geometry factor	[XBE]		0.242	0.058	
Meshing factor	[XQ]		1.000	0.894	
Tip relief factor	[XCa]		1.081	1.107	
Integral tooth flank temperature (°C)	[θint]		73.53	63.79	
Required safety	[SSmin]		1.800		
Safety factor for scuffing (intg.-temp.)	[SSint]		4.30	4.96	
Safety referring to transmittable torque	[SSL]		22.07	142.19	

Measurements for tooth thickness

		Gear 1	Gear 2	Gear 3
Tooth thickness tolerance		DIN 3967 cd25	DIN 3967 cd25	DIN 3967 cd25
Tooth thickness allowance (normal section) (mm)	[As.e/i]	-0.130 /	-0.190-0.130 /	-0.190-0.240 / -0.340
Number of teeth spanned	[k]	5.000	5.000	14.000
(Internal toothing: k = (Measurement gap number)				
Base tangent length (no backlash) (mm)	[Wk]	226.043	227.183	674.162
Base tangent length with allowance (mm)	[Wk.e/i]	225.921 /	225.865227.061 /	227.005 674.388 / 674.482
Diameter of measuring circle (mm)	[dMWk.m]	504.456	559.341	1634.140
Theoretical diameter of ball/pin (mm)	[DM]	30.971	30.592	26.440
Effective diameter of ball/pin (mm)	[DMeff]	35.000	35.000	28.000
Radial single-ball measurement backlash free (mm)	[MrK]	278.541	311.161	791.680
Radial single-ball measurement (mm)	[MrK.e/i]	278.420 /	278.364311.037 /	310.980 792.097 / 791.975
Diameter of measuring circle (mm)	[dMMr.m]	505.095	570.626	1623.030
Diametral measurement over two balls without clearance (mm)	[MdK]	557.082	622.323	1583.158
Diametral two ball measure (mm)	[MdK.e/i]	556.839 /	556.727622.074 /	621.960 1583.991 / 1583.746
Measurement over pins according to DIN 3960 (mm)	[MdR.e/i]	556.839 /	556.727622.074 /	621.960 1583.991 / 1583.746
Measurement over 3 pins, axial, according to AGMA 2002 (mm)				
	[dk3A.e/i]	556.839 /	556.727622.074 /	621.960 1583.991 / 1583.746
Measurement over 3 pins with allowance (mm)	[Md3R.e/i]	0.000 /	0.0000.000 /	0.0001583.788 / 1583.543
Chordal tooth thickness in reference circle (mm)	[sc]	32.310	32.574	9.897
(mm)	[sc.e/i]	32.182 /	32.12432.446 /	32.3889.656 / 9.556
Reference chordal height from da.m (mm)	[ha]	26.239	25.919	-6.380
Tooth thickness, arc (mm)	[sn]	32.334	32.593	9.897
(mm)	[sn.e/i]	32.204 /	32.14432.463 /	32.4039.657 / 9.557
Backlash free center distance (mm)	[aControl.e/i]	529.708 /	529.574530.448 /	530.641

KISSsoft

Backlash free center distance, allowances (mm)	[jta]	-0.292 /		-0.426	0.448 /		0.641	
dNf.i with aControl (mm)	[dNf0.i]	471.780	536.120	/	536.835	1652.635		
Reserve (dNf0.i-dFf.e)/2 (mm)	[cF0.i]	3.273	3.318	/	3.675	4.028		
Tip clearance (mm)	[c0.i(aControl)]	4.191	4.811	/	5.365	8.022		
Center distance allowances (mm)	[Aa.e/i]	0.035 /		-0.035	-0.035 /		0.035	
Circumferential backlash from Aa (mm)	[jtw_Aa.e/i]	0.032 /		-0.032	0.029 /		-0.029	
Radial backlash (mm)	[jrw]	0.461 /		0.257	0.676 /		0.413	
Circumferential backlash, transverse section (mm)	[jtw]	0.426 /		0.237	0.570 /		0.348	
Normal backlash (mm)	[jnw]	0.381 /		0.220	0.522 /		0.324	
Torsional angle on input with output fixed:								
Total torsional angle (°)	[j.tSys]	0.0505/		0.0350				

Toothing tolerances

			------- Gear 1	--------- Gear 2	--------- Gear 3 ---
According to ISO 1328-1:2013, ISO 1328-2:1997					
Accuracy grade	[Q]		A6	A6	A6
Single pitch deviation (µm)	[fptT]		17.00	17.00	18.00
Base circle pitch deviation (µm)	[fpbT]		15.80	15.90	17.30
Sector pitch deviation over k/8 pitches (µm)	[Fpk/8T]		35.00	34.00	43.00
Profile form deviation (µm)	[ffαT]		20.00	20.00	20.00
Profile slope deviation (µm)	[fHαT]		15.00	15.00	17.00
Total profile deviation (µm)	[FαT]		25.00	25.00	26.00
Helix form deviation (µm)	[ffβT]		18.00	18.00	20.00
Helix slope deviation (µm)	[fHβT]		15.00	15.00	17.00
Total helix deviation (µm)	[FβT]		24.00	24.00	26.00
Total cumulative pitch deviation (µm)	[FpT]		51.00	52.00	68.00
Adjacent pitch difference (µm)	[fuT]		24.00	24.00	26.00
Runout (µm)	[FrT]		46.00	47.00	61.00
Single flank composite, total (µm)	[FisT]		67.00	68.00	84.00
Single flank composite, tooth-to-tooth	(µm)	[fisT]	16.00	16.00	16.00
Radial composite, total (µm)	[FidT]		110.00	110.00	138.00
Radial composite, tooth-to-tooth (µm)	[fidT]		68.00	68.00	69.00

FidT (Fi''), fidT (fi'') according to ISO 1328:1997 calculated with the geometric mean values for mn and d

Axis alignment tolerances (recommendation acc. to ISO TR 10064-3:1996, Quality)			6	
Maximum value for deviation error of axis (µm)	[fΣβ]		15.60	15.60
Maximum value for inclination error of axes (µm)	[fΣδ]		31.20	31.20

Modifying and defining the tooth form

Data for the tooth form calculation :
Data not available.
Please run the calculation in the "Tooth form" tab and open the main report again.

Supplementary data

Mass (kg)	[m]	418.855	519.510	821.803
Total mass (kg)	[mGes]	2799.187		
Moment of inertia for system, relative to the input:				
calculation without consideration of the exact tooth shape				
Single gears (da+df)/2...di (kg*m²)	[J]	12.73586	20.16864	598.06844
System (da+df)/2...di (kg*m²)	[J]	inf		
Torsional stiffness at driving gear with fixed driven gear:				
Torsional stiffness (MNm/rad)	[cr]	4135.405		
Torsion when subjected to nominal torque (°)	[δcr]	0.006		
Mean coefficient of friction (as defined in Niemann)	[μ_m]	0.035	0.028	
Wear sliding coef. by Niemann	[ζw]	0.717	0.244	
Loss factor	[HV]	0.122	0.043	
Meshing power (kW)		739.175	739.175	
Gear power loss (kW)	[PVZ]	1.070	0.296	
Total power loss (kW)		4.097		

Total efficiency			0.996	
Sound pressure level according to Masuda, without contact analysis	[dB(A)]	98.2	100.9	

Service life, damage

Required safety for tooth root	[SFmin]		1.40	
Required safety for tooth flank	[SHmin]		1.00	
Service life (calculated with required safeties):				
System service life (h)	[Hatt]		> 1000000	
Tooth root service life (h)	[HFatt]	1e+06	1e+06	1e+06
Tooth flank service life (h)	[HHatt]	1e+06	1e+06	1e+06

Note: The entry 1e+006 h means that the Service life > 1,000,000 h.

Damage calculated on the basis of the required service life (20000.0 h)

F1%	F2%	F3%	H1%	H2%	H3%
0.00	0.0000	0.0000	0.0000	0.0000	0.0000

Remarks:

- Specifications with [.e/i] imply: Maximum [e] and minimum value [i] for
  Taking all tolerances into account
  Specifications with [.m] imply: Mean value within tolerance
- For the backlash tolerance, the center distance tolerances and the tooth thickness allowance are taken into account.
  The maximum and minimum clearance according to the largest or smallest allowances are defined..
  The calculation is performed for the operating pitch circle.
- Details of calculation method:
  cγ according to Method B
  Kv according to Method B
  KHβ and KFβ according to Method C
  fmα according to Equation 64, Fβx according to 52/53/56
  fsh calculated by exactly following the method in Annex D,
  ISO 6336-1:2006
  Literature: Journal "Antriebstechnik", 6/2007, p.64.
  KHα, KFα according to Method B
- The logarithmically interpolated value taken from the values for the fatigue strength and the static strength, based on the number of load cycles, is used for coefficients ZL, ZV, ZR, ZW, ZX, YdrelT, YRrelT and YX..

End of Report lines: 822

Second Planeetary Stage

Calculation of a spur planetary gear stage

Drawing or article number:					
Gear 1:	0.000.0				
Gear 2:	0.000.0				
Gear 3:	0.000.0				
Calculation method	ISO 6336:2019				
		------- Sun	---------- Planets	---------- Internal gear ---	
Number of planets	[p]	1	3	1	
Power (kW)	[P]	531.712			
Speed (1/min)	[n]	47.9		-16.3	
Speed difference for planet bearing calculation (1/min)		[n2]	49.4		
Speed planet carrier (1/min)	[nSteg]	0.0			
Power (kW)	[P]	531.712		531.712	
Planet carrier performance (kW)	[PSteg]	0.000			
Torque (Nm)	[T]	106043.0	0.0	311501.4	
Torque Pl.-Carrier (Nm)	[TSteg]	417544.375			
Application factor	[KA]	1.00			
Distribution factor	[Kγ]	1.00			
Required service life (h)	[H]	20000.00			
Gear driving (+) / driven (-)		-	+/-	+	
Working flank gear 1:	Right flank				
Gear 1 direction of rotation:	Counterclockwise				
Gear 3 direction of rotation:	clockwise				

Tooth geometry and material

Geometry calculation according to	ISO 21771:2007				
		------- Gear 1	--------- Gear 2	--------- Gear 3 ---	
Center distance (mm)	[a]	516.000			
Center distance tolerance	ISO 286:2010 Measure js7				
Normal module (mm)	[mn]	16.0000			
Normal pressure angle (°)	[αn]	20.0000			
Helix angle at reference circle (°)	[β]	0.0000			
Number of teeth	[z]	32	31	-94	
Facewidth (mm)	[b]	224.00	219.00	213.00	
Hand of gear	Spur gear				
Planetary axles can be placed in regular pitch.:	120 °				
Accuracy grade	[Q-ISO 1328:2013]	A6	A6	A6	
Inner diameter (mm)	[di]	0.00	0.00		
External diameter (mm)	[di]			1690.73	
Inner diameter of gear rim (mm)	[dbi]	0.00	0.00		
Outer diameter of gear rim (mm)	[dbi]			0.00	

Material

Gear1
18CrNiMo7-6, Case-carburized steel, case-hardened
ISO 6336-5 Figure 9/10 (MQ), Core hardness >=25HRC Jominy J=12mm<HRC28

Gear2
18CrNiMo7-6, Case-carburized steel, case-hardened

Gear3
18CrNiMo7-6, Case-carburized steel, case-hardened
ISO 6336-5 Figure 9/10 (MQ), Core hardness >=25HRC Jominy J=12mm<HRC28

		------- Gear 1	--------- Gear 2	--------- Gear 3 ---
Surface hardness		HRC 61	HRC 61	HRC 61
Material treatment according to ISO 6336:2006 Normal, life factors ZNT and YNT >=0.85				
Fatigue strength. tooth root stress (N/mm²)	[σFlim]	430.00	430.00	430.00
Fatigue strength for Hertzian pressure (N/mm²)	[σHlim]	1500.00	1500.00	1500.00
Tensile strength (N/mm²)	[σB]	1200.00	1200.00	1200.00
Yield point (N/mm²)	[σS]	850.00	850.00	850.00
Young's modulus (N/mm²)	[E]	206000	206000	206000
Poisson's ratio	[v]	0.300	0.300	0.300
Roughness average value DS, flank (µm)	[RAH]	0.60	0.60	0.60
Roughness average value DS, root (µm)	[RAF]	3.00	3.00	3.00
Mean roughness height, Rz, flank (µm)	[RZH]	4.80	4.80	4.80
Mean roughness height, Rz, root (µm)	[RZF]	20.00	20.00	20.00

Gear reference profile 1:

Reference profile	1.40 / 0.39 / 1.0 ISO 53:1998 Profil D		
Dedendum coefficient	[hfP*]	1.400	
Root radius factor	[ρfP*]	0.390	(ρfPmax*=0.394)
Addendum coefficient	[haP*]	1.000	
Tip radius factor	[ρaP*]	0.000	
Protuberance height coefficient	[hprP*]	0.000	
Protuberance angle	[αprP]	0.000	
Tip form height coefficient	[hFaP*]	0.000	
Ramp angle	[αKP]	0.000	
	not topping		

Gear reference profile 2:

Reference profile	1.40 / 0.39 / 1.0 ISO 53:1998 Profil D		
Dedendum coefficient	[hfP*]	1.400	
Root radius factor	[ρfP*]	0.390	(ρfPmax*=0.394)
Addendum coefficient	[haP*]	1.000	
Tip radius factor	[ρaP*]	0.000	
Protuberance height coefficient	[hprP*]	0.000	
Protuberance angle	[αprP]	0.000	
Tip form height coefficient	[hFaP*]	0.000	
Ramp angle	[αKP]	0.000	
	not topping		

Gear reference profile 3:

Reference profile	1.25 / 0.38 / 1.0 ISO 53:1998 Profil A		
Dedendum coefficient	[hfP*]	1.250	
Root radius factor	[ρfP*]	0.380	(ρfPmax*=0.472)
Addendum coefficient	[haP*]	1.000	
Tip radius factor	[ρaP*]	0.000	
Protuberance height coefficient	[hprP*]	0.000	
Protuberance angle	[αprP]	0.000	
Tip form height coefficient	[hFaP*]	0.000	
Ramp angle	[αKP]	0.000	
	not topping		

Information on final machining

Dedendum reference profile	[hfP*]	1.400	1.400	1.250
Tooth root radius Refer. profile	[ρfP*]	0.390	0.390	0.380
Addendum Reference profile	[haP*]	1.000	1.000	1.000
Protuberance height coefficient	[hprP*]	0.000	0.000	0.000
Protuberance angle (°)	[αprP]	0.000	0.000	0.000
Tip form height coefficient	[hFaP*]	0.000	0.000	0.000
Ramp angle (°)	[αKP]	0.000	0.000	0.000

KISSsoft

Type of profile modification:		none (only running-in)
Tip relief (µm)	[Ca L/R]	2.0 / 2.0 2.0 / 2.0 2.0 / 2.0

Lubrication type		Oil bath lubrication
Type of oil		ISO-VG 320
Lubricant base		Mineral-oil base
Oil nominal kinematic viscosity at 40°C (mm²/s)	[v40]	320.00
Oil nominal kinematic viscosity at 100°C (mm²/s)	[v100]	22.00
Specific density at 15°C (kg/dm³)	[ρ]	0.900
Oil temperature (°C)	[TS]	62.000

Gear pair 1

Overall transmission ratio	[itot]	-0.340
Gear ratio	[u]	1.032
Transverse module (mm)	[mt]	16.000
Transverse pressure angle (°)	[αt]	20.000
Working pressure angle (°)	[αwt]	23.388
	[αwt.e/i]	23.397 / 23.379
Working pressure angle at normal section (°)	[αwn]	23.388
Helix angle at operating pitch circle (°)	[βw]	0.000
Base helix angle (°)	[βb]	0.000
Reference center distance (mm)	[ad]	504.000
Pitch on reference circle (mm)	[pt]	50.265
Base pitch (mm)	[pbt]	47.234
Transverse pitch on contact-path (mm)	[pet]	47.234
Sum of profile shift coefficients	[Σxi]	0.8124
Transverse contact ratio	[εα]	1.456
Transverse contact ratio with allowances	[εα.e/m/i]	1.458 / 1.455 / 1.452
Overlap ratio	[εβ]	0.000
Total contact ratio	[εγ]	1.456
Total contact ratio with allowances	[εγ.e/m/i]	1.458 / 1.455 / 1.452
Length of path of contact (mm)	[ga, e/i]	68.796 (68.884 / 68.567)
Length T1-A (mm)	[T1A]	142.572 (142.572 / 142.503)
Length T1-B (mm)	[T1B]	121.010 (120.922 / 121.170)
Length T1-C (mm)	[T1C]	104.039 (103.994 / 104.084)
Length T1-D (mm)	[T1D]	95.337 (95.337 / 95.269)
Length T1-E (mm)	[T1E]	73.776 (73.688 / 73.936)
Length T2-A (mm)	[T2A]	62.256 (62.168 / 62.413)
Length T2-B (mm)	[T2B]	83.817 (83.817 / 83.746)
Length T2-C (mm)	[T2C]	100.788 (100.745 / 100.831)
Length T2-D (mm)	[T2D]	109.490 (109.402 / 109.647)
Length T2-E (mm)	[T2E]	131.051 (131.051 / 130.980)
Length T1-T2 (mm)	[T1T2]	204.827 (204.739 / 204.915)
Minimal length of contact line (mm)	[Lmin]	219.000

Gear pair 2

Overall transmission ratio	[itot]	-0.340
Gear ratio	[u]	-3.032
Transverse module (mm)	[mt]	16.000
Transverse pressure angle (°)	[αt]	20.000
Working pressure angle (°)	[αwt]	23.388
	[αwt.e/i]	23.379 / 23.397
Working pressure angle at normal section (°)	[αwn]	23.388
Helix angle at operating pitch circle (°)	[βw]	0.000
Base helix angle (°)	[βb]	0.000
Reference center distance (mm)	[ad]	504.000
Pitch on reference circle (mm)	[pt]	50.265
Base pitch (mm)	[pbt]	47.234

KISSsoft

Transverse pitch on contact-path (mm)	[pet]	47.234
Sum of profile shift coefficients	[Σxi]	-0.8124
Transverse contact ratio	[εα]	1.450
Transverse contact ratio with allowances	[εα.e/m/i]	1.455 / 1.451 / 1.446
Overlap ratio	[εβ]	0.000
Total contact ratio	[εγ]	1.450
Total contact ratio with allowances	[εγ.e/m/i]	1.455 / 1.451 / 1.446
Length of path of contact (mm)	[ga, e/i]	68.483 (68.747 / 68.323)
Length T1-A (mm)	[T1A]	131.051 (131.051 / 130.980)
Length T1-B (mm)	[T1B]	109.803 (109.538 / 109.891)
Length T1-C (mm)	[T1C]	100.788 (100.831 / 100.745)
Length T1-D (mm)	[T1D]	83.817 (83.817 / 83.746)
Length T1-E (mm)	[T1E]	62.569 (62.304 / 62.657)
Length T2-A (mm)	[T2A]	335.879 (335.967 / 335.719)
Length T2-B (mm)	[T2B]	314.630 (314.454 / 314.630)
Length T2-C (mm)	[T2C]	305.615 (305.747 / 305.484)
Length T2-D (mm)	[T2D]	288.645 (288.733 / 288.485)
Length T2-E (mm)	[T2E]	267.396 (267.219 / 267.396)
Length T1-T2 (mm)	[T1T2]	204.827 (204.915 / 204.739)
Minimal length of contact line (mm)	[Lmin]	213.000

Gear 1

Profile shift coefficient	[x]	0.5397
Tooth thickness, arc, in module	[sn*]	1.9637
Tip alteration (mm)	[k*mn]	-0.999
Reference diameter (mm)	[d]	512.000
Base diameter (mm)	[db]	481.123
Tip diameter (mm)	[da]	559.272
(mm)	[da.e/i]	559.272 / 559.202
Tip diameter allowances (mm)	[Ada.e/i]	0.000 / -0.070
Tip form diameter (mm)	[dFa]	559.272
(mm)	[dFa.e/i]	559.272 / 559.202
Root diameter (mm)	[df]	484.470
Generating Profile shift coefficient	[xE.e/i]	0.5285/ 0.5234
Generated root diameter with xE (mm)	[df.e/i]	484.113 / 483.948
Root form diameter (mm)	[dFf]	495.533
(mm)	[dFf.e/i]	495.284 / 495.169
Internal toothing: Calculation dFf with pinion type cutter (z0= 32 , x0= 0.000)		
Involute length (mm)	[l_dFa-l_dFf]	34.935
Addendum, $m_n(h_{aP}^*+x+k)$ (mm)	[ha]	23.636
(mm)	[ha.e/i]	23.636 / 23.601
Dedendum (mm)	[hf=mn*(hfP*-x)]	13.765
(mm)	[hf.e/i]	13.943 / 14.026
Tooth height (mm)	[h]	37.401
Virtual gear no. of teeth	[zn]	32.000
Normal tooth thickness at tip circle (mm)	[san]	10.410
(mm)	[san.e/i]	10.308 / 10.202
Normal tooth thickness at tip form circle (mm)	[sFan]	10.410
(mm)	[sFan.e/i]	10.308 / 10.202
Normal space width at root circle (mm)	[efn]	10.877
(mm)	[efn.e/i]	10.951 / 10.986

Gear 2

Profile shift coefficient	[x]	0.2727
Tooth thickness, arc, in module	[sn*]	1.7693
Tip alteration (mm)	[k*mn]	-0.999
Reference diameter (mm)	[d]	496.000
Base diameter (mm)	[db]	466.088
Tip diameter (mm)	[da]	534.729

(mm)	[da.e/i]	534.729 / 534.659
Tip diameter allowances (mm)	[Ada.e/i]	0.000 / -0.070
Tip form diameter (mm)	[dFa]	534.729
(mm)	[dFa.e/i]	534.729 / 534.659
Root diameter (mm)	[df]	459.927
Generating Profile shift coefficient	[xE.e/i]	0.2616/ 0.2564
Generated root diameter with xE (mm)	[df.e/i]	459.570 / 459.405
Root form diameter (mm)	[dFf]	474.356
(mm)	[dFf.e/i]	474.163 / 474.075
Internal toothing: Calculation dFf with pinion type cutter (z0= 31 , x0= 0.000)		
Involute length (mm)	[l_dFa-l_dFf]	32.677
Addendum, $m_n(h_{aP}$*+x+k) (mm)	[ha]	19.365
(mm)	[ha.e/i]	19.365 / 19.330
Dedendum (mm)	[hf=mn*(hfP*-x)]	18.036
(mm)	[hf.e/i]	18.215 / 18.297
Tooth height (mm)	[h]	37.401
Virtual gear no. of teeth	[zn]	31.000
Normal tooth thickness at tip circle (mm)	[san]	11.714
(mm)	[san.e/i]	11.611 / 11.509
Normal tooth thickness at tip form circle (mm)	[sFan]	11.714
(mm)	[sFan.e/i]	11.611 / 11.509
Normal space width at root circle (mm)	[efn]	0.000
(mm)	[efn.e/i]	0.000 / 0.000

Gear 3

Profile shift coefficient	[x]	-1.0852
Tooth thickness, arc, in module	[sn*]	0.7809
Tip alteration (mm)	[k*mn]	-2.186
Reference diameter (mm)	[d]	1504.000
Base diameter (mm)	[db]	1413.298
Tip diameter (mm)	[da]	1511.097
(mm)	[da.e/i]	1511.097 / 1510.972
Tip diameter allowances (mm)	[Ada.e/i]	0.000 / -0.125
Tip form diameter (mm)	[dFa]	1511.097
(mm)	[dFa.e/i]	1511.097 /1510.972
Root diameter (mm)	[df]	1578.725
Generating Profile shift coefficient	[xE.e/i]	-1.1058/ -1.1143
Generated root diameter with xE (mm)	[df.e/i]	1579.659 /1579.384
Root form diameter (mm)	[dFf]	1572.367
(mm)	[dFf.e/i]	1573.191 /1572.949
Internal toothing: Calculation dFf with pinion type cutter (z0= 31 , x0= 0.000)		
Involute length (mm)	[l_dFa-l_dFf]	33.419
Addendum, $m_n(h_{aP}$*+x+k) (mm)	[ha]	-3.548
(mm)	[ha.e/i]	-3.486 / -3.548
Dedendum (mm)	[hf=mn*(hfP*-x)]	37.363
(mm)	[hf.e/i]	37.692 / 37.830
Tooth height (mm)	[h]	33.814
Virtual gear no. of teeth	[zn]	94.000
Normal tooth thickness at tip circle (mm)	[san]	15.193
(mm)	[san.e/i]	14.952 / 14.803
Normal tooth thickness at tip form circle (mm)	[sFan]	15.193
(mm)	[sFan.e/i]	14.952 / 14.803
Normal space width at root circle (mm)	[efn]	6.481
(mm)	[efn.e/i]	6.407 / 6.376

Gear specific pair data Gear pair 1, Gear 1

Operating pitch diameter (mm)	[dw]	524.190
(mm)	[dw.e/i]	524.226 / 524.155
Active tip diameter (mm)	[dNa]	559.272
(mm)	[dNa.e/i]	559.272 / 559.202
Theoretical tip clearance (mm)	[c]	6.400
Effective tip clearance (mm)	[c.e/i]	6.731 / 6.544
Active root diameter (mm)	[dNf]	503.240
(mm)	[dNf.e/i]	503.334 / 503.188
Reserve (dNf-dFf)/2 (mm)	[cF.e/i]	4.082 / 3.952

Max. sliding velocity at tip (m/s)	[vga]	0.308
Specific sliding at the tip	[ζa]	0.549
Specific sliding at the root	[ζf]	-0.834
Mean specific sliding	[ζm]	0.508
Sliding factor on tip	[Kga]	0.299
Sliding factor on root	[Kgf]	-0.235
Roll angle at dFa (°)	[ξdFa.e/i]	33.957 / 33.941
Roll angle to dNa (°)	[ξdNa.e/i]	33.957 / 33.941
Roll angle to dNf (°)	[ξdNf.e/i]	17.610 / 17.551
Roll angle at dFf (°)	[ξdFf.e/i]	14.003 / 13.946
Diameter of single contact point B (mm)	[d-B]	538.565 (538.486 / 538.709)
Diameter of single contact point D (mm)	[d-D]	517.529 (517.529 / 517.478)
Addendum contact ratio	[ε]	0.816 (0.817 / 0.813)

Gear specific pair data Gear pair 1, Gear 2

Operating pitch diameter (mm)	[dw]	507.810
(mm)	[dw.e/i]	507.844 / 507.775
Active tip diameter (mm)	[dNa]	534.729
(mm)	[dNa.e/i]	534.729 / 534.659
Theoretical tip clearance (mm)	[c]	6.400
Effective tip clearance (mm)	[c.e/i]	6.731 / 6.544
Active root diameter (mm)	[dNf]	482.432
(mm)	[dNf.e/i]	482.513 / 482.387
Reserve (dNf-dFf)/2 (mm)	[cF.e/i]	4.219 / 4.112
Max. sliding velocity at tip (m/s)	[vga]	0.393
Specific sliding at the tip	[ζa]	0.455
Specific sliding at the root	[ζf]	-1.219
Mean specific sliding	[ζm]	0.508
Sliding factor on tip	[Kga]	0.235
Sliding factor on root	[Kgf]	-0.299
Roll angle at dFa (°)	[ξdFa.e/i]	32.220 / 32.203
Roll angle to dNa (°)	[ξdNa.e/i]	32.220 / 32.203
Roll angle to dNf (°)	[ξdNf.e/i]	15.345 / 15.284
Roll angle at dFf (°)	[ξdFf.e/i]	10.712 / 10.652
Diameter of single contact point B (mm)	[d-B]	495.317 (495.317 / 495.269)
Diameter of single contact point D (mm)	[d-D]	514.966 (514.891 / 515.099)
Addendum contact ratio	[ε]	0.641 (0.642 / 0.638)

Gear specific pair data Gear pair 2, Gear 2

Operating pitch diameter (mm)	[dw]	507.810
(mm)	[dw.e/i]	507.775 / 507.844
Active tip diameter (mm)	[dNa]	534.729
(mm)	[dNa.e/i]	534.729 / 534.659
Theoretical tip clearance (mm)	[c]	5.998
Effective tip clearance (mm)	[c.e/i]	6.535 / 6.293
Active root diameter (mm)	[dNf]	482.594
(mm)	[dNf.e/i]	482.640 / 482.457
Reserve (dNf-dFf)/2 (mm)	[cF.e/i]	4.283 / 4.147
Max. sliding velocity at tip (m/s)	[vga]	0.133
Specific sliding at the tip	[ζa]	0.155
Specific sliding at the root	[ζf]	-0.409
Mean specific sliding	[ζm]	0.231
Sliding factor on tip	[Kga]	0.080
Sliding factor on root	[Kgf]	-0.101
Roll angle at dFa (°)	[ξdFa.e/i]	32.220 / 32.203
Roll angle to dNa (°)	[ξdNa.e/i]	32.220 / 32.203
Roll angle to dNf (°)	[ξdNf.e/i]	15.405 / 15.318
Roll angle at dFf (°)	[ξdFf.e/i]	10.712 / 10.652
Diameter of single contact point B (mm)	[d-B]	515.232 (515.007 / 515.307)
Diameter of single contact point D (mm)	[d-D]	495.317 (495.317 / 495.269)
Addendum contact ratio	[ε]	0.641 (0.640 / 0.640)

Gear specific pair data Gear pair 2, Gear 3

KISSsoft

Operating pitch diameter (mm)	[dw]	1539.810
(mm)	[dw.e/i]	1539.914 /1539.705
Active tip diameter (mm)	[dNa]	1511.097
(mm)	[dNa.e/i]	1511.097 /1510.972
Theoretical tip clearance (mm)	[c]	9.585
Effective tip clearance (mm)	[c.e/i]	9.881 / 9.666
Active root diameter (mm)	[dNf]	1564.822
(mm)	[dNf.e/i]	1564.898 /1564.685
Reserve (dNf-dFf)/2 (mm)	[cF.e/i]	4.253 / 4.025
Max. sliding velocity at tip (m/s)	[vga]	0.145
Specific sliding at the tip	[ζa]	0.290
Specific sliding at the root	[ζf]	-0.183
Mean specific sliding	[ζm]	0.231
Sliding factor on tip	[Kga]	0.101
Sliding factor on root	[Kgf]	-0.080
Roll angle at dFa (°)	[ξdFa.e/i]	21.666 / 21.681
Roll angle to dNa (°)	[ξdNa.e/i]	21.666 / 21.681
Roll angle to dNf (°)	[ξdNf.e/i]	27.220 / 27.241
Roll angle at dFf (°)	[ξdFf.e/i]	27.992 / 28.015
Diameter of single contact point B (mm)	[d-B]	1547.055 (1546.911 /1547.055)
Diameter of single contact point D (mm)	[d-D]	1526.654 (1526.721 / 1526.534)
Addendum contact ratio	[ε]	0.809 (0.816 / 0.806)

General influence factors

		------- Gear 1	--------- Gear 2	--------- Gear 3 ---
Nominal circum. force at pitch circle (N)	[Ft]	138076.844	138076.844	
Axial force (N)	[Fa]	0.0	0.0	0.0
Total axial force (N)	[Fatot=Fa* 3]	0.0		0.0
Radial force (N)	[Fr]	50255.861		50255.861
Normal force (N)	[Fnorm]	146938.3	146938.3	146938.3
Nominal circumferential force per mm (N/mm)	[w]	630.49	648.25	
Only as information: Forces at operating pitch circle:				
Nominal circumferential force (N)	[Ftw]	134865.754	134865.754	
Axial force (N)	[Fa]	0.0		
Axial force (N)	[Fa]		0.0 /0.0	
Axial force (N)	[Fa]			0.0
Total axial force (N)	[Fatot=Fa* 3]	0.0		0.0
Radial force (N)	[Fr]	58327.478	58327.478	
Circumferential speed reference circle (m/s)	[v]	1.28	(Planet)	
Running-in value (µm)	[yp]	1.185	1.282	
Running-in value (µm)	[yf]	1.500	1.500	
Gear blank factor	[CR]	1.000	1.000	
Correction factor	[CM]	0.800	0.800	
Basic rack factor	[CBS]	0.900	0.937	
Material coefficient	[E/Est]	1.000	1.000	
Singular tooth stiffness (N/mm/µm)	[c']	13.495	13.858	
Meshing stiffness (N/mm/µm)	[cγα]	18.116	18.534	
Meshing stiffness (N/mm/µm)	[cγβ]	15.398	15.754	
Reduced mass (kg/mm)	[mRed]	0.2381	0.7055	
Resonance speed (min-1)	[nE1]	2603	1579	
Resonance ratio (-)	[N]	0.018	0.031	
Running-in value (µm)	[yα]	1.185	1.282	
Planet runs on rolling bearings. Planet pin fixed on both sides in the carrier..				
lpa (mm) = 284.70 b (mm) =219.00dsh (mm) =		248.00		
Tooth trace deviation (active) (µm)	[Fβy]	6.38	8.70	
from deformation of shaft (µm)	[fsh*B1]	7.99	0.57	
(fsh (µm) =7.99 / 0.57, B1 = 1.00 /	1.00, fHβ5 (µm) =	10.00 / 11.00)		
Tooth trace		0	0	
(0: without, 1: crowned, 2: end relief, 3: full modification)				
(4: slightly crowned, 5: helix angle modification, 6: helix angle modification with crowning)				
from production tolerances (µm)	[fmα*B2]	21.21	21.93	
B2 = 1.00 / 1.00				
Tooth trace deviation, theoretical (µm)	[Fβx]	7.50	10.24	
Running-in value yβ (µm)	[yβ]	1.13	1.54	

KISSsoft

Dynamic factor	[Kv=max(Kv12,Kv23)]	1.01		
	[Kv12,Kv23]	1.01	1.01	
Face load factor - flank	[KHβ]	1.08	1.11	
- Tooth root	[KFβ]	1.06	1.09	
- Scuffing	[KBβ]	1.08	1.11	
Transverse load factor - flank	[KHα]	1.00	1.00	
- Tooth root	[KFα]	1.00	1.00	
- Scuffing	[KBα]	1.00	1.00	
Number of load cycles (in mio.)	[NL]	172.4	59.3	58.7

Tooth root load capacity

Calculation of Tooth form coefficients according method: B

Internal toothing: Calculation of ρF and sFn according to ISO 6336-3:2007-04-01

Internal toothing: Calculation of YF, YS with pinion type cutter, z0= 31 , x0=0.000 , ρaP0*= 0.380

		Gear 1	Gear 2	Gear 3
Calculated with generating profile shift coefficient	[xE.i]	0.5234	0.2564	-1.1143
Tooth form factor	[YF]	1.35		
	[YF]		1.54 /1.55	
	[YF]			0.87
Stress correction factor	[YS]	2.12		
	[YS]		1.92 /1.91	
	[YS]			2.96
Bending moment arm (mm)	[hF]	20.17		
(mm)	[hF]		20.68 /20.82	
(mm)	[hF]			20.88
Load application angle (°)	[αFen]	24.47		
(°)	[αFen]		22.82 /22.89	
(°)	[αFen]			23.01
Coefficient	[fε]	1.000	1.000	
Tooth thickness at root (mm)	[sFn]	37.21		
(mm)	[sFn]		35.55 /35.55	
(mm)	[sFn]			47.37
Tooth root radius (mm)	[ρF]	7.19		
(mm)	[ρF]		8.31 /8.31	
(mm)	[ρF]			5.19

hF* = 1.261 /1.293 /1.302 / 1.305 sFn* = 2.326 /2.222 / 2.222 / 2.961

ρF* =0.449 /0.519 /0.519 / 0.324 dsFn =489.682 / 465.651 / 465.651 /-1577.961 αsFn = 30.0 / 30.0 / 30.0 / 60.0

Helix angle factor	[Yβ]	1.00	1.00	
Deep tooth factor	[YDT]	1.00	1.00	
Gear rim thickness (mm)	[sr]	483.95	459.41	55.53
Gear rim factor	[YB]	1.00	1.00	1.01
Effective facewidth (mm)	[beff]	224.00		
(mm)	[beff]		219.00 /219.00	
(mm)	[beff]			213.00
Nominal stress at tooth root (N/mm²)	[σF0]	110.67		
(N/mm²)	[σF0]		116.51 /117.00	
(N/mm²)	[σF0]			105.50
Tooth root stress (N/mm²)	[σF]	119.44		
(N/mm²)	[σF]		125.74 /129.23	
(N/mm²)	[σF]			116.52
Permissible bending stress at root of Test-gear				
Notch sensitivity factor	[YdrelT]	1.001		
Notch sensitivity factor	[YdrelT]		0.996 / 0.996	
Notch sensitivity factor	[YdrelT]			1.017
Surface factor	[YRrelT]	0.957	0.957	0.957
Size factor, tooth root	[YX]	0.890	0.890	0.890
Finite life factor	[YNT]	0.922	0.942	0.942
Alternating bending factor, mean stress influence coefficient				
	[YM]	1.000	0.700	1.000
Stress correction factor	[Yst]	2.00		
Yst*σFlim (N/mm²)	[σFE]	860.00	860.00	860.00
Permissible tooth root stress (N/mm²)	[σFP=σFG/SFmin]	482.69		
Permissible tooth root stress (N/mm²)	[σFP=σFG/SFmin]		343.68 /343.68	

Permissible tooth root stress (N/mm²)	[σFP=σFG/SFmin]				501.16	
Limit strength tooth root (N/mm²)	[σFG]	675.76				
Limit strength tooth root (N/mm²)	[σFG]			481.16	/481.16	
Limit strength tooth root (N/mm²)	[σFG]				701.62	
Required safety	[SFmin]	1.40	1.40		1.40	
Safety for tooth root stress	[SF=σFG/σF]	5.66				
	[SF=σFG/σF]			3.83	/3.72	
	[SF=σFG/σF]				6.02	
Transmittable power (kW)	[kWRating]	2148.78				
(kW)	[kWRating]			1453.36	/1414.10	
(kW)	[kWRating]				2286.84	

Flank safety

		------- Gear 1	--------- Gear 2	--------- Gear 3 ---		
Zone factor	[ZH]	2.29	2.29			
Elasticity factor (√N/mm²)	[ZE]	189.81	189.81			
Contact ratio factor	[Zε]	0.921	0.922			
Helix angle factor	[Zβ]	1.000	1.000			
Effective facewidth (mm)	[beff]	219.00	213.00			
Nominal contact stress (N/mm²)	[σH0]	632.73	374.82			
Contact stress at operating pitch circle (N/mm²)	[σHw]	661.39	397.30			
Single tooth contact factor	[ZB,ZD]	1.00	1.02	/1.13	1.00	
Contact stress (N/mm²)	[σHB, σHD]	662.89	672.48	/448.29	397.30	
Lubrication factor for NL	[ZL]	1.047	1.047 /	1.047	1.047	
Speed factor for NL	[ZV]	0.958	0.958 /	0.958	0.958	
Roughness factor for NL	[ZR]	1.006	1.006 /	1.035	1.035	
Material hardening factor for NL	[ZW]	1.000	1.000 /	1.000	1.000	
Finite life factor	[ZNT]	0.963	0.995	0.995		
Limited pitting is permitted: No						
Size factor (flank)	[ZX]	1.000	1.000	1.000		
Permissible contact stress, σHG/SHmin (N/mm²)	[σHP]	1457.05	1505.52	/1549.41	1549.92	
Pitting stress limit (N/mm²)	[σHG]	1457.05	1505.52	/1549.41	1549.92	
Required safety	[SHmin]	1.00	1.00	1.00		
Safety factor for contact stress at operating pitch circle	[SHw]	2.20	2.28	/3.90	3.90	
Safety for stress at single tooth contact	[SHBD=σHG/σHBD]	2.20	2.24	/3.46	3.90	
	Safety regarding transmittable torque[(SHBD)^2]	4.83	5.01	/	11.95	15.22
Transmittable power (kW)	[kWRating]	2568.90	2664.95	/6351.61	8092.00	

Micropitting according to **ISO/TS 6336-22:2018**

Pairing Gear 1 -2 :
Calculation has not been carried out, lubricant: Load stage micropitting test not known

Pairing Gear 2 -3 :
Calculation has not been carried out, lubricant: Load stage micropitting test not known

Scuffing load capacity

Calculation method according to	ISO/TS 6336-20/21:2017					
Helical load factor for scuffing	[KBγ]	1.00	1.00			
Lubrication coefficient for lubrication type	[XS]	1.000				
Scuffing test and load stage	[FZGtest] FZG - Test A / 8.3 / 90 (ISO 14635 - 1)	12				
Multiple meshing factor	[Xmp]	2.0	2.0			
Relative structural factor, scuffing	[XWrelT]	1.000	1.000			
Thermal contact factor (N/mm/s^.5/K)	[BM]	13.780	13.780	13.780		
Relevant tip relief (µm)	[Ca]	2.00	2.00	/ 2.00	2.00	
Optimal tip relief (µm)	[Ceff]	46.72	46.78			
Ca taken as optimal in the calculation (0=no, 1=yes)		0	0	/0	0	
Effective facewidth (mm)	[beff]	219.000	213.000			

KISSsoft

Applicable circumferential force/facewidth (N/mm)	[wBt]		688.900	728.331		
(1) KBγ = 1.000 , wBt*KBγ =688.900						
(2) KBγ = 1.000 , wBt*KBγ =728.331						
Angle factor	[Xαβ]		1.027	1.027		
Flash temperature-criteria						
Lubricant factor	[XL]		0.679	0.679		
Tooth mass temperature (°C)	[θMi]		68.48	63.44		
θMi = θoil + XS*0.47*Xmp*θflm						
Average flash temperature	(°C)	[θflm]	6.89	1.53		
Scuffing temperature (°C)	[θS]		299.98	299.98		
Γ coordinates (point of highest temperature)	[Γ]		0.370	-0.359		
(1) [Γ.A]= 0.370 [Γ.E]= -0.291						
(2) [Γ.A]= 0.300 [Γ.E]= -0.379						
Highest contact temp. (°C)	[θB]		80.41	66.02		
Flash factor (°K*N^-.75*s^.5*m^-.5*mm)	[XM]		50.058	50.058		
Approach factor	[XJ]		1.157	1.000		
Load sharing factor	[XΓ]		0.333	0.366		
Dynamic viscosity (mPa*s)	[ηM]		81.42	81.42	(62.0	°C)
Coefficient of friction	[μ_m]		0.053	0.043		
Required safety	[SBmin]		2.000			
Margin of safety for scuffing, flash temperature	[SB]		12.926	59.226		
Integral temperature-criteria						
Lubricant factor (Input)	[XL]		0.846			
Tooth mass temperature (°C)	[θMC]		67.86	62.80		
θMC = θoil + XS*0.70*θflaint						
Mean flash temperature	(°C)	[θflaint]	4.19	0.57		
Integral scuffing temperature (°C)	[θSint]		316.54	316.54		
Flash factor (°K*N^-.75*s^.5*m^-.5*mm)	[XM]		50.058	50.058		
Running-in factor, well run in	[XE]		1.000	1.000		
Contact ratio factor	[Xε]		0.342	0.342		
Dynamic viscosity (mPa*s)	[ηOil]		81.42	81.42		
Mean coefficient of friction	[μ_m]		0.037	0.023		
Geometry factor	[XBE]		0.220	0.046		
Meshing factor	[XQ]		1.000	1.000		
Tip relief factor	[XCa]		1.088	1.087		
Integral tooth flank temperature (°C)	[θint]		74.14	63.66		
Required safety	[SSmin]		1.800			
Safety factor for scuffing (intg.-temp.)	[SSint]		4.27	4.97		
Safety referring to transmittable torque	[SSL]		20.97	153.05		

Measurements for tooth thickness

		Gear 1	Gear 2	Gear 3		
Tooth thickness tolerance		DIN 3967 cd25	DIN 3967 cd25	DIN 3967 cd25		
Tooth thickness allowance (normal section) (mm)	[As.e/i]	-0.130 /	-0.190-0.130 /	-0.190-0.240 /	-0.340	
Number of teeth spanned	[k]	5.000	4.000	13.000		
(Internal toothing: k = (Measurement gap number)						
Base tangent length (no backlash) (mm)	[Wk]	225.631	175.251	623.367		
Base tangent length with allowance (mm)	[Wk.e/i]	225.509 /	225.453175.129 /	175.072	623.593 /	623.687
Diameter of measuring circle (mm)	[dMWk.m]	531.338	497.893	1544.777		
Theoretical diameter of ball/pin (mm)	[DM]	30.123	28.545	26.674		
Effective diameter of ball/pin (mm)	[DMeff]	30.000	30.000	28.000		
Radial single-ball measurement backlash free (mm)	[MrK]	286.125	274.844	748.433		
Radial single-ball measurement (mm)	[MrK.e/i]	285.992 /	285.931274.706 /	274.642	748.858 /	748.733
Diameter of measuring circle (mm)	[dMMr.m]	528.788	506.830	1536.354		
Diametral measurement over two balls without clearance (mm)	[MdK]	572.249	549.021	1496.867		
Diametral two ball measure (mm)	[MdK.e/i]	571.984 /	571.862548.745 /	548.617	1497.716 /	1497.467
Measurement over pins according to DIN 3960 (mm)	[MdR.e/i]	571.984 /	571.862548.745 /	548.617	1497.716 /	1497.467
Measurement over 3 pins, axial, according to AGMA 2002 (mm)						
	[dk3A.e/i]	571.984 /	571.862548.745 /	548.617	1497.716 /	1497.467
Measurement over 3 pins with allowance (mm)	[Md3R.e/i]	0.000 /	0.000548.079 /	547.952	-0.000 / -0.000	
Chordal tooth thickness in reference circle (mm)	[sc]	31.399	28.294	12.494		
(mm)	[sc.e/i]	31.272 /	31.21328.166 /	28.10712.253 /	12.153	
Reference chordal height from da.m (mm)	[ha]	24.101	19.751	-3.543		
Tooth thickness, arc (mm)	[sn]	31.419	28.309	12.494		

(mm)	[sn.e/i]	31.289 /	31.229	28.179 /	28.119	12.254 /	12.154
Backlash free center distance (mm)	[aControl.e/i]	515.692 /	515.549	516.437 /	516.625		
Backlash free center distance, allowances (mm)	[jta]	-0.308 /	-0.451	0.437 /	0.625		
dNf.i with aControl (mm)	[dNf0.i]	502.577	481.849	/ 481.700	1566.173		
Reserve (dNf0.i-dFf.e)/2 (mm)	[cF0.i]	3.647	3.843	/3.768	3.388		
Tip clearance (mm)	[c0.i(aControl)]	6.128	6.128	/5.891	9.075		
Center distance allowances (mm)	[Aa.e/i]	0.035 /	-0.035	-0.035 /	0.035		
Circumferential backlash from Aa (mm)	[jtw_Aa.e/i]	0.030 /	-0.030	0.030 /	-0.030		
Radial backlash (mm)	[jrw]	0.486 /	0.273	0.660 /	0.402		
Circumferential backlash, transverse section (mm)	[jtw]	0.419 /	0.236	0.573 /	0.349		
Normal backlash (mm)	[jnw]	0.381 /	0.220	0.522 /	0.324		
Torsional angle on input with output fixed:							
Total torsional angle (°)	[j.tSys]	0.0517/	0.0358				

Toothing tolerances

		------- Gear 1 ---------	Gear 2 ---------	Gear 3 ---
According to ISO 1328-1:2013, ISO 1328-2:1997				
Accuracy grade	[Q]	A6	A6	A6
Single pitch deviation (µm)	[fptT]	17.00	17.00	18.00
Base circle pitch deviation (µm)	[fpbT]	15.80	15.80	17.10
Sector pitch deviation over k/8 pitches (µm)	[Fpk/8T]	34.00	35.00	43.00
Profile form deviation (µm)	[ffαT]	20.00	20.00	20.00
Profile slope deviation (µm)	[fHαT]	15.00	15.00	17.00
Total profile deviation (µm)	[FαT]	25.00	25.00	26.00
Helix form deviation (µm)	[ffβT]	17.00	17.00	19.00
Helix slope deviation (µm)	[fHβT]	15.00	15.00	16.00
Total helix deviation (µm)	[FβT]	23.00	23.00	24.00
Total cumulative pitch deviation (µm)	[FpT]	52.00	52.00	67.00
Adjacent pitch difference (µm)	[fuT]	24.00	24.00	26.00
Runout (µm)	[FrT]	47.00	46.00	61.00
Single flank composite, total (µm)	[FisT]	67.00	67.00	83.00
Single flank composite, tooth-to-tooth (µm)	[fisT]	16.00	16.00	16.00
Radial composite, total (µm)	[FidT]	110.00	110.00	137.00
Radial composite, tooth-to-tooth (µm)	[fidT]	68.00	68.00	69.00

FidT (Fi"), fidT (fi") according to ISO 1328:1997 calculated with the geometric mean values for mn and d

Axis alignment tolerances (recommendation acc. to ISO TR 10064-3:1996, Quality)		6	
Maximum value for deviation error of axis (µm)	[fΣβ]	14.95	14.95
Maximum value for inclination error of axes (µm)	[fΣδ]	29.90	29.90

Modifying and defining the tooth form

Data for the tooth form calculation :
Data not available.
Please run the calculation in the "Tooth form" tab and open the main report again.

Supplementary data

Mass (kg)	[m]	375.169	333.106	618.003
Total mass (kg)	[mGes]	1992.489		
Moment of inertia for system, relative to the input:				
calculation without consideration of the exact tooth shape				
Single gears (da+df)/2...di (kg*m²)	[J]	12.77214	10.29861	405.20157
System (da+df)/2...di (kg*m²)	[J]	799.48558		
Torsional stiffness at driving gear with fixed driven gear:				
Torsional stiffness (MNm/rad)	[cr]	2441.902		
Torsion when subjected to nominal torque (°)	[δcr]	0.007		
Mean coefficient of friction (as defined in Niemann)	[μ_m]	0.036	0.029	
Wear sliding coef. by Niemann	[ζw]	0.739	0.311	
Loss factor	[HV]	0.124	0.042	

Meshing power (kW)		531.712	531.712
Gear power loss (kW)	[PVZ]	0.791	0.217
Total power loss (kW)		3.022	
Total efficiency		0.994	
Sound pressure level according to Masuda, without contact analysis	[dB(A)]	92.9	95.8

Service life, damage

Required safety for tooth root	[SFmin]	1.40		
Required safety for tooth flank	[SHmin]	1.00		
Service life (calculated with required safeties):				
System service life (h)	[Hatt]	> 1000000		
Tooth root service life (h)	[HFatt]	1e+06	1e+06	1e+06
Tooth flank service life (h)	[HHatt]	1e+06	1e+06	1e+06

Note: The entry 1e+006 h means that the Service life > 1,000,000 h.

Damage calculated on the basis of the required service life (20000.0 h)

F1%	F2%	F3%	H1%	H2%	H3%
0.00	0.0000	0.0000	0.0000	0.0000	0.0000

Remarks:

- Specifications with [.e/i] imply: Maximum [e] and minimum value [i] for
  Taking all tolerances into account
  Specifications with [.m] imply: Mean value within tolerance
- For the backlash tolerance, the center distance tolerances and the tooth thickness allowance are taken into account.
  The maximum and minimum clearance according to the largest or smallest allowances are defined..
  The calculation is performed for the operating pitch circle.
- Details of calculation method:
  cγ according to Method B
  Kv according to Method B
  KHβ and KFβ according to Method C
  fmα according to Equation 64, Fβx according to 52/53/56
  fsh calculated by exactly following the method in Annex D,
  ISO 6336-1:2006
  Literature: Journal "Antriebstechnik", 6/2007, p.64.
  KHα, KFα according to Method B
- The logarithmically interpolated value taken from the values for the fatigue strength and the static strength, based on the number of load cycles, is used for coefficients ZL, ZV, ZR, ZW, ZX, YdrelT, YRrelT and YX..

End of Report lines: 824

Third Planetary Stage

Calculation of a spur planetary gear stage

Drawing or article number:					
Gear 1:	0.000.0				
Gear 2:	0.000.0				
Gear 3:	0.000.0				
Calculation method	ISO 6336:2019				
		------- Sun	---------- Planets	---------- Internal gear ---	
Number of planets	[p]	1	3	1	
Power (kW)	[P]	1489.836			
Speed (1/min)	[n]	563.4		-47.9	
Speed difference for planet bearing calculation (1/min)		[n2]	313.1		
Speed planet carrier (1/min)	[nSteg]	70.1			
Power (kW)	[P]	1489.836		529.460	
Planet carrier performance (kW)	[PSteg]	960.376			
Torque (Nm)	[T]	25250.8	0.0	105594.0	
Torque Pl.-Carrier (Nm)	[TSteg]	130844.795			
Application factor	[KA]	1.00			
Distribution factor	[Kγ]	1.00			
Required service life (h)	[H]	20000.00			
Gear driving (+) / driven (-)		-	+/-	+	
Working flank gear 1:	Left flank				
Gear 1 direction of rotation:	Clockwise				
Planet carrier direction of rotation:	clockwise				
Gear 3 direction of rotation:	counterclockwise				

Tooth geometry and material

Geometry calculation according to	ISO 21771:2007				
		------- Gear 1	--------- Gear 2	--------- Gear 3 ---	
Center distance (mm)	[a]	393.000			
Center distance tolerance	ISO 286:2010 Measure js7				
Normal module (mm)	[mn]	9.0000			
Normal pressure angle (°)	[αn]	20.0000			
Helix angle at reference circle (°)	[β]	0.0000			
Number of teeth	[z]	33	52	-138	
Facewidth (mm)	[b]	183.00	178.00	174.00	
Hand of gear	Spur gear				
Planetary axles can be placed in regular pitch.:	120 °				
Accuracy grade	[Q-ISO 1328:2013]	A6	A6	A6	
Inner diameter (mm)	[di]	0.00	0.00		
External diameter (mm)	[di]			1352.64	
Inner diameter of gear rim (mm)	[dbi]	0.00	0.00		
Outer diameter of gear rim (mm)	[dbi]			0.00	

Material

Gear1
18CrNiMo7-6, Case-carburized steel, case-hardened
ISO 6336-5 Figure 9/10 (MQ), Core hardness >=25HRC Jominy J=12mm<HRC28

Gear2

KISSsoft

18CrNiMo7-6, Case-carburized steel, case-hardened
ISO 6336-5 Figure 9/10 (MQ), Core hardness >=25HRC Jominy J=12mm<HRC28

Gear3
18CrNiMo7-6, Case-carburized steel, case-hardened
ISO 6336-5 Figure 9/10 (MQ), Core hardness >=25HRC Jominy J=12mm<HRC28

		------- Gear 1	--------- Gear 2	--------- Gear 3 ---
Surface hardness		HRC 61	HRC 61	HRC 61
Material treatment according to ISO 6336:2006 Normal, life factors ZNT and YNT >=0.85				
Fatigue strength. tooth root stress (N/mm²)	[σFlim]	430.00	430.00	430.00
Fatigue strength for Hertzian pressure (N/mm²)	[σHlim]	1500.00	1500.00	1500.00
Tensile strength (N/mm²)	[σB]	1200.00	1200.00	1200.00
Yield point (N/mm²)	[σS]	850.00	850.00	850.00
Young's modulus (N/mm²)	[E]	206000	206000	206000
Poisson's ratio	[v]	0.300	0.300	0.300
Roughness average value DS, flank (µm)	[RAH]	0.60	0.60	0.60
Roughness average value DS, root (µm)	[RAF]	3.00	3.00	3.00
Mean roughness height, Rz, flank (µm)	[RZH]	4.80	4.80	4.80
Mean roughness height, Rz, root (µm)	[RZF]	20.00	20.00	20.00

Gear reference profile 1:

Reference profile	1.40 / 0.39 / 1.0 ISO 53:1998 Profil D		
Dedendum coefficient	[hfP*]	1.400	
Root radius factor	[ρfP*]	0.390	(ρfPmax*=0.394)
Addendum coefficient	[haP*]	1.000	
Tip radius factor	[ρaP*]	0.000	
Protuberance height coefficient	[hprP*]	0.000	
Protuberance angle	[αprP]	0.000	
Tip form height coefficient	[hFaP*]	0.000	
Ramp angle	[αKP]	0.000	
	not topping		

Gear reference profile 2:

Reference profile	1.40 / 0.39 / 1.0 ISO 53:1998 Profil D		
Dedendum coefficient	[hfP*]	1.400	
Root radius factor	[ρfP*]	0.390	(ρfPmax*=0.394)
Addendum coefficient	[haP*]	1.000	
Tip radius factor	[ρaP*]	0.000	
Protuberance height coefficient	[hprP*]	0.000	
Protuberance angle	[αprP]	0.000	
Tip form height coefficient	[hFaP*]	0.000	
Ramp angle	[αKP]	0.000	
	not topping		

Gear reference profile 3:

Reference profile	1.25 / 0.38 / 1.0 ISO 53:1998 Profil A		
Dedendum coefficient	[hfP*]	1.250	
Root radius factor	[ρfP*]	0.380	(ρfPmax*=0.472)
Addendum coefficient	[haP*]	1.000	
Tip radius factor	[ρaP*]	0.000	
Protuberance height coefficient	[hprP*]	0.000	
Protuberance angle	[αprP]	0.000	
Tip form height coefficient	[hFaP*]	0.000	
Ramp angle	[αKP]	0.000	
	not topping		

Information on final machining

Dedendum reference profile	[hfP*]	1.400	1.400	1.250
Tooth root radius Refer. profile	[ρfP*]	0.390	0.390	0.380
Addendum Reference profile	[haP*]	1.000	1.000	1.000
Protuberance height coefficient	[hprP*]	0.000	0.000	0.000
Protuberance angle (°)	[αprP]	0.000	0.000	0.000
Tip form height coefficient	[hFaP*]	0.000	0.000	0.000

Ramp angle (°)	[αKP]	0.000	0.000	0.000

Type of profile modification:	none (only running-in)	
Tip relief (µm)	[Ca L/R]	2.0 / 2.0 2.0 / 2.0 2.0 / 2.0

Lubrication type	Oil bath lubrication	
Type of oil	ISO-VG 320	
Lubricant base	Mineral-oil base	
Oil nominal kinematic viscosity at 40°C (mm²/s)	[v40]	320.00
Oil nominal kinematic viscosity at 100°C (mm²/s)	[v100]	22.00
Specific density at 15°C (kg/dm³)	[ρ]	0.900
Oil temperature (°C)	[TS]	62.000

Gear pair 1

Overall transmission ratio	[itot]	0.124
Gear ratio	[u]	1.576
Transverse module (mm)	[mt]	9.000
Transverse pressure angle (°)	[αt]	20.000
Working pressure angle (°)	[αwt]	23.853
	[αwt.e/i]	23.862 / 23.844
Working pressure angle at normal section (°)	[αwn]	23.853
Helix angle at operating pitch circle (°)	[βw]	0.000
Base helix angle (°)	[βb]	0.000
Reference center distance (mm)	[ad]	382.500
Pitch on reference circle (mm)	[pt]	28.274
Base pitch (mm)	[pbt]	26.569
Transverse pitch on contact-path (mm)	[pet]	26.569
Sum of profile shift coefficients	[Σxi]	1.2774
Transverse contact ratio	[εα]	1.380
Transverse contact ratio with allowances	[εα.e/m/i]	1.383 / 1.378 / 1.373
Overlap ratio	[εβ]	0.000
Total contact ratio	[εγ]	1.380
Total contact ratio with allowances	[εγ.e/m/i]	1.383 / 1.378 / 1.373
Length of path of contact (mm)	[ga, e/i]	36.671 (36.741 / 36.475)
Length T1-A (mm)	[T1A]	83.764 (83.764 / 83.709)
Length T1-B (mm)	[T1B]	73.663 (73.592 / 73.803)
Length T1-C (mm)	[T1C]	61.701 (61.673 / 61.728)
Length T1-D (mm)	[T1D]	57.195 (57.195 / 57.139)
Length T1-E (mm)	[T1E]	47.093 (47.023 / 47.233)
Length T2-A (mm)	[T2A]	75.162 (75.091 / 75.287)
Length T2-B (mm)	[T2B]	85.263 (85.263 / 85.193)
Length T2-C (mm)	[T2C]	97.225 (97.182 / 97.268)
Length T2-D (mm)	[T2D]	101.731 (101.660 / 101.857)
Length T2-E (mm)	[T2E]	111.832 (111.832 / 111.763)
Length T1-T2 (mm)	[T1T2]	158.926 (158.855 / 158.996)
Minimal length of contact line (mm)	[Lmin]	178.000

Gear pair 2

Overall transmission ratio	[itot]	0.124
Gear ratio	[u]	-2.654
Transverse module (mm)	[mt]	9.000
Transverse pressure angle (°)	[αt]	20.000
Working pressure angle (°)	[αwt]	22.279
	[αwt.e/i]	22.269 / 22.290
Working pressure angle at normal section (°)	[αwn]	22.279
Helix angle at operating pitch circle (°)	[βw]	0.000
Base helix angle (°)	[βb]	0.000
Reference center distance (mm)	[ad]	387.000
Pitch on reference circle (mm)	[pt]	28.274

KISSsoft

Base pitch (mm)	[pbt]	26.569
Transverse pitch on contact-path (mm)	[pet]	26.569
Sum of profile shift coefficients	[Σxi]	-0.7037
Transverse contact ratio	[εα]	1.218
Transverse contact ratio with allowances	[εα.e/m/i]	1.227 / 1.220 / 1.212
Overlap ratio	[εβ]	0.000
Total contact ratio	[εγ]	1.218
Total contact ratio with allowances	[εγ.e/m/i]	1.227 / 1.220 / 1.212
Length of path of contact (mm)	[ga, e/i]	32.358 (32.605 / 32.214)
Length T1-A (mm)	[T1A]	111.832 (111.832 / 111.763)
Length T1-B (mm)	[T1B]	106.043 (105.796 / 106.118)
Length T1-C (mm)	[T1C]	90.090 (90.136 / 90.045)
Length T1-D (mm)	[T1D]	85.263 (85.263 / 85.193)
Length T1-E (mm)	[T1E]	79.474 (79.227 / 79.549)
Length T2-A (mm)	[T2A]	260.828 (260.903 / 260.683)
Length T2-B (mm)	[T2B]	255.039 (254.867 / 255.039)
Length T2-C (mm)	[T2C]	239.086 (239.206 / 238.965)
Length T2-D (mm)	[T2D]	234.258 (234.334 / 234.114)
Length T2-E (mm)	[T2E]	228.469 (228.298 / 228.469)
Length T1-T2 (mm)	[T1T2]	148.995 (149.071 / 148.920)
Minimal length of contact line (mm)	[Lmin]	174.000

Gear 1

Profile shift coefficient	[x]	0.5845
Tooth thickness, arc, in module	[sn*]	1.9963
Tip alteration (mm)	[k*mn]	-0.006
Reference diameter (mm)	[d]	297.000
Base diameter (mm)	[db]	279.089
Tip diameter (mm)	[da]	325.509
(mm)	[da.e/i]	325.509 / 325.452
Tip diameter allowances (mm)	[Ada.e/i]	0.000 / -0.057
Tip form diameter (mm)	[dFa]	325.509
(mm)	[dFa.e/i]	325.509 / 325.452
Root diameter (mm)	[df]	282.321
Generating Profile shift coefficient	[xE.e/i]	0.5647/ 0.5555
Generated root diameter with xE (mm)	[df.e/i]	281.964 / 281.799
Root form diameter (mm)	[dFf]	288.268
(mm)	[dFf.e/i]	288.009 / 287.890
Internal toothing: Calculation dFf with pinion type cutter (z0= 33 , x0= 0.000)		
Involute length (mm)	[l_dFa-l_dFf]	20.475
Addendum, $m_n(h_{aP}^*+x+k)$ (mm)	[ha]	14.254
(mm)	[ha.e/i]	14.254 / 14.226
Dedendum (mm)	[hf=mn*(hfP*-x)]	7.339
(mm)	[hf.e/i]	7.518 / 7.600
Tooth height (mm)	[h]	21.594
Virtual gear no. of teeth	[zn]	33.000
Normal tooth thickness at tip circle (mm)	[san]	5.126
(mm)	[san.e/i]	5.017 / 4.917
Normal tooth thickness at tip form circle (mm)	[sFan]	5.126
(mm)	[sFan.e/i]	5.017 / 4.917
Normal space width at root circle (mm)	[efn]	5.921
(mm)	[efn.e/i]	5.984 / 6.014

Gear 2

Profile shift coefficient	[x]	0.6929
Tooth thickness, arc, in module	[sn*]	2.0752
Tip alteration (mm)	[k*mn]	-2.544
Reference diameter (mm)	[d]	468.000
Base diameter (mm)	[db]	439.776

KISSsoft

Tip diameter (mm)	[da]	493.385
(mm)	[da.e/i]	493.385 / 493.322
Tip diameter allowances (mm)	[Ada.e/i]	0.000 / -0.063
Tip form diameter (mm)	[dFa]	493.385
(mm)	[dFa.e/i]	493.385 / 493.322
Root diameter (mm)	[df]	455.273
Generating Profile shift coefficient	[xE.e/i]	0.6731/ 0.6639
Generated root diameter with xE (mm)	[df.e/i]	454.916 / 454.751
Root form diameter (mm)	[dFf]	460.431
(mm)	[dFf.e/i]	460.123 / 459.981
Internal toothing: Calculation dFf with pinion type cutter (z0= 50 , x0= 0.000)		
Involute length (mm)	[l_dFa-l_dFf]	17.868
Addendum, $m_n(h_{aP}^*+x+k)$ (mm)	[ha]	12.692
(mm)	[ha.e/i]	12.692 / 12.661
Dedendum (mm)	[hf=mn*(hfP*-x)]	6.364
(mm)	[hf.e/i]	6.542 / 6.625
Tooth height (mm)	[h]	19.056
Virtual gear no. of teeth	[zn]	52.000
Normal tooth thickness at tip circle (mm)	[san]	8.249
(mm)	[san.e/i]	8.143 / 8.049
Normal tooth thickness at tip form circle (mm)	[sFan]	8.249
(mm)	[sFan.e/i]	8.143 / 8.049
Normal space width at root circle (mm)	[efn]	5.346
(mm)	[efn.e/i]	5.373 / 5.386

Gear 3

Profile shift coefficient	[x]	-1.3967
Tooth thickness, arc, in module	[sn*]	0.5541
Tip alteration (mm)	[k*mn]	-2.110
Reference diameter (mm)	[d]	1242.000
Base diameter (mm)	[db]	1167.098
Tip diameter (mm)	[da]	1253.360
(mm)	[da.e/i]	1253.360 / 1253.235
Tip diameter allowances (mm)	[Ada.e/i]	0.000 / -0.125
Tip form diameter (mm)	[dFa]	1253.360
(mm)	[dFa.e/i]	1253.360 /1253.235
Root diameter (mm)	[df]	1289.640
Generating Profile shift coefficient	[xE.e/i]	-1.4333/ -1.4486
Generated root diameter with xE (mm)	[df.e/i]	1290.574 /1290.299
Root form diameter (mm)	[dFf]	1285.990
(mm)	[dFf.e/i]	1286.808 /1286.568
Internal toothing: Calculation dFf with pinion type cutter (z0= 45 , x0= 0.000)		
Involute length (mm)	[l_dFa-l_dFf]	17.749
Addendum, $m_n(h_{aP}^*+x+k)$ (mm)	[ha]	-5.680
(mm)	[ha.e/i]	-5.618 / -5.680
Dedendum (mm)	[hf=mn*(hfP*-x)]	23.820
(mm)	[hf.e/i]	24.150 / 24.287
Tooth height (mm)	[h]	18.140
Virtual gear no. of teeth	[zn]	138.000
Normal tooth thickness at tip circle (mm)	[san]	9.345
(mm)	[san.e/i]	9.103 / 8.952
Normal tooth thickness at tip form circle (mm)	[sFan]	9.345
(mm)	[sFan.e/i]	9.103 / 8.952
Normal space width at root circle (mm)	[efn]	3.859
(mm)	[efn.e/i]	3.800 / 3.775

Gear specific pair data Gear pair 1, Gear 1

Operating pitch diameter (mm)	[dw]	305.153
(mm)	[dw.e/i]	305.175 / 305.131
Active tip diameter (mm)	[dNa]	325.509
(mm)	[dNa.e/i]	325.509 / 325.452
Theoretical tip clearance (mm)	[c]	2.609
Effective tip clearance (mm)	[c.e/i]	2.927 / 2.759
Active root diameter (mm)	[dNf]	294.553
(mm)	[dNf.e/i]	294.643 / 294.508

Reserve (dNf-dFf)/2 (mm)	[cF.e/i]	3.376 / 3.250
Max. sliding velocity at tip (m/s)	[vga]	1.234
Specific sliding at the tip	[ζa]	0.431
Specific sliding at the root	[ζf]	-0.507
Mean specific sliding	[ζm]	0.393
Sliding factor on tip	[Kga]	0.236
Sliding factor on root	[Kgf]	-0.156
Roll angle at dFa (°)	[ξdFa.e/i]	34.393 / 34.370
Roll angle to dNa (°)	[ξdNa.e/i]	34.393 / 34.370
Roll angle to dNf (°)	[ξdNf.e/i]	19.394 / 19.307
Roll angle at dFf (°)	[ξdFf.e/i]	14.601 / 14.502
Diameter of single contact point B (mm)	[d-B]	315.587 (315.521 / 315.718)
Diameter of single contact point D (mm)	[d-D]	301.621 (301.621 / 301.579)
Addendum contact ratio	[ε]	0.830 (0.831 / 0.827)

Gear specific pair data Gear pair 1, Gear 2

Operating pitch diameter (mm)	[dw]	480.847
(mm)	[dw.e/i]	480.882 / 480.812
Active tip diameter (mm)	[dNa]	493.385
(mm)	[dNa.e/i]	493.385 / 493.322
Theoretical tip clearance (mm)	[c]	5.147
Effective tip clearance (mm)	[c.e/i]	5.468 / 5.297
Active root diameter (mm)	[dNf]	464.758
(mm)	[dNf.e/i]	464.840 / 464.713
Reserve (dNf-dFf)/2 (mm)	[cF.e/i]	2.429 / 2.295
Max. sliding velocity at tip (m/s)	[vga]	1.863
Specific sliding at the tip	[ζa]	0.336
Specific sliding at the root	[ζf]	-0.756
Mean specific sliding	[ζm]	0.393
Sliding factor on tip	[Kga]	0.156
Sliding factor on root	[Kgf]	-0.236
Roll angle at dFa (°)	[ξdFa.e/i]	29.140 / 29.122
Roll angle to dNa (°)	[ξdNa.e/i]	29.140 / 29.122
Roll angle to dNf (°)	[ξdNf.e/i]	19.617 / 19.566
Roll angle at dFf (°)	[ξdFf.e/i]	17.629 / 17.566
Diameter of single contact point B (mm)	[d-B]	471.680 (471.680 / 471.630)
Diameter of single contact point D (mm)	[d-D]	484.561 (484.502 / 484.667)
Addendum contact ratio	[ε]	0.550 (0.551 / 0.546)

Gear specific pair data Gear pair 2, Gear 2

Operating pitch diameter (mm)	[dw]	475.256
(mm)	[dw.e/i]	475.221 / 475.290
Active tip diameter (mm)	[dNa]	493.385
(mm)	[dNa.e/i]	493.385 / 493.322
Theoretical tip clearance (mm)	[c]	5.127
Effective tip clearance (mm)	[c.e/i]	5.654 / 5.429
Active root diameter (mm)	[dNf]	467.619
(mm)	[dNf.e/i]	467.670 / 467.451
Reserve (dNf-dFf)/2 (mm)	[cF.e/i]	3.844 / 3.664
Max. sliding velocity at tip (m/s)	[vga]	0.217
Specific sliding at the tip	[ζa]	0.121
Specific sliding at the root	[ζf]	-0.083
Mean specific sliding	[ζm]	0.107
Sliding factor on tip	[Kga]	0.057
Sliding factor on root	[Kgf]	-0.028
Roll angle at dFa (°)	[ξdFa.e/i]	29.140 / 29.122
Roll angle to dNa (°)	[ξdNa.e/i]	29.140 / 29.122
Roll angle to dNf (°)	[ξdNf.e/i]	20.728 / 20.644
Roll angle at dFf (°)	[ξdFf.e/i]	17.629 / 17.566
Diameter of single contact point B (mm)	[d-B]	488.245 (488.031 / 488.311)
Diameter of single contact point D (mm)	[d-D]	471.680 (471.680 / 471.630)
Addendum contact ratio	[ε]	0.818 (0.817 / 0.817)

KISSsoft

Gear specific pair data Gear pair 2, Gear 3

Operating pitch diameter (mm)	[dw]	1261.256
(mm)	[dw.e/i]	1261.347 /1261.164
Active tip diameter (mm)	[dNa]	1253.360
(mm)	[dNa.e/i]	1253.360 /1253.235
Theoretical tip clearance (mm)	[c]	6.044
Effective tip clearance (mm)	[c.e/i]	6.333 / 6.131
Active root diameter (mm)	[dNf]	1278.375
(mm)	[dNf.e/i]	1278.436 /1278.257
Reserve (dNf-dFf)/2 (mm)	[cF.e/i]	4.275 / 4.066
Max. sliding velocity at tip (m/s)	[vga]	0.129
Specific sliding at the tip	[ζa]	0.077
Specific sliding at the root	[ζf]	-0.138
Mean specific sliding	[ζm]	0.107
Sliding factor on tip	[Kga]	0.028
Sliding factor on root	[Kgf]	-0.057
Roll angle at dFa (°)	[ξdFa.e/i]	22.415 / 22.432
Roll angle to dNa (°)	[ξdNa.e/i]	22.415 / 22.432
Roll angle to dNf (°)	[ξdNf.e/i]	25.595 / 25.617
Roll angle at dFf (°)	[ξdFf.e/i]	26.580 / 26.608
Diameter of single contact point B (mm)	[d-B]	1273.694 (1273.557 / 1273.694)
Diameter of single contact point D (mm)	[d-D]	1257.627 (1257.683 / 1257.519)
Addendum contact ratio	[ε]	0.400 (0.411 / 0.395)

General influence factors

		------- Gear 1	--------- Gear 2	--------- Gear 3 ---
Nominal circum. force at pitch circle (N)	[Ft]	56679.574	56679.574	
Axial force (N)	[Fa]	0.0	0.0	0.0
Total axial force (N)	[Fatot=Fa* 3]	0.0		0.0
Radial force (N)	[Fr]	20629.678		20629.678
Normal force (N)	[Fnorm]	60317.1	60317.1	60317.1
Nominal circumferential force per mm (N/mm)	[w]	318.42	325.74	
Only as information: Forces at operating pitch circle:				
Nominal circumferential force (N)	[Ftw]	55165.234	55814.237	
Axial force (N)	[Fa]	0.0		
Axial force (N)	[Fa]		0.0 /0.0	
Axial force (N)	[Fa]			0.0
Total axial force (N)	[Fatot=Fa* 3]	0.0		0.0
Radial force (N)	[Fr]	24391.692	22867.633	
Circumferential speed reference circle (m/s)	[v]	7.67	(Planet)	
Running-in value (µm)	[yp]	0.907	0.982	
Running-in value (µm)	[yf]	1.050	1.050	
Gear blank factor	[CR]	1.000	1.000	
Correction factor	[CM]	0.800	0.800	
Basic rack factor	[CBS]	0.900	0.937	
Material coefficient	[E/Est]	1.000	1.000	
Singular tooth stiffness (N/mm/µm)	[c']	14.620	14.137	
Meshing stiffness (N/mm/µm)	[cγα]	18.789	16.447	
Meshing stiffness (N/mm/µm)	[cγβ]	15.971	13.980	
Reduced mass (kg/mm)	[mRed]	0.0985	0.5416	
Resonance speed (min-1)	[nE1]	3996	1012	
Resonance ratio (-)	[N]	0.123	0.309	
Running-in value (µm)	[yα]	0.907	0.982	
Planet runs on rolling bearings. Planet pin fixed on both sides in the carrier..				
lpa (mm) = 231.40 b (mm) =178.00dsh (mm) = 234.00				
Tooth trace deviation (active) (µm)	[Fβy]	5.95	8.29	
from deformation of shaft (µm)	[fsh*B1]	8.76	0.19	
(fsh (µm) =8.76 / 0.19, B1 = 1.00 / 1.00, fHβ5 (µm) = 10.00 / 10.00)				
Tooth trace		0	0	
(0: without, 1: crowned, 2: end relief, 3: full modification)				
(4: slightly crowned, 5: helix angle modification, 6: helix angle modification with crowning)				
from production tolerances (µm)	[fmα*B2]	19.80	20.52	
B2 = 1.00 / 1.00				
Tooth trace deviation, theoretical (µm)	[Fβx]	7.00	9.75	
Running-in value yβ (µm)	[yβ]	1.05	1.46	

KISSsoft

Dynamic factor	[Kv=max(Kv12,Kv23)]	1.18		
	[Kv12,Kv23]	1.07	1.18	
Face load factor - flank	[KHβ]	1.13	1.15	
- Tooth root	[KFβ]	1.11	1.14	
- Scuffing	[KBβ]	1.13	1.15	
Transverse load factor - flank	[KHα]	1.00	1.00	
- Tooth root	[KFα]	1.00	1.00	
- Scuffing	[KBα]	1.00	1.00	
Number of load cycles (in mio.)	[NL]	1776.0	375.7	424.7

Tooth root load capacity

Calculation of Tooth form coefficients according method: B
Internal toothing: Calculation of ρF and sFn according to ISO 6336-3:2007-04-01
Internal toothing: Calculation of YF, YS with pinion type cutter, z0= 45 , x0=0.000 , ρaP0*= 0.380

		Gear 1	Gear 2	Gear 3
Calculated with generating profile shift coefficient	[xE.i]	0.5555	0.6639	-1.4486
Tooth form factor	[YF]	1.53		
	[YF]		1.22 /1.44	
	[YF]			1.05
Stress correction factor	[YS]	2.04		
	[YS]		2.29 /2.14	
	[YS]			2.67
Bending moment arm (mm)	[hF]	13.09		
(mm)	[hF]		10.82 /12.91	
(mm)	[hF]			13.65
Load application angle (°)	[αFen]	25.96		
(°)	[αFen]		23.39 /24.51	
(°)	[αFen]			22.36
Coefficient	[fε]	1.000	1.000	
Tooth thickness at root (mm)	[sFn]	21.06		
(mm)	[sFn]		21.64 /21.64	
(mm)	[sFn]			26.26
Tooth root radius (mm)	[ρF]	3.97		
(mm)	[ρF]		3.73 /3.73	
(mm)	[ρF]			3.02

hF* = 1.455 /1.202 /1.435 / 1.516sFn* = 2.340 /2.404 / 2.404 / 2.917
ρF* =0.442 /0.414 /0.414 / 0.335dsFn =285.008 / 458.028 / 458.028 /-1289.558 αsFn = 30.0 / 30.0 / 30.0 / 60.0

Helix angle factor	[Yβ]	1.00	1.00	
Deep tooth factor	[YDT]	1.00	1.00	
Gear rim thickness (mm)	[sr]	281.80	454.75	31.03
Gear rim factor	[YB]	1.00	1.00	1.01
Effective facewidth (mm)	[beff]	183.00		
(mm)	[beff]		178.00 /178.00	
(mm)	[beff]			174.00
Nominal stress at tooth root (N/mm²)	[σF0]	106.99		
(N/mm²)	[σF0]		98.87 /109.28	
(N/mm²)	[σF0]			103.15
Tooth root stress (N/mm²)	[σF]	140.49		
(N/mm²)	[σF]		129.82 /146.82	
(N/mm²)	[σF]			138.59
Permissible bending stress at root of Test-gear				
Notch sensitivity factor	[YdrelT]	1.001		
Notch sensitivity factor	[YdrelT]		1.004 / 1.004	
Notch sensitivity factor	[YdrelT]			1.015
Surface factor	[YRrelT]	0.957	0.957	0.957
Size factor, tooth root	[YX]	0.960	0.960	0.960
Finite life factor	[YNT]	0.880	0.908	0.906
Alternating bending factor, mean stress influence coefficient				
	[YM]	1.000	0.700	1.000
Stress correction factor	[Yst]	2.00		
Yst*σFlim (N/mm²)	[σFE]	860.00	860.00	860.00
Permissible tooth root stress (N/mm²)	[σFP=σFG/SFmin]	497.16		

Permissible tooth root stress (N/mm²)	[σFP=σFG/SFmin]		359.83	/359.83		
Permissible tooth root stress (N/mm²)	[σFP=σFG/SFmin]			518.76		
Limit strength tooth root (N/mm²)	[σFG]	696.02				
Limit strength tooth root (N/mm²)	[σFG]		503.76	/503.76		
Limit strength tooth root (N/mm²)	[σFG]			726.27		
Required safety	[SFmin]	1.40	1.40	1.40		
Safety for tooth root stress	[SF=σFG/σF]	4.95				
	[SF=σFG/σF]		3.88	/3.43		
	[SF=σFG/σF]			5.24		
Transmittable power (kW)	[kWRating]	5272.31				
(kW)	[kWRating]		4129.51	/3651.21		
(kW)	[kWRating]			5576.81		

Flank safety

		------- Gear 1	--------- Gear 2	--------- Gear 3 ---		
Zone factor	[ZH]	2.26	2.35			
Elasticity factor (√N/mm²)	[ZE]	189.81	189.81			
Contact ratio factor	[Zε]	0.934	0.963			
Helix angle factor	[Zβ]	1.000	1.000			
Effective facewidth (mm)	[beff]	178.00	174.00			
Nominal contact stress (N/mm²)	[σH0]	531.46	283.05			
Contact stress at operating pitch circle (N/mm²)	[σHw]	613.27	330.62			
Single tooth contact factor	[ZB,ZD]	1.02	1.00	/1.04	1.00	
Contact stress (N/mm²)	[σHB, σHD]	622.70	613.27	/343.33	330.62	
Lubrication factor for NL	[ZL]	1.047	1.047	/ 1.047	1.047	
Speed factor for NL	[ZV]	0.993	0.993	/ 0.993	0.993	
Roughness factor for NL	[ZR]	0.998	0.998	/ 1.034	1.034	
Material hardening factor for NL	[ZW]	1.000	1.000	/ 1.000	1.000	
Finite life factor	[ZNT]	0.896	0.940	0.936		
Limited pitting is permitted: No						
Size factor (flank)	[ZX]	1.000	1.000	1.000		
Permissible contact stress, σHG/SHmin (N/mm²)	[σHP]	1394.93	1463.00	/1516.33	1510.64	
Pitting stress limit (N/mm²)	[σHG]	1394.93	1463.00	/1516.33	1510.64	
Required safety	[SHmin]	1.00	1.00	1.00		
Safety factor for contact stress at operating pitch circle	[SHw]	2.27	2.39	/4.59	4.57	
Safety for stress at single tooth contact	[SHBD=σHG/σHBD]	2.24	2.39	/4.42	4.57	
	Safety regarding transmittable torque[(SHBD)^2]	5.02	5.69	/ 19.51	20.88	
Transmittable power (kW)	[kWRating]	7476.27	8478.69	/29060.23	31103.46	

Micropitting according to **ISO/TS 6336-22:2018**

Pairing Gear 1 -2 :
Calculation has not been carried out, lubricant: Load stage micropitting test not known

Pairing Gear 2 -3 :
Calculation has not been carried out, lubricant: Load stage micropitting test not known

Scuffing load capacity

Calculation method according to ISO/TS 6336-20/21:2017

Helical load factor for scuffing	[KBγ]	1.00	1.00		
Lubrication coefficient for lubrication type	[XS]	1.000			
Scuffing test and load stage	[FZGtest] FZG - Test A / 8.3 / 90 (ISO 14635 - 1)	12			
Multiple meshing factor	[Xmp]	2.0	2.0		
Relative structural factor, scuffing	[XWrelT]	1.000	1.000		
Thermal contact factor (N/mm/s^.5/K)	[BM]	13.780	13.780	13.780	
Relevant tip relief (µm)	[Ca]	2.00	2.00	/ 2.00	2.00
Optimal tip relief (µm)	[Ceff]	21.78	23.04		
Ca taken as optimal in the calculation (0=no, 1=yes)		0	0	/0	0

Effective facewidth (mm)	[beff]		178.000	174.000	
Applicable circumferential force/facewidth (N/mm)	[wBt]		423.998	444.424	
(1) KBγ = 1.000 , wBt*KBγ =423.998					
(2) KBγ = 1.000 , wBt*KBγ =444.424					
Angle factor	[Xαβ]		1.033	1.011	
Flash temperature-criteria					
Lubricant factor	[XL]		0.679	0.679	
Tooth mass temperature (°C)	[θMi]		68.60	62.97	
θMi = θoil + XS*0.47*Xmp*θflm					
Average flash temperature	(°C)	[θflm]	7.02	1.04	
Scuffing temperature (°C)	[θS]		299.98	299.98	
Γ coordinates (point of highest temperature)	[Γ]		0.189	0.176	
(1) [Γ.A]= 0.358 [Γ.E]= -0.237					
(2) [Γ.A]= 0.241 [Γ.E]= -0.118					
Highest contact temp. (°C)	[θB]		81.18	65.28	
Flash factor (°K*N^-.75*s^.5*m^-.5*mm)	[XM]		50.058	50.058	
Approach factor	[XJ]		1.013	1.050	
Load sharing factor	[XΓ]		1.000	1.000	
Dynamic viscosity (mPa*s)	[ηM]		81.42	81.42	(62.0 °C)
Coefficient of friction	[μ_m]		0.036	0.028	
Required safety	[SBmin]		2.000		
Margin of safety for scuffing, flash temperature	[SB]		12.406	72.566	
Integral temperature-criteria					
Lubricant factor (Input)	[XL]		0.846		
Tooth mass temperature (°C)	[θMC]		67.77	62.71	
θMC = θoil + XS*0.70*θflaint					
Mean flash temperature	(°C)	[θflaint]	4.12	0.51	
Integral scuffing temperature (°C)	[θSint]		316.54	316.54	
Flash factor (°K*N^-.75*s^.5*m^-.5*mm)	[XM]		50.058	50.058	
Running-in factor, well run in	[XE]		1.000	1.000	
Contact ratio factor	[Xε]		0.278	0.319	
Dynamic viscosity (mPa*s)	[ηOil]		81.42	81.42	
Mean coefficient of friction	[μ_m]		0.027	0.015	
Geometry factor	[XBE]		0.206	0.033	
Meshing factor	[XQ]		0.997	0.854	
Tip relief factor	[XCa]		1.121	1.115	
Integral tooth flank temperature (°C)	[θint]		73.95	63.47	
Required safety	[SSmin]		1.800		
Safety factor for scuffing (intg.-temp.)	[SSint]		4.28	4.99	
Safety referring to transmittable torque	[SSL]		21.30	172.96	

Measurements for tooth thickness

		Gear 1	Gear 2	Gear 3
Tooth thickness tolerance		DIN 3967 cd25	DIN 3967 cd25	DIN 3967 cd25
Tooth thickness allowance (normal section) (mm)	[As.e/i]	-0.130 /	-0.190-0.130 /	-0.190-0.240 / -0.340
Number of teeth spanned	[k]	5.000	7.000	18.000
(Internal toothing: k = (Measurement gap number)				
Base tangent length (no backlash) (mm)	[Wk]	127.319	183.520	490.954
Base tangent length with allowance (mm)	[Wk.e/i]	127.197 /	127.141183.398 /	183.342 491.179 / 491.273
Diameter of measuring circle (mm)	[dMWk.m]	306.696	476.474	1266.263
Theoretical diameter of ball/pin (mm)	[DM]	17.054	16.560	14.867
Effective diameter of ball/pin (mm)	[DMeff]	18.000	18.000	15.000
Radial single-ball measurement backlash free (mm)	[MrK]	167.539	254.336	623.037
Radial single-ball measurement (mm)	[MrK.e/i]	167.410 /	167.351254.198 /	254.134 623.458 / 623.334
Diameter of measuring circle (mm)	[dMMr.m]	308.655	482.642	1267.569
Diametral measurement over two balls without clearance (mm)	[MdK]	334.720	508.672	1246.074
Diametral two ball measure (mm)	[MdK.e/i]	334.462 /	334.343508.396 /	508.269 1246.915 / 1246.668
Measurement over pins according to DIN 3960 (mm)	[MdR.e/i]	334.462 /	334.343508.396 /	508.269 1246.915 / 1246.668
Measurement over 3 pins, axial, according to AGMA 2002 (mm)				
	[dk3A.e/i]	334.462 /	334.343508.396 /	508.269 1246.915 / 1246.668
Measurement over 3 pins with allowance (mm)	[Md3R.e/i]	334.104 /	333.9850.000 /	0.000-0.000 / -0.000
Chordal tooth thickness in reference circle (mm)	[sc]	17.956	18.672	4.987
(mm)	[sc.e/i]	17.828 /	17.76918.544 /	18.4844.747 / 4.647
Reference chordal height from da.m (mm)	[ha]	14.512	12.863	-5.654

KISSsoft

Tooth thickness, arc (mm)	[sn]	17.967		18.677		4.987		
(mm)	[sn.e/i]	17.837 /		17.777	18.547 /	18.487	4.747 /	4.647
Backlash free center distance (mm)	[aControl.e/i]	392.697 /		392.557	393.457 /	393.654		
Backlash free center distance, allowances (mm)	[jta]	-0.303 /		-0.443	0.457 /	0.654		
dNf.i with aControl (mm)	[dNf0.i]	293.858	464.052	/	466.350	1279.779		
Reserve (dNf0.i-dFf.e)/2 (mm)	[cF0.i]	2.925	1.965	/3.113	3.394			
Tip clearance (mm)	[c0.i(aControl)]	2.345	4.883	/5.000	5.506			
Center distance allowances (mm)	[Aa.e/i]	0.029 /		-0.029	-0.029 /	0.029		
Circumferential backlash from Aa (mm)	[jtw_Aa.e/i]	0.025 /		-0.025	0.023 /	-0.023		
Radial backlash (mm)	[jrw]	0.471 /		0.274	0.682 /	0.428		
Circumferential backlash, transverse section (mm)	[jtw]	0.416 /		0.242	0.562 /	0.352		
Normal backlash (mm)	[jnw]	0.377 /		0.225	0.518 /	0.328		
Torsional angle on input with output fixed:								
Total torsional angle (°)	[j.tSys]	0.0678/		0.0469				

Toothing tolerances

			------- Gear 1 ---------	Gear 2 ---------	Gear 3 ---
According to ISO 1328-1:2013, ISO 1328-2:1997					
Accuracy grade	[Q]		A6	A6	A6
Single pitch deviation (µm)	[fptT]		13.00	13.00	14.00
Base circle pitch deviation (µm)	[fpbT]		11.80	12.10	13.10
Sector pitch deviation over k/8 pitches (µm)	[Fpk/8T]		26.00	30.00	35.00
Profile form deviation (µm)	[ffαT]		14.00	14.00	14.00
Profile slope deviation (µm)	[fHαT]		11.00	11.00	13.00
Total profile deviation (µm)	[FαT]		18.00	18.00	19.00
Helix form deviation (µm)	[ffβT]		16.00	16.00	18.00
Helix slope deviation (µm)	[fHβT]		14.00	14.00	15.00
Total helix deviation (µm)	[FβT]		21.00	21.00	23.00
Total cumulative pitch deviation (µm)	[FpT]		40.00	44.00	57.00
Adjacent pitch difference (µm)	[fuT]		18.00	18.00	20.00
Runout (µm)	[FrT]		36.00	40.00	51.00
Single flank composite, total (µm)	[FisT]		52.00	56.00	69.00
Single flank composite, tooth-to-tooth	(µm)	[fisT]	12.00	12.00	12.00
Radial composite, total (µm)	[FidT]		73.00	73.00	94.00
Radial composite, tooth-to-tooth (µm)	[fidT]		34.00	34.00	34.00

FidT (Fi''), fidT (fi'') according to ISO 1328:1997 calculated with the geometric mean values for mn and d

Axis alignment tolerances (recommendation acc. to ISO TR 10064-3:1996, Quality)		6	
Maximum value for deviation error of axis (µm)	[fΣβ]	13.65	13.65
Maximum value for inclination error of axes (µm)	[fΣδ]	27.30	27.30

Modifying and defining the tooth form

Data for the tooth form calculation :
Data not available.
Please run the calculation in the "Tooth form" tab and open the main report again.

Supplementary data

Mass (kg)	[m]	103.946	246.281	227.836	
Total mass (kg)	[mGes]	1070.625			
Moment of inertia for system, relative to the input:					
calculation without consideration of the exact tooth shape					
Single gears (da+df)/2...di (kg*m²)	[J]	1.20011	6.92628	98.15020	
System (da+df)/2...di (kg*m²)	[J]	1441.74113			
Torsional stiffness at driving gear with fixed driven gear:					
Torsional stiffness (MNm/rad)	[cr]	1984.078			
Torsion when subjected to nominal torque (°)	[δcr]	0.003			
Mean coefficient of friction (as defined in Niemann)	[μ_m]	0.027	0.018		
Wear sliding coef. by Niemann	[ζw]	0.516	0.111		

KISSsoft

Loss factor	[HV]	0.095	0.023
Meshing power (kW)		1304.500	1304.500
Gear power loss (kW)	[PVZ]	1.097	0.184
Total power loss (kW)		3.843	
Total efficiency		0.997	
Sound pressure level according to Masuda, without contact analysis	[dB(A)]	104.4	108.9

Service life, damage

Required safety for tooth root	[SFmin]	1.40	
Required safety for tooth flank	[SHmin]	1.00	

Service life (calculated with required safeties):

System service life (h)	[Hatt]	> 1000000	

Tooth root service life (h)	[HFatt]	1e+06	1e+06	1e+06
Tooth flank service life (h)	[HHatt]	1e+06	1e+06	1e+06

Note: The entry 1e+006 h means that the Service life > 1,000,000 h.

Damage calculated on the basis of the required service life (20000.0 h)

F1%	F2%	F3%	H1%	H2%	H3%
0.00	0.0000	0.0000	0.0000	0.0000	0.0000

Remarks:

- Specifications with [.e/i] imply: Maximum [e] and minimum value [i] for
  Taking all tolerances into account
  Specifications with [.m] imply: Mean value within tolerance
- For the backlash tolerance, the center distance tolerances and the tooth thickness allowance are taken into account.
  The maximum and minimum clearance according to the largest or smallest allowances are defined..
  The calculation is performed for the operating pitch circle.
- Details of calculation method:
  cγ according to Method B
  Kv according to Method B
  KHβ and KFβ according to Method C
  fmα according to Equation 64, Fβx according to 52/53/56
  fsh calculated by exactly following the method in Annex D,
  ISO 6336-1:2006
  Literature: Journal "Antriebstechnik", 6/2007, p.64.
  KHα, KFα according to Method B
- The logarithmically interpolated value taken from the values for the fatigue strength and the static strength, based on the number of load cycles, is used for coefficients ZL, ZV, ZR, ZW, ZX, YdrelT, YRrelT and YX..

End of Report lines: 825

KISSsoft

KISSsoft Release 2020 A.1

KISSsoft University license - Universidade do Porto

File

Name : Unnamed
Changed by: Rui on: 28.06.2021 at: 20:51:30

Fourth Stage: Wheel-Pinion

Calculation of a helical-toothed cylindrical gear pair

Drawing or article number:
Gear 1: z10(Z10Z11)
Gear 2: z11(Z10Z11)

Calculation method: ISO 6336:2019

		------- Gear 1	-------- Gear 2 --
Power (kW)	[P]	1474.255	
Speed (1/min)	[n]	563.4	1632.5
Torque (Nm)	[T]	24986.7	8623.7
Application factor	[KA]	1.00	
Required service life (h)	[H]	20000.00	
Gear driving (+) / driven (-)		+	-
Working flank gear 1:		Right flank	
Gear 1 direction of rotation:		Clockwise	

Tooth geometry and material

Geometry calculation according to: ISO 21771:2007

		------- Gear 1	-------- Gear 2 --
Center distance (mm)	[a]	550.000	
Center distance tolerance		ISO 286:2010 Measure js7	
Normal module (mm)	[mn]	7.0000	
Normal pressure angle (°)	[αn]	20.0000	
Helix angle at reference circle (°)	[β]	13.0000	
Number of teeth	[z]	113	39
Facewidth (mm)	[b]	194.50	191.36
Hand of gear		right	left
Accuracy grade	[Q-ISO 1328:2013]	A6	A6
Inner diameter (mm)	[di]	0.00	0.00
Inner diameter of gear rim (mm)	[dbi]	0.00	0.00

Material

Gear1
18CrNiMo7-6, Case-carburized steel, case-hardened
ISO 6336-5 Figure 9/10 (MQ), Core hardness >=25HRC Jominy J=12mm<HRC28

Gear2
18CrNiMo7-6, Case-carburized steel, case-hardened
ISO 6336-5 Figure 9/10 (MQ), Core hardness >=25HRC Jominy J=12mm<HRC28

		------- Gear 1	-------- Gear 2 --
Surface hardness		HRC 61	HRC 61
Material treatment according to ISO 6336:2006 Normal, life factors ZNT and YNT >=0.85			
Fatigue strength. tooth root stress (N/mm²)	[σFlim]	430.00	430.00
Fatigue strength for Hertzian pressure (N/mm²)	[σHlim]	1500.00	1500.00
Tensile strength (N/mm²)	[σB]	1200.00	1200.00
Yield point (N/mm²)	[σS]	850.00	850.00
Young's modulus (N/mm²)	[E]	206000	206000
Poisson's ratio	[v]	0.300	0.300
Roughness average value DS, flank (µm)	[RAH]	0.60	0.60
Roughness average value DS, root (µm)	[RAF]	3.00	3.00
Mean roughness height, Rz, flank (µm)	[RZH]	4.80	4.80
Mean roughness height, Rz, root (µm)	[RZF]	20.00	20.00

Gear reference profile 1:			
Reference profile	1.40 / 0.39 / 1.0 ISO 53:1998 Profil D		
Dedendum coefficient	[hfP*]	1.400	
Root radius factor	[ρfP*]	0.390	(ρfPmax*=0.394)
Addendum coefficient	[haP*]	1.000	
Tip radius factor	[ρaP*]	0.000	
Protuberance height coefficient	[hprP*]	0.000	
Protuberance angle	[αprP]	0.000	
Tip form height coefficient	[hFaP*]	0.000	
Ramp angle	[αKP]	0.000	
	not topping		

Gear reference profile 2:			
Reference profile	1.40 / 0.39 / 1.0 ISO 53:1998 Profil D		
Dedendum coefficient	[hfP*]	1.400	
Root radius factor	[ρfP*]	0.390	(ρfPmax*=0.394)
Addendum coefficient	[haP*]	1.000	
Tip radius factor	[ρaP*]	0.000	
Protuberance height coefficient	[hprP*]	0.000	
Protuberance angle	[αprP]	0.000	
Tip form height coefficient	[hFaP*]	0.000	
Ramp angle	[αKP]	0.000	
	not topping		

Information on final machining

Dedendum reference profile	[hfP*]	1.400	1.400
Tooth root radius Refer. profile	[ρfP*]	0.390	0.390
Addendum Reference profile	[haP*]	1.000	1.000
Protuberance height coefficient	[hprP*]	0.000	0.000
Protuberance angle (°)	[αprP]	0.000	0.000
Tip form height coefficient	[hFaP*]	0.000	0.000
Ramp angle (°)	[αKP]	0.000	0.000

Type of profile modification:	none (only running-in)	
Tip relief by running in (µm)	[Ca L/R]	2.0 / 2.0 2.0 / 2.0

Lubrication type	Oil bath lubrication	
Type of oil	ISO-VG 320	
Lubricant base	Mineral-oil base	
Oil nominal kinematic viscosity at 40°C (mm²/s)	[v40]	320.00
Oil nominal kinematic viscosity at 100°C (mm²/s)	[v100]	22.00
Specific density at 15°C (kg/dm³)	[ρ]	0.900
Oil temperature (°C)	[TS]	62.000

Gear pair

Overall transmission ratio	[itot]	-0.345
Gear ratio	[u]	2.897
Transverse module (mm)	[mt]	7.184
Transverse pressure angle (°)	[αt]	20.483
Working pressure angle (°)	[αwt]	21.572
	[αwt.e/i]	21.582 / 21.563
Working pressure angle at normal section (°)	[αwn]	21.061
Helix angle at operating pitch circle (°)	[βw]	13.092
Base helix angle (°)	[βb]	12.204
Reference center distance (mm)	[ad]	545.994
Pitch on reference circle (mm)	[pt]	22.570
Base pitch (mm)	[pbt]	21.143
Transverse pitch on contact-path (mm)	[pet]	21.143
Sum of profile shift coefficients	[Σxi]	0.5870
Transverse contact ratio	[εα]	1.643
Transverse contact ratio with allowances	[εα.e/m/i]	1.648 / 1.639 / 1.631
Overlap ratio	[εβ]	1.957
Total contact ratio	[εγ]	3.601

Total contact ratio with allowances	[εγ.e/m/i]	3.605 / 3.597 / 3.588
Length of path of contact (mm)	[ga, e/i]	34.744 (34.839 / 34.482)
Length T1-A (mm)	[T1A]	131.652 (131.557 / 131.802)
Length T1-B (mm)	[T1B]	145.253 (145.253 / 145.141)
Length T1-C (mm)	[T1C]	150.337 (150.266 / 150.407)
Length T1-D (mm)	[T1D]	152.795 (152.699 / 152.945)
Length T1-E (mm)	[T1E]	166.396 (166.396 / 166.284)
Length T2-A (mm)	[T2A]	70.571 (70.571 / 70.516)
Length T2-B (mm)	[T2B]	56.969 (56.874 / 57.177)
Length T2-C (mm)	[T2C]	51.886 (51.862 / 51.911)
Length T2-D (mm)	[T2D]	49.428 (49.428 / 49.373)
Length T2-E (mm)	[T2E]	35.827 (35.732 / 36.034)
Length T1-T2 (mm)	[T1T2]	202.223 (202.128 / 202.318)
Minimal length of contact line (mm)	[Lmin]	320.217

Gear 1

Lead height (mm)	[pz]	11046.847
Axial pitch (mm)	[px]	97.760
Profile shift coefficient	[x]	0.4083
Tooth thickness, arc, in module	[sn*]	1.8680
Tip alteration (mm)	[k*mn]	-0.706
Reference diameter (mm)	[d]	811.807
Base diameter (mm)	[db]	760.482
Tip diameter (mm)	[da]	830.110
(mm)	[da.e/i]	830.110 / 830.020
Tip diameter allowances (mm)	[Ada.e/i]	0.000 / -0.090
Tip form diameter (mm)	[dFa]	830.110
(mm)	[dFa.e/i]	830.110 / 830.020
Root diameter (mm)	[df]	797.923
Generating Profile shift coefficient	[xE.e/i]	0.3740/ 0.3583
Generated root diameter with xE (mm)	[df.e/i]	797.442 / 797.222
Root form diameter (mm)	[dFf]	801.989
(mm)	[dFf.e/i]	801.553 / 801.355
Involute length (mm)	[l_dFa-l_dFf]	15.088
Addendum, $m_n(h_{aP}^*+x+k)$ (mm)	[ha]	9.152
(mm)	[ha.e/i]	9.152 / 9.107
Dedendum (mm)	[hf=mn*(hfP*-x)]	6.942
(mm)	[hf.e/i]	7.182 / 7.292
Tooth height (mm)	[h]	16.094
Virtual gear no. of teeth	[zn]	121.397
Normal tooth thickness at tip circle (mm)	[san]	6.039
(mm)	[san.e/i]	5.898 / 5.779
Normal tooth thickness at tip form circle (mm)	[sFan]	6.039
(mm)	[sFan.e/i]	5.898 / 5.779
Normal space width at root circle (mm)	[efn]	4.123
(mm)	[efn.e/i]	4.145 / 4.155

Gear 2

Lead height (mm)	[pz]	3812.628
Axial pitch (mm)	[px]	97.760
Profile shift coefficient	[x]	0.1787
Tooth thickness, arc, in module	[sn*]	1.7009
Tip alteration (mm)	[k*mn]	0.664
Reference diameter (mm)	[d]	280.181
Base diameter (mm)	[db]	262.467
Tip diameter (mm)	[da]	298.010
(mm)	[da.e/i]	298.010 / 297.958
Tip diameter allowances (mm)	[Ada.e/i]	0.000 / -0.052
Tip form diameter (mm)	[dFa]	298.010
(mm)	[dFa.e/i]	298.010 / 297.958
Root diameter (mm)	[df]	263.083
Generating Profile shift coefficient	[xE.e/i]	0.1532/ 0.1414
Generated root diameter with xE (mm)	[df.e/i]	262.726 / 262.561

Root form diameter (mm)	[dFf]	269.115
(mm)	[dFf.e/i]	268.892 / 268.790
Involute length (mm)	[l_dFa-l_dFf]	15.609
Addendum, $m_n(h_{aP}^*+x+k)$ (mm)	[ha]	8.914
(mm)	[ha.e/i]	8.914 / 8.888
Dedendum (mm)	[hf=mn*(hfP*-x)]	8.549
(mm)	[hf.e/i]	8.728 / 8.810
Tooth height (mm)	[h]	17.464
Virtual gear no. of teeth	[zn]	41.898
Normal tooth thickness at tip circle (mm)	[san]	4.429
(mm)	[san.e/i]	4.317 / 4.227
Normal tooth thickness at tip form circle (mm)	[sFan]	4.429
(mm)	[sFan.e/i]	4.317 / 4.227
Normal space width at root circle (mm)	[efn]	5.399
(mm)	[efn.e/i]	5.494 / 5.541

Gear specific pair data Gear pair 1, Gear 1

Operating pitch diameter (mm)	[dw]	817.763
(mm)	[dw.e/i]	817.815 / 817.711
Active tip diameter (mm)	[dNa]	830.110
(mm)	[dNa.e/i]	830.110 / 830.020
Theoretical tip clearance (mm)	[c]	3.404
Effective tip clearance (mm)	[c.e/i]	3.745 / 3.547
Active root diameter (mm)	[dNf]	804.774
(mm)	[dNf.e/i]	804.872 / 804.712
Reserve (dNf-dFf)/2 (mm)	[cF.e/i]	1.758 / 1.579
Max. sliding velocity at tip (m/s)	[vga]	3.693
Specific sliding at the tip	[ζa]	0.376
Specific sliding at the root	[ζf]	-0.553
Mean specific sliding	[ζm]	0.365
Sliding factor on tip	[Kga]	0.153
Sliding factor on root	[Kgf]	-0.178
Roll angle at dFa (°)	[ξdFa.e/i]	25.073 / 25.056
Roll angle to dNa (°)	[ξdNa.e/i]	25.073 / 25.056
Roll angle to dNf (°)	[ξdNf.e/i]	19.860 / 19.823
Roll angle at dFf (°)	[ξdFf.e/i]	19.083 / 19.036
Diameter of single contact point B (mm)	[d-B]	814.080 (814.080 / 814.000)
Diameter of single contact point D (mm)	[d-D]	819.583 (819.512 / 819.695)
Addendum contact ratio	[ε]	0.760 (0.763 / 0.751)

Gear specific pair data Gear pair 1, Gear 2

Operating pitch diameter (mm)	[dw]	282.237
(mm)	[dw.e/i]	282.255 / 282.219
Active tip diameter (mm)	[dNa]	298.010
(mm)	[dNa.e/i]	298.010 / 297.958
Theoretical tip clearance (mm)	[c]	2.034
Effective tip clearance (mm)	[c.e/i]	2.445 / 2.239
Active root diameter (mm)	[dNf]	272.072
(mm)	[dNf.e/i]	272.182 / 272.022
Reserve (dNf-dFf)/2 (mm)	[cF.e/i]	1.696 / 1.565
Max. sliding velocity at tip (m/s)	[vga]	4.297
Specific sliding at the tip	[ζa]	0.356
Specific sliding at the root	[ζf]	-0.603
Mean specific sliding	[ζm]	0.365
Sliding factor on tip	[Kga]	0.178
Sliding factor on root	[Kgf]	-0.153
Roll angle at dFa (°)	[ξdFa.e/i]	30.811 / 30.787
Roll angle to dNa (°)	[ξdNa.e/i]	30.811 / 30.787
Roll angle to dNf (°)	[ξdNf.e/i]	15.732 / 15.600
Roll angle at dFf (°)	[ξdFf.e/i]	12.754 / 12.652
Diameter of single contact point B (mm)	[d-B]	286.131 (286.055 / 286.297)
Diameter of single contact point D (mm)	[d-D]	280.467 (280.467 / 280.428)
Addendum contact ratio	[ε]	0.884 (0.885 / 0.880)

General influence factors

		Gear 1	Gear 2
Nominal circum. force at pitch circle (N)	[Ft]	61558.2	
Axial force (N)	[Fa]	14211.8	
Radial force (N)	[Fr]	22994.7	
Normal force (N)	[Fnorm]	67232.0	
Nominal circumferential force per mm (N/mm)	[w]	321.69	
Only as information: Forces at operating pitch circle:			
Nominal circumferential force (N)	[Ftw]	61109.8	
Axial force (N)	[Faw]	14211.8	
Radial force (N)	[Frw]	24161.1	
Circumferential speed reference circle (m/s)	[v]	23.95	
Circumferential speed operating pitch circle (m/s)	[v(dw)]	24.12	
Running-in value (µm)	[yp]	0.9	
Running-in value (µm)	[yf]	1.0	
Correction factor	[CM]	0.800	
Gear blank factor	[CR]	1.000	
Basic rack factor	[CBS]	0.900	
Material coefficient	[E/Est]	1.000	
Singular tooth stiffness (N/mm/µm)	[c']	13.946	
Meshing stiffness (N/mm/µm)	[cγα]	20.674	
Meshing stiffness (N/mm/µm)	[cγβ]	17.573	
Reduced mass (kg/mm)	[mRed]	0.24722	
Resonance speed (min-1)	[nE1]	773	
Resonance ratio (-)	[N]	0.729	
Subcritical range			
Running-in value (µm)	[yα]	0.9	
Bearing distance l of pinion shaft (mm)	[l]	382.700	
Distance s of pinion shaft (mm)	[s]	38.270	
Outside diameter of pinion shaft (mm)	[dsh]	191.400	
Load in accordance with Figure 13, ISO 6336-1:2006 0:a), 1:b), 2:c), 3:d), 4:e)	[-]	4	
Coefficient K' according to Figure 13, ISO 6336-1:2006	[K']	-1.00	
Without stiffening			
Tooth trace deviation (active) (µm)	[Fβy]	6.38	
from deformation of shaft (µm)	[fsh*B1]	1.90	
fsh (µm) =1.90, B1= 1.00, fHβ5 (µm) = 10.00			
Tooth without tooth trace modification			
Position of contact pattern:	favorable		
from production tolerances (µm)	[fmα*B2]	20.52	
B2= 1.00			
Tooth trace deviation, theoretical (µm)	[Fβx]	7.50	
Running-in value (µm)	[yβ]	1.13	
Dynamic factor	[Kv]	1.207	
Face load factor - flank	[KHβ]	1.144	
- Tooth root	[KFβ]	1.130	
- Scuffing	[KBβ]	1.144	
Transverse load factor - flank	[KHα]	1.172	
- Tooth root	[KFα]	1.172	
- Scuffing	[KBα]	1.172	
Number of load cycles (in mio.)	[NL]	676.109	1958.983

Tooth root load capacity

Calculation of Tooth form coefficients according method: B

		Gear 1	Gear 2
Calculated with generating profile shift coefficient	[xE.i]	0.3583	0.1414
Tooth form factor	[YF]	0.85	1.07
Stress correction factor	[YS]	2.34	1.97
Load application angle (°)	[αFen]	20.57	20.68
Coefficient	[fε]	0.762	
Load application diameter (mm)	[d_{en}]	818.874	285.366
Bending moment arm (mm)	[hF]	7.58	8.24
Tooth thickness at root (mm)	[sFn]	16.84	15.69
Tooth root radius (mm)	[ρF]	3.04	3.74

Bending moment arm (-)	[hF/mn]	1.083	1.177
Tooth thickness at root (-)	[sFn/mn]	2.405	2.241
Tooth root radius (-)	[ρF/mn]	0.434	0.535
Calculation cross section diameter (mm)	[d_{sFn}]	799.975	265.463
Tangents on calculation cross section (°)	[α_{sFn}]	30.000	30.000
Notch parameter	[q_s]	2.773	2.096
Helix angle factor	[Yβ]	0.964	
Deep tooth factor	[YDT]	1.000	
Gear rim factor	[YB]	1.00	1.00
Effective facewidth (mm)	[beff]	194.50	191.36
Nominal stress at tooth root (N/mm²)	[σF0]	87.20	92.95
Tooth root stress (N/mm²)	[σF]	139.34	148.53
Permissible bending stress at root of Test-gear			
Notch sensitivity factor	[YdrelT]	1.003	0.996
Surface factor	[YRrelT]	0.957	0.957
Size factor, tooth root	[YX]	0.980	0.980
Finite life factor	[YNT]	0.897	0.878
Y_C*Y_{drelT}*Y_{RrelT}*Y_X*Y_{NT}		0.843	0.820
Alternating bending factor, mean stress influence coefficient			
	[YM]	1.000	1.000
Stress correction factor	[Yst]	2.00	
Yst*σFlim (N/mm²)	[σFE]	860.00	860.00
Permissible tooth root stress σFG/SFmin (N/mm²)	[σFP]	518.01	503.82
Limit strength tooth root (N/mm²)	[σFG]	725.22	705.35
Required safety	[SFmin]	1.40	1.40
Safety for tooth root stress	[SF=σFG/σF]	5.20	4.75
Transmittable power (kW)	[kWRating]	5480.72	5000.61

Flank safety

		------- Gear 1	-------- Gear 2 --
Zone factor	[ZH]	2.374	
Elasticity factor (√N/mm²)	[ZE]	189.812	
Contact ratio factor	[Zε]	0.780	
Helix angle factor	[Zβ]	1.013	
Effective facewidth (mm)	[beff]	191.36	
Nominal contact stress (N/mm²)	[σH0]	442.48	
Contact stress at operating pitch circle (N/mm²)	[σHw]	562.82	
Coefficient[fZCa] 1.20 (Helical gear sets without flank modifications)			
Single tooth contact factor	[ZB,ZD]	1.10	1.10
Contact stress (N/mm²)	[σHB, σHD]	616.54	616.54
Lubrication factor for NL	[ZL]	1.047	1.047
Speed factor for NL	[ZV]	1.026	1.026
Roughness factor for NL	[ZR]	0.998	0.998
Material hardening factor for NL	[ZW]	1.000	1.000
Finite life factor	[ZNT]	0.923	0.894
	[ZL*ZV*ZR*ZNT]	0.990	0.959
Limited pitting is permitted: No			
Size factor (flank)	[ZX]	1.000	1.000
Permissible contact stress, σHG/SHmin (N/mm²)	[σHP]	1485.49	1437.80
Pitting stress limit (N/mm²)	[σHG]	1485.49	1437.80
Required safety	[SHmin]	1.00	1.00
Safety factor for contact stress at operating pitch circle	[SHw]	2.64	2.55
Safety against pressure, σHG/σHBD Single contact	[SHBD]	2.41	2.33
Safety regarding transmittable torque	[(SHBD)^2]	5.81	5.44
Transmittable power (kW)	[kWRating]	8558.46	8017.74

Micropitting according to **ISO/TS 6336-22:2018**

Calculation has not been carried out, lubricant: Load stage micropitting test not known

Scuffing load capacity

Calculation method according to	ISO/TS 6336-20/21:2017		
Helical load factor for scuffing	[KBγ]	1.300	
Lubrication coefficient for lubrication type	[XS]	1.000	
Scuffing test and load stage	[FZGtest]	FZG - Test A / 8.3 / 90 (ISO 14635 - 1)	12
Multiple meshing factor	[Xmp]	1.000	
Relative structural factor, scuffing	[XWrelT]	1.000	
Thermal contact factor (N/mm/s^.5/K)	[BM]	13.780	13.780
Relevant tip relief (µm)	[Ca]	2.00	2.00
Optimal tip relief (µm)	[Ceff]	15.56	
Ca taken as optimal in the calculation (0=no, 1=yes)		0	0
Effective facewidth (mm)	[beff]	191.360	
Applicable circumferential force/facewidth (N/mm)	[wBt]	520.456	
KBγ = 1.300 , wBt*KBγ =676.593			
Angle factor	[Xαβ]	0.996	
ε1: 0.760 , ε2: 0.884			
Flash temperature-criteria			
Lubricant factor	[XL]	0.679	
Tooth mass temperature (°C)	[θMi]	66.96	
θMi = θoil + XS*0.47*Xmp*θflm			
Average flash temperature	(°C) [θflm]	10.56	
Scuffing temperature (°C)	[θS]	299.98	
Γ coordinates (point of highest temperature)	[Γ]	-0.124	
[Γ.A]= -0.124 [Γ.E]= 0.107			
Highest contact temp. (°C)	[θB]	91.94	
Flash factor (°K*N^-.75*s^.5*m^-.5*mm)	[XM]	50.058	
Approach factor	[XJ]	1.042	
Load sharing factor	[XΓ]	0.791	
Dynamic viscosity (mPa*s)	[ηM]	81.42	(62.0 °C)
Coefficient of friction	[μ_m]	0.030	
Required safety	[SBmin]	2.000	
Margin of safety for scuffing, flash temperature	[SB]	7.947	
Integral temperature-criteria			
Lubricant factor (Input)	[XL]	0.846	
Tooth mass temperature (°C)	[θMC]	65.92	
θMC = θoil + XS*0.70*θflaint			
Mean flash temperature	(°C) [θflaint]	5.60	
Integral scuffing temperature (°C)	[θSint]	316.54	
Flash factor (°K*N^-.75*s^.5*m^-.5*mm)	[XM]	50.058	
Running-in factor, well run in	[XE]	1.000	
Contact ratio factor	[Xε]	0.243	
Dynamic viscosity (mPa*s)	[ηOil]	81.42	(62.0 °C)
Mean coefficient of friction	[μ_m]	0.023	
Geometry factor	[XBE]	0.170	
Meshing factor	[XQ]	1.000	
Tip relief factor	[XCa]	1.158	
Integral tooth flank temperature (°C)	[θint]	74.31	
Required safety	[SSmin]	1.800	
Safety factor for scuffing (intg.-temp.)	[SSint]	4.260	
Safety referring to transmittable torque	[SSL]	20.672	

Measurements for tooth thickness

		------- Gear 1 --------	Gear 2 --
Tooth thickness tolerance		DIN 3967 cd25	DIN 3967 cd25
Tooth thickness allowance (normal section) (mm)	[As.e/i]	-0.175 / -0.255	-0.130 / -0.190
Number of teeth spanned	[k]	15.000	5.000
Base tangent length (no backlash) (mm)	[Wk]	313.527	97.965
Base tangent length with allowance (mm)	[Wk.e/i]	313.362 / 313.287	97.843 / 97.787
(mm)	[ΔWk.e/i]	-0.164 / -0.240	-0.122 / -0.179
Diameter of measuring circle (mm)	[dMWk.m]	819.828	279.337
Theoretical diameter of ball/pin (mm)	[DM]	11.972	12.110
Effective diameter of ball/pin (mm)	[DMeff]	12.000	14.000
Radial single-ball measurement backlash free (mm)	[MrK]	416.981	152.931
Radial single-ball measurement (mm)	[MrK.e/i]	416.759 / 416.657	152.788 / 152.722
Diameter of measuring circle (mm)	[dMMr.m]	817.054	285.822

Diametral measurement over two balls without clearance (mm)	[MdK]	833.882	305.626	
Diametral two ball measure (mm)	[MdK.e/i]	833.438 /	833.234305.340 /	305.207
Diametral measurement over pins without clearance (mm)	[MdR]	833.961	305.863	
Measurement over pins according to DIN 3960 (mm)	[MdR.e/i]	833.517 /	833.314305.576 /	305.444
Measurement over 2 pins, free, according to AGMA 2002 (mm)	[dk2f.e/i]	833.433 /	833.230305.325 /	305.193
Measurement over 2 pins, transverse, according to AGMA 2002 (mm)	[dk2t.e/i]	833.596 /	833.393305.808 /	305.676
Measurement over 3 pins, axial, according to AGMA 2002 (mm)	[dk3A.e/i]	833.517 /	833.314305.576 /	305.444

Chordal tooth thickness (no backlash) (mm)	[sc]	13.076	11.903	
Normal chordal tooth thickness with allowance (mm)	[sc.e/i]	12.902 /	12.822 11.775 /	11.716
Reference chordal height from da.m (mm)	[ha]	9.179	9.022	
Tooth thickness, arc (mm)	[sn]	13.076	11.906	
(mm)	[sn.e/i]	12.901 /	12.821 11.776 /	11.716

Backlash free center distance (mm)	[aControl.e/i]	549.600 /	549.416
Backlash free center distance, allowances (mm)	[jta]	-0.400 /	-0.584
dNf.i with aControl (mm)	[dNf0.i]	803.737	271.250
Reserve (dNf0.i-dFf.e)/2 (mm)	[cF0.i]	1.092	1.179
Tip clearance (mm)	[c0.i(aControl)]	2.998	1.690
Center distance allowances (mm)	[Aa.e/i]	0.035 /	-0.035

Circumferential backlash from Aa (mm)	[jtw_Aa.e/i]	0.028 /	-0.028
Radial backlash (mm)	[jrw.e/i]	0.619 /	0.365
Circumferential backlash (transverse section) (mm)	[jtw.e/i]	0.488 /	0.288
Normal backlash (mm)	[jn.e/i]	0.442 /	0.263
Torsional angle on input with output fixed:			
Total torsional angle (°)	[j.tSys]	0.0683/	0.0403

Toothing tolerances

		------- Gear 1	-------- Gear 2 --
According to ISO 1328-1:2013, ISO 1328-2:1997			
Accuracy grade	[Q]	A6	A6
Single pitch deviation (µm)	[fptT]	12.00	11.00
Base circle pitch deviation (µm)	[fpbT]	11.40	10.70
Sector pitch deviation over k/8 pitches (µm)	[Fpk/8T]	30.00	25.00
Profile form deviation (µm)	[ffαT]	13.00	13.00
Profile slope deviation (µm)	[fHαT]	11.00	10.00
Total profile deviation (µm)	[FαT]	17.00	16.00
Helix form deviation (µm)	[ffβT]	17.00	16.00
Helix slope deviation (µm)	[fHβT]	15.00	14.00
Total helix deviation (µm)	[FβT]	23.00	21.00
Total cumulative pitch deviation (µm)	[FpT]	48.00	38.00
Adjacent pitch difference (µm)	[fuT]	17.00	16.00
Runout (µm)	[FrT]	44.00	34.00
Single flank composite, total (µm)	[FisT]	59.00	48.00
Single flank composite, tooth-to-tooth (µm)	[fisT]	11.00	11.00
Radial composite, total (µm)	[FidT]	83.00	73.00
Radial composite, tooth-to-tooth (µm)	[fidT]	34.00	34.00

FidT (Fi''), fidT (fi'') according to ISO 1328:1997 calculated with the geometric mean values for mn and d

Axis alignment tolerances (recommendation acc. to ISO TR 10064-3:1996, Quality)

		6		
Maximum value for deviation error of axis (µm)	[fΣβ]	23.00	(Fβ=	23.00)
Maximum value for inclination error of axes (µm)	[fΣδ]	46.00		

Modifying and defining the tooth form

Data for the tooth form calculation :
Data not available.
Please run the calculation in the "Tooth form" tab and open the main report again.

Supplementary data

Mass (kg)	[m]	792.570	92.622
Total mass (kg)	[mGes]	885.191	
Moment of inertia for system, relative to the input:			
calculation without consideration of the exact tooth shape			
Single gears, (da+df)/2...di (kg*m²)	[J]	65.64685	0.91124
System (da+df)/2...di (kg*m²)	[J]	73.29681	
Torsional stiffness at driving gear with fixed driven gear:			
Torsional stiffness (MNm/rad)	[cr]	482.667	
Torsion when subjected to nominal torque (°)	[δcr]	0.003	
Mean coefficient of friction (as defined in Niemann)	[μ_m]	0.022	
Wear sliding coef. by Niemann	[ζw]	0.603	
Loss factor	[HV]	0.079	
Gear power loss (kW)	[PVZ]	2.533	
Meshing efficiency (%)	[ηz]	99.828	
Sound pressure level according to Masuda, without contact analysis			
	[dB(A)]	104.9	

Service life, damage

Required safety for tooth root	[SFmin]	1.40	
Required safety for tooth flank	[SHmin]	1.00	
Service life (calculated with required safeties):			
System service life (h)	[Hatt]	> 1000000	
Tooth root service life (h)	[HFatt]	1e+06	1e+06
Tooth flank service life (h)	[HHatt]	1e+06	1e+06

Note: The entry 1e+006 h means that the Service life > 1,000,000 h.

Damage calculated on the basis of the required service life [H] (20000.0 h)

F1%	F2%	H1%	H2%
0.00	0.0000	0.0000	0.0000

Remarks:

- Specifications with [.e/i] imply: Maximum [e] and minimum value [i] for
  Taking all tolerances into account
  Specifications with [.m] imply: Mean value within tolerance
- For the backlash tolerance, the center distance tolerances and the tooth thickness allowance are taken into account.
  The maximum and minimum clearance according to the largest or smallest allowances are defined..
  The calculation is performed for the operating pitch circle.
- Calculation of Zbet according to Corrigendum 1 ISO 6336-2:2008 with Zβ = 1/(COS(β)^0.5)
- Details of calculation method:
  cγ according to Method B
  Kv according to Method B
  KHβ and KFβ according to Method C
  fmα according to Equation 64, fsh according to 57/58, Fβx according to 52/53/54
  KHα, KFα according to Method B
- The logarithmically interpolated value taken from the values for the fatigue strength and the static strength, based on the number of load cycles, is used for coefficients ZL, ZV, ZR, ZW, ZX, YdrelT, YRrelT and YX..

End of Report lines: 628

KISSsoft

KISSsoft Release 2020 A.1

KISSsoft University license - Universidade do Porto

File

Name : Unnamed
Changed by: Rui on: 28.06.2021 at: 20:53:32

Fourth Stage: Wheel-Pump Gear

Calculation of a helical-toothed cylindrical gear pair

Drawing or article number:			
Gear 1:	z10(Z10Z12)		
Gear 2:	z12(Z10Z12)		
Calculation method	ISO 6336:2019		
		------- Gear 1 --------	Gear 2 --
Power (kW)	[P]	1.104	
Speed (1/min)	[n]	563.4	1552.9
Torque (Nm)	[T]	18.7	6.8
Application factor	[KA]	1.00	
Required service life (h)	[H]	20000.00	
Gear driving (+) / driven (-)		+	-
Working flank gear 1:	Right flank		
Gear 1 direction of rotation:	Clockwise		

Tooth geometry and material

Geometry calculation according to	ISO 21771:2007		
		------- Gear 1 --------	Gear 2 --
Center distance (mm)	[a]	558.500	
Center distance tolerance	ISO 286:2010 Measure js7		
Normal module (mm)	[mn]	7.0000	
Normal pressure angle (°)	[αn]	20.0000	
Helix angle at reference circle (°)	[β]	13.0000	
Number of teeth	[z]	113	41
Facewidth (mm)	[b]	194.50	30.00
Hand of gear		right	left
Accuracy grade	[Q-ISO 1328:2013]	A6	A6
Inner diameter (mm)	[di]	0.00	0.00
Inner diameter of gear rim (mm)	[dbi]	0.00	0.00

Material

Gear1
18CrNiMo7-6, Case-carburized steel, case-hardened
ISO 6336-5 Figure 9/10 (MQ), Core hardness >=25HRC Jominy J=12mm<HRC28

Gear2
18CrNiMo7-6, Case-carburized steel, case-hardened
ISO 6336-5 Figure 9/10 (MQ), Core hardness >=25HRC Jominy J=12mm<HRC28

		------- Gear 1 --------	Gear 2 --
Surface hardness		HRC 61	HRC 61
Material treatment according to ISO 6336:2006 Normal, life factors ZNT and YNT >=0.85			
Fatigue strength. tooth root stress (N/mm²)	[σFlim]	430.00	430.00
Fatigue strength for Hertzian pressure (N/mm²)	[σHlim]	1500.00	1500.00
Tensile strength (N/mm²)	[σB]	1200.00	1200.00
Yield point (N/mm²)	[σS]	850.00	850.00
Young's modulus (N/mm²)	[E]	206000	206000
Poisson's ratio	[v]	0.300	0.300
Roughness average value DS, flank (µm)	[RAH]	0.60	0.60
Roughness average value DS, root (µm)	[RAF]	3.00	3.00
Mean roughness height, Rz, flank (µm)	[RZH]	4.80	4.80
Mean roughness height, Rz, root (µm)	[RZF]	20.00	20.00

Gear reference profile 1:			
Reference profile	1.40 / 0.39 / 1.0 ISO 53:1998 Profil D		
Dedendum coefficient	[hfP*]	1.400	
Root radius factor	[ρfP*]	0.390	(ρfPmax*=0.394)
Addendum coefficient	[haP*]	1.000	
Tip radius factor	[ρaP*]	0.000	
Protuberance height coefficient	[hprP*]	0.000	
Protuberance angle	[αprP]	0.000	
Tip form height coefficient	[hFaP*]	0.000	
Ramp angle	[αKP]	0.000	
	not topping		

Gear reference profile 2:			
Reference profile	1.40 / 0.39 / 1.0 ISO 53:1998 Profil D		
Dedendum coefficient	[hfP*]	1.400	
Root radius factor	[ρfP*]	0.390	(ρfPmax*=0.394)
Addendum coefficient	[haP*]	1.000	
Tip radius factor	[ρaP*]	0.000	
Protuberance height coefficient	[hprP*]	0.000	
Protuberance angle	[αprP]	0.000	
Tip form height coefficient	[hFaP*]	0.000	
Ramp angle	[αKP]	0.000	
	not topping		

Information on final machining

Dedendum reference profile	[hfP*]	1.400	1.400
Tooth root radius Refer. profile	[ρfP*]	0.390	0.390
Addendum Reference profile	[haP*]	1.000	1.000
Protuberance height coefficient	[hprP*]	0.000	0.000
Protuberance angle (°)	[αprP]	0.000	0.000
Tip form height coefficient	[hFaP*]	0.000	0.000
Ramp angle (°)	[αKP]	0.000	0.000

Type of profile modification:	none (only running-in)	
Tip relief by running in (µm)	[Ca L/R]	2.0 / 2.0 2.0 / 2.0

Lubrication type	Oil bath lubrication	
Type of oil	ISO-VG 320	
Lubricant base	Mineral-oil base	
Oil nominal kinematic viscosity at 40°C (mm²/s)	[v40]	320.00
Oil nominal kinematic viscosity at 100°C (mm²/s)	[v100]	22.00
Specific density at 15°C (kg/dm³)	[ρ]	0.900
Oil temperature (°C)	[TS]	62.000

Gear pair

Overall transmission ratio	[itot]	-0.363
Gear ratio	[u]	2.756
Transverse module (mm)	[mt]	7.184
Transverse pressure angle (°)	[αt]	20.483
Working pressure angle (°)	[αwt]	21.898
	[αwt.e/i]	21.907 / 21.889
Working pressure angle at normal section (°)	[αwn]	21.378
Helix angle at operating pitch circle (°)	[βw]	13.121
Base helix angle (°)	[βb]	12.204
Reference center distance (mm)	[ad]	553.178
Pitch on reference circle (mm)	[pt]	22.570
Base pitch (mm)	[pbt]	21.143
Transverse pitch on contact-path (mm)	[pet]	21.143
Sum of profile shift coefficients	[Σxi]	0.7857
Transverse contact ratio	[εα]	1.536
Transverse contact ratio with allowances	[εα.e/m/i]	1.541 / 1.533 / 1.524
Overlap ratio	[εβ]	0.307
Total contact ratio	[εγ]	1.843

Total contact ratio with allowances	[εγ.e/m/i]	1.848 / 1.839 / 1.831
Length of path of contact (mm)	[ga, e/i]	32.486 (32.579 / 32.225)
Length T1-A (mm)	[T1A]	133.910 (133.817 / 134.059)
Length T1-B (mm)	[T1B]	145.253 (145.253 / 145.141)
Length T1-C (mm)	[T1C]	152.840 (152.771 / 152.908)
Length T1-D (mm)	[T1D]	155.053 (154.959 / 155.202)
Length T1-E (mm)	[T1E]	166.396 (166.396 / 166.284)
Length T2-A (mm)	[T2A]	74.384 (74.384 / 74.329)
Length T2-B (mm)	[T2B]	63.041 (62.947 / 63.247)
Length T2-C (mm)	[T2C]	55.455 (55.430 / 55.480)
Length T2-D (mm)	[T2D]	53.241 (53.241 / 53.187)
Length T2-E (mm)	[T2E]	41.899 (41.805 / 42.105)
Length T1-T2 (mm)	[T1T2]	208.295 (208.201 / 208.388)
Minimal length of contact line (mm)	[Lmin]	30.694

Gear 1

Lead height (mm)	[pz]	11046.847
Axial pitch (mm)	[px]	97.760
Profile shift coefficient	[x]	0.4083
Tooth thickness, arc, in module	[sn*]	1.8680
Tip alteration (mm)	[k*mn]	-0.706
Reference diameter (mm)	[d]	811.807
Base diameter (mm)	[db]	760.482
Tip diameter (mm)	[da]	830.110
(mm)	[da.e/i]	830.110 / 830.020
Tip diameter allowances (mm)	[Ada.e/i]	0.000 / -0.090
Tip form diameter (mm)	[dFa]	830.110
(mm)	[dFa.e/i]	830.110 / 830.020
Root diameter (mm)	[df]	797.923
Generating Profile shift coefficient	[xE.e/i]	0.3740/ 0.3583
Generated root diameter with xE (mm)	[df.e/i]	797.442 / 797.222
Root form diameter (mm)	[dFf]	801.989
(mm)	[dFf.e/i]	801.553 / 801.355
Involute length (mm)	[l_dFa-l_dFf]	15.088
Addendum, $m_n(h_{aP}^*+x+k)$ (mm)	[ha]	9.152
(mm)	[ha.e/i]	9.152 / 9.107
Dedendum (mm)	[hf=mn*(hfP*-x)]	6.942
(mm)	[hf.e/i]	7.182 / 7.292
Tooth height (mm)	[h]	16.094
Virtual gear no. of teeth	[zn]	121.397
Normal tooth thickness at tip circle (mm)	[san]	6.039
(mm)	[san.e/i]	5.898 / 5.779
Normal tooth thickness at tip form circle (mm)	[sFan]	6.039
(mm)	[sFan.e/i]	5.898 / 5.779
Normal space width at root circle (mm)	[efn]	4.123
(mm)	[efn.e/i]	4.145 / 4.155

Gear 2

Lead height (mm)	[pz]	4008.148
Axial pitch (mm)	[px]	97.760
Profile shift coefficient	[x]	0.3774
Tooth thickness, arc, in module	[sn*]	1.8455
Tip alteration (mm)	[k*mn]	-0.178
Reference diameter (mm)	[d]	294.549
Base diameter (mm)	[db]	275.927
Tip diameter (mm)	[da]	313.477
(mm)	[da.e/i]	313.477 / 313.425
Tip diameter allowances (mm)	[Ada.e/i]	0.000 / -0.052
Tip form diameter (mm)	[dFa]	313.477
(mm)	[dFa.e/i]	313.477 / 313.425
Root diameter (mm)	[df]	280.233
Generating Profile shift coefficient	[xE.e/i]	0.3519/ 0.3401
Generated root diameter with xE (mm)	[df.e/i]	279.876 / 279.711

Root form diameter (mm)	[dFf]	285.274
(mm)	[dFf.e/i]	285.016 / 284.898
Involute length (mm)	[l_dFa-l_dFf]	15.300
Addendum, $m_n(h_{aP}^*+x+k)$ (mm)	[ha]	9.464
(mm)	[ha.e/i]	9.464 / 9.438
Dedendum (mm)	[hf=mn*(hfP*-x)]	7.158
(mm)	[hf.e/i]	7.337 / 7.419
Tooth height (mm)	[h]	16.622
Virtual gear no. of teeth	[zn]	44.047
Normal tooth thickness at tip circle (mm)	[san]	4.988
(mm)	[san.e/i]	4.877 / 4.787
Normal tooth thickness at tip form circle (mm)	[sFan]	4.988
(mm)	[sFan.e/i]	4.877 / 4.787
Normal space width at root circle (mm)	[efn]	4.759
(mm)	[efn.e/i]	4.816 / 4.844

Gear specific pair data Gear pair 1, Gear 1

Operating pitch diameter (mm)	[dw]	819.617
(mm)	[dw.e/i]	819.668 / 819.566
Active tip diameter (mm)	[dNa]	830.110
(mm)	[dNa.e/i]	830.110 / 830.020
Theoretical tip clearance (mm)	[c]	3.329
Effective tip clearance (mm)	[c.e/i]	3.670 / 3.472
Active root diameter (mm)	[dNf]	806.263
(mm)	[dNf.e/i]	806.362 / 806.201
Reserve (dNf-dFf)/2 (mm)	[cF.e/i]	2.503 / 2.324
Max. sliding velocity at tip (m/s)	[vga]	3.004
Specific sliding at the tip	[ζa]	0.306
Specific sliding at the root	[ζf]	-0.531
Mean specific sliding	[ζm]	0.330
Sliding factor on tip	[Kga]	0.124
Sliding factor on root	[Kgf]	-0.173
Roll angle at dFa (°)	[ξdFa.e/i]	25.073 / 25.056
Roll angle to dNa (°)	[ξdNa.e/i]	25.073 / 25.056
Roll angle to dNf (°)	[ξdNf.e/i]	20.200 / 20.164
Roll angle at dFf (°)	[ξdFf.e/i]	19.083 / 19.036
Diameter of single contact point B (mm)	[d-B]	814.080 (814.080 / 814.000)
Diameter of single contact point D (mm)	[d-D]	821.278 (821.207 / 821.391)
Addendum contact ratio	[ε]	0.641 (0.644 / 0.633)

Gear specific pair data Gear pair 1, Gear 2

Operating pitch diameter (mm)	[dw]	297.383
(mm)	[dw.e/i]	297.402 / 297.364
Active tip diameter (mm)	[dNa]	313.477
(mm)	[dNa.e/i]	313.477 / 313.425
Theoretical tip clearance (mm)	[c]	2.800
Effective tip clearance (mm)	[c.e/i]	3.212 / 3.006
Active root diameter (mm)	[dNf]	288.371
(mm)	[dNf.e/i]	288.491 / 288.316
Reserve (dNf-dFf)/2 (mm)	[cF.e/i]	1.796 / 1.650
Max. sliding velocity at tip (m/s)	[vga]	4.195
Specific sliding at the tip	[ζa]	0.347
Specific sliding at the root	[ζf]	-0.441
Mean specific sliding	[ζm]	0.330
Sliding factor on tip	[Kga]	0.173
Sliding factor on root	[Kgf]	-0.124
Roll angle at dFa (°)	[ξdFa.e/i]	30.892 / 30.869
Roll angle to dNa (°)	[ξdNa.e/i]	30.892 / 30.869
Roll angle to dNf (°)	[ξdNf.e/i]	17.486 / 17.361
Roll angle at dFf (°)	[ξdFf.e/i]	14.827 / 14.729
Diameter of single contact point B (mm)	[d-B]	303.369 (303.291 / 303.540)
Diameter of single contact point D (mm)	[d-D]	295.761 (295.761 / 295.721)
Addendum contact ratio	[ε]	0.895 (0.896 / 0.892)

General influence factors

		------- Gear 1	-------- Gear 2 --
Nominal circum. force at pitch circle (N)	[Ft]	46.1	
Axial force (N)	[Fa]	10.6	
Radial force (N)	[Fr]	17.2	
Normal force (N)	[Fnorm]	50.3	
Nominal circumferential force per mm (N/mm)	[w]	1.54	
Only as information: Forces at operating pitch circle:			
Nominal circumferential force (N)	[Ftw]	45.6	
Axial force (N)	[Faw]	10.6	
Radial force (N)	[Frw]	18.3	
Circumferential speed reference circle (m/s)	[v]	23.95	
Circumferential speed operating pitch circle (m/s)	[v(dw)]	24.18	
Running-in value (µm)	[yp]	0.9	
Running-in value (µm)	[yf]	1.0	
Correction factor	[CM]	0.800	
Gear blank factor	[CR]	1.000	
Basic rack factor	[CBS]	0.900	
Material coefficient	[E/Est]	1.000	
Singular tooth stiffness (N/mm/µm)	[c']	10.135	
Meshing stiffness (N/mm/µm)	[cγα]	14.213	
Meshing stiffness (N/mm/µm)	[cγβ]	12.081	
The formula for c' and cγ at w*KA < 25 N/mm is imprecise!			
c' and cγ are calculated using w*KA = 25 N/mm.			
Reduced mass (kg/mm)	[mRed]	0.27648	
Resonance speed (min-1)	[nE1]	606	
Resonance ratio (-)	[N]	0.930	
Range of the main resonance!			
Running-in value (µm)	[yα]	0.9	
Bearing distance l of pinion shaft (mm)	[l]	60.000	
Distance s of pinion shaft (mm)	[s]	6.000	
Outside diameter of pinion shaft (mm)	[dsh]	30.000	
Load in accordance with Figure 13, ISO 6336-1:2006	[-]	4	
0:a), 1:b), 2:c), 3:d), 4:e)			
Coefficient K' according to Figure 13, ISO 6336-1:2006	[K']	-1.00	
Without stiffening			
Tooth trace deviation (active) (µm)	[Fβy]	6.34	
from deformation of shaft (µm)	[fsh*B1]	0.03	
fsh (µm) =0.03, B1= 1.00, fHβ5 (µm) = 7.50			
Tooth without tooth trace modification			
Position of contact pattern:		favorable	
from production tolerances (µm)	[fmα*B2]	13.35	
B2=			
1.00			
Tooth trace deviation, theoretical (µm)	[Fβx]	7.46	
Running-in value (µm)	[yβ]	1.12	
Dynamic factor	[Kv]	2.000	
Note: Kv is limited by preset Kv <= Kvmax =2.00			
Face load factor - flank	[KHβ]	5.000	
- Tooth root	[KFβ]	3.047	
- Scuffing	[KBβ]	5.000	
Note: KHβ is limited by KHβ <= KHβmax = 5.00			
Transverse load factor - flank	[KHα]	1.560	
- Tooth root	[KFα]	1.625	
- Scuffing	[KBα]	1.625	
Number of load cycles (in mio.)	[NL]	676.109	1863.423

Tooth root load capacity

Calculation of Tooth form coefficients according method: B

		------- Gear 1	-------- Gear 2 --
Calculated with generating profile shift coefficient	[xE.i]	0.3583	0.3401
Tooth form factor	[YF]	1.18	1.23
Stress correction factor	[YS]	2.24	2.10
Load application angle (°)	[αFen]	20.91	21.90
Coefficient	[fε]	0.940	

Load application diameter (mm)	[d_{en}]	820.560	302.571
Bending moment arm (mm)	[hF]	8.52	8.25
Tooth thickness at root (mm)	[sFn]	16.84	16.18
Tooth root radius (mm)	[ρF]	3.04	3.36
Bending moment arm (-)	[hF/mn]	1.217	1.179
Tooth thickness at root (-)	[sFn/mn]	2.405	2.311
Tooth root radius (-)	[ρF/mn]	0.434	0.480
Calculation cross section diameter (mm)	[d_{sFn}]	799.975	282.443
Tangents on calculation cross section (°)	[α_{sFn}]	30.000	30.000
Notch parameter	[q_s]	2.773	2.410
Helix angle factor	[Yβ]	1.045	
Deep tooth factor	[YDT]	1.000	
Gear rim factor	[YB]	1.00	1.00
Effective facewidth (mm)	[beff]	44.00	30.00
Nominal stress at tooth root (N/mm²)	[σF0]	0.41	0.59
Tooth root stress (N/mm²)	[σF]	4.09	5.88
Permissible bending stress at root of Test-gear			
Notch sensitivity factor	[YdrelT]	1.003	0.999
Surface factor	[YRrelT]	0.957	0.957
Size factor, tooth root	[YX]	0.980	0.980
Finite life factor	[YNT]	0.897	0.879
Y_C*Y_{drelT}*Y_{RrelT}*Y_X*Y_{NT}		0.843	0.824
Alternating bending factor, mean stress influence coefficient			
	[YM]	1.000	1.000
Stress correction factor	[Yst]	2.00	
Yst*σFlim (N/mm²)	[σFE]	860.00	860.00
Permissible tooth root stress σFG/SFmin (N/mm²)	[σFP]	518.01	505.89
Limit strength tooth root (N/mm²)	[σFG]	725.22	708.25
Required safety	[SFmin]	1.40	1.40
Safety for tooth root stress	[SF=σFG/σF]	177.30	120.55
Transmittable power (kW)	[kWRating]	139.75	95.02

Flank safety

		------- Gear 1	-------- Gear 2 --
Zone factor	[ZH]	2.354	
Elasticity factor (√N/mm²)	[ZE]	189.812	
Contact ratio factor	[Zε]	0.877	
Helix angle factor	[Zβ]	1.013	
Effective facewidth (mm)	[beff]	30.00	
Nominal contact stress (N/mm²)	[σH0]	33.46	
Contact stress at operating pitch circle (N/mm²)	[σHw]	132.18	
Coefficient [fZCa] 1.20 (Helical gear sets without flank modifications)			
Single tooth contact factor	[ZB,ZD]	1.00	1.04
Contact stress (N/mm²)	[σHB, σHD]	132.57	137.26
Lubrication factor for NL	[ZL]	1.047	1.047
Speed factor for NL	[ZV]	1.026	1.026
Roughness factor for NL	[ZR]	1.000	1.000
Material hardening factor for NL	[ZW]	1.000	1.000
Finite life factor	[ZNT]	0.923	0.895
	[ZL*ZV*ZR*ZNT]	0.992	0.961
Limited pitting is permitted: No			
Size factor (flank)	[ZX]	1.000	1.000
Permissible contact stress, σHG/SHmin (N/mm²)	[σHP]	1487.61	1442.06
Pitting stress limit (N/mm²)	[σHG]	1487.61	1442.06
Required safety	[SHmin]	1.00	1.00
Safety factor for contact stress at operating pitch circle	[SHw]	11.25	10.91
Safety against pressure, σHG/σHBD Single contact	[SHBD]	11.22	10.51
Safety regarding transmittable torque	[(SHBD)^2]	125.91	110.37
Transmittable power (kW)	[kWRating]	138.94	121.80

Micropitting according to **ISO/TS 6336-22:2018**

Calculation has not been carried out, lubricant: Load stage micropitting test not known

Scuffing load capacity

Calculation method according to	ISO/TS 6336-20/21:2017		
Helical load factor for scuffing	[KBγ]	1.000	
Lubrication coefficient for lubrication type	[XS]	1.000	
Scuffing test and load stage	[FZGtest]	FZG - Test A / 8.3 / 90 (ISO 14635 - 1)	12
Multiple meshing factor	[Xmp]	1.000	
Relative structural factor, scuffing	[XWrelT]	1.000	
Thermal contact factor (N/mm/s^.5/K)	[BM]	13.780	13.780
Relevant tip relief (µm)	[Ca]	2.00	2.00
Optimal tip relief (µm)	[Ceff]	0.11	
Ca taken as optimal in the calculation (0=no, 1=yes)		0	0
Effective facewidth (mm)	[beff]	30.000	
Applicable circumferential force/facewidth (N/mm)	[wBt]	24.965	
KBγ = 1.000 , wBt*KBγ = 24.965			
Angle factor	[Xαβ]	1.000	
ε1: 0.641 , ε2: 0.895			
Flash temperature-criteria			
Lubricant factor	[XL]	0.679	
Tooth mass temperature (°C)	[θMi]	62.20	
θMi = θoil + XS*0.47*Xmp*θflm			
Average flash temperature	(°C) [θflm]	0.43	
Scuffing temperature (°C)	[θS]	299.98	
Γ coordinates (point of highest temperature)	[Γ]	-0.120	
[Γ.A]= -0.124 [Γ.E]= 0.089			
Highest contact temp. (°C)	[θB]	62.91	
Flash factor (°K*N^-.75*s^.5*m^-.5*mm)	[XM]	50.058	
Approach factor	[XJ]	1.000	
Load sharing factor	[XΓ]	0.382	
Dynamic viscosity (mPa*s)	[ηM]	81.42	(62.0 °C)
Coefficient of friction	[μ_m]	0.016	
Required safety	[SBmin]	2.000	
Margin of safety for scuffing, flash temperature	[SB]	260.719	
Integral temperature-criteria			
Lubricant factor (Input)	[XL]	0.846	
Tooth mass temperature (°C)	[θMC]	62.11	
θMC = θoil + XS*0.70*θflaint			
Mean flash temperature	(°C) [θflaint]	0.15	
Integral scuffing temperature (°C)	[θSint]	316.54	
Flash factor (°K*N^-.75*s^.5*m^-.5*mm)	[XM]	50.058	
Running-in factor, well run in	[XE]	1.000	
Contact ratio factor	[Xε]	0.249	
Dynamic viscosity (mPa*s)	[ηOil]	81.42	(62.0 °C)
Mean coefficient of friction	[μ_m]	0.012	
Geometry factor	[XBE]	0.164	
Meshing factor	[XQ]	1.000	
Tip relief factor	[XCa]	1.784	
Integral tooth flank temperature (°C)	[θint]	62.33	
Required safety	[SSmin]	1.800	
Safety factor for scuffing (intg.-temp.)	[SSint]	5.078	
Safety referring to transmittable torque	[SSL]	254.540	

Measurements for tooth thickness

		------- Gear 1 --------	Gear 2 --
Tooth thickness tolerance		DIN 3967 cd25	DIN 3967 cd25
Tooth thickness allowance (normal section) (mm)	[As.e/i]	-0.175 / -0.255	-0.130 / -0.190
Number of teeth spanned	[k]	15.000	6.000
Base tangent length (no backlash) (mm)	[Wk]	313.527	119.793
Base tangent length with allowance (mm)	[Wk.e/i]	313.362 / 313.287	119.671 / 119.614
(mm)	[ΔWk.e/i]	-0.164 / -0.240	-0.122 / -0.179
Diameter of measuring circle (mm)	[dMWk.m]	819.828	299.684
Theoretical diameter of ball/pin (mm)	[DM]	11.972	12.415

Effective diameter of ball/pin (mm)	[DMeff]	12.000	14.000	
Radial single-ball measurement backlash free (mm)	[MrK]	416.981	161.247	
Radial single-ball measurement (mm)	[MrK.e/i]	416.759 /	416.657	161.107 / 161.042
Diameter of measuring circle (mm)	[dMMr.m]	817.054	302.306	
Diametral measurement over two balls without clearance (mm)	[MdK]	833.882	322.268	
Diametral two ball measure (mm)	[MdK.e/i]	833.438 /	833.234	321.988 / 321.859
Diametral measurement over pins without clearance (mm)	[MdR]	833.961	322.494	
Measurement over pins according to DIN 3960 (mm)	[MdR.e/i]	833.517 /	833.314	322.214 / 322.085
Measurement over 2 pins, free, according to AGMA 2002 (mm)	[dk2f.e/i]	833.433 /	833.230	321.974 / 321.845
Measurement over 2 pins, transverse, according to AGMA 2002 (mm)	[dk2t.e/i]	833.596 /	833.393	0.000 / 0.000
Measurement over 3 pins, axial, according to AGMA 2002 (mm)	[dk3A.e/i]	833.517 /	833.314	322.214 / 322.085

Chordal tooth thickness (no backlash) (mm)	[sc]	13.076	12.915	
Normal chordal tooth thickness with allowance (mm)	[sc.e/i]	12.902 /	12.822	12.787 / 12.728
Reference chordal height from da.m (mm)	[ha]	9.179	9.585	
Tooth thickness, arc (mm)	[sn]	13.076	12.919	
(mm)	[sn.e/i]	12.901 /	12.821	12.789 / 12.729

Backlash free center distance (mm)	[aControl.e/i]	558.106 /	557.925
Backlash free center distance, allowances (mm)	[jta]	-0.394 /	-0.575
dNf.i with aControl (mm)	[dNf0.i]	805.240	287.486
Reserve (dNf0.i-dFf.e)/2 (mm)	[cF0.i]	1.843	1.235
Tip clearance (mm)	[c0.i(aControl)]	2.932	2.465
Center distance allowances (mm)	[Aa.e/i]	0.035 /	-0.035

Circumferential backlash from Aa (mm)	[jtw_Aa.e/i]	0.028 /	-0.028
Radial backlash (mm)	[jrw.e/i]	0.610 /	0.359
Circumferential backlash (transverse section) (mm)	[jtw.e/i]	0.489 /	0.288
Normal backlash (mm)	[jn.e/i]	0.442 /	0.263
Torsional angle on input with output fixed:			
Total torsional angle (°)	[j.tSys]	0.0684/	0.0403

Toothing tolerances

		------- Gear 1	-------- Gear 2 --
According to ISO 1328-1:2013, ISO 1328-2:1997			
Accuracy grade	[Q]	A6	A6
Single pitch deviation (µm)	[fptT]	12.00	11.00
Base circle pitch deviation (µm)	[fpbT]	11.40	10.70
Sector pitch deviation over k/8 pitches (µm)	[Fpk/8T]	30.00	24.00
Profile form deviation (µm)	[ffαT]	13.00	13.00
Profile slope deviation (µm)	[fHαT]	11.00	10.00
Total profile deviation (µm)	[FαT]	17.00	16.00
Helix form deviation (µm)	[ffβT]	17.00	11.00
Helix slope deviation (µm)	[fHβT]	15.00	9.50
Total helix deviation (µm)	[FβT]	23.00	14.00
Total cumulative pitch deviation (µm)	[FpT]	48.00	38.00
Adjacent pitch difference (µm)	[fuT]	17.00	16.00
Runout (µm)	[FrT]	44.00	34.00
Single flank composite, total (µm)	[FisT]	59.00	49.00
Single flank composite, tooth-to-tooth (µm)	[fisT]	11.00	11.00
Radial composite, total (µm)	[FidT]	83.00	73.00
Radial composite, tooth-to-tooth (µm)	[fidT]	34.00	34.00

FidT (Fi"), fidT (fi") according to ISO 1328:1997 calculated with the geometric mean values for mn and d

Axis alignment tolerances (recommendation acc. to ISO TR 10064-3:1996, Quality)

		6		
Maximum value for deviation error of axis (µm)	[fΣβ]	16.00	(Fβ=	16.00)
Maximum value for inclination error of axes (µm)	[fΣδ]	32.00		

Modifying and defining the tooth form

Data for the tooth form calculation :
Data not available.
Please run the calculation in the "Tooth form" tab and open the main report again.

Supplementary data

Mass (kg)	[m]	792.570	16.258
Total mass (kg)	[mGes]	808.828	
Moment of inertia for system, relative to the input:			
calculation without consideration of the exact tooth shape			
Single gears, (da+df)/2...di (kg*m²)	[J]	65.64685	0.17908
System (da+df)/2...di (kg*m²)	[J]	67.00719	
Torsional stiffness at driving gear with fixed driven gear:			
Torsional stiffness (MNm/rad)	[cr]	51.903	
Torsion when subjected to nominal torque (°)	[δcr]	0.000	
Mean coefficient of friction (as defined in Niemann)	[μ_m]	0.018	
Wear sliding coef. by Niemann	[ζw]	0.496	
Loss factor	[HV]	0.072	
Gear power loss (kW)	[PVZ]	0.001	
Meshing efficiency (%)	[ηz]	99.871	
Sound pressure level according to Masuda, without contact analysis			
	[dB(A)]	57.0	

Service life, damage

Required safety for tooth root	[SFmin]	1.40	
Required safety for tooth flank	[SHmin]	1.00	
Service life (calculated with required safeties):			
System service life (h)	[Hatt]	> 1000000	
Tooth root service life (h)	[HFatt]	1e+06	1e+06
Tooth flank service life (h)	[HHatt]	1e+06	1e+06

Note: The entry 1e+006 h means that the Service life > 1,000,000 h.

Damage calculated on the basis of the required service life [H] (20000.0 h)

F1%	F2%	H1%	H2%
0.00	0.0000	0.0000	0.0000

Remarks:

- Specifications with [.e/i] imply: Maximum [e] and minimum value [i] for
  Taking all tolerances into account
  Specifications with [.m] imply: Mean value within tolerance
- For the backlash tolerance, the center distance tolerances and the tooth thickness allowance are taken into account.
  The maximum and minimum clearance according to the largest or smallest allowances are defined..
  The calculation is performed for the operating pitch circle.
- Calculation of Zbet according to Corrigendum 1 ISO 6336-2:2008 with Zβ = 1/(COS(β)^0.5)
- Details of calculation method:
  cγ according to Method B
  Kv according to Method B
  KHβ and KFβ according to Method C
  fmα according to Equation 64, fsh according to 57/58, Fβx according to 52/53/54
  KHα, KFα according to Method B
- The logarithmically interpolated value taken from the values for the fatigue strength and the static strength, based on the number of load cycles, is used for coefficients ZL, ZV, ZR, ZW, ZX, YdrelT, YRrelT and YX..

End of Report lines: 632